Surface composition profiles in some polymer mixtures

Ian Hopkins

Surface Composition Profiles in Some Polymer Mixtures

October 1994

Ian Hopkinson

University of Durham

Supervisor

Randal W. Richards

University of Durham

A thesis submitted to the University of Durham in partial fulfilment of the regulations for the Degree of Doctor of Philosophy

Surface Composition Profiles in Some Polymer Mixtures

Ian Hopkinson

PhD Thesis October 1994

Abstract

The surface composition of selected polymer mixtures has been studied to a depth of circa 4000Å with a resolution of up to 10Å using neutron reflectometry (NR) and nuclear reaction analysis (NRA). The effective interaction parameters, χ, of several blends have been measured as a function of both composition and temperature, using Small Angle Neutron Scattering (SANS) and the incompressible random phase approximation, in order to understand the surface segregation behaviour of the polymer blends. No surface segregation was observed in annealed blends of syndiotactic poly (methyl methacrylate) (h-PMMA) with perdeuterated poly (methyl methylacrylate) (d-PMMA), where the h-PMMA was the majority component with a high molecular weight and the d-PMMA had lower molecular weights. Values of χ for these blends showed a chain length disparity effect, higher disparity led to a small negative χ. Increases in χ were observed at low volume fractions of d-PMMA. Surface segregation of perdeuterated poly (ethylene oxide) (d-PEO) to the polymer - silicon oxide interface of an annealed d-PEO/h-PMMA blend was observed, where the bulk volume fraction of the d-PEO was <0.30. The surface composition profile could not be described by current theory. Measured χ values were small and negative and there was a change in χ on changing the locus of deuteration from PEO to PMMA in a PEO/PMMA blend. These blends exhibited a decrease in χ at low volume fractions of PEO. Polymer brushes were found at the air - polymer interface of a blend of low molecular weight polystyrene (h-PS) with perdeuterated polystyrene with a single perfluorohexane end group (d-PS(F)) or two perfluorohexane end groups (d-PS(F2)). These results were in good agreement with a self consistent field theory. Similar blends of high molecular h-PS / d-PS(F) showed enhanced surface segregation, compared to blends with no perfluorohexane end groups. NR data showed that the surface of a blend of polystyrene with perdeuterated dibutyl phthalate (d-DBP) (a model additive) was enriched with d-DBP over a 30Å length scale. The loss of d-DBP from a thin film (~ 800Å thick) was observed using NR and attenuated total reflection (ATR) infra red spectroscopy.

Acknowledgements

I am grateful to Randal Richards for his persistent and enthusiastic supervision and for tolerating my scepticism of anything he said even though he was nearly always right! I'd also like to thank Prof. W.J. Feast our leader, for making the IRC a good place to work.

A number of people at the IRC in Polymer Science have been directly involved in this work and I'd like to thank: F.T. Kiff who has synthesised all the polymers I have used, with a degree of competence I could only dream of emulating. Gordon 'Backup' Forrest who was responsible for the size exclusion chromatography and J. Say and Dr A. Kenwright who ran and helped in the analysis of n.m.r spectra. I am also grateful to the Mechanical Workshop, who have made various oddly shaped bits of metal for me and the Glassblowers.

I have had the pleasure of working with a number of instrument scientists, these are: Dr J. Penfold, Dr J. Webster and Dr D. Bucknall (on CRISP at the Rutherford Appleton Laboratory), Dr S. King and Dr. R. Heenan (on LOQ at the Rutherford Appleton Laboratory) and Dr A. Clough (nuclear reaction analysis at Surrey University), these people have all put up with my incessant questions and have made useful suggestions in the analysis of data, thanks are also due here to Dr D. Sivia, also at Rutherford Appleton Laboratory for allowing me to use his neutron reflectivity data analysis programs.

I'd like to thank Prof. K.R. Shull for allowing me to use LAYERS, his self consistent field theory program and also for useful discussions.

I have enjoyed many stimulating meetings with my collaborators at Strathclyde University (Prof. R.A. Pethrick, Dr S. Affrossman, M. Hartshorne (also responsible for the synthesis of perdeuterated dibutyl phthalate)) and at Courtaulds Plc (Dr H. Munro, Dr T. Farren, S. Wills, Dr J. Connell). I would like to thank Courtaulds Plc and SERC for funding this work.

The IRC has been a fun place to work and I'd like to mention specifically my immediate cohort: Norman 'Sleepwalker' Clough, Neil 'Red shoes' Stainton, Don 'whoops' Davison and Cecilia 'Disk full' Backson and some distinguished others 'Red' Lian Hutchings, Stella 'Sainsbury's' Gissing, Dave 'The Viking' Parker, Pangiotis 'PD' Dounis, all other members of the IRC are mentioned implicitly.

Finally I'd like to thank Sharon who has kept me relatively sane over the last three years, and has put up with my occasional sanity lapses during writing up and my parents who haven't seen me very often recently (my fault!).

To Sharon

Contents

Declaration

All work contained within this thesis is my own work, unless stated otherwise, and has not previously been submitted for any other qualification.

1. Introduction

1.1 Surfaces

The aim of this work was to study and understand the surface segregation behaviour of polymer - polymer blends and a polymer - 'additive' system. The reason for this interest is that the surface composition of a polymer mixture influences properties of the mixture. In blends this includes wettability, adhesion, solvent penetration and weathering. For 'additives' the interest will be in whether certain additives accumulate preferentially at the surface, in some situations this will be desirable such as when the additive is used to lubricate the polymer during processing or alternatively such segregation could be undesirable because the additive is required to modify the bulk properties of the blend and hence is at best wasted at the surface. Ultimately the hope is that by understanding the processes and conditions which influence surface segregation behaviour it will be possible to control the phenomena to produce industrially useful properties at lower cost than current methods. However this work is not concerned with such properties, but rather in the near surface composition profile from which the properties ultimately stem.

Two processes by which the surface composition of a miscible polymer blend can differ from the bulk composition have been considered. These are ***surface enrichment*** and ***brush formation***, illustrated schematically in Figures 1.1a and 1.1b. ***Surface enrichment*** is the 'wetting' of the surface of a blend by the component of lower surface energy, ***brush formation*** is driven by end groups on polymers in the blend which will attach these polymers to an interface.

The study of ***surface enrichment*** behaviour in polymer blends has developed over the past ~15 years since the general theoretical work of Cahn[1], who considered the surface enrichment behaviour of blends in general. This work was followed by development of a theory specifically for polymer blends by Pincus and Nakanishi[2] and Schmidt and Binder[3]. Subsequently these theories have been explored more thoroughly and in addition Monte Carlo[4] and Self Consistent Field[5] theory models have been developed.

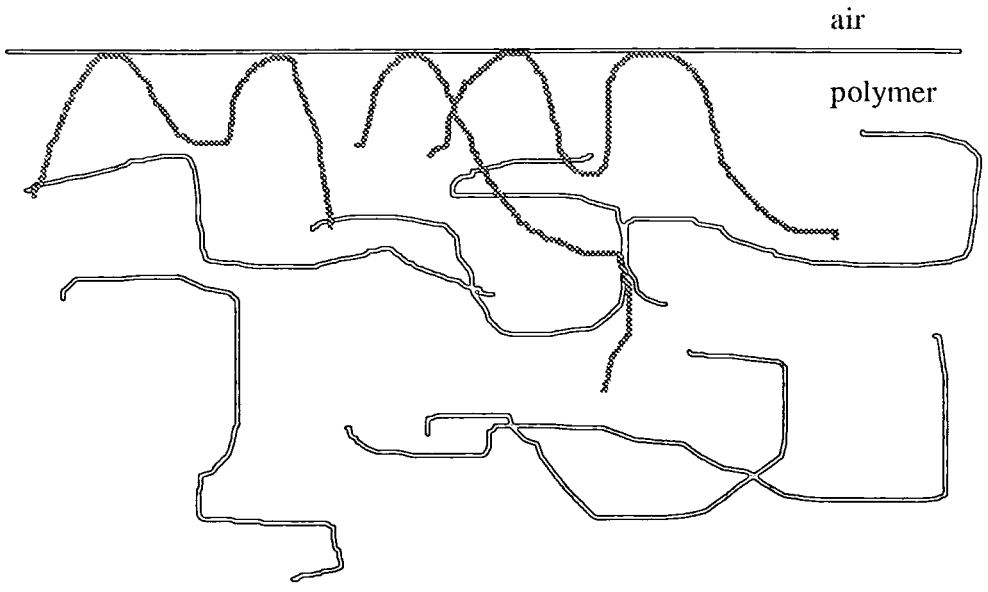

Figure 1.1a: Schematic of Surface enrichment

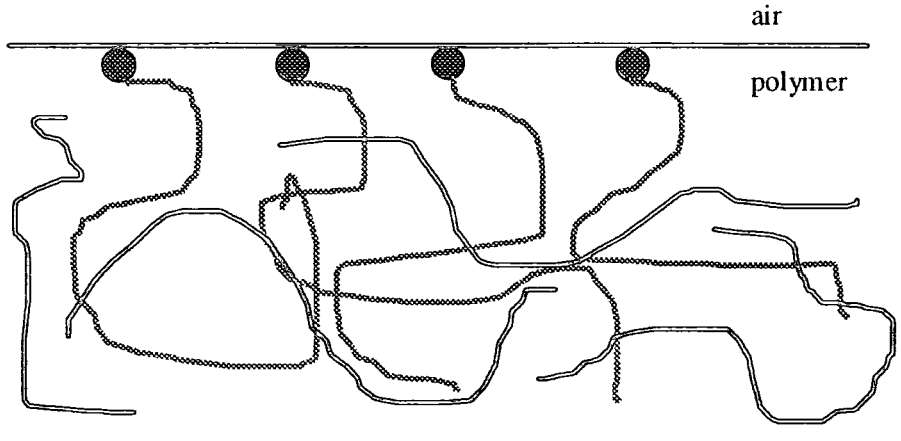

Figure 1.1b: Schematic of brush formation

These theories predict that the variation of volume fraction of the enriching polymer as a function of depth from the interface occurs over lengths ~R_g (where R_g is the radius of gyration of the enriching polymer). This corresponds typically to distances of the order ~50Å to ~200Å, a typical composition versus depth profile for a blend sustaining surface enrichment is shown in Figure 1.2. Enrichment may equally occur at the air - polymer or polymer - substrate interface of a film. The horizontal axis in this figure indicates the depth, z, from the interface and the vertical axis is the volume fraction, ϕ, of the enriching component. In a binary blend it will be assumed that $\phi + (1-\phi) = 1$, where $(1-\phi)$ is the volume fraction of the second component of the blend.

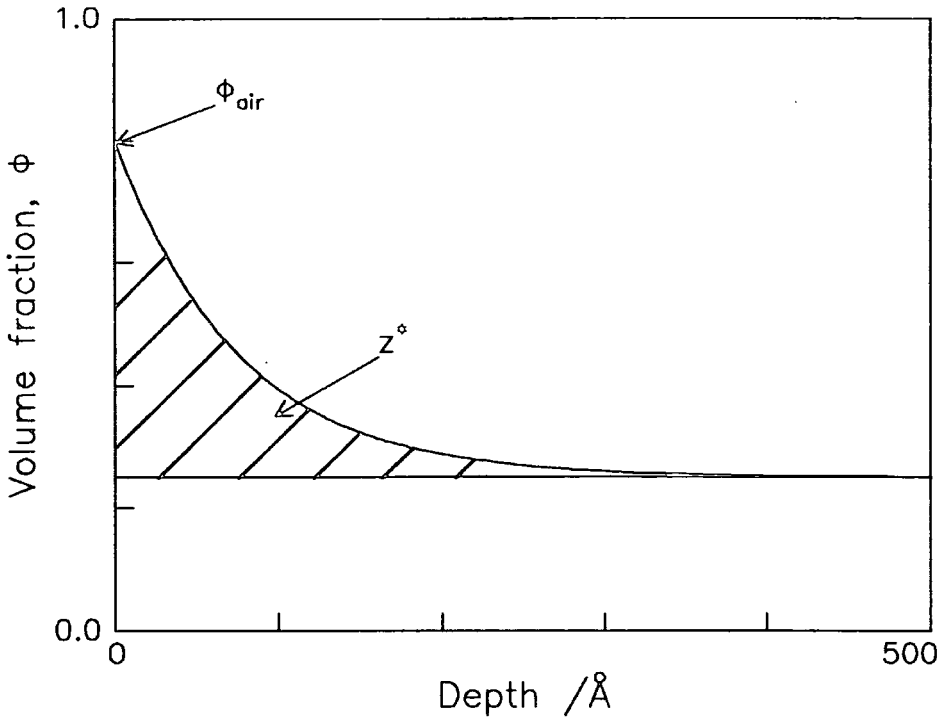

Figure 1.2: Generic surface enrichment composition versus depth profile.

Figure 1.2 also illustrates the definitions of the surface volume fraction, ϕ_{air}, and the surface excess, z^*, which is given in Equation 1.1. ϕ_B is the bulk volume fraction of the enriching polymer.

$$z^* = \int (\phi(z) - \phi_B)\, dz$$

Equation 1.1

The surface analysis techniques that can be used to study near surface structure at the required length scale will be introduced shortly.

Theories[2,3] show that the bulk thermodynamics of the polymer blend are important in determining the shape of the near surface composition profile of the enriching polymer. When the blend is close to one phase - two phase coexistence the characteristic decay length of the enrichment profile increases since the free energy cost of maintaining a region at the surface with a composition different from that in the bulk is lower closer to the phase boundary. For this reason the bulk thermodynamics of the polymer blends used in this work have been investigated using Small Angle Neutron Scattering (SANS) using the theoretical results of de Gennes[6], an 'effective' Flory -

Huggins interaction parameter is determined and hence the thermodynamics of the blend are revealed in the context of the Flory - Huggins lattice theory of polymer blends[7].

Following theoretical predictions there has been an experimental interest in the surface enrichment behaviour of polymer blends. The primary interest, for making detailed comparisons between theory and experiment, has been in the perdeuterated polystyrene (d-PS) / polystyrene (h-PS) blend system. It has been found by Bates and Wignall[8] that, rather than being completely ideal such blends of a polymer with its perdeuterated isomer are characterised by a small positive Flory - Huggins interaction parameter, χ_{FH}, and so at sufficiently high degrees of polymerisation such blends will exhibit 'upper critical solution temperature' (UCST) phase behaviour, where the one phase region is found at higher temperatures. Subsequently non-zero values of χ_{FH} have been measured for a range of blends of hydrogenous polymers with their perdeuterated isomers (see section 5.1.3 for examples). In addition to introducing simple phase behaviour the deuteration acts as a 'label' for a variety of experimental techniques.

The initial work on the surface enrichment behaviour of the d-PS/h-PS blend was by Jones *et al*[9,10] who showed that surface enrichment of the d-PS to the air - polymer interface occurred in 'symmetric' high molecular weight blends (that is where the degrees of polymerisation of the hydrogenous, N_H, and deuterated, N_D, components are approximately equal). The variation of the degree of enrichment as a function of the bulk volume fraction of d-PS, ϕ_B, was obtained and from these data it was concluded that the enrichment was driven by a surface energy difference of 0.078 mJ m^{-2} in favour of the deuterated polymer. This difference is small when compared to surface energy differences that can be measured directly and when compared to the differences in surface energy typically found between the components of a miscible blend. Because the high molecular weight of the polymers forces the blend close to the phase boundary this tiny surface energy difference is sufficient to drive enrichment. The work of Jones *et al* culminated in showing that although the surface enrichment behaviour of d-PS/h-PS was described quite accurately by the theory of Schmidt and Binder, the shape of the near surface composition profile differed subtly from theoretical prediction. This has been attributed, at least in part, to the use of the approximation that the surface energy difference can be assumed to act like a delta function potential at the interface, rather than acting over a longer range that extends a short distance into the blend.

Further work by Hariharan *et al*[11] on d-PS/h-PS blends has explored the effect that a difference in molecular weight between the d-PS and h-PS has on the surface enrichment behaviour. Entropy favours lower molecular weight polymers at the surface and Hariharan *et al* were able to force h-PS to the surface of d-PS/h-PS blends by lowering the molecular weight of the h-PS to values well below that of the d-PS. Budkowski *et al*[12] have shown that in contrast to the work of Jones *et al* where no enrichment was observed to the polymer - substrate interface (the substrate was silicon), enrichment of d-PS does occur to a silicon surface which retains its native silicon dioxide layer. The surface energy difference between d-PS and h-PS against silicon dioxide is rather smaller than that versus air.

In addition to this work on d-PS/h-PS there has also been experimental work on the poly (ethylene oxide) (PEO) / poly (methyl methacrylate) (PMMA)[13] and polystyrene / poly (vinyl methyl ether) (PVME)[14,15,16] systems although detailed determinations of the near surface composition profile have not been made. There has also been a short paper on surface enrichment in the perdeuterated PMMA / hydrogenous PMMA blend[17] , showing a very narrow region of surface enrichment of the d-PMMA at the air - polymer interface although, as will be discussed later, the conclusions in this paper may well be in error.

Polymer brushes have typically been studied in the context of brushes forming on the surface of particles in solution, the effect of such brush formation is to stabilise the formation of a colloidal suspension of the particles, there has recently been a general review of the theoretical and experimental aspects of such systems[18] . The properties of brush systems have been studied using Small Angle Neutron Scattering, force balance experiments and very recently coupled neutron reflectometry / force balance experiments (see reference 18 and references therein). Again the length scales involved are typically ~R_g. Theoretically the behaviour of brushes in solution has been described using the scaling theories of de Gennes[19] and Alexander[20] and there have also been Monte Carlo models[21] and self consistent field models[22] .

However the behaviour of polymer brushes in polymer melts has been less well studied. Scaling theories do not generally apply to the polymer melt case since the entropy of the 'matrix' polymer becomes important and scaling theories do not account for this effect. Shull[23] has developed a self consistent field theory for brush formation in a polymer matrix. The expected composition profiles for the brush are not dissimilar

from those for the surface enrichment profile, and again the variables of interest in the melt case will be the surface volume fraction of the brush forming polymer, ϕ_{air}, and the surface excess, z^*. Since, in principle, the brush forming polymer is only attached to the surface at one end then the expectation is that for the same surface volume fraction a brush will extend further into the bulk than an equivalent surface enrichment profile where the polymer is attached to the surface at several points along its length. Some progress has been made experimentally in the study of butadiene[24] and carboxyl[25] and terminated d-PS brushes in a h-PS matrix. The carboxyl and butadiene groups are found to end attach the deuterated polymer to a silicon substrate to form a brush. The interest in this work is not the effect that the end groups will have on the surface properties but the effect that bringing the attached polymer to the surface will have on the surface properties.

A topic related to that of polymer brushes is the behaviour of A-B diblock copolymers at interfaces between A and B homopolymers[26,27], where the homopolymers are immiscible. The junctions of the A-B copolymers will locate at the interface between the A and B homopolymers, this effectively 'grafts' each half of the copolymer in the identical homopolymer. The profiles of the brushes thus formed can be studied by deuterating the diblock copolymer. This situation is illustrated schematically in Figure 1.3.

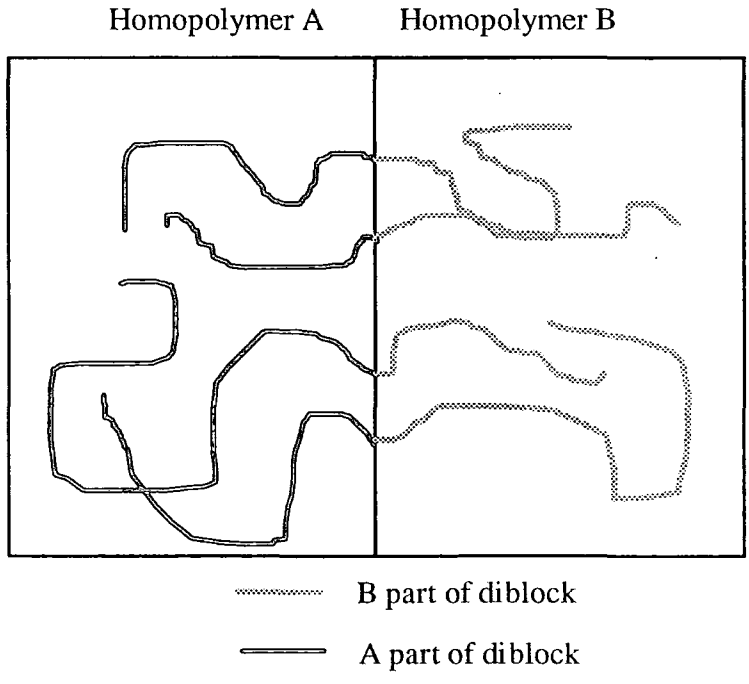

Figure 1.3: Schematic diagram of an A-B diblock copolymer forming two brushes at the interface between homopolymers of A and B.

In practical terms brush formation is probably of more interest than surface enrichment, because the relative surface energies of the components of a blend system are essentially predetermined, whereas the addition of surface active end groups to one component of a polymer blend to form a brush at the surface can be done without significantly altering the bulk properties of the blend.

1.2 Surface Analysis Techniques

Earlier the subject of techniques which may be used to study the near surface composition was mentioned. The requirements for such techniques are that they be able to determine the surface composition of the polymer blend, here the 'surface' refers to the top 10-15Å, and the shape of the composition profile up to a depth of ~1000Å into the sample. For polymer - polymer blends the sample environment is relatively unimportant, however if the behaviour of a blend of a polymer with a low molecular additive is of interest then there is a problem in the use of high vacuum techniques because even relatively high boiling point additives will leach out of at least the surface region of the polymer by evaporation. Outlines of the main techniques used to study the surface and near surface composition profiles of polymers will follow, the details of the techniques actually used in this work can be found in Section 3.1 (theoretical basis) and Section 4 (experimental). The introduction to these analytical techniques will be divided into two broad areas ***surface specific*** techniques and ***depth profiling*** techniques.

Surface Specific

X-ray photoelectron spectroscopy (XPS or ESCA)[28], this is a high vacuum technique which provides information on the chemical environment, in terms of bond types, of electrons ejected from the surface of the sample. The sample surface is illuminated with X-rays, causing the excitation of electrons from inner shell orbitals to the continuum state. These electrons are detected, their energy will vary according to the type and bonding of the atom from which they originated. The depth probe is limited to the maximum escape distance for the electrons, which is ~40Å. XPS can be used on

polymer blends where the components are chemically distinct, deuteration is of no use as a label.

Static Secondary Ion Mass Spectrometry (SSIMS or SIMS)[28] provides chemical information on the near surface (~10Å) layers of a polymer blend. Like XPS it is a high vacuum technique. The sample surface is bombarded with a beam of ions (commonly Ar^+ with energy ~2 KeV), this penetrates the sample and causes a degree of chain scission producing polymer fragments that, if generated close enough to the surface, will escape. These fragments are collected electrostatically and mass spectrometry is carried out on them. SIMS is very surface specific because the escape depths for these large fragments is very small. The masses of the fragments produced are characteristic of the parent polymer. Deuteration will produce shifts in the masses of fragments used and so will act as a label, but in a blend of two chemically different polymers deuterium labelling is not necessary since the fragmentation patterns of the two polymers will be different.

Depth Probing

Forward Recoil Elastic Scattering (FRES)[29] this again is a high vacuum technique which will provide a composition depth profile with a resolution of ~800Å and a probe depth of ~1μm (although recent refinements will provide a slightly improved resolution). Deuterium labelling is necessary. $^4He^+$ are fired into the sample at a low incident angle, nuclei of, in particular, ^1H and ^2H are knocked from the sample by elastic collisions. The elastically scattered $^4He^+$, ^1H and ^2H are collected at forward angles. The energies of the detected ^1H and ^2H will be characteristic of the depth beneath the sample surface at which they are produced. This technique is insensitive to chemical environment, but gives a measure of the ^1H / ^2H ratio as a function of depth.

Nuclear Reaction Analysis (NRA)[30], again a high vacuum technique which relies on deuterium labelling to produce composition depth profiles with a resolution of up to 150Å. The technique relies on the nuclear reaction:

$$^3He^+ + {}^2H \rightarrow {}^1H^+ + {}^4He + Q$$

Equation 1.2

where Q = 18.352 MeV. The sample of interest is bombarded with $^3He^+$ with an energy of 0.7 MeV. These react with ^2H at various depths within the sample, $^1H^+$ are then

detected at backward angles. The energy of the detected $^{1}H^{+}$ is characteristic of the depth at which the source nuclear reaction occurred. NRA is only sensitive to ^{2}H and so calibration to obtain absolute concentration is required. The penetration depth and resolution are related, a greater penetration depth can be obtained by sacrificing resolution.

Dynamic Secondary Ion Mass Spectrometry (DSIMS)[31] this technique is closely related to SSIMS, but whereas SSIMS is carried out at low ion beam currents to avoid sample damage, in DSIMS the beam current is increased and controlled sample damage is produced by rastering the ion beam repeatedly across a small area of the sample surface, this gradually produces an 'open cast mine' structure. The mass spectrum of the ejected fragments will vary as a function of time as the bottom of the 'mine' penetrates deeper into the sample. The composition profile is obtained from the mass spectrum versus time, the resolution is ~150Å. Run times are very long since the sample is eroded very slowly and there are worries over the degree of mixing that the continuous bombardment produces in the surface layers.

Attenuated Total Reflection (ATR)[32] infra red spectroscopy utilises the evanescent wave that is found at the surface of a material undergoing total internal reflection. The intensity of the evanescent wave decays exponentially over a length scale of microns. This property can be used to produce infra red spectra which are heavily weighted with contributions from the region close to the surface of the material sustaining total reflection (~1 μm). In principle ATR can be used to produce depth profiles of the near surface composition profile with a resolution ~0.5 μm, i.e. too poor for the work described here. However there are advantages to ATR, principally that it can be used for solutions and in ambient conditions and it is a relatively cheap laboratory based technique which will provide chemical information on thin film samples.

Neutron Reflectometry (NR)[33] this is essentially a scattering technique. The intensity of a neutron beam reflected specularly (i.e. with incident and reflected angles equal) from the surface of the sample is measured as a function of the scattering vector (which is related to both the angle of incidence and neutron wavelength). The variation of the reflectivity ((incident/reflected) intensity) with the scattering vector contains information on the variation of nuclear scattering length density (a property of nuclei) perpendicular to the surface. The scattering lengths of ^{1}H and ^{2}H are very different and so determination of the composition profile is through isotopic substitution. The analysis of

NR data is not straightforward since the reflectivity is in reciprocal space and there is a loss of phase information in the measurement. The analysis of neutron reflectometry data requires the use of a model fitting procedure, however the resolution approaches 10Å. In this work samples are studied in ambient conditions, however since neutrons are not readily absorbed the sample can be studied in a wide range of conditions, the neutron beam passes easily through the sample containment

In practice no one technique is used exclusively, the very high resolution of NR is highly desirable, but the data analysis is made far easier by the addition of further information from other techniques. Neutron reflectometry is not readily available, there are a very limited number of reflectometers in the world and they are typically over subscribed. For this reason other techniques are used to 'screen' samples so that reflectometer time is best utilised. The majority of this work has been done using neutron reflectometry, collaborators in this project at Strathclyde University have done SSIMS work on the same systems as those used here and these results along with NRA experiments have been used to assist the analysis of the neutron reflectometry data. On the additive - polymer system ATR spectroscopy was used in addition to neutron reflectometry.

1.3 Overview of This Work

There are a number of factors that determine the systems that can be used in surface segregation studies of this type. First of all it must be possible to synthesise the polymers with a controlled molecular weight and a narrow molecular weight distribution, since a wide molecular weight distribution will make comparisons with theory more difficult. This constraint obliges the use of anionic polymerisation, which does give good control of molecular weight and distribution. Secondly it must be possible (and financially reasonable) to deuterate at least one component of the blend, preferably the component that segregates to the surface. The blends that were chosen for study are as follows:

perdeuterated poly (methyl methacrylate) (d-PMMA) / hydrogenous poly (methyl methacrylate) (h-PMMA) the original intention was to study the effect of tacticity and chain length disparity on surface enrichment and also to study the kinetics of the enrichment process as a function of molecular weight. It is possible to synthesise

PMMA in both isotactic and syndiotactic forms and the perdeuterated monomer is relatively cheap. However it was found that it was not possible to synthesise the isotactic polymer with a narrow molecular weight distribution and control of the molecular weight was poor. PMMA differs from polystyrene in that it contains polar groups and there was some interest in seeing if this had any influence on the surface enrichment behaviour. In addition to neutron reflectometry work, Small Angle Neutron Scattering (SANS) work was also required in order to understand the surface enrichment behaviour and as a separate question whether composition and chain length disparity had an effect on the effective interaction parameter measured for this system.

poly (ethylene oxide) (PEO) / syndiotactic PMMA this is a mixture of two chemically different polymers which are both available in perdeuterated and hydrogenous form and can be synthesised anionically. The blend is semi - crystalline for volume fractions of PEO above ~0.30. This blend represents an opportunity to make a detailed study of the surface enrichment behaviour in a system that is rather more complex than the d-PS/h-PS system that has been used previously. Although there has been a considerable amount of work on the bulk thermodynamics of PEO/PMMA, SANS measurements were made in order to determine the effective interaction parameter, in particular the effect of swapping deuteration from the PEO to PMMA could be studied and the variation of the effective interaction parameter with composition could be compared with that obtained for d-PMMA/h-PMMA, the difference being that the expectation for the PEO/PMMA blend is that there are favourable interactions that drive compatibility.

End capped perdeuterated polystyrene (d-PS(F)) / h-PS a small perfluorinated group (perfluorohexane) is attached to one or both ends of the perdeuterated polymer. The intention is that the very low surface energy of this group, when compared to that of the polystyrene, will end attach the perdeuterated polymer to the air - polymer interface to form a polymer brush. Results from these experiments can be compared to the theoretical predictions of self consistent field theory. The d-PS(F)/h-PS system was chosen for this work because the surface enrichment behaviour in the 'normal' blend (with no end caps) has been thoroughly investigated and the bulk thermodynamics have also been described.

perdeuterated dibutyl phthalate (d-DBP) / polystyrene this is a polymer - additive system. The perdeuterated dibutyl phthalate is a 'model' plasticiser, a plasticiser lowers the glass transition temperature of a polymer. Dibutyl phthalate is no longer used industrially, since despite its high boiling point it is lost from the polymer substrate

during use, the dioctyl phthalates are more commonly used. However for this work dibutyl phthalate was used because the precursors required to synthesise the perdeuterated form are relatively cheap and readily available.

The structure of this thesis is as follows: the next two sections are an outline of the current theories of polymer - polymer thermodynamics, surface enrichment and brush formation followed by the theoretical underpinnings of the surface analysis techniques used. The general experimental procedures for all the work are in Section 4. Sections 5 - 8 contain details of the experiments, results, discussion and conclusions for each of the blend systems introduced above, divided up by blend system rather than technique. Where appropriate sections are divided into two parts, covering the bulk thermodynamics and surface segregation behaviour of an individual system separately, references are found at the end of each part (this does mean some references are repeated). The final Section 9, draws together conclusions from all the different blend systems and contains suggestions for further work.

1.4 References for Section 1

1 . J.W. Cahn, *Journal of Chemical Physics*, 66(8), 1977, 3667.

2 . H. Nakanishi, P. Pincus, *Journal of Chemical Physics*, 79(2), **1983**, 997.

3 . I. Schmidt, K. Binder, *Journal de Physique*, 46, **1985**, 1631.

4 . P. Cifra, F. Bruder, R. Brenn, *Journal of Chemical Physics*, 99(5), **1993**, 4121.

5 . A. Hariharan, S.K. Kumar, T.P. Russell, *Macromolecules*, 24, **1991**, 4909.

6 . P.G. de Gennes, 'Scaling Concepts in Polymer Physics', Cornell University Press, 1985.

7 . P.J. Flory, 'Principles of Polymer Chemistry', Cornell University Press, 1953.

8 . F.S. Bates, G.D. Wignall, *Physical Review Letters*, 57(12), **1986**, 1429.

9 . R.A.L. Jones, E.J. Kramer, M.H. Rafailovich, J. Sokolov, S.A. Schwarz, *Physical Review Letters*, 62, **1989**, 280.

10 . R.A.L. Jones, L.J. Norton, E.J. Kramer, R.J. Composto, R.S. Stein, T.P. Russell, A. Mansour, A. Karim, G.P. Felcher, M.H. Rafailovich, J. Sokolov, X. Zhao, S.A. Schwarz, *Europhysics Letters*, 12(1), **1990**, 41.

11 . A. Hariharan, S.K. Kumar, T.P. Russell, *Journal of Chemical Physics*, 98(5), **1993**, 4163.

12 . A. Budkowski, U. Steiner, J. Klein, *Journal of Chemical Physics*, 97(7), **1992**, 5229.

13 . P. Sakellariou, *Polymer*, 34(16), **1993**, 3408.

14 . D.H. Pan, W.M. Prest, *Journal of Applied Physics*, 58, **1985**, 2861.

15 . Q.S. Bhatia, D.H. Pan, J.T. Koberstein, *Macromolecules*, 21, **1988**, 2166.

16 . J.M.G. Cowie, B.G. Devlin, I.J. McEwen, *Macromolecules*, 26, **1993**, 5628.

17 . S. Tasaki, H. Yamaoka, F. Yoshida, *Physica B*, 180&181, **1992**, 480.

18 . G.J. Fleer, M.A. Cohen Stuart, J.M.H.M Scheutjens, T. Cosgrove, B. Vincent, 'Polymers at Interfaces', Chapman & Hall, 1993.

19 . P.G. de Gennes, *Macromolecules*, 13, **1980**, 1069.

20 . S. Alexander, *Journal de Physique*, 38, **1977**, 983.

21 . P-Y. Lai, K. Binder, *Journal of Chemical Physics*, 97, **1992**, 586.

22 . J.M.H.M. Scheutjens, G.J. Fleer, *Journal of Physical Chemistry*, 84, **1980**, 178.

23 . K.R. Shull, *Journal of Chemical Physics*, 94(8), **1991**, 5723.

24 . R.A.L. Jones, L.J. Norton, K.R. Shull, E.J. Kramer, G.P. Felcher, A. Karim, L.J. Fetters, *Macromolecules*, 25, **1992**, 2359.

25 . C.J. Clarke, R.A.L. Jones, J.L, Edwards, A.S. Clough, J. Penfold, *Polymer*, 35, **1994**, 4065.

26 . H.R. Brown, K. Char, V.R. Deline, *Macromolecules*, 23, **1990**, 3385.

27 . D.G. Bucknall, M.L. Fernandez, J.S. Higgins, to be published in *Faraday Discussion*, 98, **1994**.

28 . D. Briggs in 'Comprehensive Polymer Science Volume 1', Pergamon, 1989.

29 . P.J. Mills, P.F. Green, C.J. Palmstrom, J.W. Mayer, E.J. Kramer, *Applied Physics Letters*, 45(9), **1984**, 957.

30 . R.S. Payne, A.S. Clough, P. Murphy, P.J. Mills, *Nuclear Instruments and Methods in Physics Research B*, 42, **1989**, 130.

31 . S.J. Whitlow, R.P. Wool, *Macromolecules*, 24, **1991**, 5926.

32 . L.J. Leslie, G. Chen, *Vibrational Spectroscopy*, 1, **1991**, 353.

33 . T.P. Russell, *Materials Science Reports*, 5, **1990**, 171.

This page left intentionally blank

2. Theory

2.1 Polymer - polymer thermodynamics

The purpose of this section is to introduce Flory - Huggins lattice theory[1], paying particular attention to the polymer-polymer interaction parameter, χ_{FH}, and how this parameter may be extracted from experimental scattering data by use of the incompressible random phase approximation (i-RPA)[2].

In the Flory - Huggins model the properties of a binary polymer blend, with components A and B, are calculated by assuming that the blend can be represented by a cubic lattice in which each lattice site is the same size and contains one repeat unit of either the A or B polymer. Using the basic Flory - Huggins theory the Gibbs free energy of mixing, ΔG_m, of the blend is given by:

$$\frac{\Delta G_m}{k_B T} = \frac{\phi}{N_A}\ln\phi + \frac{(1-\phi)}{N_B}\ln(1-\phi) + \chi_{FH}\phi(1-\phi)$$

Equation 2.1

ϕ is the volume fraction of component A, it is assumed that the blend is incompressible, hence the volume fraction of component B is (1 - ϕ). N_A and N_B are the degrees of polymerisation of components A and B. The Flory - Huggins interaction parameter is defined as:

$$\chi_{FH} = \frac{z_c(2\varepsilon_{AB} - \varepsilon_{AA} - \varepsilon_{BB})}{2k_B T}$$

Equation 2.2

where ε_{ij} are the nearest neighbour pair exchange interaction energies between monomers i and j. z_c is the co-ordination number. Implicit in Equation 2.1 is a clear division between entropic (the first two terms) and enthalpic (the final term) contributions to the free energy. The entropic terms represent the purely combinatorial entropy of the mixture. Ideally $\chi_{FH} \propto 1/T$ and has no dependence on either molecular weight or composition. However it is generally found that even in the simplest systems χ_{FH} is better described by:

$$\chi = A + \frac{B}{T}$$

Equation 2.3

where A is an entropic term that accounts for the inadequacies in the entropy calculation that leads to the ln terms in Equation 2.1, B is an enthalpic term. The blend will phase separate if it reduces its free energy by doing so, two phases will form with volume fractions of A, ϕ' and ϕ''. These compositions lie at or close to the minima in the free energy curve illustrated in Figure 2.1, which shows free energy as a function of ϕ for a blend in the one phase region (M), a blend well below the 'upper critical solution temperature' (UCST), (the highest temperature at which phase separation occurs) labelled (UM) and a blend a little below the UCST which separates into phases with compositions ϕ' and ϕ'', labelled PM. The locus of points in the composition (ϕ) - temperature (T) plane at which the free energy of the blend is reduced by phase separation is given by Equation 2.3:

$$\left(\frac{\partial \Delta G_m}{\partial \phi'}\right)_{T,P} = \left(\frac{\partial \Delta G_m}{\partial \phi''}\right)_{T,P} \quad \begin{cases} = 0 & if\ N_A = N_B \\ \neq 0 & if\ N_A \neq N_B \end{cases}$$

Equation 2.4

this locus is known as the coexistence or binodal curve, there is an additional constraint for the binodal curve for $N_A \neq N_B$ which is shown graphically in Figure 2.1. The binodal curve indicates when phase separation is thermodynamically favoured, the spinodal curve is when phase separation occurs spontaneously and is given by Equation 2.4:

$$\left(\frac{\partial^2 \Delta G_m}{\partial \phi^2}\right)_{T,P} = 0$$

Equation 2.5

therefore the value of χ_{FH} at the spinodal curve, calculated from Equations 2.1 and 2.5 is:

$$\chi_s = \frac{1}{2N_A\phi} + \frac{1}{2N_B(1-\phi)}$$

Equation 2.6

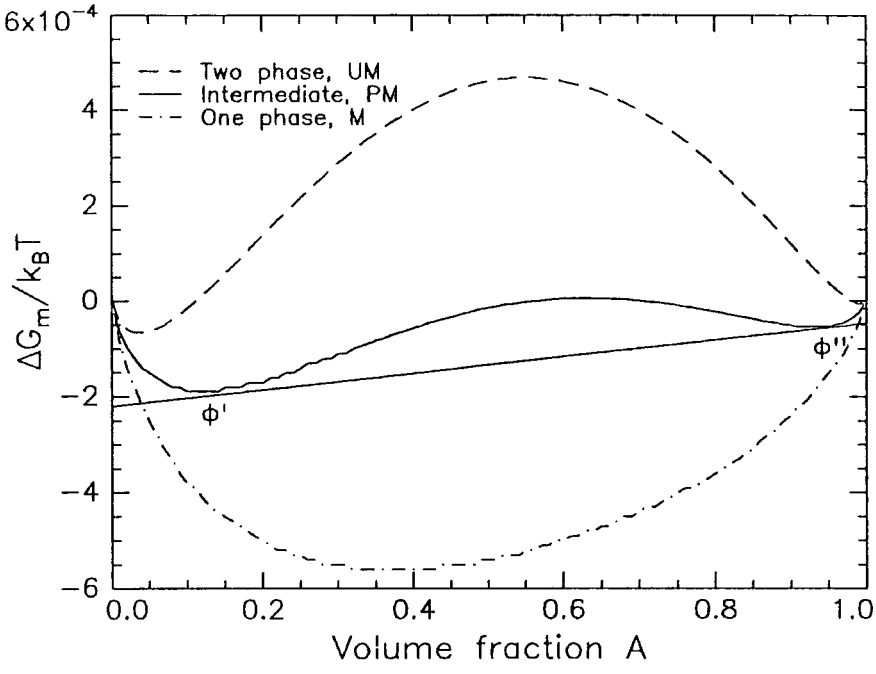

Figure 2.1: Free energy of mixing for a blend at various points in the ϕ - T phase diagram. The different curves are obtained by varying χ_{FH}. Straight line is the common tangent for ϕ' and ϕ''.

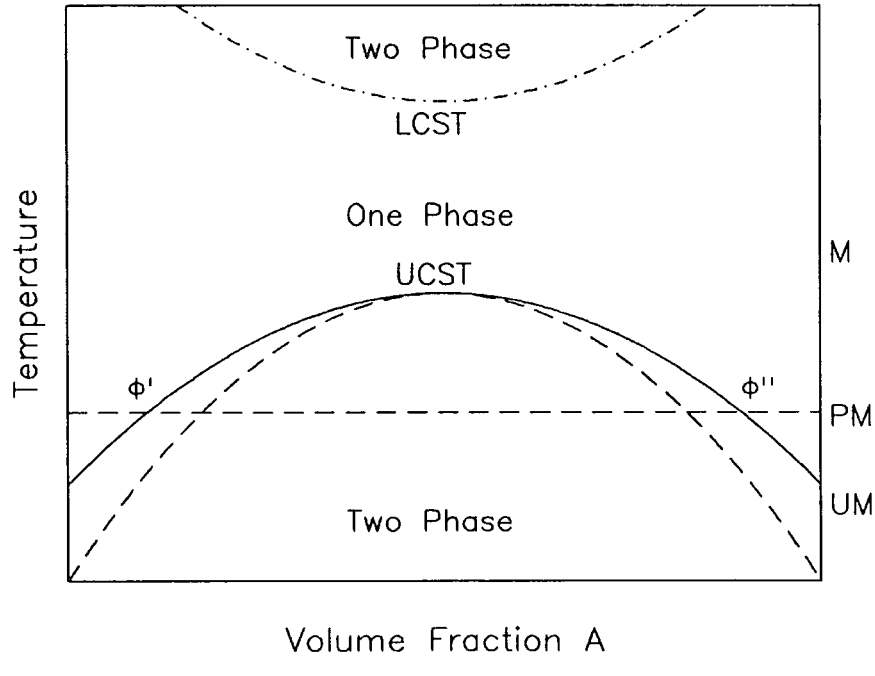

Figure 2.2: Phase diagram for the situation shown in Figure 2.1, LCST is not predicted by Flory - Huggins original theory. Solid line - coexistence or binodal curve, bottom broken line - spinodal curve. PM, U and M indicated in Figure 2.1.

When $N_A = N_B = N$ a simple expression is available for χ_{FH} at the coexistence curve, χ_b:

$$\chi_b = \frac{1}{N(1-2\phi)} \ln \frac{(1-\phi)}{\phi}$$

Equation 2.7

The phase diagram of an ideal 'Flory - Huggins' blend is shown in Figure 2.2, this phase diagram corresponds to the free energy plot in Figure 2.1. This phase diagram exhibits an upper critical solution temperature (UCST), i.e. the two phase region is found at lower temperatures. Basic Flory - Huggins theory is only able to predict UCST phase diagrams, experimentally other behaviours such as lower critical solution temperatures (LCST), where phase separation occurs at higher temperatures are observed. Note that the spinodal curve lies inside the coexistence curve.

In the context of the Flory - Huggins theory, de Gennes[2] has used the incompressible random phase approximation to predict the scattering law, S(Q) of a blend as:

$$S^{-1}(Q) = \frac{1}{\phi N_A g_D(R_{gA}, Q)} + \frac{1}{(1-\phi) N_B g_D(R_{gB}, Q)} - 2\chi_{FH}$$

Equation 2.8

where $g_D(R_g, Q)$ is the Debye function[3] which describes the intensity of scattering from a single Gaussian polymer chain with radius of gyration, R_g:

$$g_D(R_g, Q) = \left(\frac{2}{u^2}\right)(\exp(-u) + u - 1)$$
$$u = Q^2 R_g^2$$
$$Q = \frac{4\pi}{\lambda} \sin\theta$$

Equation 2.9

λ is the radiation wavelength and 2θ is the scattering angle. The coherent elastic neutron scatter, I(Q), for a blend, with segment volumes, v_A and v_B, and scattering lengths b_A and b_B, respectively is given by[4]:

$$I(Q) = v_o\left(\frac{b_A}{v_A} - \frac{b_B}{v_B}\right)^2\left(\frac{v_o}{\phi N_A v_A \bar{g}_D(R_{gA},Q)} + \frac{v_o}{(1-\phi)N_B v_B g_D(R_{gB},Q)} - 2\chi\right)^{-1}$$

Equation 2.10

Note that the Flory - Huggins interaction parameter, χ_{FH}, is replaced by an effective interaction parameter, χ, the reason for this will be discussed shortly. v_o is a 'reference' volume:

$$v_o = \left(\frac{\phi}{v_A} + \frac{(1-\phi)}{v_B}\right)^{-1}$$

Equation 2.11

In this situation where the segments have different volumes, the value of χ_s is also modified:

$$\chi_s = \frac{v_o}{2}\left(\frac{1}{v_A \phi N_A} + \frac{1}{v_B(1-\phi)N_B}\right)$$

Equation 2.12

If the blend components are not monodisperse but can be described by the Schultz - Zimm distribution then Equation 2.10 can be used with the substitution of a modified Debye function[5], $g'_D(R_g, Q)$:

$$g'_D(R_g,Q) = \frac{2}{u^2}\left[\left(\frac{h}{h+u}\right)^h - 1 + u\right]$$

Equation 2.13

where u was defined above and:

$$h = \left(\frac{M_W}{M_N} - 1\right)^{-1}$$

Equation 2.14

The complete form of Equation 2.10 can be fitted to scattering data of I(Q), to obtain χ and the radii of gyration of the components. This discussion will continue,

concentrating on the scattering structure factor, S(Q). Figure 2.3 shows the effect that varying the parameters in the model has on the scattering S(Q), in the form of Kratky plots of $Q^2S(Q)$ versus Q. It does appear that the effect of varying the radii of gyration and the interaction parameter is essentially the same - if this were the case then fitted values of χ would be determined entirely by the values of the radii of gyration used. However Figure 2.4 shows that there are in fact differences between the scattering from a blend with $\chi \neq 0$ and a best fit to the same scattering with $\chi = 0$. The discrepancy between the original model data and the best fit with $\chi = 0$ is at a maximum for intermediate values of Q.

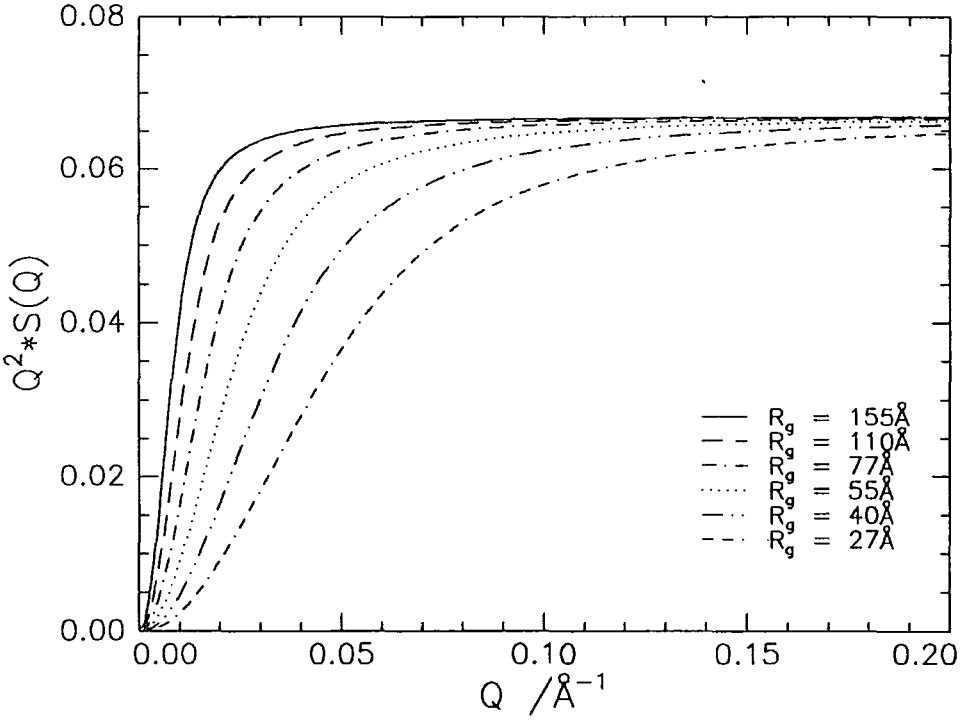

Figure 2.3a: Scattering for a blends with $R_{gA} = R_{gB} = R_g$, $\phi = 0.5$ and $\chi = 0$.

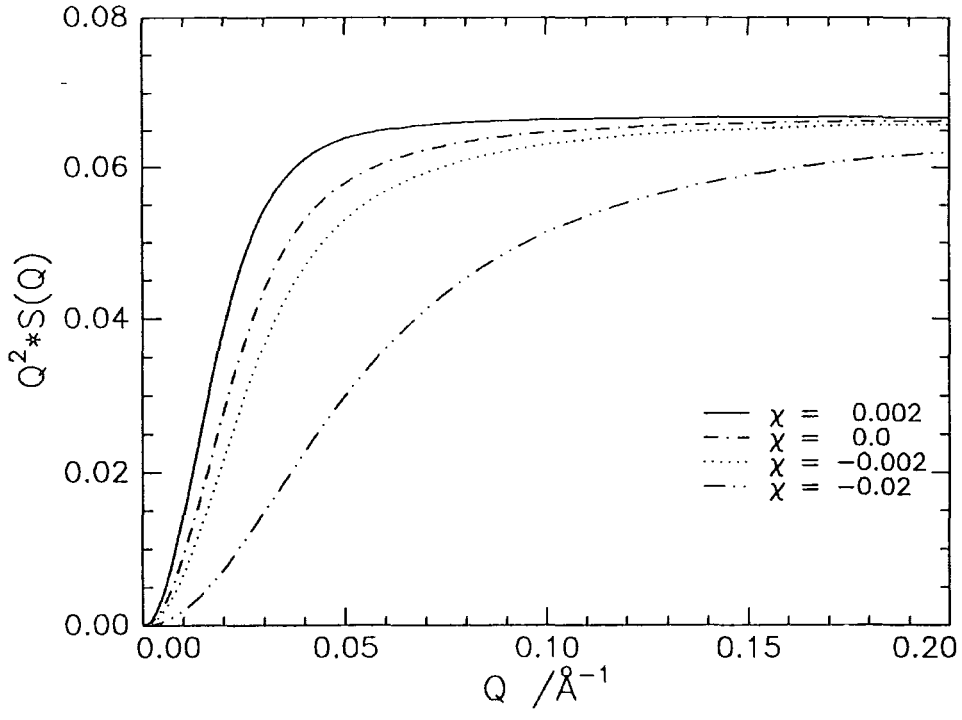

Figure 2.3b: Scattering from blends with $R_{gA} = R_{gB} = 55$Å, $\phi = 0.5$ and various χ values.

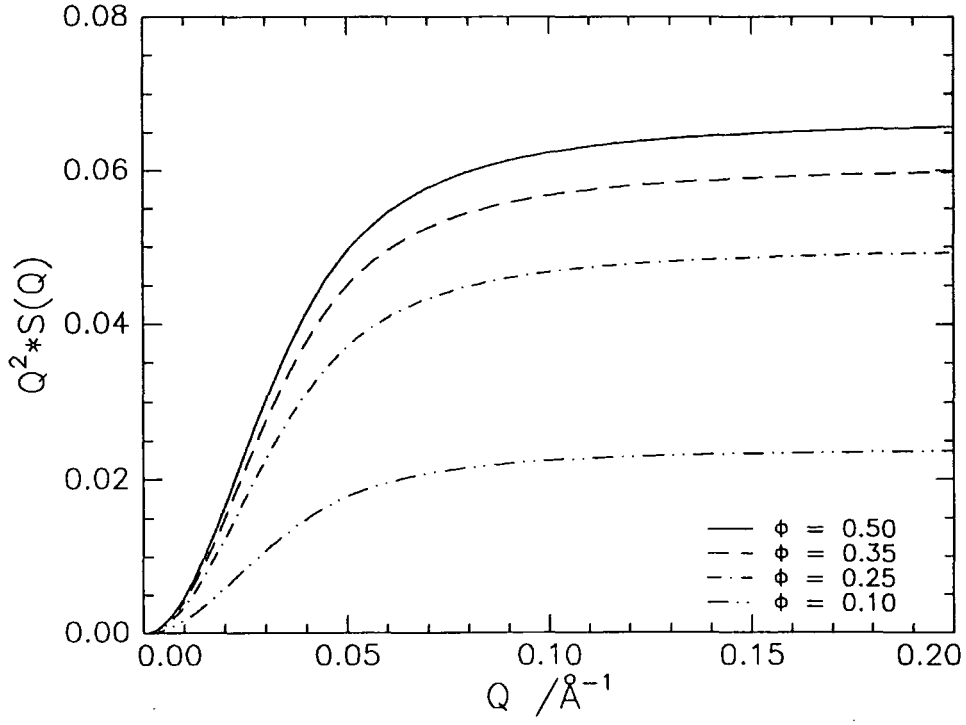

Figure 2.3c: Scattering from blends with $R_{gA} = R_{gB} = 55$Å, $\chi = 0$ and various ϕ values note for $R_{gA} = R_{gB}$ blends with composition ϕ and $(1 - \phi)$ have the same scattering function.

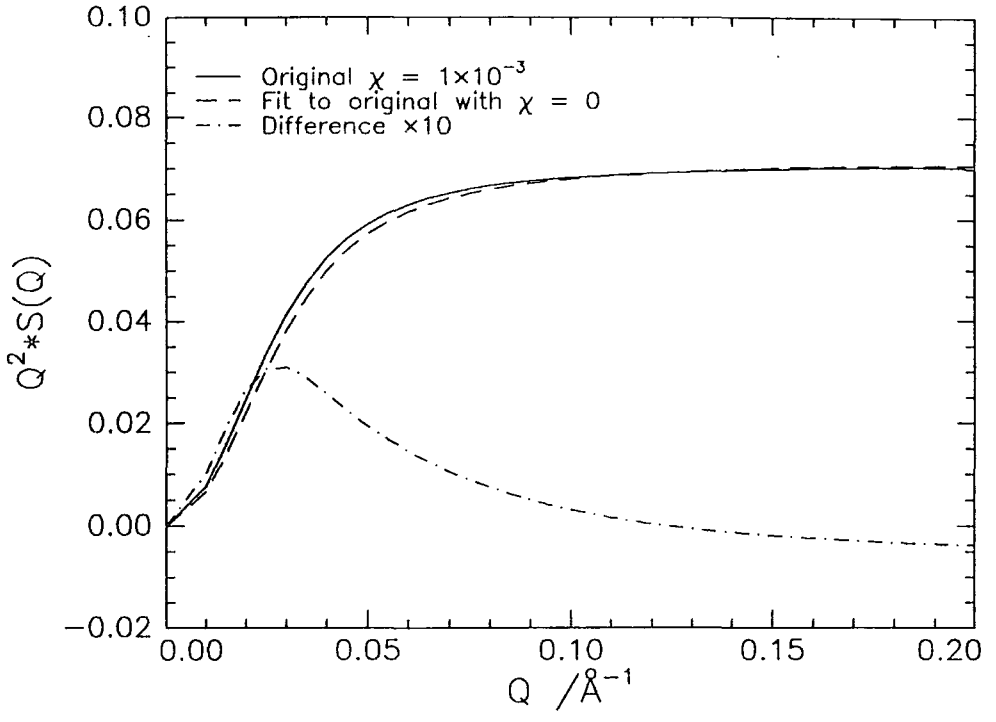

Figure 2.4: Scatter from a blend (details in text) with $\chi = 1\times10^{-3}$ fitted with an S(Q) with $\chi = 0$, along with the difference ×10.

It is possible to approximate Equation 2.8, such that thermodynamic parameters can be derived from simple linear fits to functions of the scattering data over limited ranges of the scattering vector Q. For simplicity these approximations will be considered in the context of a blend with $v_A = v_B = v_o$. At values of Q such that $R_gQ << 1$, the exponential term in the Debye function $g_D(R_g, Q)$ can be replaced by the first terms of a series expansion:

$$g_D(R_g, Q) \approx 1 - \frac{Q^2 R_g^2}{3}$$

Equation 2.15

when this is substituted into Equation 2.8 we obtain:

$$S(Q) \approx \frac{1}{2(\chi_s - \chi)(1 + Q^2\xi^2)}$$

Equation 2.16

where ξ is the correlation length for composition fluctuations defined as:

$$\xi = \frac{a}{6} \frac{1}{\sqrt{\phi(1-\phi)(\chi_s - \chi)}}$$

Equation 2.17

a is the statistical segment or Kuhn length of the polymer. To obtain a straight line, $S^{-1}(Q)$ is plotted versus Q^2, the intercept of this line is $2(\chi_s - \chi)$ and the gradient is $2\xi^2(\chi_s - \chi)$ (or ξ^2 = (gradient/intercept)). This is sometimes known as the Ornstein - Zernike plot. At high Q, $g_D(R_g, Q)$ becomes small and the -2χ term negligible and therefore:

$$S(Q) \approx \frac{12\phi(1-\phi)}{Q^2 a^2}$$

Equation 2.18

hence the statistical segment length can be obtained from the gradient of the high Q region of the Ornstein - Zernike plot. However if the scatter from a single coil deviates from the Debye function erroneous values for the statistical segment length will be obtained.

There are three main assumptions made in these derivations for the scattering behaviour of a polymer blend:

(i) The blend can be described by the Flory - Huggins lattice.

(ii) The incompressible random phase approximation applies - this assumes that there is no change in the total volume of the system when the pure components are mixed.

(iii) The chains have a Gaussian distribution of segments and so the scattering from a single chain can be described by the Debye function.

In practice all of these approximations are violated to some extent. The Flory _ Huggins theory is known to fail, in that is not able to predict any phase behaviour other than UCST behaviour. This occurs for a number of reasons; the physical 'un-naturalness' of the lattice, the discounting of specific interactions, the assumptions made in calculating the entropy of mixing and so forth. A number of attempts have been made to modify the Flory - Huggins theory, by taking into account the presence of free volume[6], differing surface areas for the different segment types[7], the presence of composition fluctuations[8], and adding structure to the individual segments by spreading each segment across several lattice cells (lattice cluster theory)[9]. Additionally there have

also been Monte Carlo simulations[10,11], polymer reference interaction site models (PRISM)[12], Born - Green - Yvon integral equation treatments[13] and equation of state theories[14]. These various theories are reviewed and compared by Binder[15] and Cui and Donohue[16], it is beyond the scope of this work to describe these various theories and the intention is simply to provide a starting point for any further study and give some idea as to the amount of theoretical activity there is in this important area. The overall conclusion that can be drawn from these various articles is that the interaction parameter that is extracted from Small Angle Neutron Scattering (SANS) data is not the simple χ_{FH} described in Equation 2.2, but is a function of both composition and molecular weight. However these more recent theories offer no new, straightforward method to analyse SANS data. For this work the most useful ideas have been those of Kumar[10] who has considered the effect of volume changes on mixing, and found that for 'repulsive' blends where there is a slightly unfavourable interaction, such as in the blends of a polymer with it's deuterated isomer, a small increase in volume is expected leading to slight increases in the effective χ parameter at the limits of the composition range. For 'attractive' blends, on the other hand, a small decrease in volume on mixing is expected and this leads to a downturn in the effective χ parameter at the limits of the composition range. Examples of 'attractive' blends would include poly (ethylene oxide) / poly (methyl methacrylate) and polystyrene / poly (vinyl methyl ether). These ideas are also incorporated in the compressible Random Phase Approximation of Tang and Freed[17].

Turning finally to the third assumption, that the segment distribution is Gaussian, this assumption is obeyed moderately well for polystyrene but for other polymers, such as poly (methyl methacrylate) it does breakdown, generally this occurs at intermediate and higher values of Q. A better prediction of the segment distribution and thus the single coil scattering of a polymer chain is obtained using the Rotational Isomeric State (RIS) model of Flory[18], again the problem is that this gives no simple analytic form for the single coil scattering function.

2.2 Surface Enrichment

Figure 2.5 shows a schematic phase diagram of a simple binary polymer blend, with components A and B. If we consider such a blend with a bulk composition corresponding to one of the coexisting phases, X for example, then under certain circumstances the other coexisting phase Y will be found to be preferentially absorbed at the 'walls' of the container in which the blend resides. The component with the lower surface energy will be expected to be found at the surface. Two sorts of wetting behaviour are expected: firstly the wetting layer may be thick, this will occur close to the critical point of unmixing and secondly as the blend is moved away from the critical point of unmixing along the coexistence curve a transition, W, to a much thinner 'partially' wet state will occur. The transition between these two states may be, in theory, first or second order. A precursor phenomena, often called 'prewetting', will sometimes be observed in the one phase region close to the coexistence curve. The type of transition that is observed and its location on the coexistence curve will be determined by the thermodynamics of the blend; the interactions between the component polymers and the relative strengths of their interactions with the container wall.

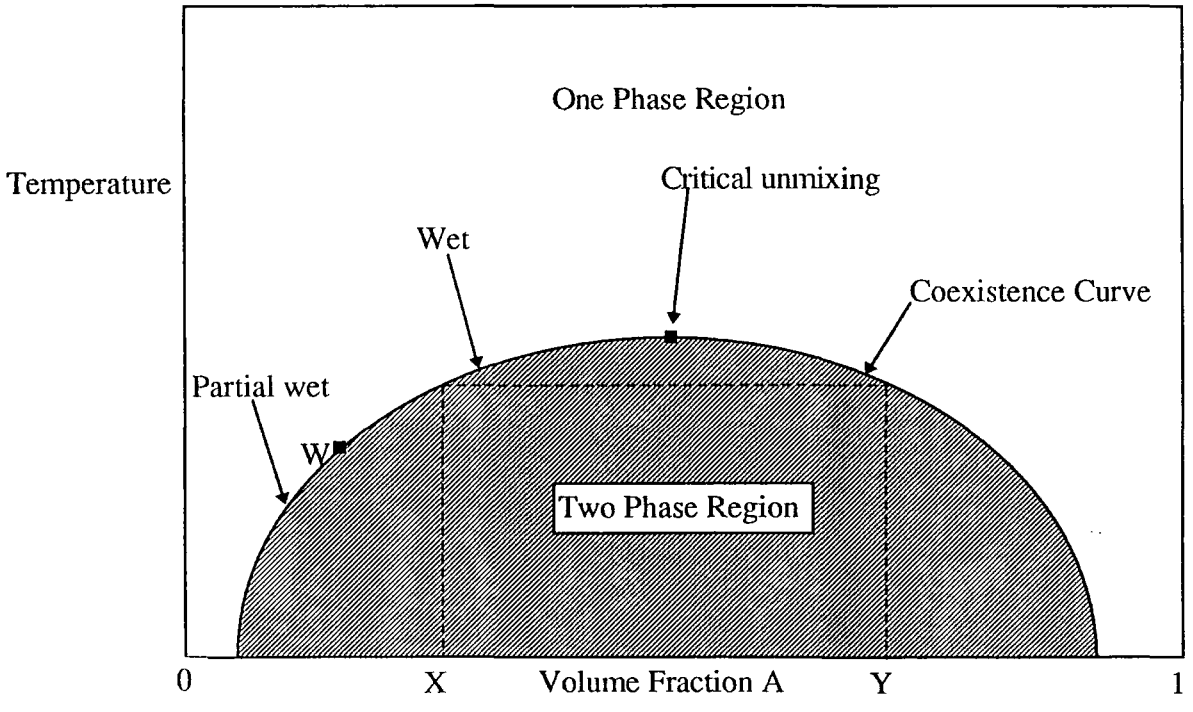

Figure 2.5: Phase diagram for a simple binary blend

The surface enrichment behaviour of a blend can be analysed by writing an expression for the free energy of the blend, incorporating contributions from the bulk, a surface energy contribution and a contribution accounting for the free energy cost of maintaining composition gradients in the blend. The general theory for blends was discussed by Cahn[19], a theory for polymers based on the Flory - Huggins lattice representation of the blend was presented by Nakanishi and Pincus[20] and Schmidt and Binder[21]. Subsequently Carmesin and Noolandi[22] have used an integral representation of the polymer blend in the same context. Jones and Kramer[23] have made approximations to the theory of Schmidt and Binder that allow some results to be obtained from simple analytical expressions. The main concern here is the shape of the near surface composition profile, the derivations presented here are drawn broadly from all the above references. The form of the transition between partial wet and wet state is not discussed here, the nature and location of this transition is discussed further by Jones[24].

The expression for the free energy of a two component polymer blend, on a simple cubic Flory - Huggins lattice, including a surface energy contribution is:

$$\frac{\Delta G}{k_B T} = f_s(\phi_{air}) + \int_0^\infty dz \left[\frac{\phi}{N_A} \ln\phi + \frac{(1-\phi)}{N_B} \ln(1-\phi) + \chi_{FH}\phi(1-\phi) - \Delta\mu\phi + \frac{a^2}{36\phi(1-\phi)} (\nabla\phi)^2 \right]$$

Equation 2.19

N_A ,N_B are the degrees of polymerisation of A and B respectively.

a is the statistical segment length.

ϕ is the volume fraction of component A

χ_{FH} is the Flory - Huggins interaction parameter.

$\Delta\mu$ is the exchange chemical potential evaluated at the bulk composition.

$f_s(\phi_{air})$ is the surface free energy contribution, the surface composition is ϕ_{air}.

This expression assumes a semi - infinite system with an interface located at z = 0, the final term in the expression is the contribution to the free energy from concentration gradients. This term is valid only in the long wavelength approximation:

$$a^2(\nabla\phi)^2 << \frac{1}{N}$$

Equation 2.20

where $N = N_A = N_B$. i.e. the concentration gradients in the bulk are not sharp. It is also assumed that the system is isotropic in the x-y plane, hence:

$$(\nabla\phi)^2 = \left(\frac{\partial\phi}{\partial z}\right)^2$$

Equation 2.21

In general it is assumed that the surface free energy contribution is localised at the surface as a δ - function and so only depends on the surface composition. This approximation makes the ensuing maths more manageable and is not unreasonable. Chen, Noolandi and Izzo[25] discuss the effect of a non-δ-function surface free energy. $f_S(\phi_{air})$, can be expressed as the first two terms of a Taylor series in ϕ_{air}:

$$f_s(\phi_{air1}) = -\mu_1\phi_{air} - \frac{1}{2}g\phi_{air}^2$$

Equation 2.22

μ_1 is related to the surface energy difference, $\Delta\gamma$, between components A and B:

$$\mu_1 = \frac{b^3}{k_B T}\Delta\gamma$$

Equation 2.23

Where b is the parameter of the Flory - Huggins lattice. g is known as the 'missing bond' term and is equal to $-\chi_{FH}b$. To find the composition profile within the blend we must minimise the free energy given by Equation 2.19 with respect to ϕ. Variational calculus shows that this free energy minimum is obtained when:

$$\frac{a^2}{36\phi(1-\phi)}\left(\frac{\partial\phi}{\partial z}\right)^2\Bigg|_{z'=0}^{z'=z} = \left[\frac{\phi}{N_A}\ln\phi + \frac{(1-\phi)}{N_B}\ln(1-\phi) + \chi_{FH}\phi(1-\phi) - \Delta\mu\phi\right]_{\phi_1}^{\phi(z)}$$

Equation 2.24

This is known as the 'phase portrait'. The boundary conditions at $z = 0$ and $z \rightarrow \infty$ are used to find ϕ_{air} and indicate which solutions of Equation 2.19 are acceptable and also

gives an indication as to what physical situation they represent. Using these boundary conditions Equation 2.24 becomes:

$$\mu_1 + g\phi_{air} = \pm\frac{a}{3}\left[\frac{\Delta G_m(\phi_{air},\chi_{FH}) - \Delta G_m(\phi_B,\chi_{FH}) - \Delta\mu(\phi_{air}-\phi_B)}{\phi_{air}(1-\phi_{air})}\right]^{1/2}$$

Equation 2.25

ϕ_B is the bulk volume fraction of component A (i.e. when $z\rightarrow\infty$). $\Delta G_m(\phi,\chi_{FH})$ is the Gibbs free energy per lattice site:

$$\Delta G_m(\phi,\chi_{FH}) = \frac{\phi}{N_A}\ln\phi + \frac{(1-\phi)}{N_B}\ln(1-\phi) + \chi_{FH}\phi(1-\phi)$$

Equation 2.26

By plotting both sides of Equation 2.25 together, as a function of ϕ_{air}, the crossing points give possible values of values ϕ_{air} and the areas bisected indicate the physical situation which will be observed. Figures 2.6 are examples of this type of plot, both figures represent a situation with a blend at the coexistence curve (i.e. $\Delta\mu = 0$ for a blend with $N_A = N_B$). $\phi^{a}_{air1}, \phi^{b}_{air}$ and ϕ^{c}_{air} are possible values for the surface volume fraction, in fact ϕ^{b}_{air} is at a <u>maximum</u> in the free energy and so is unstable. ϕ^{a}_{air} is the surface volume fraction in the partial wet case, i.e. the volume fraction decays directly from the surface, and ϕ^{c}_{air} is the surface volume fraction in the wet case, i.e. with a thick uniform layer at the surface. The solution which occurs, wet or partially wet, depends on the relative areas W and PW. If area PW is larger than area W then , the partial wet state, ϕ^{a}_{air} is the correct solution and if area W is larger than area PW then , the wet state, ϕ^{c}_{air} is the correct solution. So in this case Figure 2.6a represents a blend where complete wetting is occurring and Figure 2.6b partial wetting, in this illustration the transition is driven by a change in the surface energy difference. These diagrams can also be used to work out the location and type of transition between the wet and partial wet states.

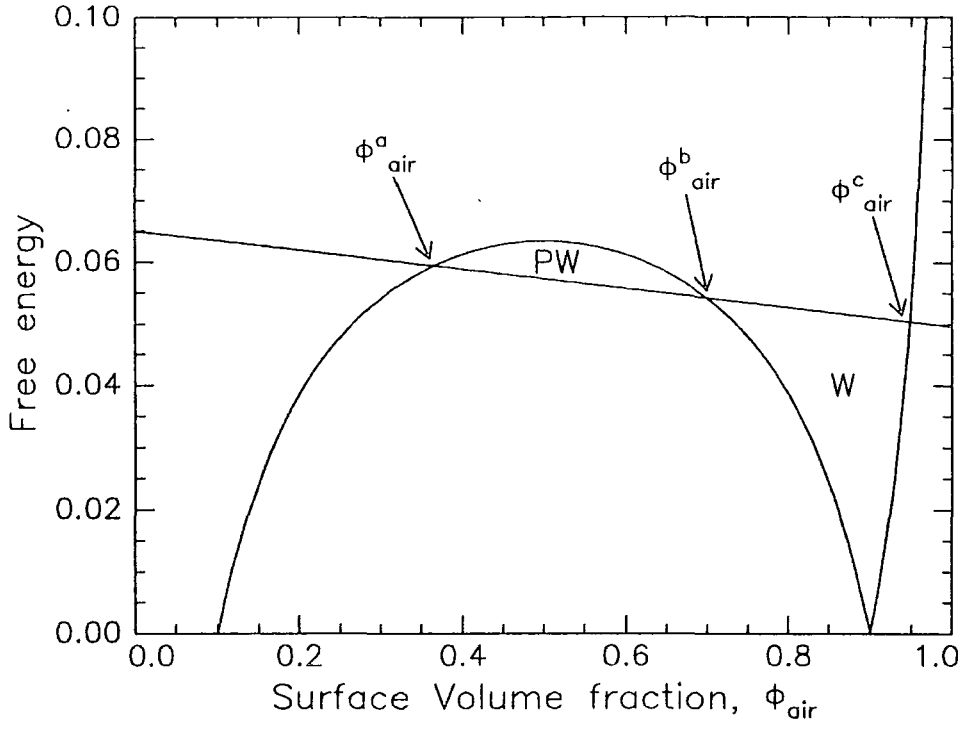

Figure 2.6a: Phase portrait for a blend on the coexistence curve exhibiting complete wetting, with surface volume fraction, ϕ^c_{air}.

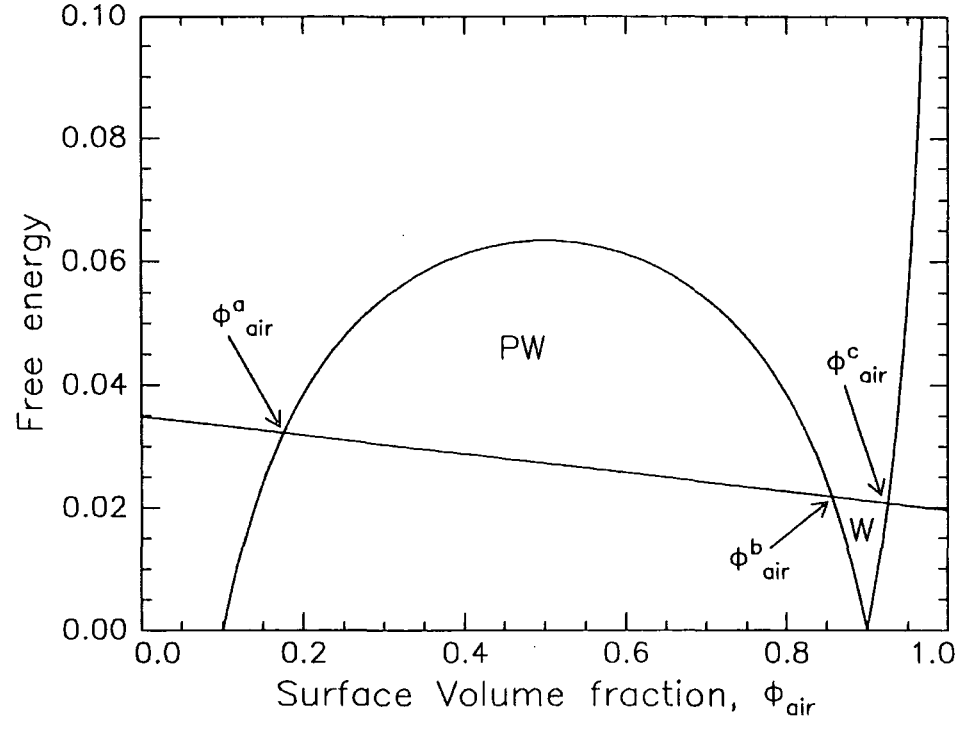

Figure 2.6b: Phase portrait for the same blend as above, in this instance exhibiting partial wetting, due to a reduction in the surface energy difference, surface volume fraction, ϕ^a_{air}.

The concentration profile at the surface can be found by rearranging and integrating Equation 2.24 to give:

$$z = \frac{a}{6}\int_{\phi_{air}}^{\phi(z)} \frac{d\phi}{\sqrt{\phi(1-\phi)[\Delta G_m(\phi,\chi_{FH}) - \Delta G_m(\phi_B,\chi_{FH}) - \Delta\mu(\phi-\phi_B)]}}$$

Equation 2.27

This expression shows that there is a 'master profile', determined by the bulk thermodynamics of the blend and this master profile is truncated at the appropriate point (the surface volume fraction, ϕ_{air}) to give the observed profile. For ϕ_{air} close to ϕ_B the profile is exponential in form, with a decay length equal to the correlation length of concentration fluctuations at the coexistence curve, ξ_{coex}:

$$\xi_{coex} = \frac{a}{6}\sqrt{2N}\left(1 - \frac{2\phi_B(1-\phi_B)\ln((1-\phi_B)/\phi_B)}{1-2\phi_B}\right)^{-1/2}$$

Equation 2.28

Figure 2.7 shows schematic composition versus depth profiles for the (a) wet state and the (b) partially wet state, note that the wet state has a plateau at the composition corresponding to the 'other side' of the coexistence curve, in a blend with $N_A = N_B$ this will be at $(1-\phi_B)$.

Jones and Kramer have simplified the mean field theory for blends with $N = N_A = N_B$, where $|\chi_{FH}|N$ is large and ϕ_B is not too close to 1 or 0. They introduce the variable χ_b, the interaction parameter at the coexistence curve:

$$\chi_b = \frac{1}{N(1-2\phi_B)}\ln\left(\frac{1-\phi_B}{\phi_B}\right)$$

Equation 2.29

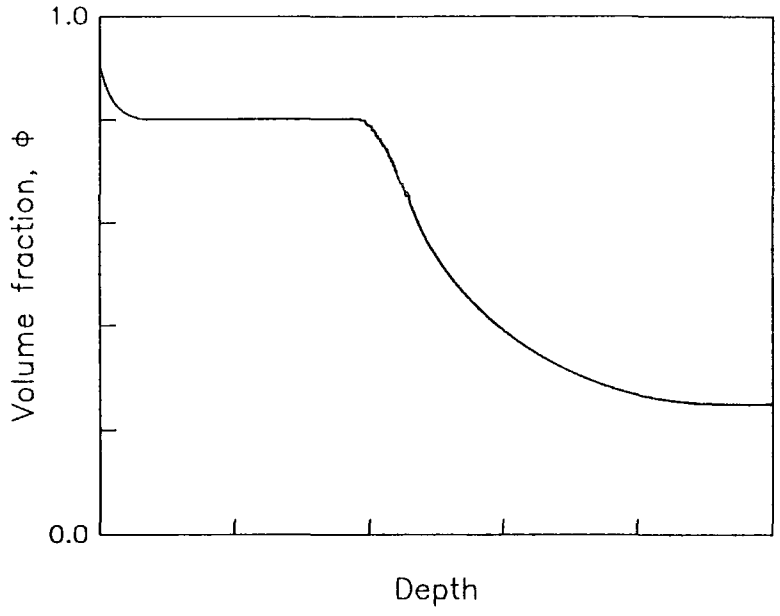

Figure 2.7a: A 'wet' profile, note that the plateau region is at volume fraction (1 - ϕ_B) for a symmetric blend and is of indeterminate thickness in the Schmidt and Binder formulation.

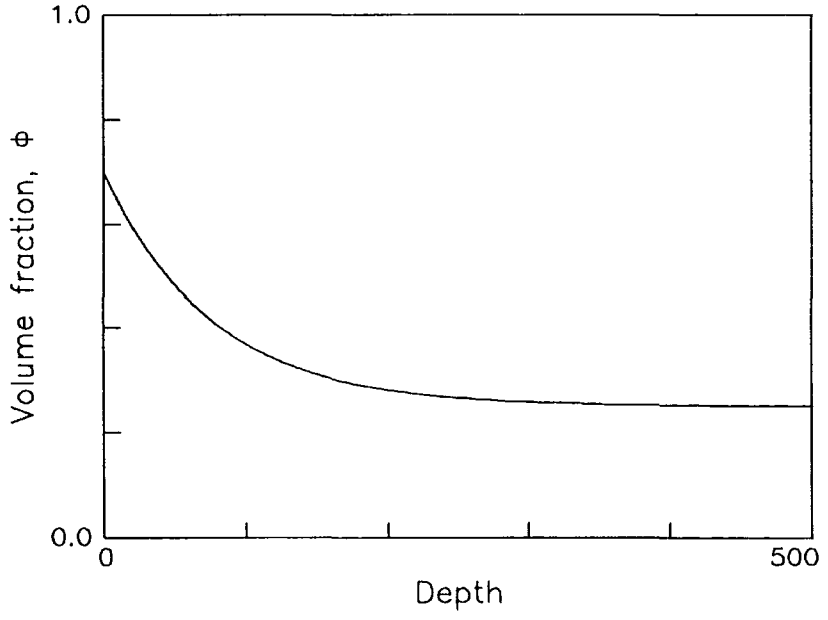

Figure 2.7b: A 'partial wet' profile, note that the surface volume fraction is less than (1 - ϕ_B) for a symmetric blend, the length scale of the decay is of the order of the radius of gyration of the enriching polymer.

The surface volume fraction for the wetting profile is given by:

$$\phi_{air} = \frac{\phi_B + t}{1+t}$$

Equation 2.30

where the parameter, t, is given by:

$$t = 9\left(\frac{\mu_1}{a}\right)^2 \frac{1}{(\chi_b - \chi_{FH})}$$

Equation 2.31

and the composition profile is obtained from the expression:

$$z = \frac{a}{6}\int_{\phi_B}^{\phi(z)} \frac{d\phi}{\sqrt{\phi(1-\phi)(\chi_b - \chi_{FH})(\phi - \phi_B)^2}}$$

Equation 2.32

In addition to these models based on the theory of Cahn, there are also self consistent field theories[26,27] and Monte Carlo simulations[28,29,30]. (It is possible to use the LAYERS program, used in section 2.3.1 to do self consistent field calculations for surface enrichment.)

There is good agreement between Monte Carlo models and the mean field theory, the small deviations observed can be attributed to the effect of finite compressibility and distortion of polymer chains at the surface from the ideal Gaussian chain segment distribution, the mean field takes no account of these effects.

The self consistent field theory of Hariharan *et al*[26] has been used to study the effects of chain length disparity ($N_A \neq N_B$), a small entropic effect is observed, whereby the shorter chains are found preferentially at the surface in the absence of a surface energy difference. For long chains this amounts to a surface composition different from the bulk by only 1% or so.

2.3 Polymer Brushes

A polymer brush is formed when polymer chains 'end absorb' to an interface, this 'brush' may significantly alter the properties of the interface. Commonly such brushes have been considered in the context of polymers in solution end absorbing onto some substrate, in this work the interest is in two component polymer blends where one component has a low surface energy end group and that is intended to form brushes at the blend / air interface. These two different situations are known as 'wet' brushes, where the polymer is in solution (or the molecular weight of the matrix polymer is less than that of the brush polymer), and 'dry' brushes, where the 'solvent' is another polymer (with molecular weight higher than that of the brush forming polymer). Two theoretical methods of treating brushes are considered; a self consistent field (SCF) theory developed by Shull[31,32], based on the mean field ideas originating from Edwards[33] and the self consistent field methods of Scheutjens and Fleer[34] and a scaling theory developed by de Gennes[35].

2.3.1 Self Consistent Field Theory

All the models presented here were obtained using the program LAYERS, written by K.R. Shull.

We will consider a two component polymer blend with components A, a homopolymer with degree of polymerisation N_A and component B a polymer with degree of polymerisation N_B and a surface active group at one end. The discussion here concentrates on a component B with only one surface active end group, for clarity, however the modifications for a surface active end group at each end are relatively straight forward and have been included in the program LAYERS. The blend is characterised by a Flory - Huggins interaction parameter, χ_{FH}.

This binary blend exists on a Flory - Huggins like cubic lattice with an impenetrable interface at $x = 0$, x is the number of lattice layers from this impenetrable surface. For the purposes of the calculations in this work the number of layers, x_n, in the lattice is not important so long as the brush has reached bulk composition well before (i.e. 5-10 layers) the far edge of the lattice is reached.

The interaction of the surface active end is characterised by two parameters, χ^b_e is the interaction of the ends with the bulk of the blend and χ^s_e is the interaction of the ends with the surface, so the ends may be found at the surface because they have been 'expelled' by the bulk or because they feel an attraction to the surface. It is the difference χ^b_e-χ^s_e that determines the number of B ends absorbed at the surface.

The quantities of interest are the volume fractions of components A and B as a function of x, $\phi_A(x)$ and $\phi_B(x)$. These values are calculated from the distribution functions $q_A(x,j)$, $q_{B1}(x,j)$ and $q_{B2}(x,j)$. $q_k(x,j)$ is the probability that a chain has reached position x, after j steps along its length from end k. Two functions are required to describe the B component because the two ends of the B chains are distinct - one end has a surface active group ($q_{B1}(x,j)$) and the other does not ($q_{B2}(x,j)$). The volume fractions are calculated from the $q_k(x,j)$ thus:

$$\phi_A(x) = A_A \int_0^{N_A} q_A(x,j) q_A(x, N_A - j) dj$$

Equation 2.33

$$\phi_B(x) = A_B \int_0^{N_B} q_{B1}(x,j) q_{B2}(x,j) dj$$

Equation 2.34

A_k are normalisation constants. The distribution functions $q_k(x,j)$ are analogous to concentration, in a modified diffusion equation:

$$\frac{\partial q_k(x,j)}{\partial j} = \frac{a^2}{6} \frac{\partial^2 q_k(x,j)}{\partial x^2} - \frac{w_k(x)}{k_B T} q_k(x,j)$$

Equation 2.35

$w_k(x)$ is a mean field acting on the polymer segments, arising from the neighbouring segments. In fact Equation 2.35 is based on a continuous form for $q_k(x,j)$

and not the discrete form implied by the lattice on which the polymers are placed. The discrete form for Equation 2.35 is given by the following recursion relations:

$$q_A(x,j) = \left\{\frac{1}{6}q_A(x-1,j-1) + \frac{2}{3}q_A(x,j-1) + \frac{1}{6}q_A(x+1,j-1)\right\}\exp\left(\frac{-w_A(x)}{k_BT}\right)$$

$$q_{B1}(x,j) = \left\{\frac{1}{6}q_{B1}(x-1,j-1) + \frac{2}{3}q_{B1}(x,j-1) + \frac{1}{6}q_{B1}(x+1,j-1)\right\}\exp\left(\frac{-w_B(x)}{k_BT}\right)$$

$$q_{B2}(x,j) = \left\{\frac{1}{6}q_{B2}(x-1,j-1) + \frac{2}{3}q_{B2}(x,j-1) + \frac{1}{6}q_{B2}(x+1,j-1)\right\}\exp\left(\frac{-w_B(x)}{k_BT}\right)$$

Equation 2.36

The terms in $q_k(x,j)$ occur by virtue of the chain connectivity, each chain segment has six nearest neighbours one each in the layers x-1 and x+1 and four in the layer x and the probability $q_k(x,j)$ depends on the probabilities of the previous segment, j-1, being in any of the neighbouring cells. The exponential is a Boltzmann distribution function, evaluating the probability of finding a polymer segment in a state with energy $w_k(x)$, from the mean field. The only unknowns in this set of equations are the mean fields, since all the values $q_k(x,j)$ can be calculated using the following initial conditions:

$$\left.\begin{aligned} q_A(x,0) &= 1 \\ q_{B1}(x,0) &= 1 \\ q_{B2}(x,0) &= 1 \end{aligned}\right\} x = 1 \rightarrow x_n$$

Equation 2.37

$$\left.\begin{aligned} q_A(0,j) &= 0, \quad q_A(n+1,j) = 0 \\ q_{B1}(0,j) &= 0, \quad q_{B1}(n+1,j) = 0 \\ q_{B2}(0,j) &= 0, \quad q_{B2}(n+1,j) = 0 \end{aligned}\right\} j = 0 \rightarrow \max(N_A, N_B)$$

Equation 2.38

Equation 2.37 is a 'book-keeping' boundary condition, so that the chain connectivity of the end groups is accounted for properly. Equation 2.38 expresses the

fact that no chain segments lie beyond the polymer layer, they are a confinement condition. In addition the following conditions apply for first segments in the bulk of the lattice i.e. not in layer 1:

$$\left.\begin{aligned} q_A(x,1) &= \exp\left(\frac{-w_A(x)}{k_B T}\right) \\ q_{B1}(x,1) &= \exp\left(-\chi_c^b - \frac{w_B(x)}{k_B T}\right) \\ q_{B2}(x,1) &= \exp\left(\frac{-w_B(x)}{k_B T}\right) \end{aligned}\right\} x = 2 \rightarrow x_n$$

Equation 2.39

Finally there are the conditions for first segments in the surface layer:

$$\left.\begin{aligned} q_A(x,1) &= \exp\left(\frac{-w_A(x)}{k_B T}\right) \\ q_{B1}(x,1) &= \exp\left(-\chi_c^s - \frac{w_B(x)}{k_B T}\right) \\ q_{B2}(x,1) &= \exp\left(\frac{-w_B(x)}{k_B T}\right) \end{aligned}\right\} x = 1$$

Equation 2.40

The mean fields $w_A(x)$ and $w_B(x)$ can be divided in two parts:

$$w_A(x) = w_A^o(x) - w'(x)$$
$$w_B(x) = w_B^o(x) - w'(x)$$

Equation 2.41

The difference between these mean fields lies solely in the $w_k^o(x)$ parts which are given by:

$$w_A^o(x) = \chi_{FH}\phi_B^2(x)$$
$$w_B^o(x) = \chi_{FH}\phi_A^2(x) - w_{ext}(x)$$

Equation 2.42

The term $w_{ext}(x)$ is a field that acts equally on all B segments not arising from A-B interactions, for 'pure' brushes this term is zero but it can be used to include a preferential attraction to the interface of A or B segments. This allows us to study both surface enrichment where composition gradients are driven by differences between the surface energies of the chain segments and brushes where composition gradients are driven by end absorption, in addition it is also possible to consider combinations of these effects.

$w'(x)$ is given by:

$$w'(x) = \zeta(1 - \phi_A(x) - \phi_B(x)) + \frac{\phi_A^{bulk}}{N_A} + \frac{\phi_B^{bulk}}{N_B}$$

Equation 2.43

ζ is inversely proportional to the bulk compressibility and ϕ_A^{bulk} and ϕ_B^{bulk} are the bulk volume fractions of components A and B respectively. The procedure to calculate the equilibrium volume fraction profile is firstly to calculate volume fractions $\phi_A(x)$ and $\phi_B(x)$ using an initial estimate for the mean fields based on the assumed bulk volume fractions, $w_k(x)$. These calculated volume fractions are used to determine a new set of 'image' mean fields, $w_{kI}(x)$. New values for the mean fields are calculated from a linear combination of $w_k(x)$ and $w_{kI}(x)$, this procedure is repeated until some convergence criteria is met.

The preceding section outlined the details of the mechanics of the self consistent field theory calculations. Some results will now be discussed, there are a number of factors influencing the size and shape of the near surface composition profile these are:

(a) The value of $(\chi_e^b - \chi_e^s)$, this is the enthalpic contribution to the end attachment free energy, larger values will result in larger values of the surface excess.

(b) N_B and the ratio N_A/N_B, smaller values of N_B will enhance brush formation since the entropic cost of confining the end of a shorter chain to the interface is smaller than that for longer chains. Larger ratios of N_A/N_B will also enhance brush formation.

(c) χ_{FH}, the Flory - Huggins interaction parameter, all the modelling work done here was in the one phase region of the phase diagram. Brush formation is enhanced in blends that lie closer to the coexistence curve, i.e. with small positive values of χ_{FH}.

(d) The bulk volume fraction, ϕ_B ($\equiv \phi_B^{bulk}$), of the brush forming polymer.

Figure 2.8 illustrates some typical composition versus depth profiles. The data here are shown versus lattice layer, but the depth z is often normalised by the radius of gyration, R_g, of the brush forming polymer, as part of the procedure used to relate results obtained theoretically, which for computational tractability are done on polymers with relatively small values of N_A and N_B, to the experimental data.

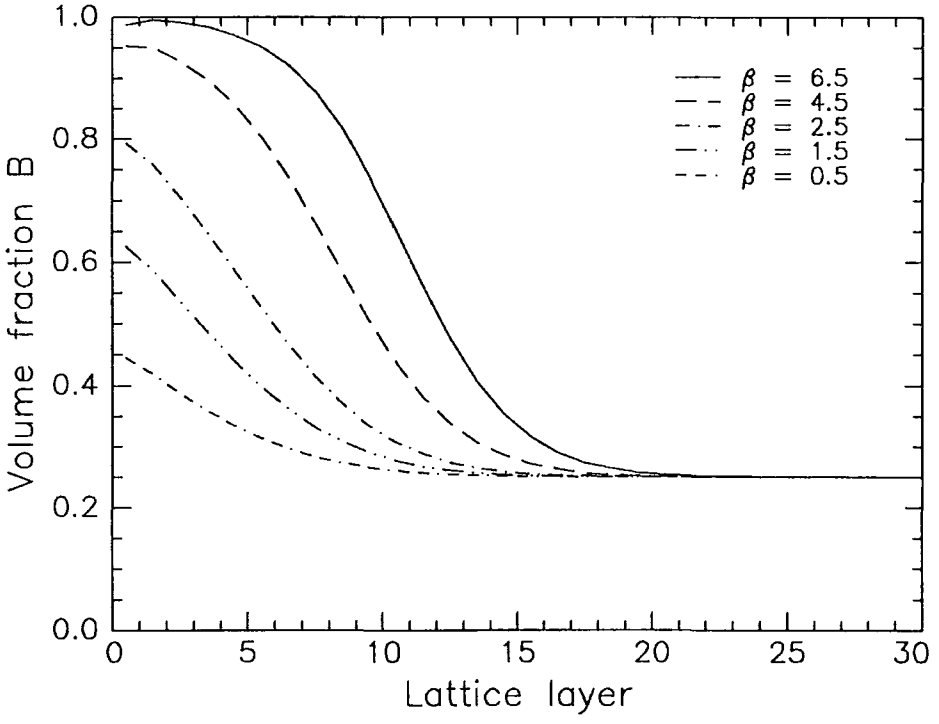

Figure 2.8 Example brush profiles for a series of model blends with $N_A = N_B = 100$, $\phi_B = 0.25$ and $\chi = 0$, the free energy of end attachment, β, is defined in Equation 2.44.

Throughout this work two parameters will be used to characterise the shape of the composition profiles - these are the normalised surface excess z^*/R_g and the difference between the surface, ϕ_{air}, and bulk, ϕ_B, composition (ϕ_{air} - ϕ_B). Figure 2.9 shows a plot of (ϕ_{air} - ϕ_B) vs z^*/R_g for two series of calculations, firstly where ϕ_B is fixed and the enthalpic attachment energy increased (leading to an increasing z^*/R_g) and secondly where the enthalpic attachment energy is fixed and ϕ_B is increased (similarly leading to an increasing z^*/R_g), for small values of z^*/R_g the two curves overlay but at higher values the data with varying ϕ_B 'curl over'. This is because the excess is constrained to be zero when ϕ_B is one, so there must be a maximum in z^*/R_g with respect to ϕ_B, this is illustrated in Figure 2.10.

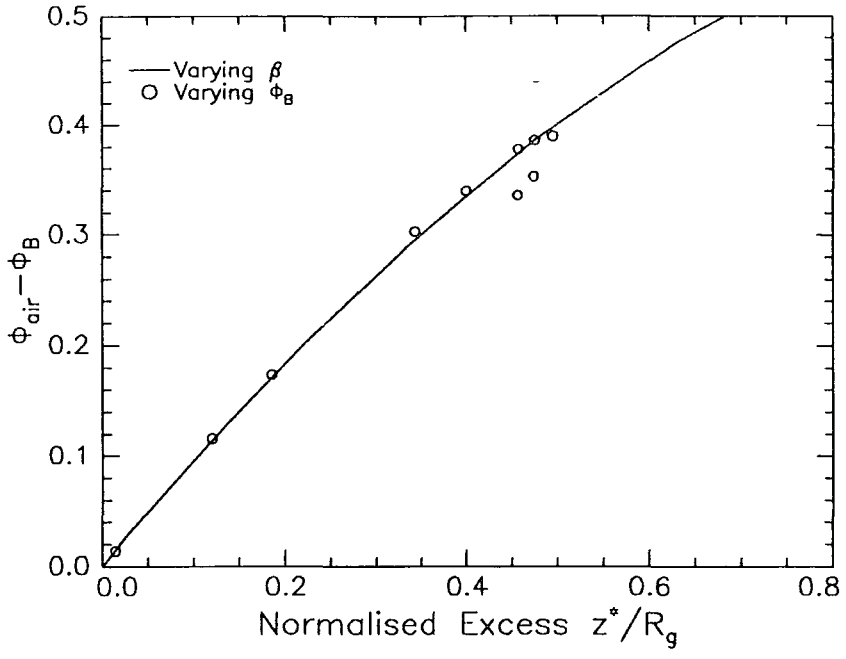

Figure 2.9: (ϕ_{air} - ϕ_B) **versus normalised excess for two series of blends: (1) the excess is increased by increasing the attachment free energy and (2) the excess is increased by increasing the bulk volume fraction of the absorbing polymer.**

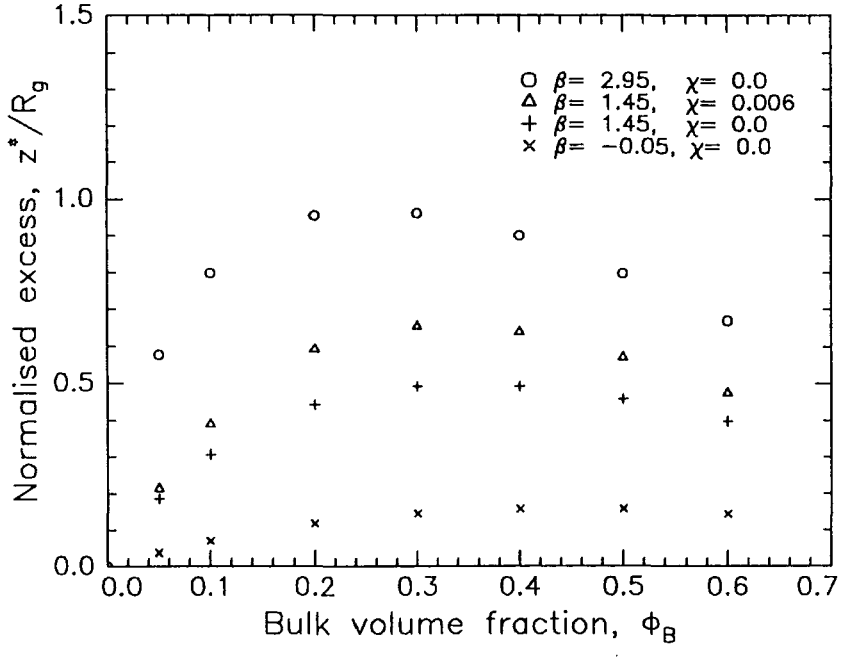

Figure 2.10: Normalised excess, z^*/R_g, versus ϕ_B showing the maximum in z^*/R_g which arises at intermediate ϕ_B. Brush formation occurs at $\beta < 0$, stabilised by entropy of mixing in the plane of the surface.

Shull concentrates mainly on the behaviour of strongly absorbed polymer brushes with a bulk volume fraction of the absorbing polymer, ϕ_B, of zero and with generally large ratios of N_A/N_B. In this work the interest is in systems where the absorption is generally weak, ϕ_B ranges from ~0.05 to ~0.5 and N_A/N_B is close to 1. However the general comments of Shull will apply to these systems, the brush formation behaviour of blends can be more readily described in terms of two reduced parameters, the intention is that blends with the same values for these parameters will have the same near surface composition profiles. These parameters are the free energy of end attachment, β:

$$\beta = (\chi_e^b - \chi_e^s) + 1.1 \ln \frac{\delta_s}{R_g}$$

Equation 2.44

and the modified chemical potential function, $\bar{\mu}_b$:

$$\frac{\bar{\mu}_b}{k_B T} = \ln \phi_B + (1-\phi_B)\left(1 - \frac{N_B}{N_A}\right) + N_B \chi_{FH} (1-\phi_B)^2 + \beta$$

Equation 2.45

Turning first to the β parameter, which incorporates the enthalpic driving force (χ_e^b - χ_e^s) and an entropic term (1.1ln ($\delta s/R_g$)), where δ_s is the thickness of the surface region to which absorbing end groups are localised. In this work it has been assumed that δ_s = a (the lattice dimension) this means that δ_s/R_g can be replaced by $\sqrt{(6/N_B)}$ since assuming Gaussian chain statistics R_g = a $\sqrt{(N_B/6)}$. Back calculating δ_s from the discrepancy between β measured and β estimated from literature values in Section 7 implies a value of δ_s = 6.1Å. However this figure should be treated with some scepticism - granted it is of the order of magnitude that is expected, but the estimated β is obtained from solubility parameters and surface energy differences for which the values used are a little crude. β does not account for chain length disparity (N_A/N_B) or thermodynamic effects (ϕ_B and χ_{FH}), so to compare theoretical results with experimental data the same conditions of ϕ_B, N_A/N_B, and χ_{FH} should be used in both experiment and theoretical calculations.

$\bar{\mu}_b$ should in principle, allow for these further effects, however in practice this is only true in the strong absorption limit for small values of ϕ_B. Figure 2.11 shows z^*/R_g

versus ($\bar{\mu}_b/k_BT$) for this case (the solid line) with N_A/N_B = 8 along with points calculated for a host of models with various ϕ_B and χ_{FH} and values of N_A/N_B in the range 1 to 2. These points generally lie above the line for N_A/N_B = 8, particularly around $\bar{\mu}_b$ = 0, the points lying below the line for $\bar{\mu}_b$ > 0 correspond to profiles where the bulk volume fraction is above the value where z^*/R_g reaches a maximum. These deviations mean that the $\bar{\mu}_b$ is rather less useful in this work than the simpler β parameter.

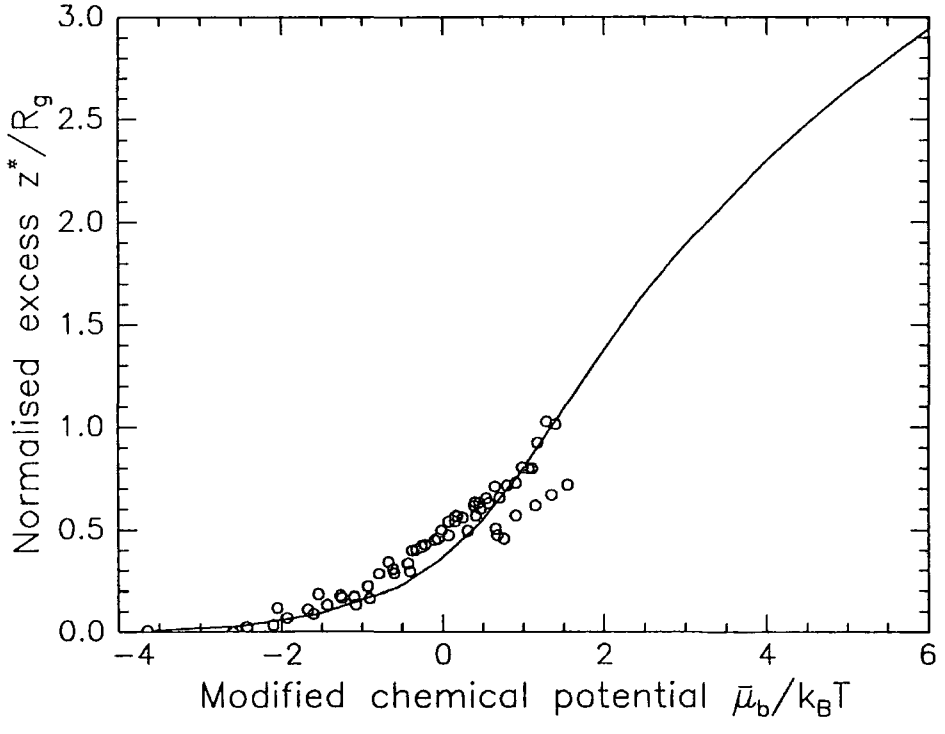

Figure 2.11: Plot of normalised excess, z^*/R_g, versus modified chemical potential for data from Shull (with N_A/N_B) and a range of data calculated for this work.

2.3.2 Scaling Theory

The basics of the scaling theory of polymer brushes will be introduced, however this must be done with the understanding that the results will only give, at best, a feel for the underlying behaviour of the brushes observed in this work. The reason for this is that scaling theory is not able to account properly for the entropy of mixing between the brush forming polymer N_B with the matrix polymer N_A, when $N_A > N_B$. Additionally it is assumed in scaling theory that the brush composition depth profile is a step function, self consistent field theories[36] and Monte Carlo studies[37,38] show that this is not the case.

This outline of scaling theory draws on the paper by de Gennes[35], who considers the end absorption of polymers with N_B repeat units to a solid surface, in a solution of 'mobile' polymers with N_A repeat units. So the system consists of absorbed polymers, mobile polymers and a solvent, in de Gennes paper the mobile polymers are referred to as P, rather than N_A. The notation used here is to remain consistent with the preceding section on self consistent field theory. The important parameters in the scaling theory are the dimensionless grafting density, σ, and the volume fraction of mobile chains, ϕ. The size of the lattice cell is a and the height of the grafted brush is L. A further parameter, D_G, the distance between graft points is also defined:

$$D_G = \frac{a}{\sqrt{\sigma}}$$

Equation 2.46

The results of de Gennes are summarised in Figure 2.12. This figure shows where stretching of the grafted chains from their unperturbed dimensions occurs (US - unstretched, WS - weakly stretched and SS - strongly stretched) and where mixing between the grafted chains and the mobile chains is predicted (M - mixed and UM - unmixed). The extreme left of this diagram ($\phi = 0$) corresponds to a grafted polymer in a pure solvent with no mobile chains.

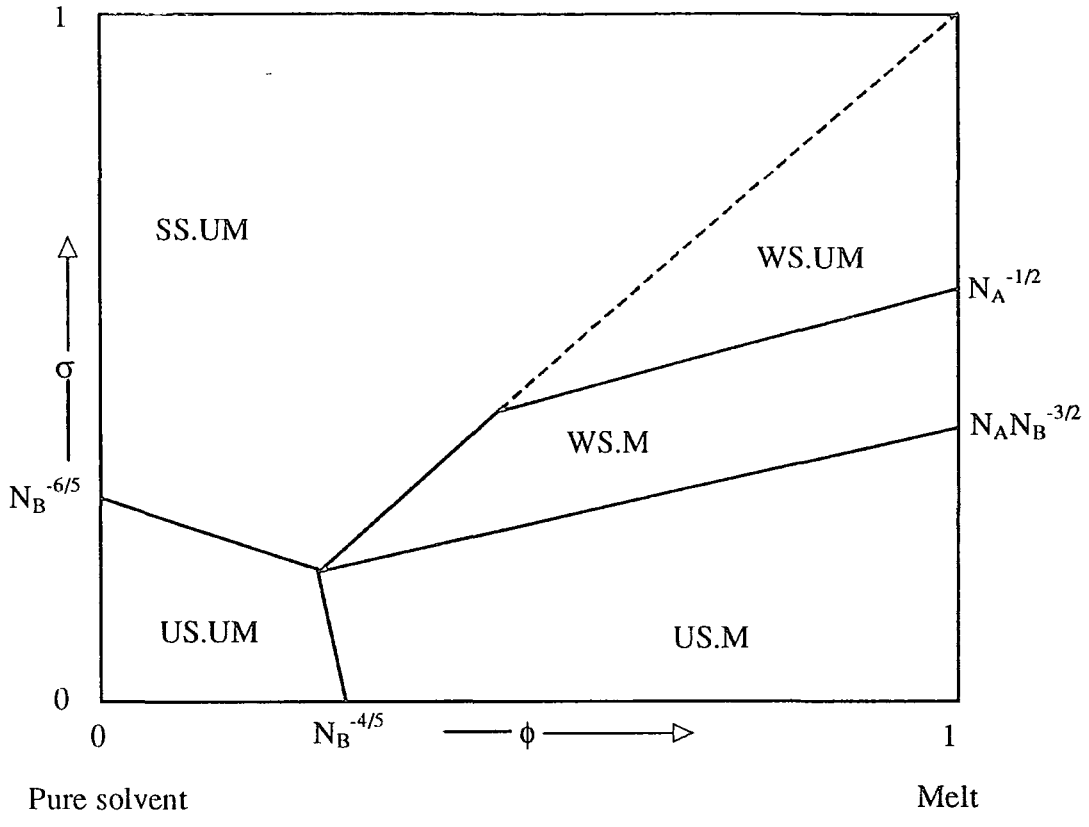

Figure 2.12: Schematic representation of de Gennes scaling results for brushes (from reference 35).

There are two regimes predicted in this case, the unstretched regime where chains are grafted sufficiently far apart that they do not overlap, it can be shown that this is when $\sigma < N_B^{-6/5}$. In this situation the brush height, $L \approx N_B^{3/5}a$, the dimensions of a chain in a good solvent. When the grafted chains overlap they are stretched out away from the surface and the brush height is found to scale as:

$$L \approx N_B a \sigma^{1/3}$$

Equation 2.47

Both of these chains are denoted UM because there are no mobile chains to mix with!

The polymer melt case appears on the far right of Figure 2.12, where $\phi = 1$. The behaviour in this case is slightly more complex, again at the lowest grafting densities chains do not penetrate and so as long as $N_A > N_B^{1/2}$ they have ideal dimensions and the length of the brush will be given by $L \approx N_B^{1/2}a$. Clearly the mobile chains can easily penetrate this brush. The cross over to the stretched regime is different to that for the

polymer - pure solvent system, as the grafting density increases the absorbed chains will start to overlap, however initially they will not be stretched because the penetration of the mobile chains screens interactions between the grafted chains. It can be shown that stretching of the grafted chains starts to occur when:

$$\sigma = N_A N_B^{-3/2}$$

Equation 2.48

At this point the grafted layer is still mixed with the mobile chains. The final regime is reached when mobile chains are expelled from the grafted layer, ultimately as the graft density reaches one the brush length will be $L \approx aN_B$. The cross over to the regime where this occurs is when:

$$\sigma = N_A^{-1/2}$$

Equation 2.49

For $N_A = N_B$ the stretched mixed regime (WS.M) will not exist since $N_A N_B^{-3/2} = N_A^{-1/2}$. The free energy of the grafted brush in the melt can be calculated by summing the free energy of mixing ΔG_m and the elastic energy ΔG_{el} of the brush, (the equations used here are those of Brown[39], which include a non-zero interaction parameter, χ_{FH}). The free energy of mixing term is given by:

$$\frac{\Delta G_m}{k_B T} = \left(\frac{LD_G^2}{a^3 N_A}\right)\phi_A \ln\phi_A + \chi_{FH} N_B \phi_A$$

Equation 2.50

and the elastic energy is given by:

$$\frac{\Delta G_{el}}{k_B T} = \left(\frac{L^2}{R_o^2} + \frac{R_o^2}{L^2}\right)$$

Equation 2.51

(where $R_o = N_B^{1/2} a$)

Minimising $\Delta G_m + \Delta G_{el}$ with respect to the volume fraction of N_B in the brush, ϕ_B, gives Equation 2.52 below. (In the context of the scaling theory the composition of the brush is uniform)

$$\phi_B \ln(1-\phi_B) + \phi_B^2 + \chi_{FH}\phi_B^3 N_A = -2N_A\sigma^2\left[1-\left(\frac{\phi_B^2}{N_B\sigma^2}\right)^2\right]$$

Equation 2.52

This relates the volume fraction of the grafted polymer in the brush, ϕ_B, to the parameters σ, N_B, N_A and χ_{FH}. The brush height is given by:

$$L = \frac{N_B a^3}{D_G^2 \phi_B}$$

Equation 2.53

These expressions fail for $N_A > N_B$, because the expression for ΔG_m is no longer accurate. The remainder of Figure 2.12 represents the semidilute regime where there is absorbed polymer, mobile polymer and solvent present, de Gennes discusses the behaviour in this region in some detail.

2.4 References to Section 2

1 . P.J. Flory, 'Principles of Polymer Chemistry', Cornell University Press, 1953.

2 . P.G. de Gennes, 'Scaling Concepts in Polymer Physics', Cornell University Press, 1979.

3 . P. Debye, *Journal of Physical Colloid Chemistry*, 51, **1947**, 18.

4 . M. Shibayama, H. Yang, R.S. Stein, C.C. Han, *Macromolecules*, 18, **1985**, 2179.

5 . S. Sakurai, H. Hasegawa, T. Hashimoto, I. Glen Hargis, S.L. Aggarwai, C.C. Han, *Macromolecules*, 23, **1990**, 451.

6 . M.G. Bawendi, K.F. Freed, *Journal of Chemical Physics*, 88(4), **1988**, 2741.

7 . G. Beaucage, R.S. Stein, R. Koningsveld, *Macromolecules*, 26, **1993**, 1603.

8 . M. Muthukumar, *Journal of Chemical Physics*, 85(8), **1986**, 4722.

9 . J. Dudowicz, K.F. Freed, *Macromolecules*, 24, **1991**, 5074.

10 . S.K. Kumar, *Macromolecules*, 27, **1994**, 260.

11 . A. Sariban, K. Binder, *Macromolecules*, 21, **1988**, 711.

12 . A. Yethiraj, K.S. Schweizer, *Journal of Chemical Physics*, 98(11), **1993**, 9080.

13 . H.M. Sevian, P.K. Brazhnik, J.E.G. Lipson, *Journal of Chemical Physics*, 99(5), **1993**, 4112.

14 . I.C. Sanchez, R.H. Lacombe, *Macromolecules*, 11, **1978**, 1145.

15 . K. Binder, *Advances in Polymer Science*, 112, **1994**, 181.

16 . Y. Cui, M.D. Donohue, *Macromolecules*, 25, **1992**, 6489.

17 . H. Tang, K.F. Freed, *Macromolecules*, 24, **1991**, 958.

18 . D.Y. Yoon, P.J. Flory, *Macromolecules*, 9, **1976**, 299.

19 . J.W. Cahn, *Journal of Chemical Physics*, 66(8), **1977**, 3667.

20 . H. Nakanishi, P. Pincus, *Journal of Chemical Physics*, 79(2), **1983**, 997.

21 . I. Schmidt, K. Binder, *Journal de Physique*, 46, **1985**, 1631.

22 . I. Carmesin, J. Noolandi, *Macromolecules*, 22, **1989**, 1689.

23 . R.A.L. Jones, E.J. Kramer, *Polymer*, 34(1), **1993**, 115.

24 . R.A.L. Jones, *Polymer*, 35(10), **1994**, 2160.

25 . Z. Y. Chen, J. Noolandi, D. Izzo, *Physical Review Letters*, 66(6), **1991**, 727.

26 . A. Hariharan, S.K. Kumar, T.P. Russell, *Macromolecules*, 24, **1991**, 4909.

27 . A. Hariharan, S.K. Kumar, T.P. Russell, *Macromolecules*, 23, **1990**, 3584.

28 . P. Cifra, F.E. Karasz, W.J. MacKnight, *Macromolecules*, 25, **1992**, 3895.

29 . J.-S. Wang, K. Binder, *Journal of Chemical Physics*, 94(12), 1991, 8537.

30 . P. Cifra, F. Bruder, R. Brenn, *Journal of Chemical Physics*, 99(5), 1993, 4121.

31 . K.R. Shull, *Journal of Chemical Physics*, 94(8), 1991, 5723.

32 . K.R. Shull, E.J. Kramer, *Macromolecules*, 23, 1990, 4769.

33 . S.F. Edwards, *Proceedings of the Physical Society*, 85, 1965, 613.

34 . J.M.H.M. Scheutjens, G.J. Fleer, *Journal of Physical Chemistry*, 84, 1980, 178.

35 . P.G. de Gennes, *Macromolecules*, 13, 1980, 1069.

36 . S.T. Milner, T.A. Witten, M.E. Cates, *Macromolecules*, 21, 1988, 2610.

37 . P-Y. Lai, K. Binder, *Journal of Chemical Physics*, 97, 1992, 586.

38 . T. Cosgrove, T. Heath, B. van Lent, F. Leermakers, J. Scheutjens, *Macromolecules*, 20, 1987, 1692.

39 . H.R. Brown, K. Char, V.R. Deline, *Macromolecules*, 23, 1990, 3385.

This page left intentionally blank

3. Techniques

3.1 Neutron Techniques

All the neutron scattering (small angle and reflectivity) done in this work was carried out at the Rutherford Appleton Laboratory, Chilton. At this source neutrons are produced by 'spallation'. Protons are accelerated to high energies (~800MeV) in a synchrotron and then fired at a tantalum or uranium target, neutrons are 'chipped off' or 'spalled' from the target nuclei, the yield is around 25-30 per incident proton. Initially the neutrons have a high energy (~40MeV), but they are passed through a moderator where they are thermalised by repeated collisions to give a Maxwell - Boltzmann distribution of energies. For this work a liquid hydrogen moderator is used which is at a temperature of 22K. The most probable neutron energy, E_{max}, in the Maxwell - Boltzmann distribution is given by:

$$E_{\max} = \frac{3}{2} k_B T$$

Equation 3.1

Where k_B is the Boltzmann constant and T is the absolute temperature. The velocity of neutrons with such energy is given by:

$$v_{\max} = \left(\frac{2E_{\max}}{m_n} \right)^{1/2}$$

Equation 3.2

where m_n is the neutron mass (= 1.7×10^{-27} kg). For the 22K hydrogen moderator this corresponds to a velocity of ~740 m s^{-1}, the wavelength of a particle / wave such as the neutron, with velocity, v, is given by the de Broglie relationship:

$$\lambda = \frac{h}{m_n v}$$

Equation 3.3

where h is Planck's constant. For the most probable energy in the distribution from the hydrogen moderator this wavelength is ~5.4Å. The finite velocity of the neutron, which determines its wavelength, leads to the manner in which neutrons of different wavelength are discriminated at the Rutherford Appleton Laboratory. The proton beam does not bombard the target continuously, instead very short pulses are used at a rate of 50Hz. This means that bunches of neutrons leave the target at known times, they then travel through the experiment and are detected. Shorter wavelength neutrons travel faster than longer wavelength neutrons and so the first neutrons to arrive at the detector from any pulse of neutrons are those of shortest wavelength, i.e. wavelengths are determined by time of flight.

A particular wavelength range can be selected by the use of a 'chopper', a chopper is a disc of material (fairly) opaque to neutrons (see Figure 3.1) that has a segment cut out of it. This disk rotates at 50Hz and is synchronised with the arrival of the proton pulse at the target such that when neutrons of the correct velocity arrive the segment cut out of the disk is in the path of neutron beam, other neutrons with the wrong velocity, miss the gap and are stopped.

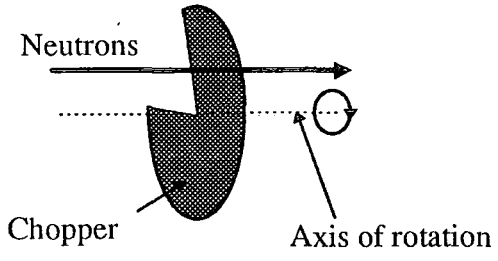

Figure 3.1: Schematic diagram of a disk chopper, allowing the passage of desirable neutrons.

A general review of the various experiments that can be performed on polymers using neutrons is by Higgins and Benoit[1].

3.1.1 Small Angle Neutron Scattering (SANS)

The aim of a small angle neutron scattering experiment is to measure the 'normalised' flux of neutrons scattered through scattering vectors Q (= $(4\pi/\lambda)\sin\theta$). Normalised by both the incident neutron flux and the volume of the sample. The particular interest in this work is neutrons that have been scattered elastically (i.e. with no energy loss) and coherently (that is neutrons arising from the interference between neutrons scattered from two different points in the sample). This elastic coherent scatter contains information on the 'structural' correlations in the sample. To take a polymer blend, with components A and B, as an example and imagine standing on a segment of type A, the segments closest to this 'home' segment will most probably also be of type A, in the same chain as the 'home' segment. The exact distribution of other A segments as a function of distance from the 'home' segment will depend on the conformation of the polymer chain and so the small angle scattering is sensitive to the chain conformation.

If, in addition, there are interactions between chains of type A then there will be an additional structural correlation for distances beyond the polymer chain in which the 'home' segment lies, this inter - molecular correlation will also influence the scattering.

The following paragraphs are an attempt to introduce the principal mathematical relationships that define the scattering, the details of the scattering arising from polymer blends are given in Section 2.1. This section is by necessity highly summarised, Lovesey[2] gives a more in depth presentation of the fundamentals of neutron scattering. In this section vector quantities will appear in bold type and scalar quantities in normal type.

Neutrons behave as if they are scattered from a so called Fermi pseudo potential, $V(\mathbf{r})$, which is given by:

$$V(\mathbf{r}) = \frac{h^2}{2\pi m_n} b\delta(\mathbf{r} - \mathbf{R})$$

Equation 3.4

R is the position of the scattering nucleus and **r** is a position vector. $\delta(x)$ is the Dirac delta function, argument x. b is known as the scattering length of the nucleus and is a property of nuclei that varies irregularly as a function of atomic weight and is different

for different isotopes of the same element. This is at the crux of neutron scattering from polymers since the scattering lengths of ^1H and ^2H are very different, and most polymers and their solvents contain hydrogen, the polymer or part of a polymer of interest can be labelled by isotopic substitution. What Equation 3.4 is essentially saying is that the nucleus which scatters the incident neutron can be considered to be a point i.e. is much smaller than the wavelength of the neutron.

The number of neutrons scattered into solid angle dΩ per unit time $\frac{d\sigma}{d\Omega}$ from a single nucleus at position $\mathbb{R}$ is given by the expression:

$$\frac{d\sigma}{d\Omega} = \left| \frac{2\pi m_n}{h^2} \int d\mathbf{r} \exp(-i\mathbf{k}'.\mathbf{r}) V(\mathbf{r}) \exp(i\mathbf{k}.\mathbf{r}) \right|^2$$

Equation 3.5

where $\mathbf{k}$ is the wavevector of the incident neutron and $\mathbf{k}'$ is the wavevector of the scattered neutron. The exponential terms are the (conjugate) wavefunctions for the incident and (scattered) neutron. A further quantity, $\mathbb{Q}$, the scattering vector is defined:

$$\mathbb{Q} = \mathbb{k}' - \mathbb{k}$$

Equation 3.6

This is illustrated graphically in Figure 3.2.

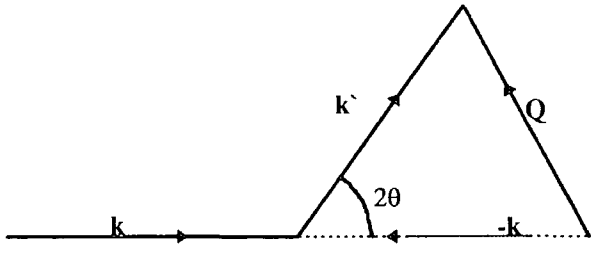

Figure 3.2: Diagram showing the relationship between the scattering vector, Q, and the incident and scattered wave vectors k and k`.

To complicate matters, outside this section the magnitude of the scattering vector, Q, will be used exclusively and referred to as the 'scattering vector', this is technically incorrect but accepted by custom! Substituting Equations 3.6 and 3.4 into Equation 3.5:

$$\frac{d\sigma}{d\Omega} = \left| \left(\frac{2\pi m_n}{h^2} \right) \int d\mathbf{r} V(\mathbf{r}) \exp(-i\mathbf{Q}.\mathbf{r}) \right|^2 = |b|^2$$

Equation 3.7

To calculate the scattering from an ensemble of, N, nuclei at positions $\mathbb{R}_j$, we replace V(r) with a summation and so:

$$\frac{d\sigma}{d\Omega} = \sum_{jk} \exp(i\mathbf{Q}.(\mathbb{R}_j - \mathbb{R}_k)) \overline{b_j b_k}$$

Equation 3.8

where $\overline{b_j b_k}$ is the value of $b_j b_k$ averaged over a random distribution of isotopes. Clearly the behaviour of $\overline{b_j b_k}$ will be different for j = k than for j ≠ k. It can be shown that:

$$\frac{d\sigma}{d\Omega} = \left(|\bar{b}|^2 \left| \sum_j \exp(i\mathbf{Q}.\mathbb{R}_j) \right| \right)_{coh} + \left(N \overline{|b - \bar{b}|^2} \right)_{incoh}$$

Equation 3.9

The subscripts 'coh' and 'incoh' refer to the coherent and incoherent contributions to the elastic scatter. When the scattering from polymer chains is being considered it is often the case that the Q range covered does not extend to high enough values for the internal structure of the monomers to be resolved and so the scattering from polymer segments with scattering lengths b_H and b_D for hydrogenous or deuterated components respectively are used. In this case the elastic coherent scattering, which will now be referred to as I(Q) follows the general form:

$$I(Q) = \left(\frac{b_H}{V_H} - \frac{b_D}{V_D} \right)^2 S(Q)$$

Equation 3.10

where S(Q) is the scattering structure factor and is derived eventually from the coherent part of Equation 3.9. de Gennes[3] has calculated S(Q) for polymer blends, with an interaction parameter, using the incompressible Random Phase Approximation. The behaviour of S(Q) in this situation is discussed in Section 2.1, it contains contributions from the scattering of a single polymer coil with a Gaussian distribution of chain

segments and a 'correction' term allowing for the structure arising from the thermodynamic interaction.

3.1.2 Neutron Reflectometry (NR)

A neutron reflectometry experiment determines the variation of the intensity of a beam of neutrons reflected from a surface as a function of Q (= $(4\pi/\lambda)$ sin θ), the scattering vector. The reflectivity R(Q), is defined as $I_r(Q)/I_o(Q)$, where $I_r(Q)$ is the reflected and $I_o(Q)$ is the incident intensity, λ is the neutron wavelength and 2θ is the scattering angle. The angle between the plane of the sample and the incident beam is θ. These terms are illustrated in Figure 3.3.

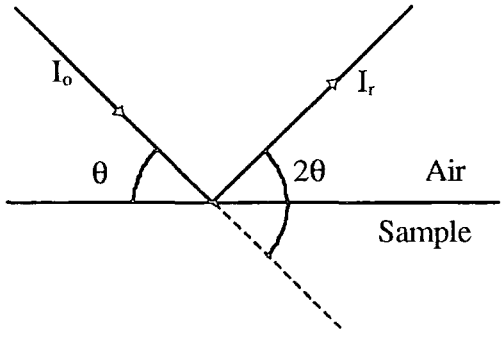

Figure 3.3: Schematic diagram of reflectivity experiment.

The reflectivity R(Q) provides information on the variation of nuclear scattering length density perpendicular to the sample surface, $\rho_N(z)$. The shape of the reflectivity profile, R(Q) arises from the interference of neutrons reflected from the air - polymer surface and from scattering length density gradients within the sample. The section that follows is based principally on the reviews of Penfold[4] and Russell[5], a more detailed description of the mathematics of reflection and optical matrix methods can be found in Lekner[6], Born and Wolf[7] or Heavens[8].

The nuclear scattering length density, ρ_N, of a polymer is given by:

$$\rho_N = \frac{\rho N_A \sum b_i}{m}$$

Equation 3.11

where ρ is the physical density of the polymer, m is the monomer mass, N_A is Avogadro's number and Σb_i is the sum of the nuclear scattering lengths of the atoms, i, in the monomer unit. The scattering lengths of ^1H and ^2H nuclei are very different and this means that composition gradients in polymer blends can be obtained from the scattering length density gradient if one component of the blend has been selectively deuterated. This is because scattering length density is additive, i.e. $\rho_N(z) = \phi_D(z)\rho_D + (1-\phi_D(z))\rho_H$, ρ_D and ρ_H are the scattering length densities of the deuterated and the hydrogenous polymers, respectively, $\phi_D(z)$ is the volume fraction of the deuterated polymer as a function of depth, $\phi_D(z)$ will be abbreviated to $\phi(z)$.

Extracting the real space scattering length density depth profile, $\rho_N(z)$ from the reflectivity data R(Q) is not straightforward. In general there is no direct transform from R(Q) to $\rho_N(z)$ and a model fitting procedure is generally used. The reflectivity of neutrons from a surface is entirely analogous to the reflectivity of electromagnetic radiation from a surface, the optical refractive index is simply replaced by the neutron refractive index, n:

$$n = 1 - \frac{\lambda^2}{2\pi}\rho_N + i\lambda\frac{\rho N_A(\sigma_i + \sigma_a)}{m4\pi}$$

Equation 3.12

where σ_i and σ_a are the incoherent cross section and absorption cross section respectively. This final complex term accounts for incoherent and absorption effects, in this work the complex term has been disregarded since it typically has a very small effect on the calculated neutron reflectivity profiles of the systems studied here, Penfold[9] has discussed these effects. The neutron refractive index for most materials is very slightly less than 1 (1-n is of the order 1×10^{-6}). This means that most materials exhibit critical external reflection at very small incident angles. The critical angle, θ_c, below which total external reflection occurs is calculated from Snell's Law:

$$\cos\theta_c = n$$

Equation 3.13

Since θ_c is small, $\cos\theta_c$ can be expanded to $1-(\theta_c^2/2)$, therefore:

$$\theta_c = \lambda\left(\frac{\rho_N}{\pi}\right)^{1/2}$$

Equation 3.14

Below the critical angle the reflectivity is one. Above the critical angle the reflectivity, R, at a single sharp interface between medium 0 and medium 1 is given by:

$$r_{01} = \frac{k_0 - k_1}{k_0 + k_1}$$
$$R = r_{01} r_{01}^*$$

Equation 3.15

r_{01} is known as the Fresnel reflection coefficient and r_{01}^* is its complex conjugate. k_i ($Q = 2k$) is the component of the neutron wavevector perpendicular to the surface in medium i:

$$k_i = \frac{2\pi}{\lambda}\sin\theta_i$$

Equation 3.16

Given the angle of incidence, θ_0, in medium 0, the angle of refraction, θ_1, in medium 1 can be calculated from Snell's Law:

$$n_0 \cos\theta_0 = n_1 \cos\theta_1$$

Equation 3.17

where n_0 and n_1 are the neutron refractive indices of mediums 0 and 1 respectively.

This approach can be extended to calculate the reflectivity from a stack of uniform layers, using matrix methods. The neutron reflectivity of an arbitrary nuclear scattering length density profile can be obtained by representing the profile as a stack of uniform layers, this is illustrated in Figure 3.4.

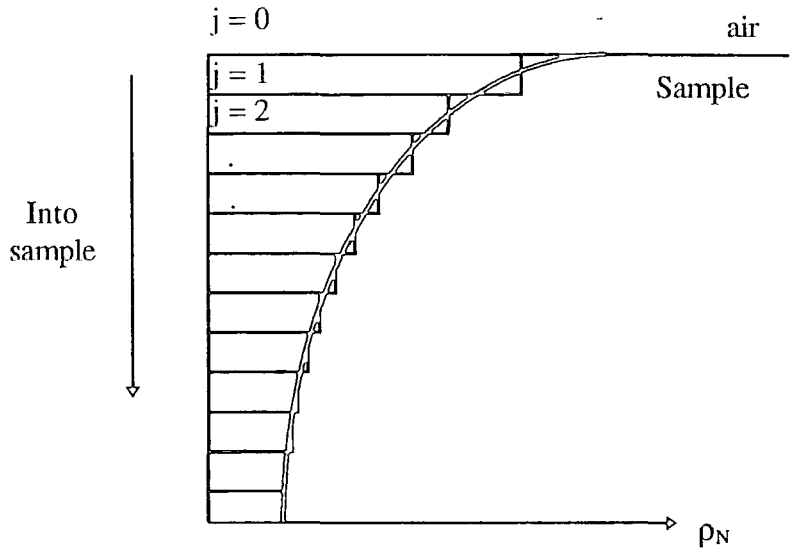

Figure 3.4: Illustration of a 'multilayer' representation of a nuclear scattering length density profile perpendicular to the sample surface.

The properties of the j^{th} sheet in the structure are given by the matrix:

$$M_j = \begin{pmatrix} e^{i\beta_{j-1}} & r_j e^{i\beta_{j-1}} \\ r_j e^{-i\beta_{j-1}} & e^{-i\beta_{j-1}} \end{pmatrix}$$

Equation 3.18

where r_j is a modified Fresnel coefficient for the interface between layers j-1 and j:

$$r_j = \frac{p_{j-1} - p_j}{p_{j-1} + p_j} \exp(-0.5 Q_{j-1} Q_j \langle\sigma\rangle^2)$$

Equation 3.19

the exponential term allows for the incorporation of Gaussian roughness at the interface with a root mean square value of $<\sigma>$.

$$p_j = n_j \sin\theta_j = (n_j^2 - n_{j-1}^2 \cos^2\theta_{j-1})^{1/2}$$

Equation 3.20

where $\sin\theta_j$ has been expressed in terms of the θ and n for the previous layer, j-1, using Snell's Law.

$$\beta_j = (2\pi/\lambda) n_j z_j \sin\theta$$

Equation 3.21

n_j and z_j are the neutron refractive index and the thickness of the j^{th} layer respectively. The reflectivity, R, is then given by:

$$R = \frac{M_{21} M_{21}^*}{M_{11} M_{11}^*}$$

Equation 3.22

M_{11} and M_{21} are elements of the resultant matrix, M_R, obtained as the product of all the individual matrices for each separate layer, i.e.

$$M_R = \prod_{j=1}^{n} M_j$$

Equation 3.23

This system of equations facilitates the extraction of the composition profile via a model fitting procedure. Figure 3.5 shows some reflectivity profiles for situations that are typically encountered in this work. The effect of instrument resolution has been included in these profiles by integrating the reflectivity profile, with no resolution included, over intervals of the resolution, ΔQ, for each data point. Figure 3.5a shows reflectivity profiles for a series of layers of different thickness, these exhibit 'Kiessig fringes' whose spacing is inversely proportional to the film thickness. Figure 3.5b shows the effect that a surface excess of material with higher scattering length density has at the surface of a film (a two layer profile with a large roughness between the two layers has been used for these data, the ρ_N at the surface is at a volume fraction equivalent to 0.5 d-PMMA in h-PMMA and the bulk volume fraction is fixed at 0.25, the thickness of the surface excess layer is varied), these are compared to the reflectivity of uniform films with volume fractions of 0.25 and 0.5 d-PMMA . Finally, since all samples used in this work were cast onto silicon oxide substrates which have a layer of native silicon dioxide at the

surface approximately 15Å thick, which has a different scattering length density to silicon Figure 3.5c shows the effect that this silicon dioxide layer has on the reflectivity of uniform films with various thicknesses and a scattering length density which matches that of the underlying substrate. For thicker films the effect of the SiO_2 layer is negligible.

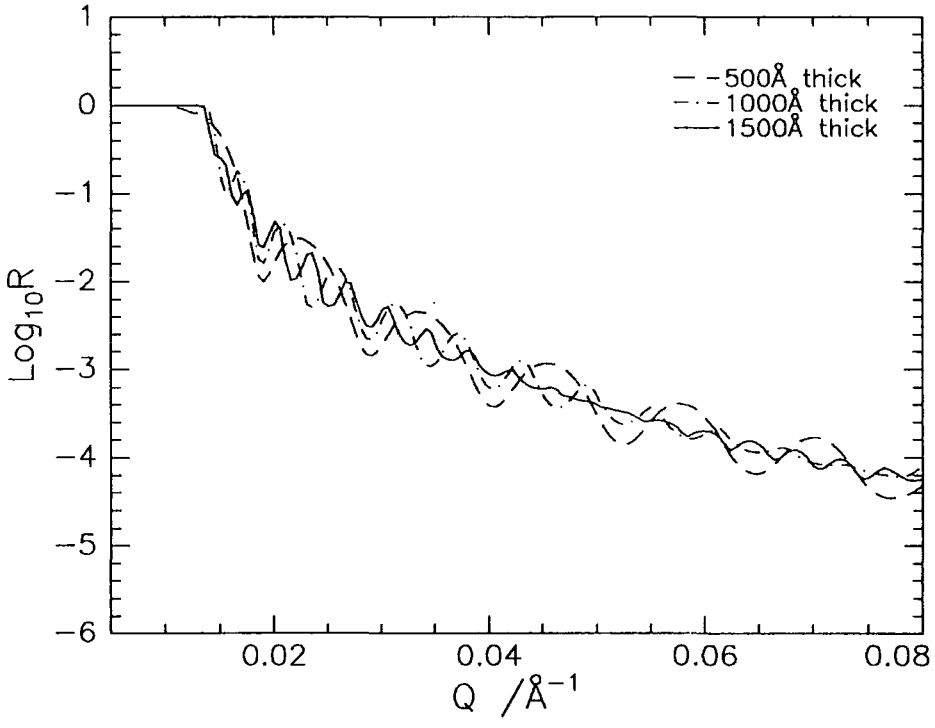

Figure 3.5a: Calculated reflectivity from uniform layers of varying thickness (4% resolution.

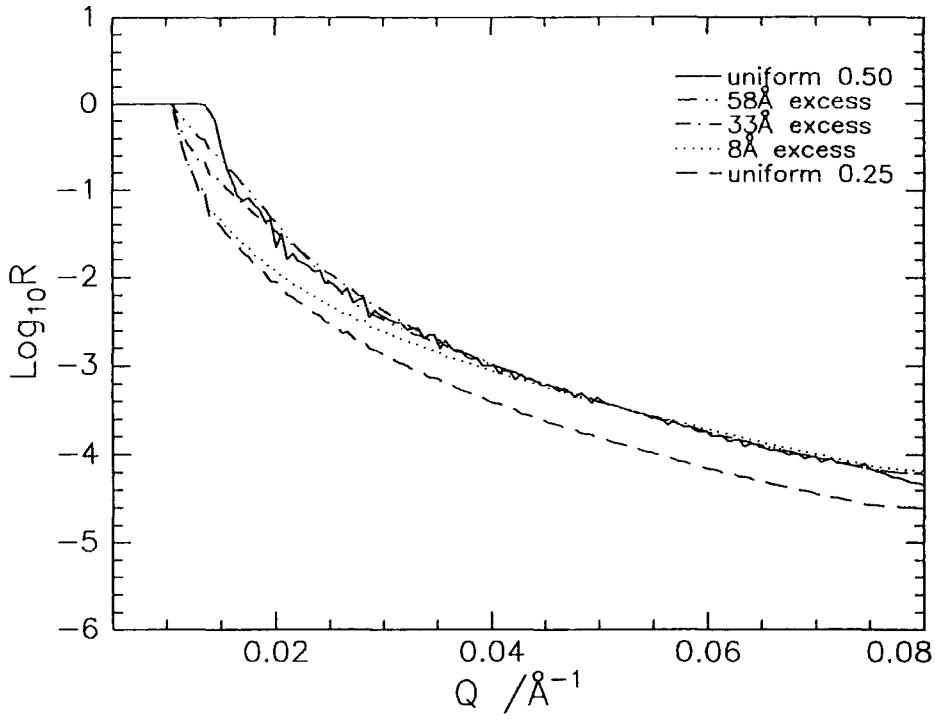

Figure 3.5b: Calculated reflectivity from layers with various surface excesses, see text for details.

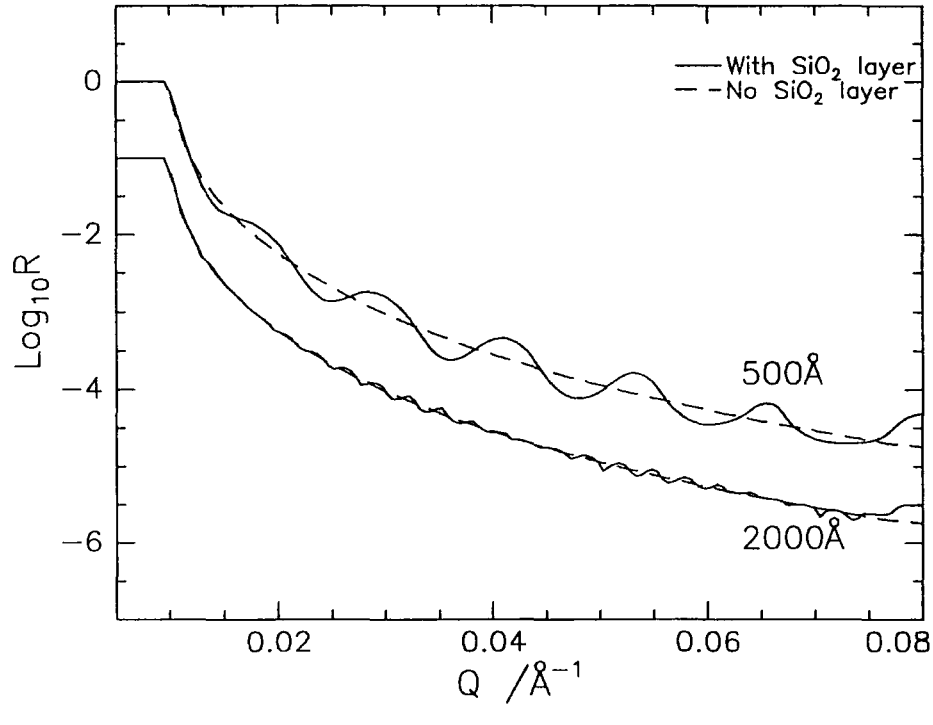

Figure 3.5c: Calculated reflectivity of layers of (top) 500Å and (bottom) 2000Å with and without a 15Å SiO_2 layer at the substrate. (2000Å data offset by -1 for clarity.

Even in an ideal world where data can be collected over an infinite Q range with no resolution effects the reflectivity, R(Q), is not unique to a single composition profile because of the loss of phase information[10], furthermore a host of different composition profiles may all have very similar reflectivity profiles and in a real experimental situation these profiles will be essentially indistinguishable. On top of this fundamental problem there is the practical problem of fitting the parameters. Ideally we would like to divide our model composition profile into a large number of layers so that the model can accurately represent the composition profile in the sample. Fitting a profile with such a large number of parameters is difficult and if the usual non-linear least squares methods are used then a smaller number of parameters are fitted by resorting to the use of functional form models or multilayer models with Gaussian roughness between the layers where the number of layers is small (<5).

The preceding paragraph represents the pessimistic side of neutron reflectivity data analysis, in practice there are reasons to be more optimistic. A substantial subset of the composition profiles are physically or chemically unreasonable and further to this additional information can be obtained for the system of interest using techniques which are sensitive to the surface composition (such as SIMS or XPS) or give a lower resolution picture of the composition profile (such as NRA) these data can be used to give starting parameters for the fitting process and discard unreasonable fits.

This section has concentrated on one method of data analysis - the optical matrix method, which is suitable for the systems studied here. Two further methods are that of partial structure factors[11] and indirect Fourier transform[12] methods. It is also possible to obtain some information more directly from the reflectivity profile by using the Born or kinematic approximation which is at the root of the partial structure factor method. The kinematic approximation is that observed neutrons have undergone only one collision, i.e. there is no multiple scattering, this approximation breaks done as the region of total reflection is approached. In the kinematic approximation:

$$R(Q) = \frac{16\pi^2}{Q^4}\left|\underline{\rho}'_N(Q)\right|^2$$

Equation 3.24

$\underline{\rho}'_N(Q)$ is the Fourier transform of the composition gradients, $(\partial\rho_N/\partial z)$, in the sample. In the limit of large Q, $\underline{\rho}'_N(Q) \rightarrow \Sigma\delta(\rho_N(z))$, where $\Sigma\delta(\rho_N(z))$ is the sum of the 'jumps' in the

scattering length density, i.e. at large Q, $\rho'_N(Q)$ is directly related to abrupt changes in the scattering length density. Commonly such sharp changes in scattering length density are only observed at the air / polymer and polymer / substrate interfaces. Formally:

$$\lim_{Q\to\infty} R(Q)Q^4 = 16\pi^2 \Sigma(\delta(\rho_N(z)))^2$$

Equation 3.25

This means that the air / polymer surface composition of a sample can be obtained directly from the value of the asymptote of the $R(Q)*Q^4$ vs. Q at large Q, if it can be arranged that the polymer and substrate have the same scattering length density.

3.2 Nuclear Reaction Analysis (NRA)

Nuclear reaction analysis, as applied to polymers, is based on the nuclear reaction:

$$^3He^+ + ^2H \rightarrow ^4He + ^1H^+ + Q$$

Equation 3.26

where Q = 18.352 MeV, the reaction proceeds via the short lived $^5Li^+$. The reaction has a maximum cross-section at an incident $^3He^+$ energy of 0.7 MeV. The basis of NRA is to fire $^3He^+$ into the partially deuterated sample of interest and measure the energy spectrum of the resultant ^4He (as α particles) or $^1H^+$ (as protons, p). The depth profiling technique was developed by Dieumegard *et al*[13] to probe the composition profiles of ^2H in silicon. Only more recently has it been developed by Payne *et al*[14] and Chaturvedi *et al*[15] for use in polymer systems.

Figure 3.6 is a schematic illustration of the NRA experiment, showing the angles α_{nra} and θ_{nra}, which are the beam / sample angle and the detection angle, respectively. These angles will influence the depth probed and the resolution.

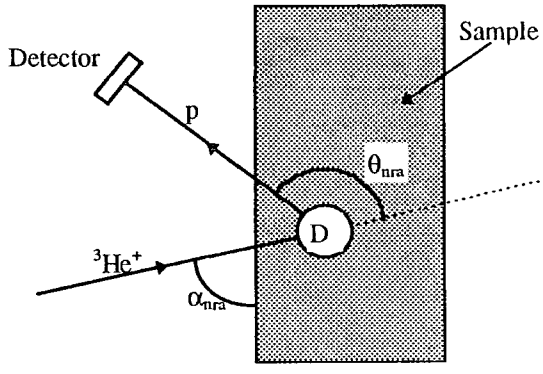

Figure 3.6: Schematic illustration of the NRA experiment with α_{nra} and θ_{nra} defined

The energies of the resultant p and ^4He can be calculated from kinematics, the situation is illustrated in Figure 3.7. We consider two frames of reference, the laboratory reference frame (referred to using the superscript 'lab') and the centre of mass reference frame (referred to using the superscript 'cm'). The ^3He, ^4He, ^2H and protons (^1H) will

be referred to using the subscripts 3He, α, D and p respectively. V_x^y and m_x will denote the velocities and masses of the particles, respectively.

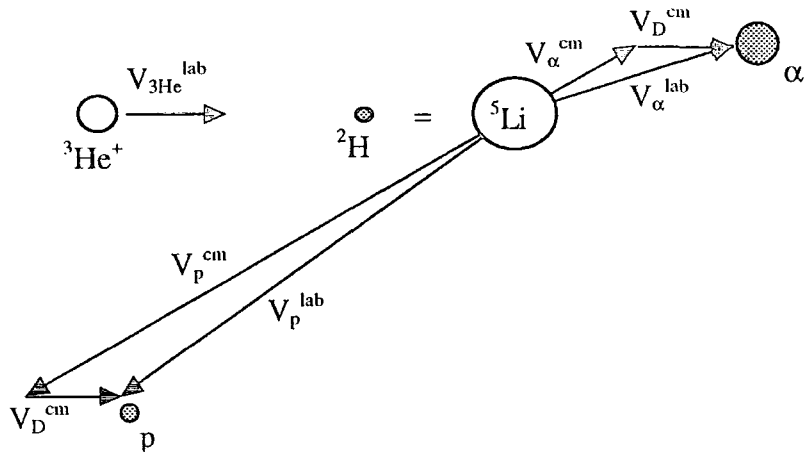

Figure 3.7: Kinematics of the reaction between $^3He^+$ and ^2H

In the centre of mass reference frame the ^2H (or D) is no longer stationary but moves towards the incoming $^3He^+$ with velocity, V_D^{cm}, such that the net momentum in the system is zero:

$$m_{3He}(V_{3He}^{lab} + V_D^{cm}) = m_D V_D^{cm}$$

$$\therefore V_D^{cm} = \frac{m_{3He} V_{3He}^{cm}}{(m_{3He} + m_D)} = -\frac{3}{5} V_{3He}^{lab}$$

Equation 3.27

After the reaction the net momentum in the centre of mass reference frame is still zero:

$$m_\alpha V_\alpha^{cm} = -m_p V_p^{cm}$$

$$\therefore 4V_\alpha^{cm} = -V_p^{cm}$$

Equation 3.28

This is illustrated schematically in Figure 3.7, the resultant velocities in the laboratory reference frame are obtained by adding the velocity of the centre of mass, V_D^{cm}, to the velocities in the centre of mass reference frame. In the centre of mass frame of reference the protons will have energy 14.8 MeV and the ^4He will have energy 3.7

MeV, this means that the signals from the protons, ^{4}He and Rutherford backscattered ^{3}He are all well separated in energy.

As the incident ^{3}He penetrates into the sample it losses energy through electronic collisions, thus the centre of mass velocity becomes less as the ^{3}He travels deeper into the sample. This means that protons collected at backward detection angles (θ_{nra}>90°) have an energy in the laboratory reference frame that depends on how deep in the sample the reaction in which they originated occurred. Protons originating at the surface will have a lower energy than protons generated deep within the sample. The energy lost by the proton as it leaves the sample is relatively small, since it travels much faster than the incident ^{3}He. To maximise the depth resolution the protons should be detected at the largest θ_{nra} available.

NRA experiments have been done on polymers in two modes, with protons detected at backward angles[14] (as was assumed in the discussion above) or with ^{4}He detected at forward angles[15], in which case ^{4}He or p from the surface have a higher energy than those from deeper within the sample.

The resolution perpendicular to the sample surface can be improved by tilting the sample with respect to the incident beam, this increases the path length of the ^{3}He in the sample for a given depth perpendicular to the surface. Payne *et al*[14] found a resolution of 300Å (Full Width Half Maximum) for samples at 15° to the incident beam and with a backward detection angle of 165°.

3.3 Attenuated Total Reflection Infrared Spectroscopy (ATR)

If a material, such as an ATR crystal, is sustaining total internal reflection then an evanescent wave will be found 'protruding' from the surface of the material. ATR spectroscopy takes advantage of this by placing the sample of interest in good optical contact with the ATR crystal such that the evanescent wave penetrates the sample. Mirabella[16] gives a general review of various aspects of total internal reflection spectroscopy. The notation used here follows that of Fina and Chen[17]. Total internal reflection occurs if the angle of incidence[§], θ_{atr}, is greater than the critical angle, θ_c defined below:

$$\theta_c = \sin^{-1} \frac{n_{atr}}{n_{sam}}$$

Equation 3.29

where n_{atr} is the refractive index of the ATR crystal and n_{sam} is the refractive index of the sample placed on the ATR crystal. The intensity of the evanescent wave decays exponentially away from the surface of the material. In the case of zero absorption in the surrounding medium no energy is radiated away. The intensity of the electric field, $\langle E_{sam}^2 \rangle$, in the evanescent wave is given by:

$$\left\langle E_{sam}^2 \right\rangle = \left\langle E_0^2 \right\rangle \exp\left(-\frac{z}{d_p} \right) dz$$

Equation 3.30

where $\langle E_0^2 \rangle$ is the electric field intensity at the interface between the ATR crystal and the sample. d_p is the penetration depth, defined below:

$$d_p = \frac{\lambda}{2\pi \sqrt{n_{atr}^2 \sin^2 \theta_{atr} - n_{sam}^2}}$$

Equation 3.31

[§] The angle of incidence is defined relative to the normal in this section on ATR and relative to the surface for NR, this is to maintain consistency with the literature.

where λ is the wavelength of the radiation in free space. Intuitively it can be seen that the evanescent wave will lead to a depth weighted absorption spectrum of the sample, with the spectrum dominated by contributions from closest to the crystal surface.

A further parameter, d_e, is also used in ATR spectroscopy, this is defined as the thickness of a sample in transmission that would produce the same absorption as the ATR sample. This is defined by the equation:

$$d_e = \frac{n_{sam}\langle E_0^2 \rangle}{n_{atr}\cos\theta_{atr}} \int_0^{\infty} \exp\left(-\frac{z}{d_p}\right) dz$$

Equation 3.32

$1/\cos\theta_{atr}$ is a geometric weighting factor and the term $(n_{sam}/n_{atr})\langle E_0^2 \rangle$ arises because the intensities of the electric fields in the sample and the ATR crystal are related by the expression:

$$n_{sam}\langle E_{sam}^2 \rangle = n_{atr}\langle E_{atr}^2 \rangle$$

Equation 3.33

With a direct analogy to the Beer Law for absorption in the transmission:

$$A_{atr} = \exp(-\alpha_\lambda d_e)$$

Equation 3.34

where A_{atr} is the measured absorption and α_λ is the absorption coefficient at wavelength λ, for small α_λ the following approximation can be made:

$$A_{atr} = 1 - \alpha_\lambda d_e$$

Equation 3.35

This is the result of two approximations, that of the exponential term and that of the exact Fresnel coefficients used in deriving the Beer Law. Combining equations 3.35 and 3.32 gives the equation:

$$1 - A_{atr}(\theta_{atr}) = \frac{n_{sam}\langle E_0^2 \rangle}{n_{atr}\cos\theta_{atr}} \int_0^{\infty} \alpha_\lambda(z) \exp\left(-\frac{z}{d_p}\right) dz$$

Equation 3.36

This shows that the ATR absorption spectrum as a function of incident angle, $A_{atr}(\theta_{atr})$, is the Laplace transform of the absorption coefficient as a function of depth, $\alpha_\lambda(z)$. Fina and Chen have shown that for the Laplace transform to be successfully inverted the absorption spectrum must be measured over a range in d_p of 2.76, i.e.:

Maximum $d_p \geq 2.76 \times$ minimum d_p

Equation 3.37

The depth resolution of ATR is around 0.5 μm with a probe depth of up to 10 μm. In the derivation above it was assumed that a single total internal reflection occurred this can be attained using a hemispherical ATR crystal which allows the incident angle to be varied with no regard to refraction of the beam at the 'entry' and 'exit' air - crystal interfaces, this is illustrated in Figure 3.8a. Experimentally it is more usual to use a parallelepiped ATR crystal illustrated in Figure 3.8b the multiple reflections enhance the absorption spectrum although the fixed angle of the end faces limits the range of incident angles available and introduces uncertainty in the angle θ_{atr} at the crystal sample interface. In practice very little work has been done on quantitative depth profiling using ATR spectroscopy. Although ATR has been used to obtain the surface excess or total amount of a substance in the region adjacent to the ATR crystal, this has included measurements of the absorption of polymers onto the surface of an ATR crystal[18], the penetration of water in poly (acrylonitrile)[19] and a semi-quantitative investigation of the surface enrichment behaviour of polystyrene / poly (vinyl methyl ether)[20].

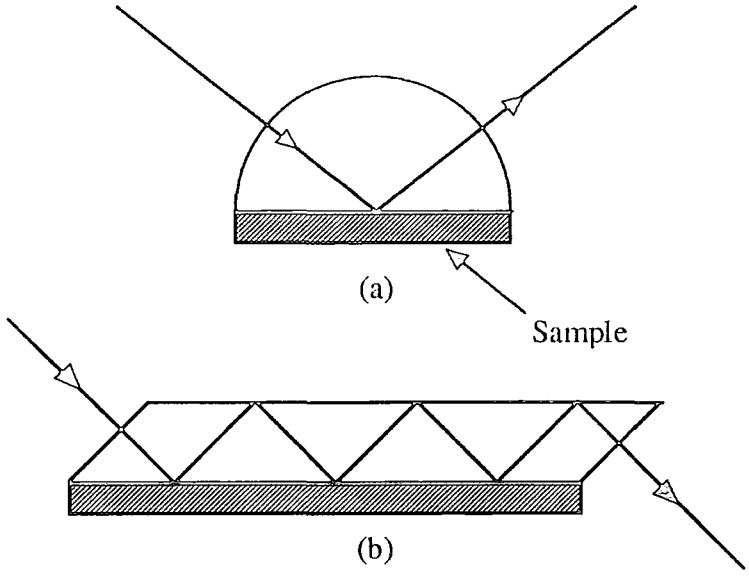

Figure 3.8: Schematic diagrams of two modes of ATR spectroscopy

3.4 References for Section 3

1 . J.S. Higgins, H.C. Benoit, 'Polymers and Neutron Scattering', Clarendon Press, 1994.

2 . S.W. Lovesey, 'Theory of Neutron Scattering from Condensed Matter, Volume 1', Clarendon Press, 1986.

3 . P.G. de Gennes, 'Scaling Concepts in Polymer Physics', Cornell University Press, 1985.

4 . J. Penfold, Rutherford Appleton Laboratory Report, RAL-88-088, 1988.

5 . T.P. Russell, *Material Science Reports*, 5, **1990**, 173.

6 . J. Lekner, 'Theory of Reflection', Martinus Nijhoff Publishers, 1987.

7 . M. Born, E. Wolf, 'Principles of Optics 6th ed.', Pergamon, 1980.

8 . O. Heavens, 'Optical Properties of Thin Films', Butterworth, 1955.

9 . J.Penfold, Rutherford Appleton Laboratory Report, RAL-91-023, 1991.

10 . D.S. Sivia, W.A. Hamilton, G.S. Smith, *Physica B*, 173, **1991**, 121.

11 . T.L. Crowley, E.M. Lee, E.A. Simister, R.K. Thomas, *Physica B*, 173, **1991**, 143.

12 . J. S. Pedersen, *Journal of Applied Crystallography*, 25, **1992**, 129.

13 . D. Dieumegard, D. Dubreuil, G. Amsel, *Nuclear Instruments and Methods*, 166, **1979**, 431.

14 . R.S. Payne, A.S. Clough, P. Murphy, P.J. Mills, *Nuclear Instruments and Methods B*, 42, **1989**, 130.

15 . U.K. Chaturvedi, U. Steiner, O. Zak, G. Krausch, G. Schatz, J. Klein, *Applied Physics Letters*, 56(13), **1990**, 1228.

16 . F.M. Mirabella, *Applied Spectroscopy Reviews*, 21(1&2), **1985**, 45.

17 . L.J. Fina, G. Chen, *Vibrational Spectroscopy*, 1, **1991**, 353.

18 . H.E. Johnson, S. Granick, *Macromolecules*, 23, **1990**, 3367.

19 . G.T. Fieldson, T.A. Barbari, *Polymer*, 34(6), **1993**, 1146.

20 . J.M.G. Cowie, B.G. Devlin, I.J. McEwan, *Macromolecules*, 26, **1993**, 5628.

This page left intentionally blank

4. Experimental

4.1 Materials

4.1.1 Synthesis

All the polymers used in this work were synthesised by F.T. Kiff and the perdeuterated dibutyl phthalate was synthesised by M. Hartshorne. Outlines of the synthesis methods used are included here to provide evidence of the provenance of the polymers used but no expertise in these synthetic methods is claimed. All the deuterated polymers were prepared by polymerisation of the fully deuterated monomers. In this work the following abbreviations will be used:

h-PMMA	hydrogenous poly (methyl methacrylate)
d-PMMA	perdeuterated poly (methyl methacrylate)
h-PEO	hydrogenous poly (ethylene oxide)
d-PEO	perdeuterated poly (ethylene oxide)
h-PS	hydrogenous polystyrene
d-PS	perdeuterated polystyrene
d-PS(F)	perdeuterated polystyrene with one end 1H,1H,2H,2H-perfluoro octyl dimethyl chlorosilane terminated, this end group will often be described as 'perfluorohexane' as a short hand.
d-PS(F2)	perdeuterated polystyrene with both ends terminated with 1H,1H,2H,2H-perfluoro octyl dimethyl chlorosilane.
h-DBP	hydrogenous dibutyl phthalate
d-DBP	perdeuterated dibutyl phthalate

Syndiotactic Poly (methyl methacrylate)

Deuterated and hydrogenous syndiotactic poly (methyl methacrylate) were prepared by anionic polymerisation of the purified monomers in tetrahydrofuran solution

at 195K using 9-fluorenyllithium as initiator. After termination by addition of degassed methanol, the polymers were isolated by precipitation in hot hexane, filtered off washed and dried under vacuum at 313K for 1 week.

Isotactic Poly (methyl methacrylate)

Deuterated and hydrogenous isotactic poly (methyl methacrylate) were prepared by the anionic polymerisation of the purified monomers in toluene at 273K using phenyl magnesium bromide as initiator. After termination by addition of degassed methanol, the polymers were isolated by precipitation in chilled hexane. A chilled methanol / HCl mixture was added to the dried polymer in order to remove magnesium residues from the initiator. The initial broad molecular weight distribution was narrowed somewhat by re-precipitation.

Poly (ethylene oxide)

Deuterated and hydrogenous poly (ethylene oxide) were prepared by the anionic polymerisation of the purified monomer in tetrahydrofuran at 340K. The initiator was diphenyl methyl potassium. The reaction was terminated using degassed ethanoic acid and the product was then precipitated into hexane, filtered off and dried in a vacuum oven at 313K.

Polystyrene ('normal' and functionally end capped)

Deuterated and hydrogenous polystyrene were prepared by anionic polymerisation of the purified monomer in benzene at room temperature. The initiator was secondary butyl lithium. To produce 'normal' polystyrene the reaction was terminated using degassed methanol, the end capped polystyrene was terminated with 1H,1H,2H,2H-perfluoro octyl dimethyl chlorosilane This end capped polymer is illustrated in Figure 4.1.

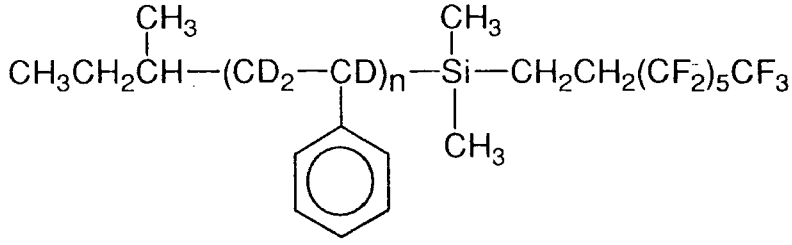

Figure 4.1: End capped polystyrene

In addition to 'normal' polystyrene and polystyrene capped at one end with 1H,1H,2H,2H-perfluoro octyl dimethyl chlorosilane, polystyrene capped at both ends with this group was prepared. This polymer was synthesised by anionic polymerisation using the difunctional initiator shown in Figure 4.2.

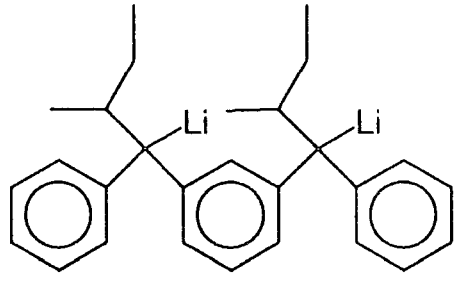

Figure 4.2: Difunctional initiator used in the synthesis of d-PS(F2)

Polymerisation was carried out at room temperature in benzene, with the addition of 1% v/v tetrahydrofuran, which is required to maintain a monomolecular weight distribution. The polymerisation was terminated using 1H,1H,2H,2H-perfluoro octyl dimethyl chlorosilane. After reprecipitation and drying the polymer the polymer was re-dissolved in methyl ethyl ketone and reprecipitated in methanol to remove any unreacted excess silane.

^{19}F n.m.r was used to establish that the reprecipitation procedure was adequate to remove unreacted silane from the polymer and to attempt to quantify the average number of perfluorohexane end groups per polymer chain, details of this procedure can be found elsewhere[1]. These measurements showed that within the substantial uncertainties of the procedure, each polymer chain had 2 perfluorohexane end groups.

Dibutyl phthalate

Hydrogenous dibutyl phthalate was purchased from Aldrich Chemical Company Ltd, Gillingham, Dorset. Perdeuterated dibutyl phthalate was synthesised by M. Hartshorne at Strathclyde University. Both compounds were used as received.

4.1.2 Molecular weights and distributions

The molecular weights and distributions of the polymers produced were determined by size exclusion chromatography, the eluting solvent was $CHCl_3$, in all cases the calibration was by polystyrene standards. The results of these analyses are summarised in Table 4.1. The codes used in this table will be referred to as 'global codes', and will be used to indicate which polymers were used at the beginning of each results and discussion section. These codes are the original codes used to designate these polymers at Durham.

Polymer	Code	M_w	M_w/M_n
syndiotactic h-PMMA	TK21	994,000	1.3
	TK76	148,000	1.3
syndiotactic d-PMMA	TK24	12,400	1.2
	TK20	17,900	1.1
	TK25	25,200	1.1
	TK22	118,000	1.2
	TK26	136,000	1.1
	TK23	417,000	1.3
isotactic h-PMMA	TK118	322,000	9.4
isotactic d-PMMA	TK120	65,500	9.1
h-PEO	TK74	124,000	1.1
d-PEO	TK77	102,000	1.2
h-PS	TK79	44,700	1.1
	TK58	1,710,000	1.2
	TK85	891,000	1.2
	TK45*	87,000	1.0
49% d-PS/h-PS copolymer	TK47*	80,000	1.0
d-PS	TK48*	86,000	1.0
	TK93	816,000	1.7
d-PS(F)	TK89	31,700	1.1
	TK92	658,000	1.1
d-PS(F2)	TK145	56,000	1.0

*eluting solvent tetrahydrofuran.

Table 4.1: Molecular weights and distributions of polymers used.

4.1.3 Tacticity

The tacticity of a selected subset of the poly (methyl methacrylate) polymers used was determined using ^{13}C n.m.r spectroscopy. Spectra were run on a Varian VXR 400 NMR spectrometer, the solvent was $CDCl_3$ and the operating frequency was 100Mhz. The method of data analysis is from reference 2 , in this work the CH_2–^{13}C (quaternary carbon) resonances in the 44-46 ppm region and the C–$^{13}CH_3$ resonances in the 15-22 ppm region were used to measure the relative proportions of meso-meso, meso-racemic and racemic-racemic dyads. The positions of these resonances are shown in Table 4.2 and the proportions of each dyad, as a percentage, shown in Table 4.3, these values are calculated from the resonances in both regions.

Polymer	Code	mm		mr		rr	
syndiotactic h-PMMA	TK21	-	-	18.60	44.78	16.41	44.4
syndiotactic d-PMMA	TK24	-	-	17.84	44.37	15.64	44.07
	TK25	-	-	-	44.32	15.66	44.00
	TK23	-	-	17.77	44.31	15.69	43.98
isotactic h-PMMA	TK118	21.94	45.47	-	44.87	-	-
isotactic d-PMMA	TK120	20.95	44.86	-	44.28	-	-
h-PMMA (ref 2)		21.8	45.4	18.8	44.9	16.3	44.5

Table 4.2: Positions of dyad resonances in ppm

Polymer	Code	mm dyads	mr dyads	rr dyads
syndiotactic h-PMMA	TK21	0	23	77
syndiotactic d-PMMA	TK24	0	20	80
	TK25	0	22	78
	TK23	0	25	75
isotactic h-PMMA	TK118	97	3	0
isotactic d-PMMA	TK120	100	0	0

Table 4.3: Tacticities of PMMA, in terms of percentages of dyads.

4.2 Small Angle Neutron Scattering (SANS)

4.2.1 Sample Preparation

For the SANS work plaques of the polymer mixture 12mm in diameter and approximately 1mm thick were required. These were prepared by, first, co-dissolving the appropriate polymers in an approximately 5% total weight polymer solution. This solution was then poured slowly into a non-solvent (either chilled methanol or hexane), the resulting precipitate was then filtered off using a sintered glass filter and a Buchner flask. The precipitate was washed with the non-solvent and allowed to dry in air at room temperature. Final drying was for 2 days under vacuum at 313K. Plaques were made from the mixtures prepared in this way using a heated Specac Infrared press, the appropriate weight of the polymer mixture to be used was placed between the die plates of the press. Typically a pressure of 2 tonnes was then applied and the temperature of the die increased to 453K, in the early compression stage a vacuum was applied to the die although in the later compression stage no vacuum was applied. The die was held at 453K for approximately one hour then it was allowed to cool, this took around 1.5 hours, then the resulting plaque was removed from the die. The plaques were uniform in thickness and free of macroscopic air bubbles, when prepared. The thickness of the samples was determined using the average of three micrometer readings and the plaques were then placed in cylindrical brass and aluminium cells with quartz windows approximately 1mm thick.

4.2.2 LOQ

All the Small Angle Neutron Scattering (SANS) data presented in this work were collected using the LOQ diffractometer at ISIS, Rutherford Appleton Laboratory, Chilton, near Oxford. Figure 4.3 is a schematic diagram of LOQ. The diffractometer views the liquid hydrogen moderator which is at 22K.

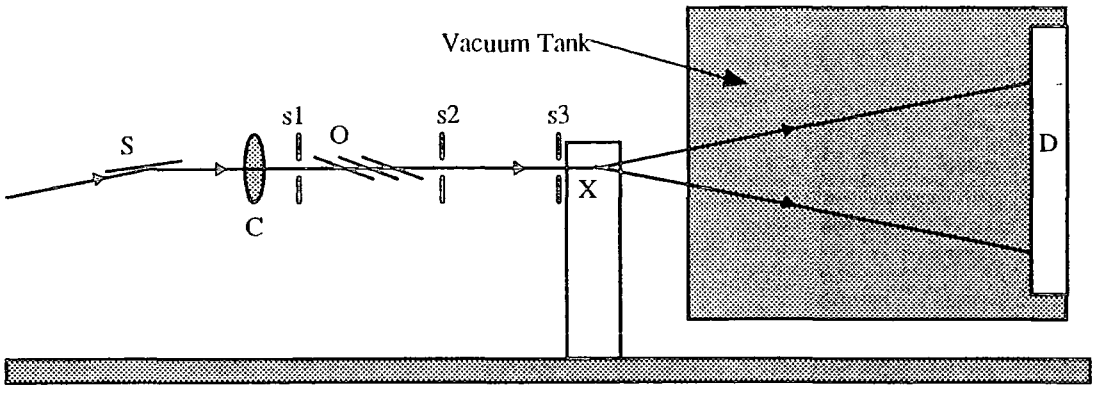

Figure 4.3: Schematic diagram of LOQ, side elevation. Key to symbols in text. (Not to scale)

The LOQ disc chopper (C) operates at 25Hz, i.e. selecting alternate pulses of neutrons from the target, this provides a useful wavelength range of 2.0-9.8Å. The neutrons are collimated by three apertures (s1, s2, s3) producing a beam at the sample (X) 8mm in diameter. Frame overlap mirrors (O) remove long wavelength neutrons (>13.7Å) which would otherwise interfere with neutrons from preceding pulses. The Soller bending mirror (S) deflects all but the shortest wavelength neutrons, this means that the detector (D) does not have a direct 'view' of the source and reduces the background radiation. The available Q range on LOQ is 0.006Å^{-1} to 0.22Å^{-1}, limited by the size of the beam stop at low Q and the size of the detector at high Q. The neutron flight path from the source to the sample position and from the sample position to the detector is evacuated to minimise neutron losses through air scattering, although the sample position itself is typically under ambient conditions. Neutrons scattered from the sample are detected by a ^{3}He-CF_4 filled area detector 64cm×64cm, this is encoded as 128×128 pixels. The detector is arranged such that the direct beam falls in the middle of the detector. The vacuum tank and the detector are heavily shielded to reduce background.

Samples were placed in an eight position, temperature controlled sample rack driven by the LOQ CAMAC electronics. The temperature of the rack was monitored by a single thermocouple at the centre of the rack. At the temperatures used in this work the thermocouple shows the rack temperature fluctuating in a regular sinusoid with a period of ~5 minutes and an amplitude ±3K, the mid point of this range is within 0.5K of the temperature set. The positions on the sample rack were aligned using a laser coincident with the neutron beam. Rack position, rack temperature and sample

'exposure' time can be controlled automatically using a command file on the LOQ front end computer.

For each sample run at each temperature two measurements are made, firstly the transmission of the sample as a function of wavelength is measured by applying a small collimation aperture to the incident beam, and placing a scintillation monitor immediately after the sample position. The sample transmission can be calculated given this measurement and a similar measurement of the 'direct beam' with no sample in place. Secondly the total small angle neutron scattering, $I_{tot}(\theta,\phi,\lambda)$, is measured using the area detector. Where 2θ is the scattering angle from the direct beam, ϕ is the azimuthal angle and λ is the neutron wavelength. The raw scattering data is corrected for incident beam flux, detector efficiency and sample transmission, in addition the data were converted from $I_{tot}(\theta,\phi,\lambda)$ to $I_{tot}(Q, \phi)$ where $Q = (4\pi/\lambda)\sin\theta$. Finally because the data were azimuthally isotropic $I_{tot}(Q, \phi)$ was azimuthally averaged to give $I_{tot}(Q)$. All these procedures were carried out at the Rutherford Appleton Laboratory using the COLLETTE program. The output from COLLETTE is nominally in absolute intensity units (cm^{-1}), but as a further calibration procedure blends of d-PS/h-PS were run at room temperature on each occasion that LOQ was used. This calibration will be discussed further in the next section.

4.2.3 Calibration

The absolute calibration of the Small Angle Neutron Scattering is important if accurate values of χ are to be obtained, in principle data from LOQ is in absolute units[3], but as a further calibration procedure a d-PS/h-PS blend with 0.47 volume fraction of d-PS was run on each occasion that scattering data were collected. Polymer blends have been used previously for the calibration of SANS[4,5], principally because they exhibit very strong scattering at low Q, this is important because it minimises the time required to make the calibration measurement. For the calibration procedure in this work two samples were run at room temperature, a blend containing 0.47 volume fraction d-PS in h-PS and a random copolymer of h-PS and d-PS with the same volume fraction of d-PS as the blend. The copolymer is run in order to measure the background scatter for the blend, background subtraction is discussed in the next Section 4.2.4. The molecular weights of the polymers used were measured by size exclusion chromatography (SEC)

with either chloroform ($CHCl_3$) or tetrahydrofuran (THF) as the eluting solvent, these values are shown in Table 4.4, along with values of the degree of polymerisation, N, calculated from these weights.

	Solvent	M_w	M_w/M_n	N
h-PS	$CHCl_3$	73,500	1.1	710
	$CHCl_3$	77,050	1.1	740
	$CHCl_3$	80,350	1.1	770
	THF	86,900	1.0	835
d-PS	$CHCl_3$	71,100	1.1	635
	THF	86,200	1.0	770

Table 4.4: Molecular weights of polymers used in calibration

There is a fairly large variation in the molecular weights determined in this manner, this will be discussed later. After background subtraction, the scattering was fitted using the Random Phase Approximation (see Section 2.1). Polystyrene is known to scatter in an ideal manner according to the Debye function[6]. The constants used were as follows: $b_H = 2.328\times10^{-12}$ cm, $b_D = 10.660\times10^{-12}$ cm, the average value of the segmental volume[7], $V = 1.725\times10^{-22}$ cm^3 , the average degree of polymerisation N = 800, χ was fixed at zero. The data were fitted using the FORTRAN program BANTAM (listing in Appendix 10.4) which is based on the interactive fitting library FITFUN, statistical error weighting was used. The radii of gyration of the two polymers were allowed to vary but the constraint $R_{gH} = R_{gD}$ was applied. Figure 4.4 shows a representative fit to the data, there are small deviations from the ideal scattering at high Q. This may be due to a slight over subtraction of the background scatter. Table 4.5 shows values of the normalisation constant, k_N, and R_g (= R_{gH}, R_{gD}) fitted to the calibration sample on the four occasions on which the SANS data were collected.

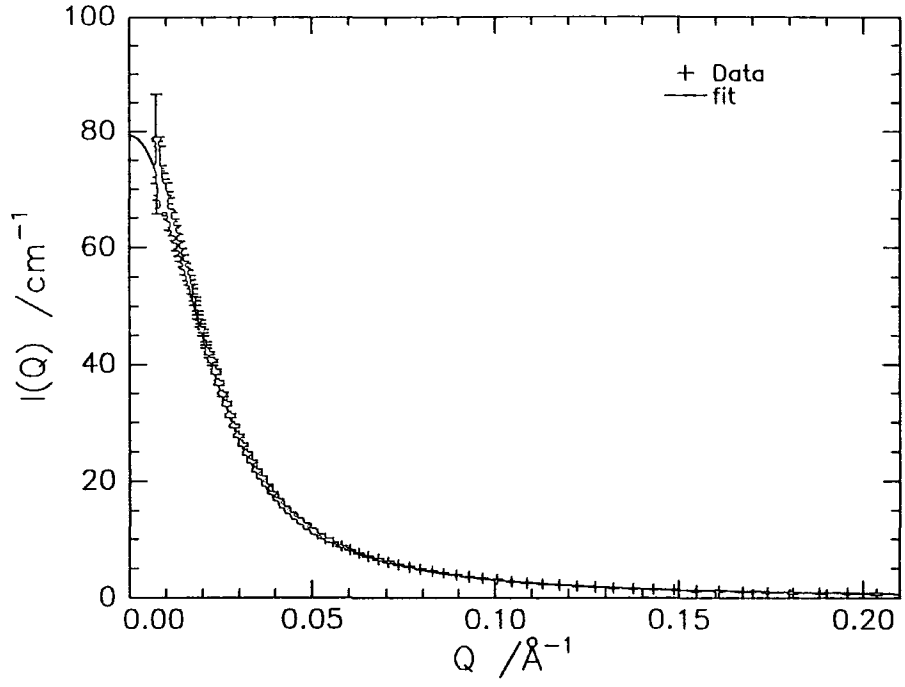

Figure 4.4: Fit to the July 1993 calibration sample using the Random Phase Approximation. Error bars from Poisson statistics.

	R_g /Å	k_N
September 1992	68.8(2)	0.940(3)
December 1992	68.3(2)	0.841(3)
June 1993	72.5(2)	0.948(3)
July 1993	71.1(2)	0.952(3)

Table 4.5: Values fitted for the radii of gyration and the normalisation constant

The normalisation constant, k_N, is the amount by which the model function must be multiplied in order to fit the data - the data must be multiplied by $1/k_N$ to convert to absolute units. Figure 4.5 shows the scattering from the calibration sample runs in the Kratky mode following multiplication by the normalisation factor ($1/k_N$), Figure 4.6 is a detail of the low Q region. These data are, in principle, on an absolute scale and so should be identical. The overlap at low Q is good, but at higher Q values (0.05Å^{-1} to 0.10Å^{-1} there are discrepancies. There is a difference between data collected in 1992 and that collected in 1993, this is probably due to an adjustment of the detector electronics between the end of 1992 and mid-1993.

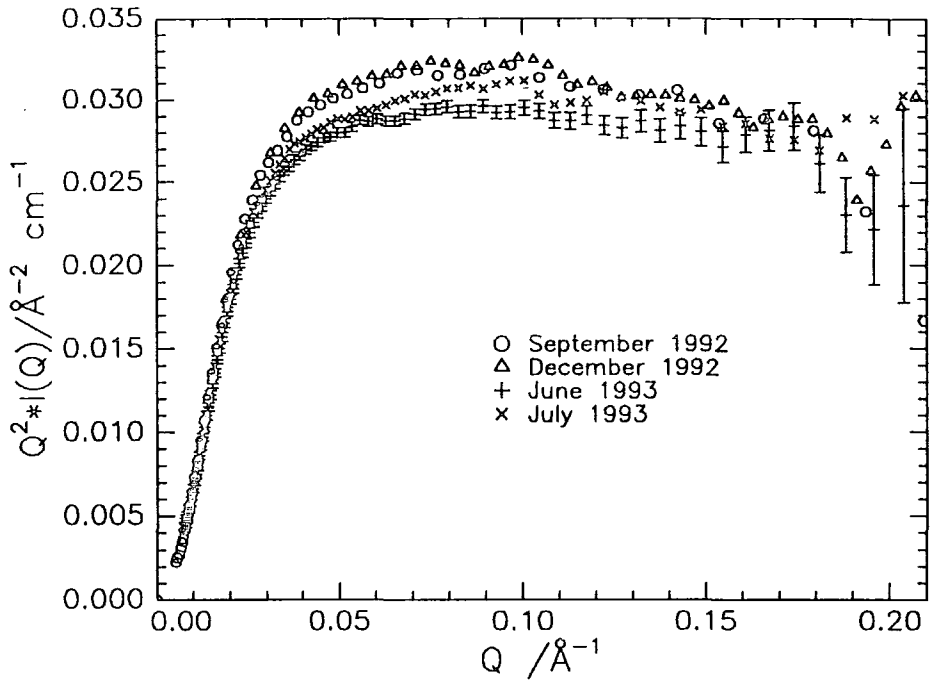

Figure 4.5: Kratky plots of data collected from calibration samples and normalised by calibration constant.

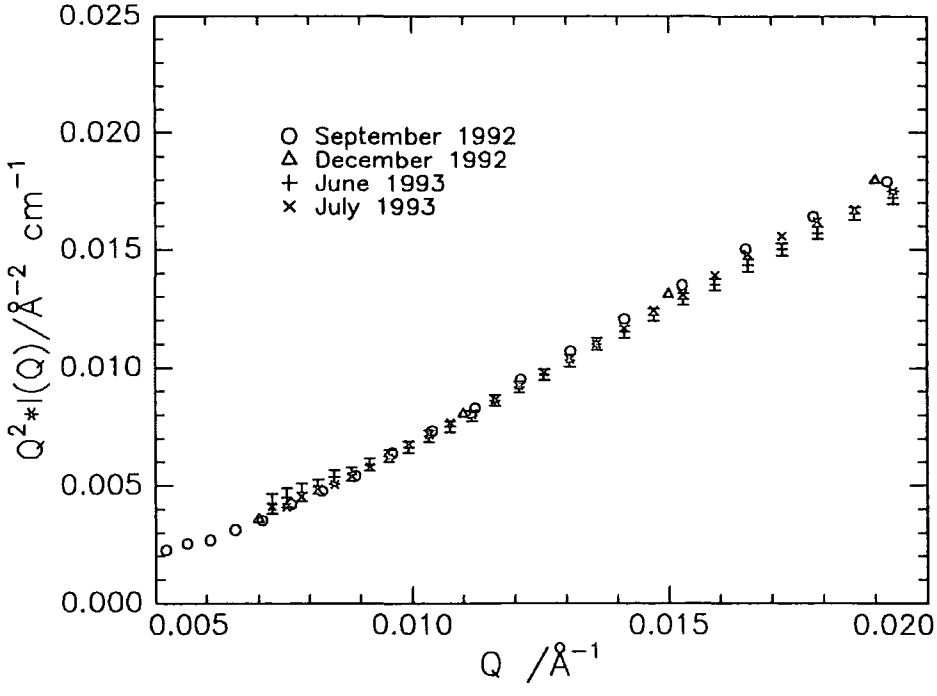

Figure 4.6: Detail of Figure 4.5 (above) showing the low Q region of the Kratky plots.

There are several sources of error in this calibration procedure: the uncertainty in the molecular weights of the polymers and hence in N, the influence of non-zero χ values and the uncertainty in the density and hence the segmental volume and the possibility that the copolymer is not a sufficiently good measure of the background scatter. Segmental volumes for d-PS and h-PS were calculated from values for the density of d-PS and h-PS in Russell[7] (a general review of neutron reflectometry). Davidson[8] has measured values for the density of h-PS and d-PS, the average value for the segmental volume is lower (1.653×10^{-22} cm^3 compared to 1.725×10^{-22} cm^3), Davidson's value for the density of h-PS is in agreement with the value for h-PS in Brandrup and Immergut[9]. This difference in segmental volumes results in a 4% reduction in the fitted value of k_N.

The N used were the average of values obtained using THF SEC, using the average of N_H and N_D makes a small difference to the value of k_N fitted, but values of N obtained using the $CHCl_3$ SEC are rather lower than those measured by THF SEC. Using the average of the values obtained using $CHCl_3$ SEC to calculate N produces a 20% increase in the fitted value of k_N. Finally there is the influence of χ on the fitted value of k_N, Wignall *et al*[4] states that the influence of χ on the scattering from low molecular weight polymers is negligible, thus χ was initially set to zero. However, if χ is fixed at values indicated by Bates *et al*[10] then values of k_N fitted are up to 10% lower than for $\chi = 0$, the normalised χ^2 parameter is slightly lower for $\chi \neq 0$ than for $\chi = 0$. Table 4.6 is a compendium of k_N values that have been obtained by fitting the data from the July 1993 calibration measurements.

	N_H	N_D	R_g /Å	V /cm^3	χ	k_N	'χ^2/N_p'
1	800	800	71.1	1.725×10^{-22}	0	0.952	2.12
2	835	770	71.1	1.725×10^{-22}	0	0.989	2.12
3	835	770	71.2	1.653×10^{-22}	0	0.948	2.12
4	740	635	71.1	1.653×10^{-22}	0	1.149	2.12
5	740	635	69.5	1.653×10^{-22}	1.6×10^{-4}	1.092	2.12
6	740	635	68.9	1.653×10^{-22}	2.1×10^{-4}	1.074	2.09
7	740	635	67.3	1.653×10^{-22}	3.7×10^{-4}	1.016	2.06

Table 4.6: Compendium of fitted k_N values. Average value of k_N = 1.03(7)

Items 1 and 2 in this table show the effect of averaging N_H and N_D, 2 and 3 show the effect of using values of V calculated from Davidson rather than Russell, 3 and 4 show the effect of using values of N_H and N_D from $CHCl_3$ rather than THF SEC and finally items 4-7 show the effect of non-zero values of χ. The values of χ are those calculated at the measurement temperature (2.1×10^{-4}) and the temperatures at which the sample was pressed (3.7×10^{-4}). 'χ^2/N_p' is the normalised χ^2 parameter of the fit, the values in this table represent good fits.

The conclusion from this calibration work is that uncertainty in the molecular weights of the polystyrenes used in the calibration sample limit the accuracy of the calibration procedure to ±10%, this accuracy could be improved by measuring the molecular weight of the polymers using light scattering and by running this calibration sample on other neutron sources. Despite the uncertainty in the absolute accuracy of the calibration procedure all the data in this thesis should be on the same relative scale.

4.2.4 Background Subtraction

The scattering function of interest in this work is the elastic coherent scattering, I(Q), of the polymer blend. What was initially measured was the total scattering of the sample and the sample cell which is a sum of elastic coherent, elastic incoherent, and inelastic incoherent scattering from the sample and the sample cell. The sum of all of the scattering that is not elastic coherent scattering will be referred to as the 'background' scatter. To correct for the background scatter pure hydrogenous and pure deuterated samples of the polymers in each blend were run at each temperature at which the blends were run. A weighted sum of the scattering from the pure components was made such that it matched the composition of the blend. These pure polymers produce no elastic coherent scattering but will provide a measure of all the incoherent and inelastic processes that the blend exhibits. Subtraction of the sample cell scattering is implicit because both blend and pure polymer samples are held in identical cells and the weighted sum of scattering from the pure polymers will contain contributions from the equivalent of one sample cell. Figure 4.7 shows representative scattering from various pure hydrogenous and deuterated polymers and the scatter from a sample cell.

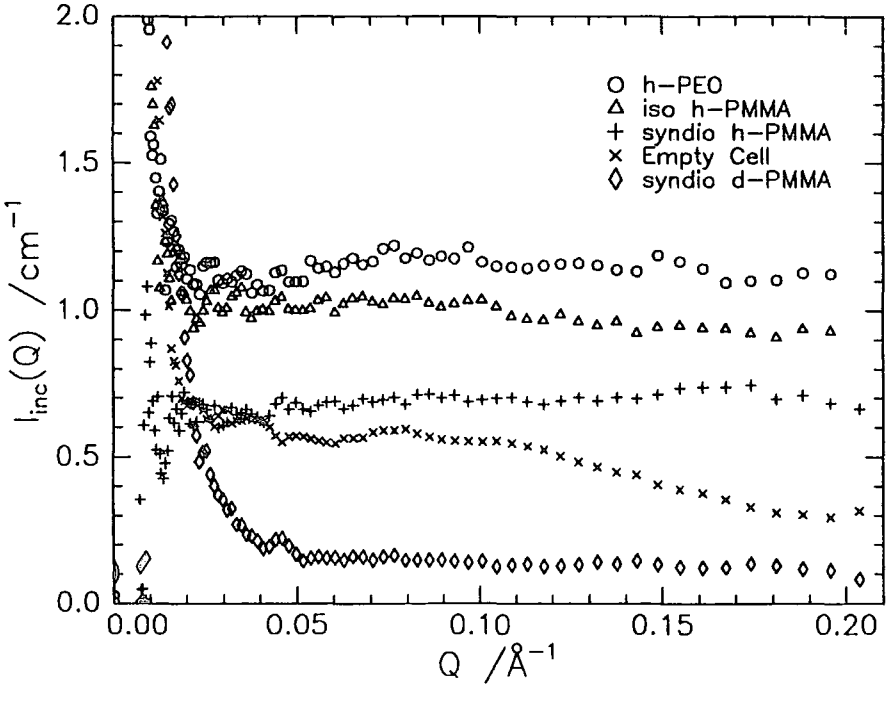

Figure 4.7: Scattering from pure hydrogenous and deuterated polymers, and the empty sample cell.

It is clear that the background scattering arises substantially from the hydrogenous polymers, this is due to the much larger incoherent scattering power of hydrogen compared to deuterium. This method of background subtraction has been used extensively in SANS work of this type. Comparisons of the scattering from pure hydrogenous polymers with scattering predicted solely from the bound atom incoherent scattering cross-sections of the constituent atoms show that there are considerable contributions to the background scattering from inelastic processes. This has been commented on in the literature[11,12,13] , these inelastic processes cannot be evaluated theoretically and so an a priori calculation of the background scattering is not possible.

4.2.5 Data Analysis Methods

The equations used to analyse the Small Angle Neutron Scattering (SANS) were presented in Section 2.1, in this section the 'mechanics' of the fitting process are described. A series of FORTRAN programs were written to perform non-linear least squares to the scattering data, using the Random Phase Approximation. These programs were based on the FITFUN[14] interactive fitting routine, which uses a Marquardt - Levenson[15] fitting algorithm, in this work the fit was weighted by the error in I(Q). Four programs were used in the analysis of the scattering data:

Pullet	the most basic version, which assumes that both blend components are monodisperse and have equal segment volumes, V.
Pullet2	mondisperse blend components with different segment volumes.
Pullet3	blend components with a Schultz - Zimm distribution of molecular weights and different segment volumes.
Pullet4	monodisperse blend components with different segment volumes and a residual background.

Listings of these programs are in Appendix 10.4. All the programs display the data in Kratky form, $Q^2I(Q)$ vs Q, in this form the differences between the fit and the data are more apparent, particularly at higher Q. Values for the volume fraction of deuterated polymer, ϕ, degrees of polymerisation, N_i, segment volumes, V_i, and scattering lengths, b_i. were all fixed. Values for V_i were calculated from literature values for the polymer densities (see Table 4.7), values for the nuclear scattering length were calculated from the literature, values of N_i were calculated from the weight average molecular weight of

the polymers (measured by size exclusion chromatography) and the monomer masses. It was assumed that there was no volume change on deuteration. R_{gH}, R_{gD} and χ were fitted, after an initial attempt the 'step size', i.e. the amount by which parameters were varied during each iteration of the fit, was reduced. FITFUN generates estimates of the uncertainty in the fitted parameters, based on the shape of the local fitting minimum. It was found that χ rapidly reached a well defined value, i.e. with a small uncertainty, the radii of gyration of the blend components were fitted rather poorly because the scattering is sensitive to the combination of the radii of gyration rather than the individual values.

Straight line fits to the Ornstein - Zernike plot were carried out using GENPLOT[16]. No statistical error weighting was used, so the points at low Q where the error due to the subtraction of the direct beam is large were excluded from the fit.

Polymer	Scattering length /cm^{-1}	Segment volume /cm^3
isotactic d-PMMA	[a]9.821×10^{-12}	[c]1.359×10^{-22}
isotactic h-PMMA	[a]1.493×10^{-12}	[c]1.361×10^{-22}
syndiotactic d-PMMA	[a]9.821×10^{-12}	[d]1.446×10^{-22}
syndiotactic h-PMMA	[a]1.493×10^{-12}	[d]1.444×10^{-22}
d-PEO	[b]4.58×10^{-12}	[e]0.716×10^{-22}
h-PEO	[b]0.41×10^{-12}	[e]0.718×10^{-22}

Table 4.7: Segment volumes, V_i, and scattering lengths, b_i, of the polymers used in this work. Values from (a) T.P. Russell, *Material Science Reports*, 5, (1990), 171, (b) J.R. Henderson, PhD Thesis, 1992, (c) 'Polymer Handbook 3rd edition pp V/19', J. Brandrup, E.H. Immergut, John Wiley & Sons, 1989. (d) *ibid*, V/77, (e) S. Cimmino, E. Martesculli, C. Silvestre, *Polymer*, 30, (1989), 393.

4.3 Neutron Reflectometry

4.3.1 Sample Preparation

Thin film samples for neutron reflectometry and nuclear reaction analysis were prepared by spin casting. In both cases polished silicon substrates were used with orientations <100> and <110>, no attempt was made to remove the silicon oxide layer that is found on such substrates. Substrates for neutron reflectometry were disks 50mm in diameter and 5mm thick, for the nuclear reaction analysis similar disks 1.25mm thick were used. The silicon was used as received or if re-used the following cleaning procedure was applied: washing in chloroform followed by wiping using optical tissue, soaking overnight in AR toluene followed by 15 minutes in an ultrasound bath, whilst immersed in fresh toluene, and a final wipe with optical tissue.

Spin casting was done using a Dynapert Precima Ltd photoresist spinner. An aliquot of the required polymer solution was placed on the silicon substrate, typically circa 0.5cm^3 was used and this covered 75% of the polished surface, the substrate was immediately spun for 30-60 seconds. The thickness of films prepared in this way can be controlled by varying the concentration of the casting solution or the spinning speed. It was found that varying the casting solution concentration was the more flexible method of controlling the film thickness. A discussion of the film formation process during spin casting can be found in reference 17 .

After spin casting all but the dibutyl phthalate/polystyrene films were allowed to dry overnight under vacuum at room temperature. Any annealing procedure was further to this initial treatment.

The thicknesses of films were measured using contact profilometry. This is a mechanical measurement achieved by measuring the displacement of a stylus as it is drawn across small scratches made in the film, exposing the substrate. The precision of this technique is of the order of 50 to 100Å.

4.3.2 CRISP

All the neutron reflectometry results presented in this work were carried out using the CRISP reflectometer on the ISIS pulsed neutron source at the Rutherford Appleton Laboratory. The aim of the neutron reflectometry experiment is to measure the neutron reflectivity, R, as a function of the scattering vector Q where:

$$Q = \frac{4\pi}{\lambda}\sin\theta$$

Equation 4.1

and

$$R = \frac{I_r}{I_o}$$

Equation 4.2

where λ is the neutron wavelength and 2θ is the scattering angle (the angle between the plane of the sample and the incident beam is θ). I_r is the reflected intensity and I_o is the incident intensity of the neutron beam. CRISP is a variable wavelength instrument, where the principle method of covering the Q range is by variation of λ.

Figure 4.8 is a schematic of the CRISP instrument. Neutrons travel from the moderator, which lies to the left of the region shown in this figure through the sample position (X) to the detector (D) on the right. CRISP uses neutrons from the hydrogen moderator and utilises every pulse generated (i.e. has an operating frequency of 50Hz). The disc chopper (C) selects a wavelength range circa 2Å - 6.4Å. This gives the Q ranges shown in Table 4.8, for the incident angles θ of 0.25°, 0.6° and 1.2° used in this work.

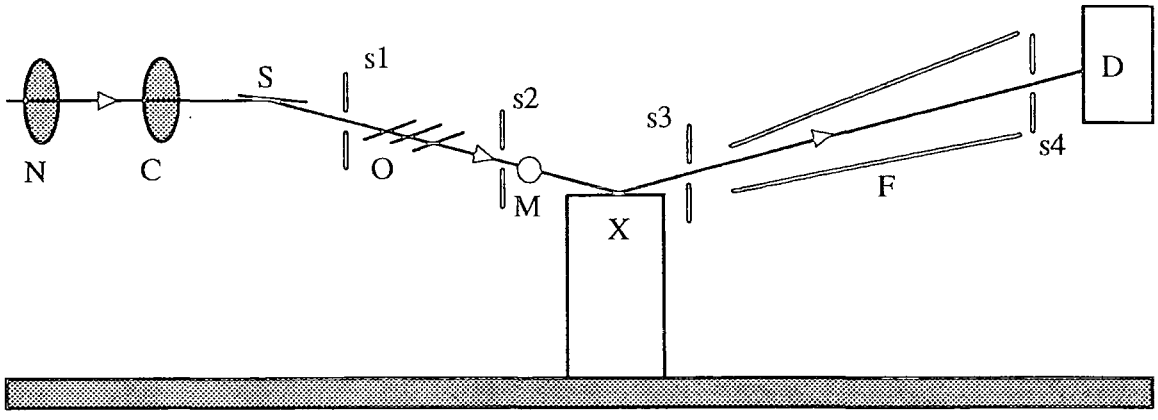

Figure 4.8: Schematic illustration of CRISP, side elevation. Key to symbols is in text.

Incident Angle (θ/2)	$Q/Å^{-1}$ range	
0.25°	0.009	0.027
0.60°	0.021	0.065
1.20°	0.041	0.132

Table 4.8: Q ranges probed by CRISP using various incident angles.

The neutron beam is crudely collimated between the moderator and the region shown in this figure. It is subsequently collimated more finely by slits, s1 and s2, the aperture height of these slits determines the geometric resolution, ΔQ/Q, given by the equation below:

$$\left(\frac{\Delta Q}{Q}\right) = \frac{\tan^{-1}\frac{(s1+s2)}{2d_s}}{\theta}$$

Equation 4.3

s1 and s2 are the heights of the two collimation slits, d_s is the sample to detector distance and θ is the incident angle. The slit widths are generally fixed at 30mm, these widths do not effect the resolution in Q. The collimated neutrons are reflected from the sample at X and then pass through further slits, s3, and the funnel, F, to the detector which is either a single detector or a 1-dimenional multidetector.

The function of the funnel, which is covered in boron impregnated resin - a strong absorber of neutrons - is to reduce the level of background radiation impinging on the detector. The detectors are also heavily shielded with boron impregnated resin. A number of other measures are taken to reduce background count rates; when the protons strike the tantalum or uranium target a pulse of high energy neutrons and γ-rays is produced, a proportion of the neutrons are not moderated and these along with the γ-rays, will contribute to the background. The nimonic chopper, N, is timed such that it blocks the view of the target during the period of the proton pulse and the supermirror, S, will reflect neutrons in the useful wavelength range but high energy neutrons and γ-rays will pass straight through. This means that the sample position and detectors are offset from a direct line view of the target and a major source of background counts. The frame overlap mirrors, O, reflect long wavelength (slow) neutrons originating from previous pulses, the shorter wavelength pass straight through. In addition to these measures further procedures in the data analysis are used to measure background counts and correct for them in the output data.

The beam monitor, M, is used to measure the incident beam flux, I_o, this and a further beam monitor are also used for diagnostic purposes to ensure useable neutrons are reaching the sample position.

The function of the sample position is to present the samples to the neutron beam at the appropriate angle, in addition provision for the automatic changing can be made. Since the samples used here are reflective to light the sample is aligned with a laser coincident with the neutron beam. In this work the sample position was used in two configurations:

(1) Single sample, (automatic) angle control.

(2) Multiple sample, manual angle control.

In the first configuration a single sample is run at all the required incident angles and the sample is then changed manually. The second configuration is a four position sample changer which moves the samples horizontally and perpendicular to the neutron beam. The samples are attached, by suction, to four separate manual goniometers. The four samples are aligned and can then be run in sequence under automatic control. Some problems were experienced with the goniometers shifting during movement of the sample rack, this is particularly worrying when the single detector is used because if the sample angle changes the specularly reflected beam misses the detector.

Two detectors are available for use on CRISP:

(1) 1 dimensional position sensitive multidetector, this is a BF_3 gas filled detector with a sensitive area 250mm high, this area is encoded as horizontal strips with a spatial resolution of around 1mm. The advantages of the multidetector are that it is flexible - able to measure specular and off specular reflectivity in a single measurement and the alignment is less demanding since there is a large detector area to aim at and the position of the specular reflection can be determined precisely. The background level can be measured quickly and directly from the signal collected away from the specular peak in the plane of the detector.

(2) Single detector, this is a single scintillation detector element providing no information on the vertical position of the detected neutrons. The single detector is used with additional slits, s4, immediately before the detector position. The advantage of the single detector is that it has a higher sensitivity and lower intrinsic background than the multidetector.

For this work the preference was to use the multidetector, however this is not a critical decision since the specular reflectivity, R, is identical regardless of the detector.

On each occasion that experiments were done a direct beam measurement was made in order to provide a reference position for determining the angle of reflection. Data were then obtained for each sample in terms of counts versus time (for the single detector or counts versus (time, position) for the multidetector. Where the time is the time of the last proton pulse and is directly related to the wavelength of the detected neutron. The initial data reduction was carried out using a suite of programs in the GENIE environment. Single detector data was reduced in a single step to un-normalised R(Q) using the program @g:norm which corrects for detector efficiency and incident beam flux, as measured by the beam monitor, M. Multidetector data was reduced in a two stage process, firstly a plot of total counts versus position on the multidetector, x, was obtained using @g:multidet. A typical example of such a plot is shown in Figure 4.9. The exact angle of incidence was calculated from the centre of the specular peak, which is found either by eye or using a Gaussian peak fitting routine. The second stage of the reduction was done using the program @g:norm_md2. The reflectivity, R, at each value of Q was obtained by integrating over x. At this point a background subtraction can be made by assuming that the background under the specular peak can be obtained by interpolating the background level either side of the specular peak and subtracting this from the specular peak.

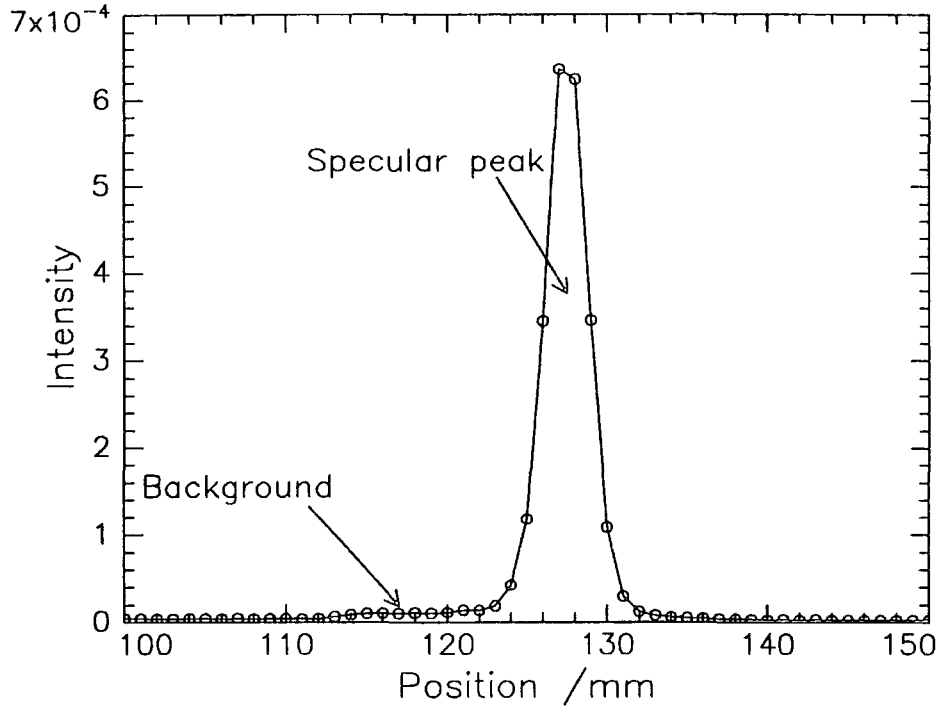

Figure 4.9: Typical output from the program @g:multidet of total neutron intensity versus position on neutron detector, showing the specular reflection peak and some background counts.

Using either the single or multidetector, data was produced in the form of up to three separate datasets per sample of R(Q), covering different overlapping Q ranges, arising from the different incident angles. This is illustrated in Figure 4.10.

The reflectivity, R, may be on different scales, and this scale will not be an absolute scale. Normalisation was carried out by multiplying the data collected at the lowest angle by a factor such that the reflectivity in the region of total reflection, observed for all the samples in this work, is one. Data collected at higher angles were normalised by eye to this lowest angle dataset using the region of overlap.

After normalisation the data from different incident angles were 'rebinned' into the same Q interval and Q resolution and then combined into a single dataset using either the program @g:combine or the program WELDER written at Durham. @g:combine will crash if there are negative values of R in any of the datasets to be combined, negative values of R arise in multidetector detector at high Q values where there may be slight over-subtraction of the background.

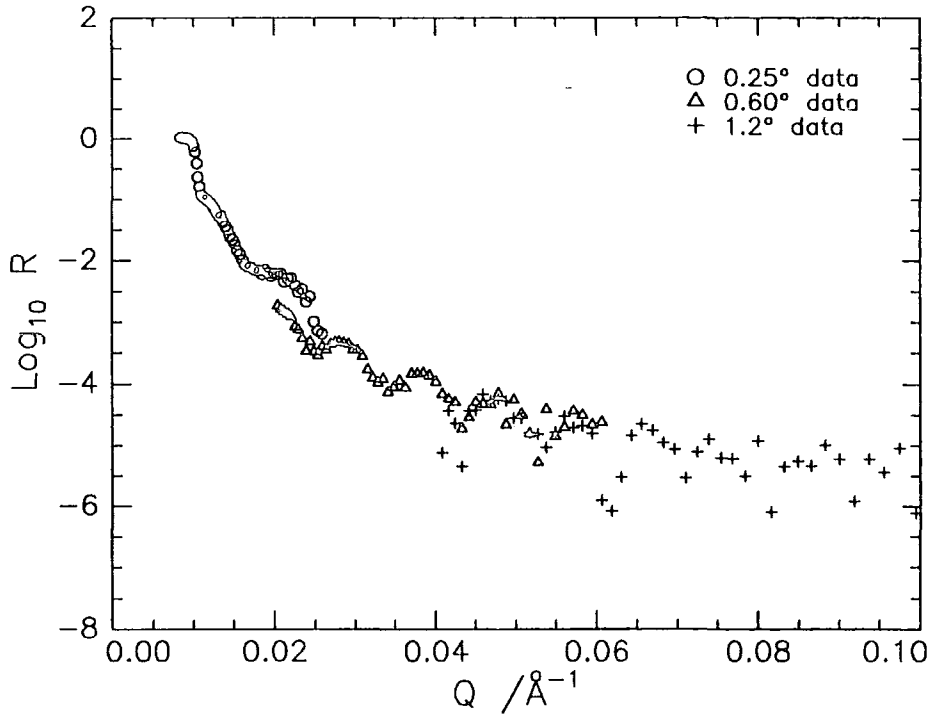

Figure 4.10: Reflectivity data collected from the same sample at three different incident angles. 0.25° data normalised to 1 in region of total reflectivity, other data un-normalised.

If the single detector was used then the reflectivity was measured up to a Q value where R is independent of Q. This value is taken to be the background level and is then subtracted from the whole Q range. For the samples used here the background for the single detector was very small and the subtraction of this background had little effect on the fitted composition profile.

The result of this data reduction was to produce a single file of R(Q) data, with errors in R calculated from Poisson statistics, for each sample run. Before continuing two comments will be made:

(1) For the purposes of combining data collected at different angles the presence of Kiessig fringes in the reflectivity can be very useful because they provide a rigorous check on the incident angles θ used in the data analysis, if the values are wrong then there will be a mismatch in the fringes in the overlap regions.

(2) Throughout this work data collected at different angles has been combined to form one large dataset. There may be some merit in keeping the data collected at different angles separate and analysing the separate datasets as a group.

4.3.3 Data Analysis Methods

The principles by which the neutron reflectivity of a model profile can be calculated were outlined in Section 3.1.2. Model composition profiles were fitted to the reflectivity data using two methods:

(1) The FORTRAN program PHOENIX, written at Durham. PHOENIX utilises the FITFUN[14] routine, which is itself based on a Marquardt-Levenson[15] algorithm. A listing of this program can be found in Appendix 10.4. The program includes multilayer models, with Gaussian roughness, for up to 4 layers, in addition there are also functional form models based on the modified exponential function:

$$\phi(z) = \phi_B + (\phi_1 - \phi_B)\exp\left(-\left(\frac{z}{\xi}\right)^{\beta}\right)$$

Equation 4.4

and a Tanh profile:

$$\phi(z) = \phi_B + \frac{(\phi_1 - \phi_B)}{2}\left\{1 + \tanh\left(\frac{2(z_{off} - z)}{w}\right)\right\}$$

Equation 4.5

Where $\phi(z)$ is the volume fraction of the deuterated component as a function of depth, z, from the air - polymer interface. These profiles are approximated using layers of equal thickness - generally 15Å thick -although this thickness is under user control. These functional form profiles can be placed either at the air - polymer, polymer substrate or both interfaces. Resolution effects are accounted for by convoluting the model reflectivity with a box function of the appropriate width. PHOENIX uses the Fit Index (F.I) as the measure of the fit quality. The Fit Index is given by:

$$F.I. = \frac{1}{N_p}\sum_i\left(\frac{\log R_m - \log R_D}{(\Delta R_D / R_D)}\right)^2$$

Equation 4.6

Where N_P is the number of data points, R_m is the calculated reflectivity and R_D is the experimentally measured reflectivity and ΔR_D is the statistical error in the measured reflectivity. The Fit Index differs slightly from the usual measure of the merit of fit, the normalised χ^2 parameter (χ^2/N_P) which is given by:

$$\frac{\chi^2}{N_P} = \frac{1}{N_P}\sum_i \left(\frac{R_m - R_D}{\Delta R_D} \right)$$

Equation 4.7

The relationship between χ^2/N_P and F.I. is illustrated in Figure 4.11. The original motivation for using the Fit Index was a rather small computational advantage, limited tests show that the fits obtained using the normalised χ^2 parameter and the Fit Index are identical within the statistical error. However it would be wise to convert PHOENIX to use the more common χ^2/N_P.

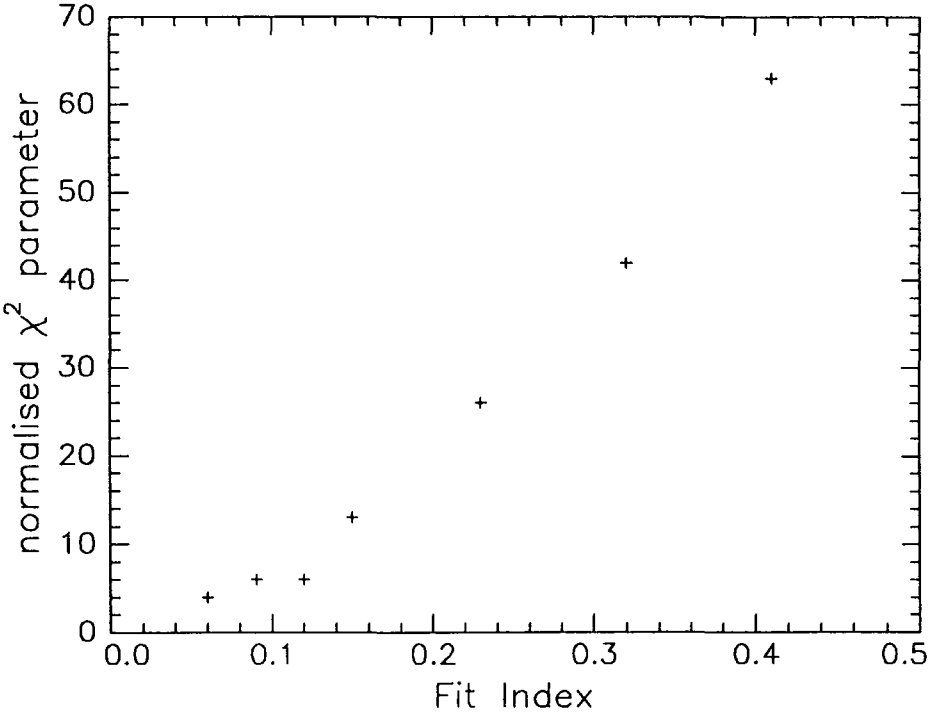

Figure 4.11: Plot to illustrate the relationship between the Fit Index and the normalised χ^2 parameter. (Data from multilayer fits to d-DBP/PS data).

In addition to fitting data, PHOENIX can also be used to generate model reflectivity profiles either from its intrinsic functional forms or from arbitrary $\phi(z)$, read

in from an ASCII file. Furthermore 'maps' of the Fit Index as a function of 1 or 2 model parameters can be made.

(2) The program VOLFMEM, written by D. Sivia currently at the Rutherford-Appleton Laboratory. VOLFMEM is based on a maximum entropy algorithm, the principles of which are outlined in reference 18 . Briefly, in addition to the merit parameter χ^2/N_P, the 'entropy' of the current model is also evaluated. The 'entropy' of a model corresponds crudely to how 'reasonable' a model looks, without reference to the experimental data. Models with high entropy will be favoured over models with low entropy even if both models have the same normalised χ^2 parameter. The entropy of the model can be measured relative to a uniform profile (as was done in this work) or some sort of preferred prior model. Using the additional entropy constraint it is possible to fit the composition profile with a 'free form' where the composition profile is divided into a large number of layers (up to 255) of equal thickness and the composition of each layer is allowed to vary. This can lead to unphysical profiles, in particular sharp changes in the composition profile - which in general are unphysical because of the size of the polymer chain - are observed. So as an additional constraint a so called 'internal correlation function (ICF)' is applied to the composition profile, this smoothes out sharp changes in composition, typically an ICF of scale 75Å - 100Å was required to obtain composition profiles with the minimum of sharp changes in composition.

In both these programs the composition profile data is presented in terms of the volume fraction of the deuterated component as a function of depth, it is the scattering length densities, ρ_N, that are actually used in the calculation of the reflectivity. Table 4.9 (overleaf) is a compendium of the values of ρ_N for pure polymers used in this work.

Component	$\rho_N / Å^{-2} \times 10^6$
h-PMMA	1.034
d-PMMA	6.792
h-PS	1.399
d-PS	6.409
h-PEO	0.652
d-PEO	7.062
d-DBP	6.186
Si	2.095
SiO_2	3.676

Table 4.9: Nuclear scattering length densities used in this work.

4.4 Nuclear Reaction Analysis (NRA)

Samples for NRA experiments were prepared in a manner very similar to that used for the NR experiments, but instead of spin casting onto thick silicon blocks, thin silicon wafers were used. After the film had been cast the wafer was broken up into pieces, ideally 30mm×10mm, using a diamond tipped glass knife, in practice the pieces varied in size.

Figure 4.12 is a schematic illustration of the instrument used in this work, the SERC Device Fabrication Facility at the University of Surrey, Guildford. $^3He^+$ are accelerated by a Van der Graaf generator to energies of up to 3 MeV. The bending magnet, B, guides the $^3He^+$ down the appropriate beam line. The slits s1 and s2 are used to guide the beam to the target via a feedback loop, if the beam falls preferentially on either the left or right hand side of the slits then a small current is produced and this is used to steer the beam back to the centre of the slits The entire beam path is held under high vacuum, to maximise the flux of $^3He^+$ to the sample. The beam then strikes the sample at X, in this work the sample was generally fixed at an angle of 15° to the incident beam, in order to optimise the resolution perpendicular to the sample surface. The sample holder can be cooled with liquid nitrogen, if the sample is susceptible to

beam damage. The sample holder is earthed to prevent a build up of charge on the sample. Samples are introduced to the sample chamber via an airlock.

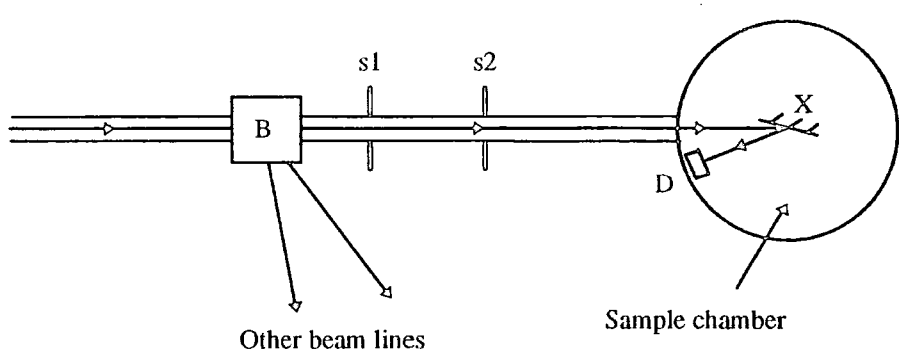

Figure 4.12: Schematic diagram of the NRA apparatus, plan view. Key to symbols in text. (Not to scale).

Particles generated at the sample are detected by the silicon surface barrier detector, D, which is at an angle of 165° to the incident beam. These particles include elastically scattered $^{3}He^{+}$, which have a relatively low energy and the products of the nuclear reaction ^{4}He and p. Data of counts versus channel number (which is related linearly to energy) are collected using a dedicated I/O board on a PC. It is the p energy spectrum that is used to produce the composition depth profile in this work. In order to calibrate the channel number to an absolute energy scale, a calibration package containing three α-emitters (^{244}Cm, ^{241}Am, ^{239}Pu) with known energies is included in the sample chamber.

Samples were run with a $^{3}He^{+}$ beam energy of 0.7 MeV or 0.75 MeV for the background sample (a ~1 μm thick pure d-PS film). The beam current used was generally in the range 70-100nA. Typical count times were of the order of 15-20 minutes for the samples containing most deuterated material, and up to 1½ hours for samples containing only 0.05 volume fraction deuterated material.

The raw experimental data of counts versus channel number were reduced using programs written by A. Clough at University of Surrey. The first stage of this reduction is to convert the data to an absolute energy scale using the energy per channel calculated from the calibration package (typically 9.6 Kev/channel). The sample counts are then divided by the background (d-PS) sample counts to correct for the cross-section of the $^{3}He^{+}$ + ^{2}H reaction which varies as a function of incident $^{3}He^{+}$ energy. The maximum cross-section is at an energy of 0.7 MeV. The background sample is run at a slightly

higher incident beam energy than the sample so that the front edge of the p energy spectrum (corresponding to protons produced in reactions at the very surface of the polymer film) lies at a slightly lower energy than the front edge for the sample of interest. This reduces the risk of a slight mismatch in beam energies leading to a poor background correction at the front edge.

Following the background correction the data are converted to counts versus depth scale using the known stopping powers of $^3He^+$ in polystyrene and the theory of elastic collisions. The counts are normalised to a composition scale by multiplying the data by a normalisation constant such that the integral of the data over the sample thickness matches the nominal volume fraction of the deuterated component in the film. Statistical errors are calculated from the counts using Poisson statistics.

4.5 Attenuated Total Reflection (ATR) infra-red spectroscopy

Samples for ATR spectroscopy were prepared by spin casting the polymer solution directly onto the ATR crystal, which in this case was a silicon parallelepiped (10mm × 5mm × 50mm) with an angle 45°. No attempt was made to remove the native silicon oxide layer that will be present on this substrate. The casting procedure was virtually identical to that used to cast films for NR and NRA; a special adapter was designed to facilitate the attachment of the ATR crystal to the chuck of the spin caster. No problems were encountered, in terms of damage to the ATR crystal, for spinning speeds up to and above 4000 rpm. The shape of the ATR crystal - a narrow rectangle as opposed to a disk - means that the film cast on the crystal is uneven in thickness towards the ends of the crystal. For this reason the polymer film was removed from the first ~1 cm from each end (as well as from the entry and exit faces of the crystal) using an optical tissue moistened with AR toluene.

All the ATR data presented in this work were obtained using a Perkin Elmer 1600 with a Specac variable angle ATR unit, which is illustrated in Figure 4.13.

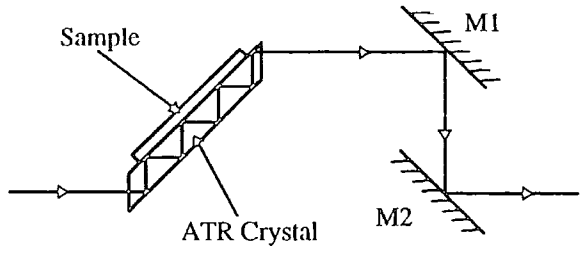

Figure 4.13: Schematic illustration of the Specac Variable ATR unit, plan view. Key to symbols in text. (Not to scale)

The infra red beam enters at the left and passes through the entry face of the ATR crystal, where it undergoes multiple internal reflections. The stage on which the ATR crystal is mounted can be rotated, however in this work it was fixed such that the incident beam past through the entry face of the crystal normal to its surface. The mirrors M1 and M2 are used to couple the infra red beam leaving the ATR crystal to the detector, which lies to the right of the region illustrated in the figure. The first step in each measurement is to take an 'empty beam' spectrum without the ATR unit in the optical path, this spectrum is used to correct data for absorption by atmospheric water and carbon dioxide and for the variable energy output of the infra-red source across the wavelength range. All spectra are automatically ratioed by this empty beam measurement. The ATR unit is then placed in the optical path and the energy throughput is maximised by adjusting the mirrors m1 and m2. Before any measurements are made on a polymer sample, the ATR spectra of the bare silicon crystal is obtained, this is done so that the absorption of the silicon crystal can be accounted for. The spectrum of the polymer film alone is obtained by subtracting the absorption spectrum of the bare silicon from the spectrum of silicon crystal with polymer film.

The water and carbon dioxide absorption bands are not exactly subtracted, because the concentration of water vapour and carbon dioxide varies as a function of time (particularly if the experimenter breathes too close to the sample position!) and also because the fine structure of the water band varies as a function of pressure and so the bands will not subtract exactly if collected at different atmospheric pressures. These effects contribute to the random error found in Section 8.

All the spectra used in this work were the average of 64 scans (acquisition time ~ 5 minutes) and run at a resolution of $4.0cm^{-1}$. Some use was made of the intrinsic spectrometer functions to give background subtracted spectra a flat baseline - this is a cosmetic alteration. Absorption peak areas were calculated using the intrinsic peak area function of the spectrometer. If necessary data can be obtained in the form of an ASCII file of wavenumber versus absorption by converting the data to Lotus 1-2-3 format using the Perkin Elmer 1720 spectrometer software and then reading the Lotus 1-2-3 data into Microsoft Excel.

4.6 References for Section 4

1 . T. Kiff, unpublished results.

2 . I. R. Peat, W. F. Reynolds, *Tertrahedron Letters*, 14, **1972**, 1359.

3 . R.K. Heenan, S.M. King, ISSI Conference, Dubna, September 1992.

4 . G.D. Wignall, F.S. Bates, *Journal of Applied Crystallography*, 20, **1987**, 28.

5 . J. Schelten, reported in reference 4

6 . M. Rawiso, R. Duplessix, C.Picot, *Macromolecules*, 20, **1987**, 630.

7 . T.P. Russell, *Materials Science Reports*, 5, **1990**, 173.

8 . Neil Davidson, PhD Thesis, University of Strathclyde, 1984.

9 . J. Brandrup, E.H. Immergut, 'Polymer Handbook 3rd ed.', J. Wiley & Sons 1989, pp V/82.

10 . F.S. Bates, G.D. Wignall, *Physical Review Letters*, 57(12), **1986**, 1429.

11 . A.R. Rennie, R.K. Heenan, ISSI Conference, Dubna, September 1992.

12 . R.E. Ghosh, A.R. Rennie in 'Neutron Scattering Data Analysis 1990', ed. M.W. Johnson, Institute of Physics Conference Proceedings.

13 . A. Maconnachie, *Polymer*, 25, **1984**, 1068.

14 . FITFUN, R.E. Ghosh, Institut Laue Langevin, 1989.

15 . W.H. Press, S.A. Teukolsky, W.T. Vetterling, B.P. Flannery, 'Numerical Recipes in FORTRAN 2nd ed.', Cambridge University Press, 1992.

16 . GENPLOT, Computer Graphics Service Ltd, Ithaca, New York, 1991.

17 . D. Meyerhofer, *Journal of Applied Physics*, 49(7), **1978**, 3993.

18 . J. Skilling in 'Maximum Entropy in Action' ed. B. Buck and V.A. Macaulay, Oxford University Press, 1991.

This page left intentionally blank

The scattering data for blend I collected at temperatures 408K to 473K was analysed using the RPA modified for polymers with a Schultz - Zimm distribution of molecular weights. Fitting was carried out using the FORTRAN program Pullet3. Fitting was carried out over the range $0.0 < Q < 0.1 Å^{-1}$, the Q range was limited because deviations from the RPA expression were observed at higher Q values for all three blends (B, D and I), these deviations will be discussed later. Three variables were allowed to vary in the fitting process: χ, R_{gD} and R_{gH}. Values fitted for R_{gH} varied over a wide range, because the scattering was relatively insensitive to this parameter. Fits were generally rather poor, see Figure 5.3, with consistent mis-fitting in the low Q region, where the scattering is most sensitive to χ.

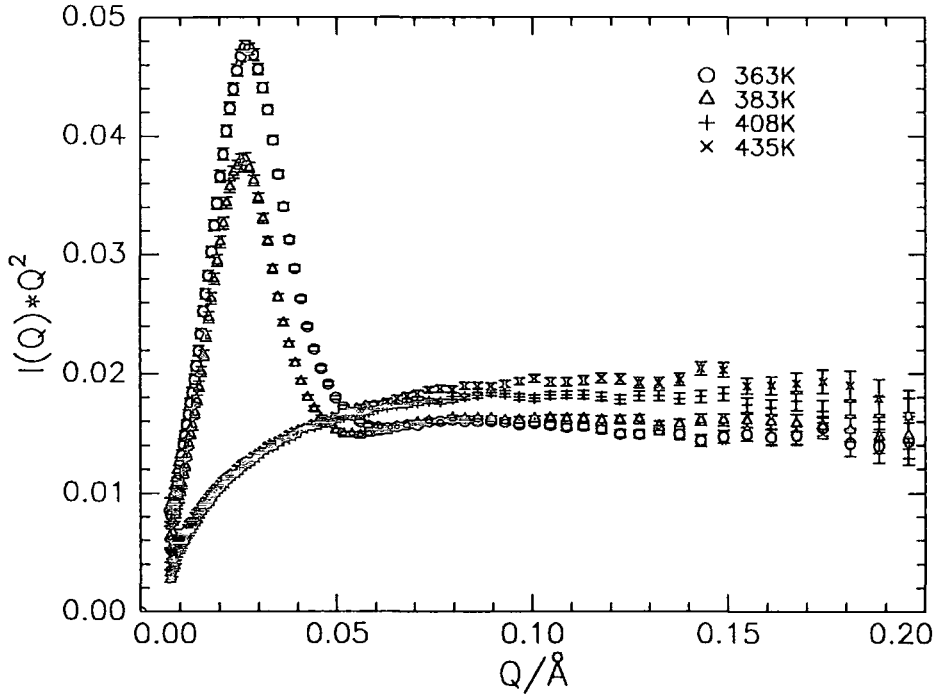

Figure 5.2: Kratky plots of blend I $\phi = 0.725$ data as a function of temperature, error bars from Poisson statistics.

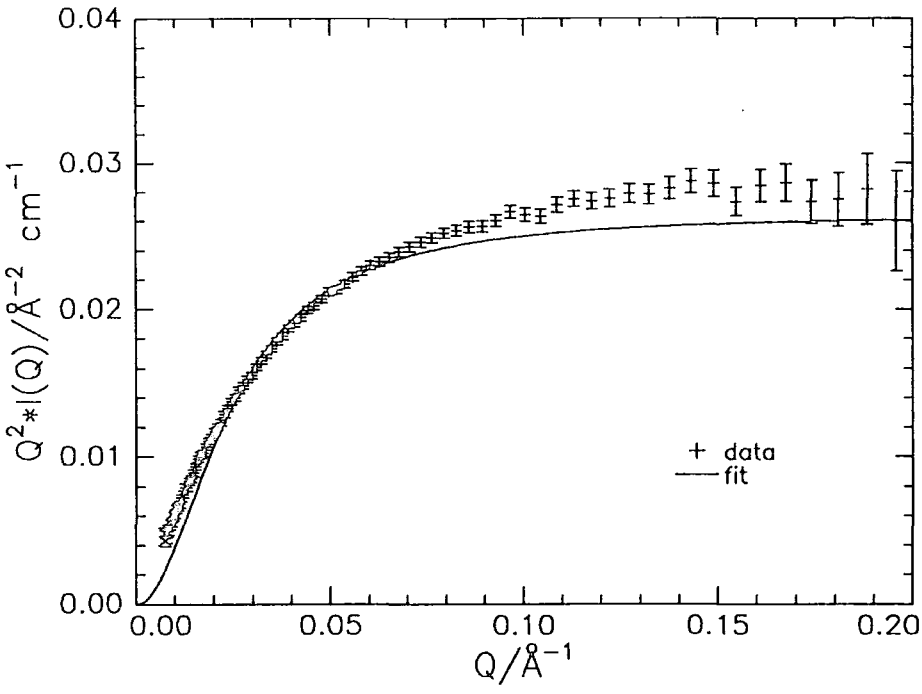

Figure 5.3: Sample fit of the modified RPA to the blend I data, ϕ = 0.478 at 453K, experimental error from Poisson statistics.

Figure 5.4 shows the variation of χ with reciprocal temperature and composition. Error bars are those calculated from the fitting procedure and do not include uncertainty derived from errors in input parameters such as the degrees of polymerisation of the blend components and their polydispersities. The χ values for the blends at 473K are rather more negative than the values obtained at lower temperatures. This may be caused by sample degradation at higher temperatures, at the end of the experiment the samples had turned brown and had a strong acrid odour. Flory - Huggins theory suggests a χ parameter which varies linearly with reciprocal temperature, for this reason fits of the form shown in Equation 5.1 were made to the χ data:

$$\chi = A + \frac{B}{T}$$

Equation 5.1

The parameters of these fits can be found in Table 5.3, the 473K data were excluded from these fits.

Composition ($\phi_{d\text{-}PMMA}$)	A	B
0.253	-0.016(3)	2(1)
0.478	0.010(5)	-7(2)
0.725	0.002(2)	-3(1)

Table 5.3: Parameters fitted to blend I χ data according to Equation 5.1

There is a fairly large variation of χ with composition, in particular values for the ϕ = 0.253 blend are rather more negative than for ϕ = 0.478 and ϕ = 0.725. Figure 5.1 shows that the scattering from the ϕ = 0.253 blend is considerably weaker than for the other two compositions, one would expect that at higher Q values the scattering from the ϕ = 0.253 and ϕ = 0.725 would be similar, having corrected properly for background scattering. This behaviour could be explained by an inappropriate transmission correction arising from the presence of macroscopic air bubbles in the sample.

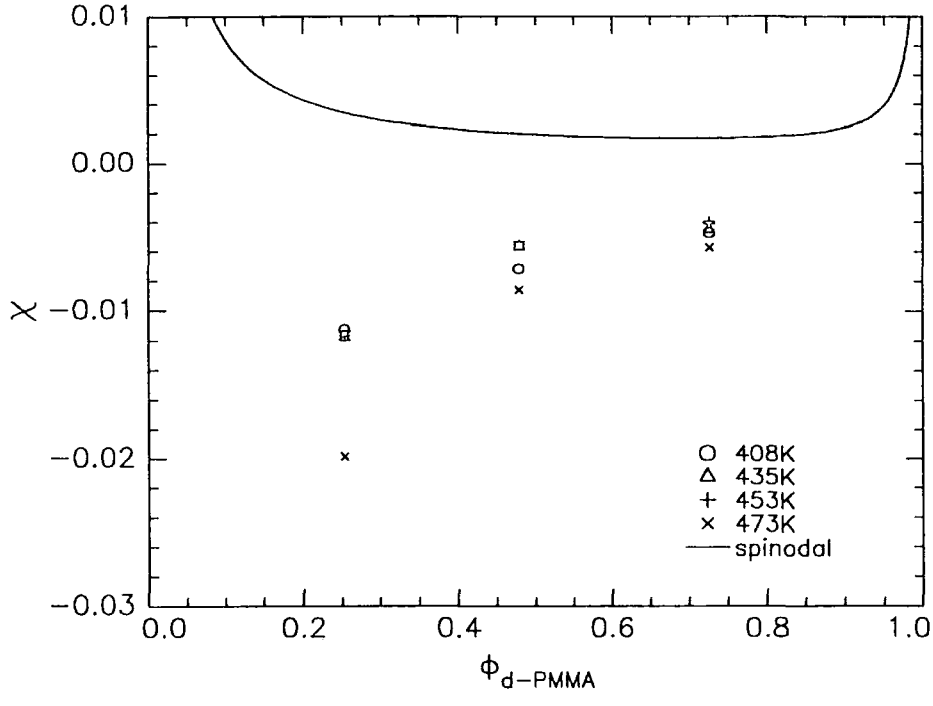

Figure 5.4a: χ vs $\phi_{d\text{-}PMMA}$ for blend I, with χ_s calculated from measured molecular weights, error bars on 453K data from fitting statistics

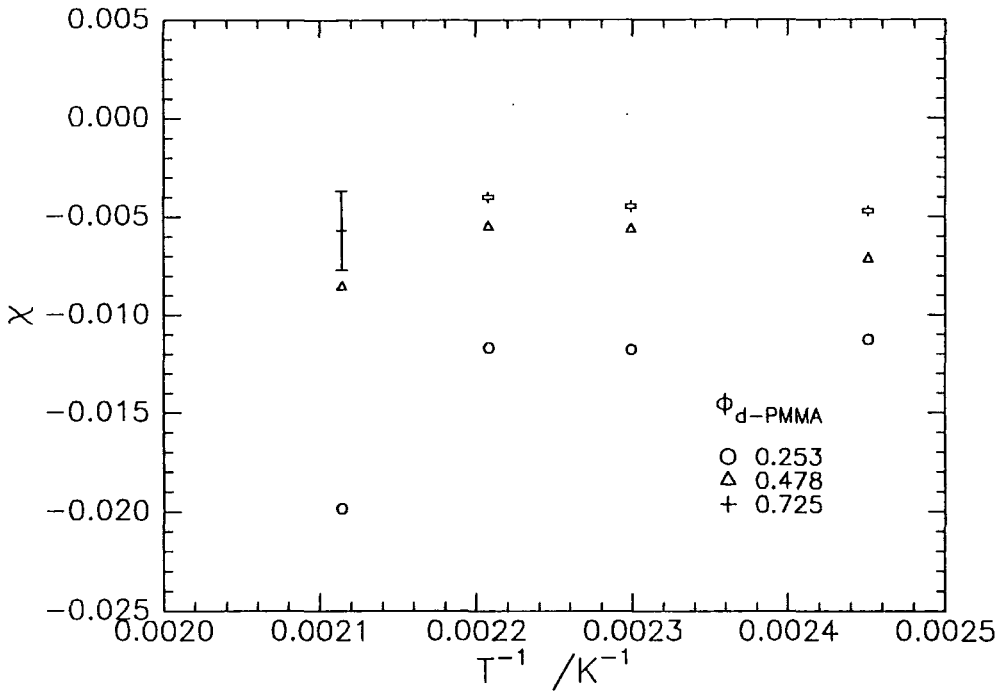

Figure 5.4b: χ vs 1/T for blend I, error bars on ϕ = 0.725 from fitting statistics

The average value for R_{gD} fitted for these data is 105±20Å this compares with 68Å calculated from literature[1] values of $<S_0/M_w^{½}>$ and the weight average molecular weight.

Turning to the syndiotactic blends B and D, it is apparent from Figure 5.1 that the scattering from blend B varies rather more with composition than for blend D. This is because the deuterated polymer in blend B has a smaller radius of gyration and so more of the scattering law is probed using the available Q range of LOQ. To use the low Q limit of the Debye expression QR_{gD} must be rather less than 1, using the literature values to calculate the radii of gyration for the deuterated polymers the low Q limit for blends B and D fall in the following regions:

Blend B	$R_{gD} \approx 40$Å	$0.0 < Q < 0.025$Å^{-1}
Blend D	$R_{gD} \approx 150$Å	$0.0 < Q < 0.0066$Å^{-1}

These values imply that the low Q limit may be used for the blend B data but for blend D the low Q limit lies below the Q range available on the LOQ diffractometer.

Figure 5.5 shows data from blend B plotted in the Ornstein - Zernike mode ($I^{-1}(Q)$ vs Q^2) suggested by the low Q limit of the Debye expression, the error bars are calculated from Poisson statistics. The fluctuation correlation length ξ is calculated from the slopes and

intercepts of these plots and χ is obtained from the intercept (given the value of χ_s calculated from the degrees of polymerisation of the blend components and the volume fraction of the d-PMMA). In general the data are linear over the Q^2 range $0.0002 < Q^2 < 0.0008 Å^{-2}$ but the data collected at 408K all show strong downward deviation from linearity at low Q (this corresponds to excess scattering at low Q), for this reason data collected at this temperature were fitted over the range $0.0004 < Q^2 < 0.0008 Å^{-2}$. This downturn in the Ornstein - Zernike plot may be due to phase separation[2] or the presence of voids that are subsequently annealed out at the higher measurement temperatures. If this is the case then χ and ξ values calculated at this temperature may well be meaningless. Data collected at 435K, 453K and 473K were fitted over the range $0.0002 < Q^2 < 0.0008 Å^{-2}$, the first few points, (below $Q^2 < 0.0002 Å^{-2}$) were not used because of difficulty in subtracting the remnants of the straight through beam not masked by the beam stop in this region. The straight line fit has been extended a little higher in Q^2 than the calculations of R_{gD} would seem to allow because the data remain linear in this slightly extended region.

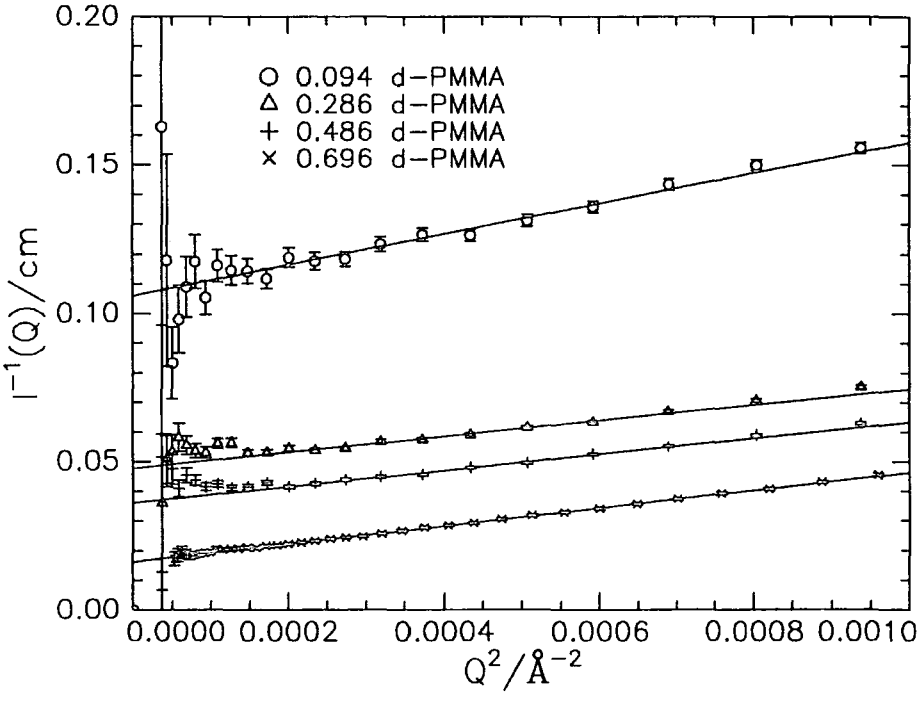

Figure 5.5: Scattering from blend B plotted in Ornstein - Zernike mode with linear fits, errors from Poisson statistics (473K data)

Figure 5.6 shows χ as a function of composition obtained from blend B, an upturn in χ is observed at low d-PMMA concentrations. Figure 5.7 shows χ and ξ^{-2} as a function of reciprocal temperature (in K^{-1}), extrapolating these plots to $\chi = \chi_s$ and $\xi^{-2} = 0$, respectively, for each composition gives the spinodal temperature, T_s, at that composition.

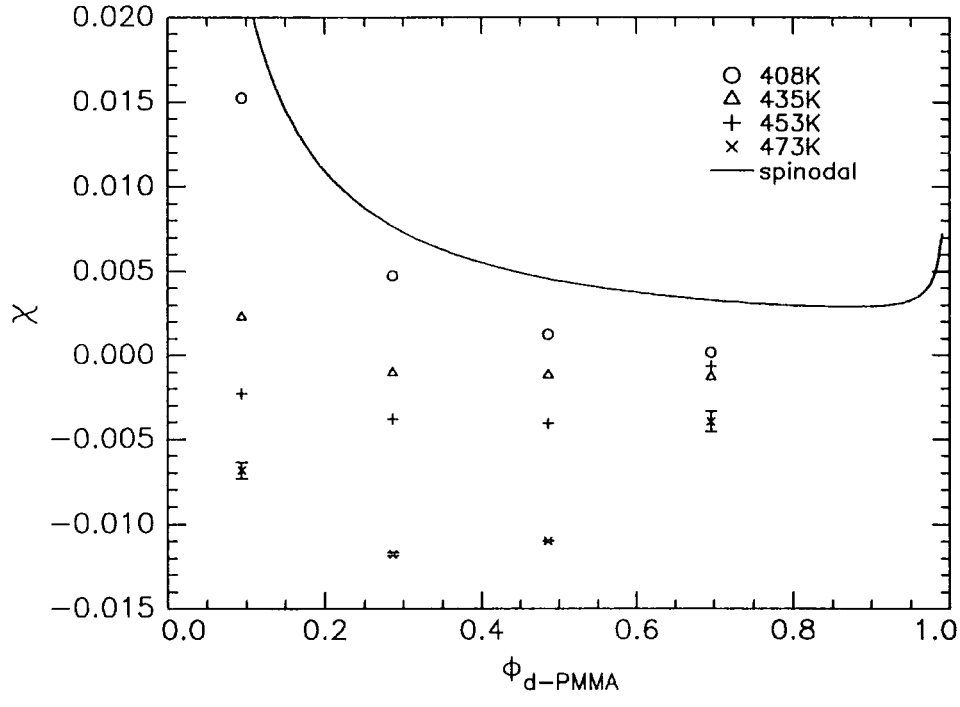

Figure 5.6: χ vs ϕ data for blend B, with χ_s calculated error bars on 473K data derived purely from fitting error.

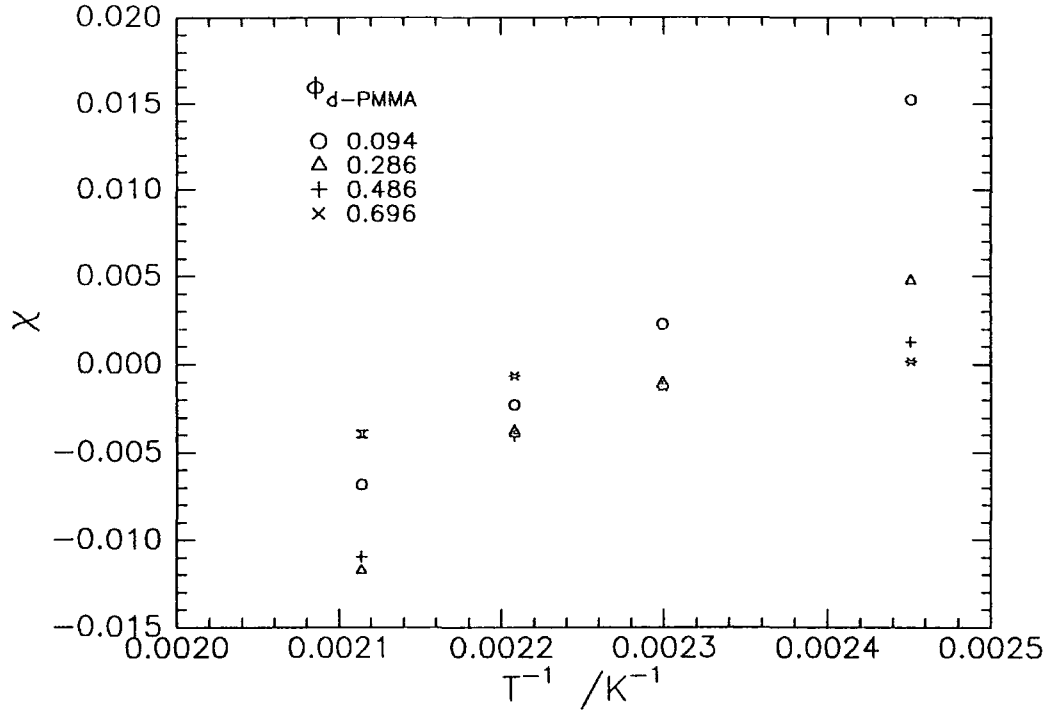

Figure 5.7a: χ vs 1/T for blend B, error bars on ϕ = 0.486 from fitting statistics.

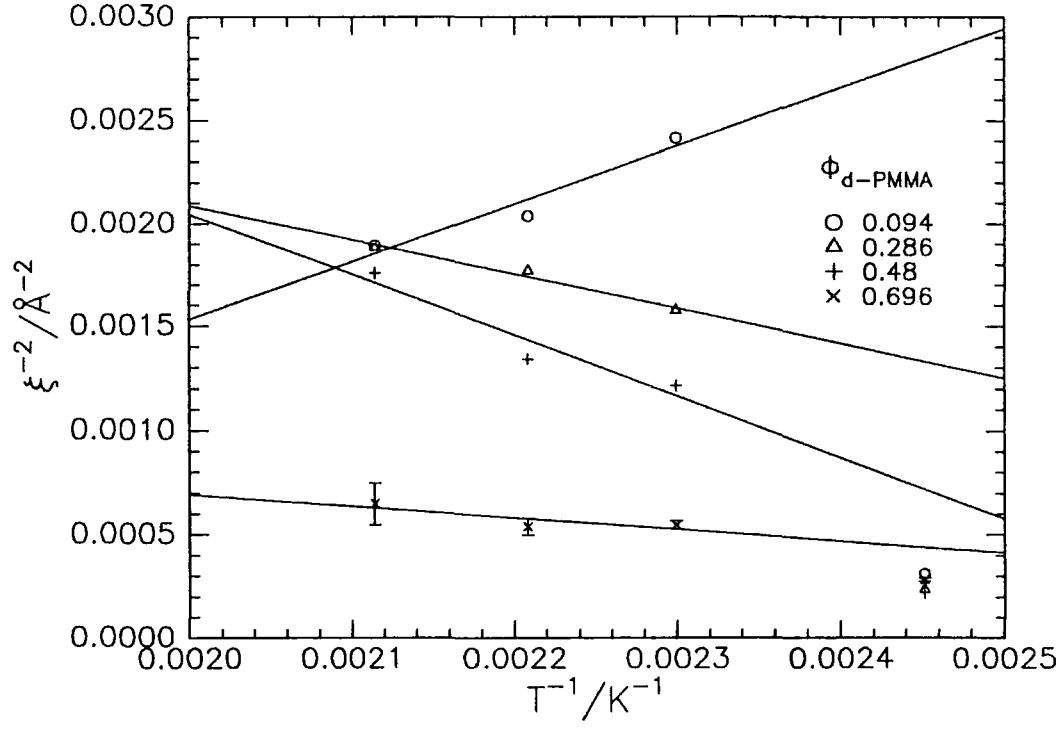

Figure 5.7b: ξ^{-2} vs 1/T for blend B, with straight line fits to 435K-473K data, error bars on ϕ = 0.696 from fitting statistics.

For all four blend compositions the values of ξ^{-2} at 408K are very similar and deviate from the trends indicated by the values measured at 435K, 453K and 473K, phase separation may be occurring in these blends and for this reason data collected at 408K has not been used in the spinodal temperature calculations. The data for blend B with ϕ = 0.094 are anomalous showing ξ^{-2} increasing with increasing reciprocal temperature, the data from the other three compositions show ξ^{-2} decreasing with increasing reciprocal temperature. The spinodal temperatures extracted in this manner are shown in Table 5.4. The error bars shown are calculated from the fitting errors and do not include contributions from other sources, most significant of which is the uncertainty in the determination of the molecular weight of the deuterated polymer. Assuming an uncertainty in this value of 10% a composition dependent systematic error occurs in χ, this error is ~1×10^{-3} for ϕ = 0.094 and ~2×10^{-4} for the other compositions. The calculated spinodal temperature is not affected by this error.

Within the experimental error the spinodal temperatures calculated from χ and ξ^{-2} are in agreement and show values of T_s that vary little over the composition range, although it should be emphasised that the experimental error is large due to the limited number of temperatures at which data were collected. Parameters to fits of the χ data of the form shown in Equation 5.1 can be found in Table 5.5.

Blend	Composition ($\phi_{d\text{-PMMA}}$)	Spinodal temperature (in K)	
		from $\chi = \chi_s$	from $\xi^{-2} = 0$
B	0.094	370 ± 20	690 ± 250
	0.286	410 ± 50	310 ± 60
	0.486	420 ± 20	370 ± 180
	0.696	520 ± huge	360 ± huge
D	0.096	400	-
	0.287	380	-
	0.480	430	-

Table 5.4: Spinodal temperatures calculated for blends B and D

The blend B data were also analysed by fitting the full RPA expression using the FORTRAN analysis program Pullet - the data were fitted over the Q range 0.0 < Q < 0.1

$Å^{-1}$, χ, R_{gH} and R_{gD} were allowed to vary. The fit was not extended over the full Q range because the data clearly deviates from the RPA expression at high Q, this is observed for both the blends B and D and will be discussed later.

Blend	Composition ($\phi_{d\text{-}PMMA}$)	A	B
B	0.094	-0.11(3)	49.3(5)
	0.286	-0.13(4).	60(16)
	0.486	-0.12(3)	53(12)
	0.696	-0.03(3)	15(12)
D	0.096	0.40×10^{-2}	1.84
	0.287	-0.20×10^{-2}	0.98
	0.480	-0.32×10^{-2}	1.86

Table 5.5: Values of A and B parameters for the temperature dependence of χ

Values of χ obtained were the same as those calculated using the Ornstein - Zernike plots, within the experimental error. The average value of R_{gD} fitted using this procedure was 44±6Å, which is consistent with the values calculated from literature values of $<S_0/M_w^{½}>$ and the measured molecular weight of the polymer which give radii of gyration in the range 33Å - 40Å.

Moving on to the blend D data, the results from blend B and data in the literature indicate that the low Q limit of the Debye expression is not probed by the LOQ diffractometer for this blend. For this reason the data were only analysed by fitting the RPA expression using the FORTRAN program Pullet. Fitting was over the Q range 0.0 $< Q < 0.1Å^{-1}$ (the fitting range was limited for the reasons mentioned in relation to blends I and B) and the parameters R_{gD}, R_{gH} and χ were allowed to vary. The average value of R_{gD} was 120 ± 50Å which compares with values calculated from literature data of 130Å - 170Å. Scattering was relatively insensitive to R_{gH} and this was reflected in a huge range of R_{gH} values. Figure 5.8 shows typical fits obtained using this procedure, the Kratky plot is used to emphasise the deviations from the RPA at higher Q values.

Figure 5.9 shows fitted values of χ as a function of composition and reciprocal temperature, in common with the data from blend B there is an upturn in χ at low volume fractions of d-PMMA. Uncertainty in the molecular weight of the deuterated

polymer leads to systematic errors approximately one order of magnitude smaller than those for blend B. Within these errors the size of the upturn in χ at low d-PMMA volume fractions is the same for both blend D and blend B. The variation of χ with reciprocal temperature is interesting, the χ values measured at room temperature and at 408K are quite similar and coupled with the behaviour observed in blend B this would indicate that phase separation was present in the samples at room temperature and that this persisted at 408K but was absent in the blend at temperatures above 408K

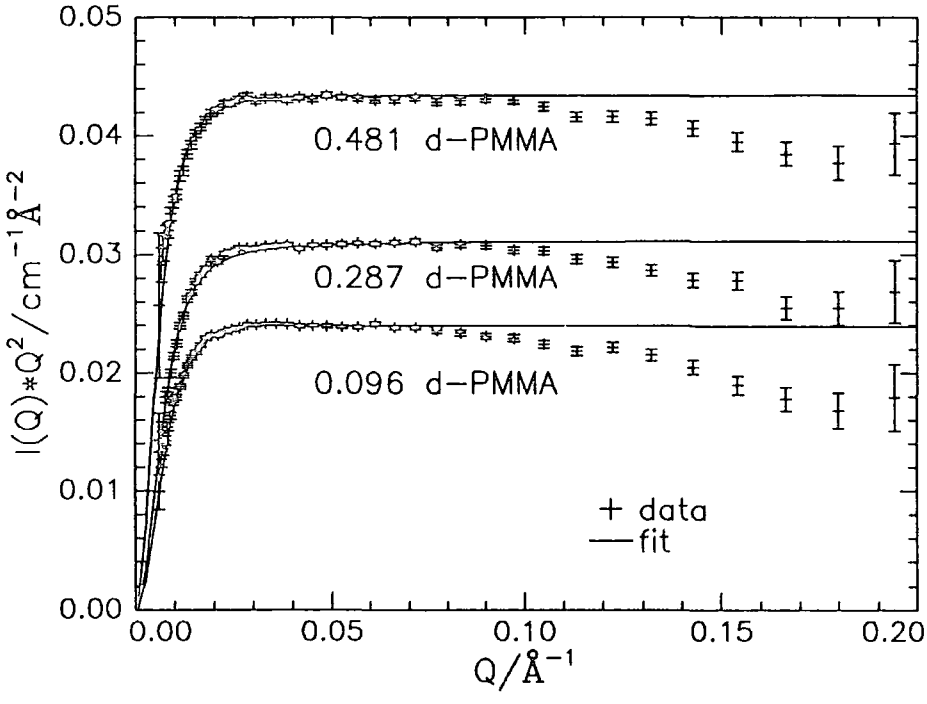

Figure 5.8: Typical fits to blend D data (453K) obtained using Pullet plotted in Kratky mode, error bars from Poisson statistics.

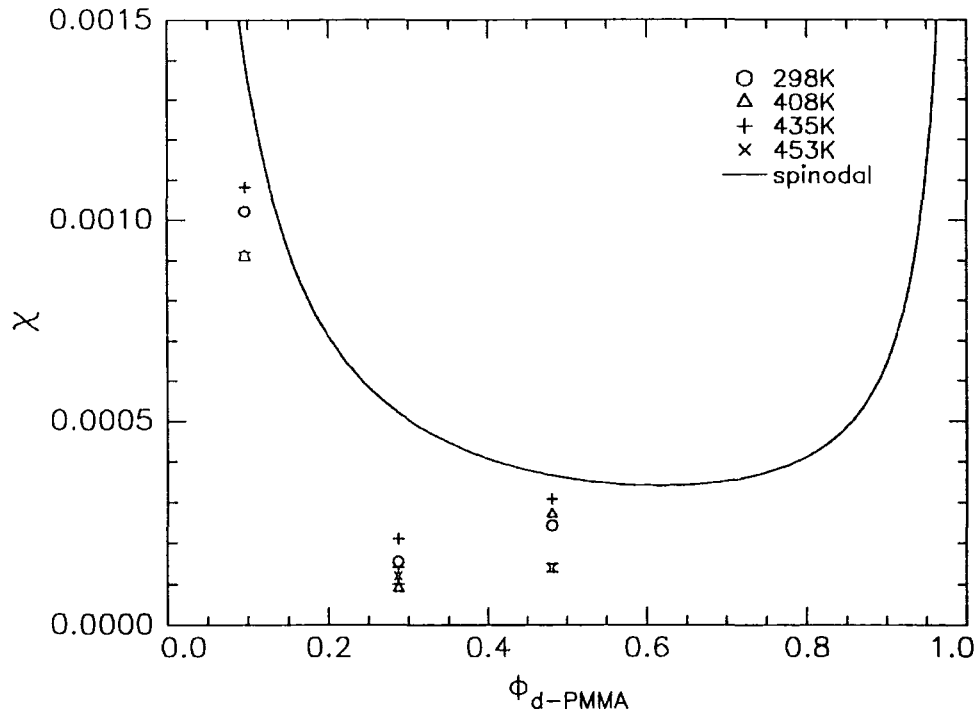

Figure 5.9a: χ vs ϕ data for blend D, with χ_s calculated from molecular weights, error bars on 453K data from Poisson statistics.

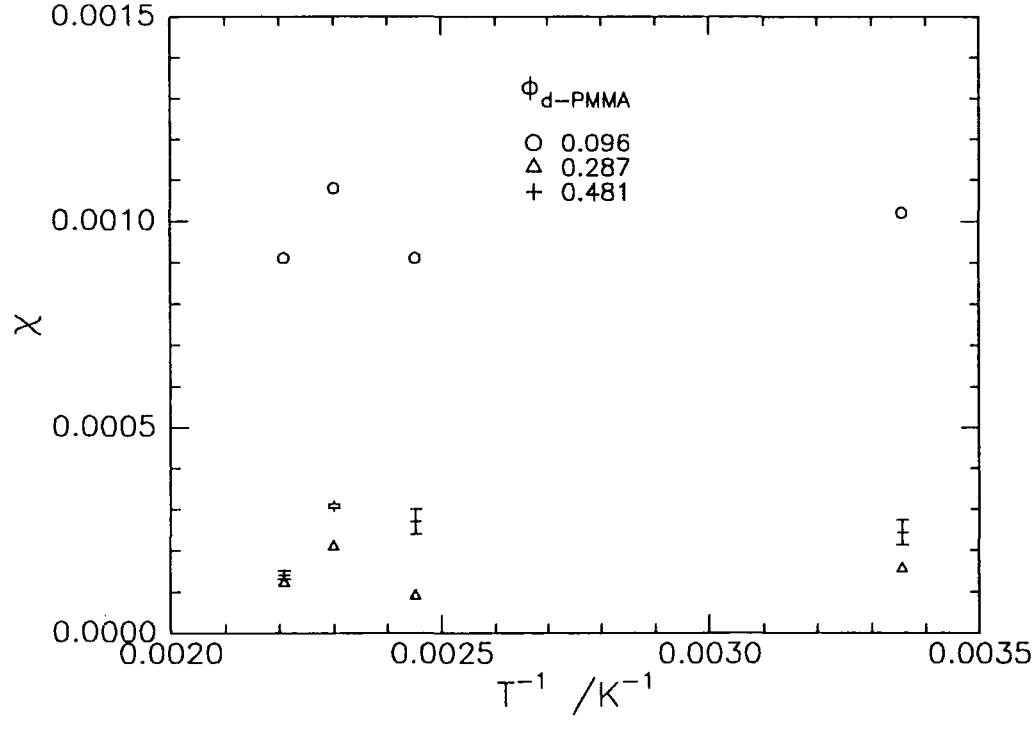

Figure 5.9b: χ vs 1/T data for blend D, error bars on ϕ = 0.481 calculated using Poisson statistics.

It is interesting to note that the errors purely from the fitting procedure are larger for the data collected at room temperature and 408K than for data collected at 435K and 453K. Spinodal temperatures calculated from the χ values measured at 435K and 453K can be found in Table 5.4 and parameters of the fits to these data of the form shown in Equation 5.1 are in Table 5.5. Clearly both these parameters and the spinodal temperatures that have been calculated for this blend are somewhat tentative because they are derived from data collected at only two temperatures.

5.1.3 Discussion

Two issues arise from the analysis of the scattering data from the isotactic blend I: firstly the existence of crystallinity in the blends at 363K and 383K and secondly the reliability of the χ values extracted.

To recap the sample preparation and measurement procedure, which will have a bearing on any crystallisation behaviour observed; powdered blends were held under two tonnes of pressure at 373K for ~1 hour and then allowed to cool for 1-2 hours before being removed from the sample press, typically samples resided in the heated rack on the LOQ diffractometer for periods of several hours at any particular measurement temperature, pure h-PMMA and pure d-PMMA were run first at any particular temperature and lower temperatures were run before higher temperatures. de Boer*et al*[3] have measured crystal growth rates, G, and melting points, T_m for hydrogenous isotactic PMMA (M_v = 213,000) crystallised from the melt at a range of crystallisation temperatures, T_c. For T_c = 373K de Boer *et al* observed a growth rate of ~3Å min^{-1}, producing crystals with melting temperatures of around 413K. This behaviour broadly matches that observed in this work, the characteristic length scale of ~215Å calculated from the position of the peak in the Kratky plots at low Q corresponds to crystal growth times of ~1 hour and the disappearance of the peak between 383K and 408K for the ϕ = 0.725 blend and between 363K and 383K for the other two blends suggests melting temperatures a little lower than those measured by de Boer, this lower melting temperature could be due to the lower molecular weight of the isotactic d-PMMA - work on polyethylene[4] shows that T_m decreases with decreasing molecular weight. Crystallisation appears to be predominantly in the deuterated component. Given the limited data collected from the crystalline samples in this work no further conclusions can be drawn about the crystallisation behaviour of isotactic PMMA.

The validity of the χ data extracted from the scattering from blend I relies on the modified RPA that was used to analyse the data. The isotactic polymers used are clearly highly polydisperse and the modified RPA was used in order to make some allowance for this polydispersity but this modified RPA is based on a Schultz - Zimm distribution of molecular weights. The reason that this distribution was used is that a simple analytical expression for the scattering from this distribution is available, for general distributions such a simple expression is not available. Figure 5.10 shows the actual distributions of

the isotactic polymers vs Log M measured using SEC and the Schultz - Zimm distribution[5] calculated from the polydispersity and molecular weight parameters derived from the SEC.

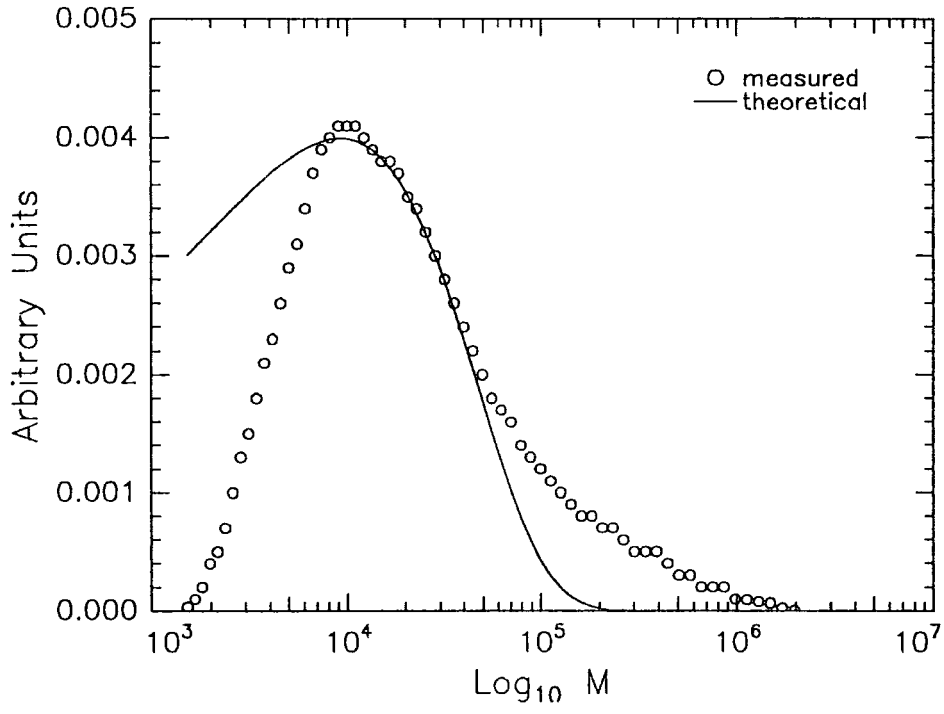

Figure 5.10a: Molecular weight distribution for isotactic d-PMMA, with 'theoretical' Schultz - Zimm distribution calculated using parameters from SEC.

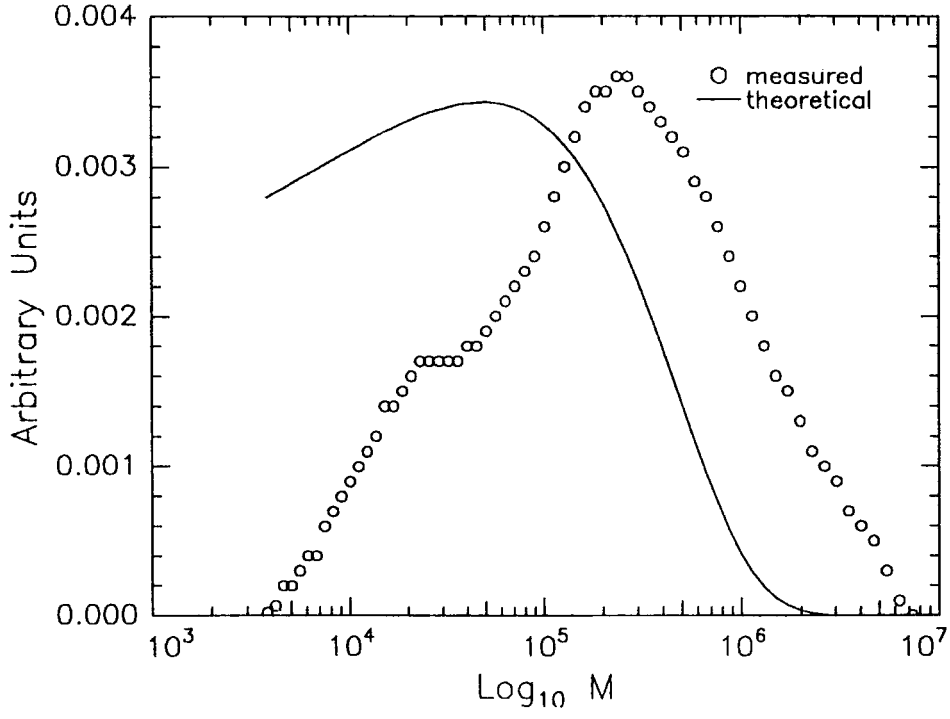

Figure 5.10b: Molecular weight distribution for isotactic h-PMMA, (see above)

The equation for the Schultz - Zimm distribution is:

$$w(M_x) = PM_x^{\lambda+1} \exp(-\tau M_x)$$

Equation 5.2

where P is an arbitrary scaling constant and :

$$h = \frac{M_w}{M_n} - 1$$
$$\lambda = \frac{1-h}{h}$$
$$\tau = \frac{\lambda+1}{M_n}$$

Equation 5.3

The shapes of the experimentally measured distributions and the 'theoretical' distributions are quite different and for this reason the χ values extracted using the modified RPA are at best tentative. In addition there is some possibility that, even at temperatures above 383K there is some crystallinity which even if not obvious could effect the values of χ calculated using the RPA, this may explain the rather poor fits to the low Q region.

In summary: the results from the isotactic blend are tentative for two reasons: the broad molecular weight distribution of the polymers and the presence of crystallinity. It would be possible to fractionate broad molecular weight distribution isotactic PMMA to give narrow molecular weight distributions, but the yield would be poor and this would be particularly expensive for the deuterated polymer. Polymerisation at low temperature to produce narrower molecular weight distributions is also possible but to produce high molecular weight polymers reaction times are prohibitively long. Once narrow distribution polymers have been obtained the crystallinity could be investigated using SAXS or DSC. The χ values measured for the isotactic blends will be discussed further in the context of results from the syndiotactic blends and values for other hydrogenous / deuterated blends found in the literature.

Isotopic blends of a single polymer have been used as simple model systems in a number of studies, these include work on polystyrene[6,7], 1,4-polybutadiene[2], polydimethylsiloxane[8], poly(ethylene-propylene)[9,10], poly(ethyl-ethylene)[11], poly(vinyl

ethylene)[11] and poly(ethylene-co-butene)[10]. Table 5.6 shows typical values of χ obtained from the purely isotopic blends, along with A and B values according calculated to Equation 5.1. Values of χ are generally slightly positive and with magnitude of order 1×10^{-4} or 1×10^{-3}.

	A	B	χ at ~300K
polystyrene (exp.)	$-2.9(4)\times10^{-4}$	0.20(1)	3.7×10^{-4}
theory		0.19(2)	
1,4-polybutadiene (exp.)	$-2(2)\times10^{-4}$	0.326(4)	8.7×10^{-4}
theory		0.33(2)	
poly(methyl methacrylate) [1] blend B	-0.12(1)	54(5)	6.0×10^{-2}
blend D	$0(4)\times10^{-4}$	1.6(5)	5.3×10^{-3}
blend I	$6(4)\times10^{-3}$	-5(2)	-1×10^{-2}
theory		0.25(2)	
polydimethylsiloxane			1.7×10^{-3}
poly(ethylene-propylene)	$-6.6(2)\times10^{-4}$	0.57(1)	1.2×10^{-3}
poly(ethyl ethylene)			9.8×10^{-4}
poly(vinyl ethylene)			7.7×10^{-4}
poly(ethylene-co-butene)	$-3.6(2)\times10^{-4}$	0.181(6)	2.4×10^{-4}

Table 5.6: Typical χ values for isotopic blends, with theoretical calculations by the method of Bates and Wignall.

These blends are almost exclusively either 'symmetric' with $N_H = N_D$ or nearly symmetric, the exception being the polydimethylsiloxane blend for which only a single χ value is available. Several studies have observed variations of χ with the volume fraction of the deuterated component, for polystyrene a very weak downturn is observed at the limits of the composition range (or 'wings') and for poly(ethyl ethylene) and poly(vinyl ethylene) a weak upturn is seen. The magnitude of this upturn is of the order of 1×10^{-3}.

[1] Excluding $\phi = 0.696$ data.

These values for χ and the magnitude of the upturn in the 'wings' of the composition are in accordance with the values obtained for blend-D in this work, but the low molecular weight blend B exhibits rather larger, more negative values for χ than have previously been observed in other isotopic blends. Although the size of the upturn in the 'wings' of the composition range is similar to that seen in other isotopic blends. Both the A and B parameters for blend B are far larger than are measured for any other isotopic blend. The χ value for blend I in Table 5.6 is negative because the temperature coefficient of χ is negative (unlike any other of the isotopic blends), at the measurement temperatures values of χ for blend I are broadly similar to those for blend B.

The range of χ values measured exists in the context of a range of theoretical work. Bates and Wignall[12] have estimated χ for isotopic polystyrene and polybutadiene blends. They consider the mixing of two components as a two stage process, firstly compressing or expanding each component to the segmental volume of the mixture and then mixing the components at constant volume. Hence χ is the sum of two terms, χ_v, from the volume change and χ_d from the mixing. It can be shown that:

$$\chi_v \cong \left(\frac{1}{k_B T}\right)\frac{(V_H - V_D)^2}{2\kappa V}$$

Equation 5.4

where κ is the compressibility of the polymers, V_H, V_D and V are the segmental volumes of the two components and of the mixture, k_B is the Boltzmann constant and T is the temperature in K. χ_d can further be divided into two, an enthalpic term $\chi_{d\varepsilon}$ and an entropic term χ_{ds}:

$$\chi_d = \chi_{d\varepsilon} - \chi_{ds}$$

Equation 5.5

χ_{ds} is cannot be easily calculated but they state that it is small and positive and is independent of temperature:

$$\chi_{d\varepsilon} \cong \frac{1}{k_B T}\frac{2}{3}\frac{\pi^2}{V^2} I(\alpha_H - \alpha_D)^2$$

Equation 5.6

α_H and α_D are the segmental polarisabilities for the hydrogenous and deuterated monomers and I is the segmental ionisation potential estimated from literature values[13]. Comparing these expressions with Equation 5.1:

$$A = -\chi_{ds}$$
$$B = (\chi_v + \chi_{d\varepsilon})T$$

Equation 5.7

Table 5.6 shows the values that Bates and Wignall calculate for the B parameter for polystyrene and 1,4-polybutadiene along with a value calculated for poly(methyl methacrylate). The calculated values for PMMA are very similar to those for polystyrene and polybutadiene, these values being close to the experimentally measured values B for the two polymers.

Freed and Bawendi[14] have solved, exactly, the Flory-Huggins lattice model (rather than using the mean field solutions) and they provide corrections for χ as a function of ϕ and the degree of polymerisation of the blend components.

$$\chi = \frac{\varepsilon(z-2)}{2} + \frac{z_c\varepsilon^2}{4} + \varepsilon\left[\frac{2}{N_D+1} - \frac{1}{N_H+1}\right] + \left(\frac{1}{N_D} - \frac{1}{N_H}\right)^2\left(\frac{z_c+4}{z_c^2}\right) - 3\varepsilon\phi\left[\frac{1}{N_D+1} - \frac{1}{N_H+1}\right] - \frac{3z_c\varepsilon^2}{2}\phi(1-\phi)$$

Equation 5.8

where ε is an effective interaction energy parameter and z_c is the lattice co-ordination number, ϕ is the volume fraction of the deuterated polymer. These calculations show relatively large entropic corrections to χ as the degree of polymerisation of one component is reduced relative to the other, but the absolute size of this correction is far smaller than that observed here. Similarly calculations using Equation 5.8 show upturns in the 'wings' of the composition range, but again the absolute magnitude of these variations is far smaller than those measured here.

Several models have been developed which are appropriate to describe these simple isotopic blends, these include Monte Carlo lattice models[15,16], polymer reference interaction site models (PRISM)[17] and Flory-Huggins mean field theory, modified by Muthukumar to allow for concentration fluctuations[18]. (note equation 14 in reference 11,

based on this theory is incorrect[19] as it is when repeated in relation to this work in reference 20) generally though the affect of asymmetry ($N_D \neq N_H$) has not been commented upon. Monte Carlo lattice models and PRISM do suggest a weak upturn in χ at the wings of the composition, but these upturns are typically small and indicate downturns for negative χ values. These calculations are all essentially aimed at correcting or replacing the Flory-Huggins lattice stage of modelling.

Kumar[16] has suggested that additionally contributions to effective χ values arise from failures of incompressible random phase approximation in particular non-ideal volume changes on mixing. The size of the volume change required to produce the observed upturn in χ is very small (of the order of 0.05%). The data for blends B and D are characteristic of 'repulsive' blends where there is a slight increase in the volume on mixing, leading to upturns in χ at the extremes of the composition range. Tang and Freed[21] have developed a compressible RPA theory, but its application to experimental data is difficult.

In summary: for the 'high' molecular weight blend D the χ values measured in this work are very much in line with the χ values measured for other isotopic systems, both in magnitude and in the upturn in the 'wings' of the composition. The χ values measured for blend B, on the other hand, are negative and larger in magnitude than values measured in any other isotopic blend. This striking difference in behaviour is attributed to entropic contributions arising from chain length disparity. It is interesting to note that the size of the upturn in blends B and D is very similar, this upturn is due largely to failures in the incompressible RPA.

When using the RPA to extract χ parameters from small angle neutron scattering data the fitting range has been limited to lower Q values, this is because polymer chains are known to deviate from the ideal; Gaussian distribution of chain segments upon which the RPA is based. This behaviour has been known in PMMA for a long time, and has been discussed by Yoon and Flory[22]. In addition to the non-Gaussian distribution of chain segments, at higher Q values the 'rigid rod' nature of the chain at the level of the monomer becomes apparent in the scattering. In order to further investigate this behaviour the BIOSYM Polymer modelling software suite[23] has been used to perform Monte Carlo rotational isomeric state(RIS)[24] theory calculations on PMMA chains. Several model molecules were studied, in all cases the model molecule had 470 main chain bonds and the scattering from 400 chain configurations was calculated at a

simulated temperature of 450K. Polymer molecules with 100% isotactic or 75% syndiotactic dyads were used. For the 100% isotactic models only the backbone scattering was calculated, but for the 75% syndiotactic blends the monomer units were divided into scattering centres of the methylene groups on the main chain backbone, the α methyl groups and the ester methyl groups. The total scattering from this molecule is the sum of contributions between scattering centres of the same type and cross terms of scattering from pairs of different types.

Figure 5.11a shows a comparison between the scattering calculated for a 100% isotactic chain and the scattering from blend I, $\phi = 0.478$ at 453K. In principle it should be possible to scale the data by fixing I(0) = 1 for both model and experiment, but the excess scattering at low Q for the experimental data renders this impossible so the data have been multiplied by an arbitrary scaling constant. The match is relatively good at intermediate Q values. At low Q values the scattering is strongly influenced by the molecular weight of the deuterated polymer and given that the molecular weight distribution is broad the poor correspondence is unsurprising. Figure 5.11b shows the scattering from blend B, $\phi = 0.486$ at 453K, along with various scattering functions calculated for a 75% syndiotactic chain, in this case it was possible to scale the model successfully and experimental data by setting I(0) = 1. The scattering from the ester methyl groups appears to be dominant in the observed experimental scattering. These model scattering profiles all show an upturn at Q values above ~0.2Å^{-1}, this corresponds to the scattering from a chain consisting of short 'rigid rods'. Unfortunately the available Q range of LOQ does not extend far enough to test this behaviour in the experimental system.

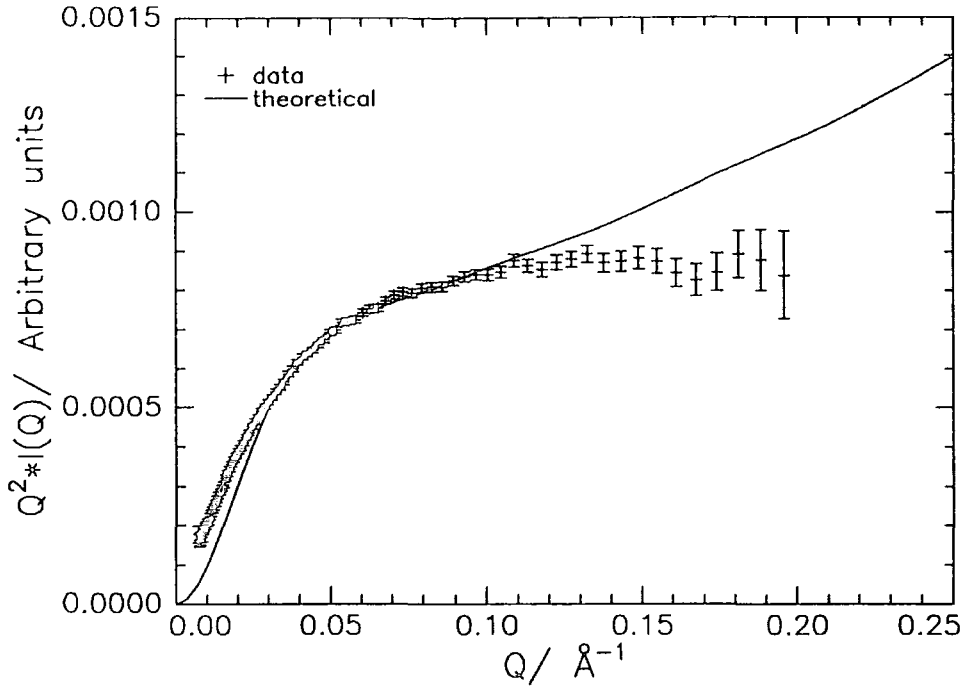

Figure 5.11a: Comparison between scattering from blend I, ϕ = 0.478 at 453K and a RIS calculation for the backbone scattering from a 100% isotactic chain.

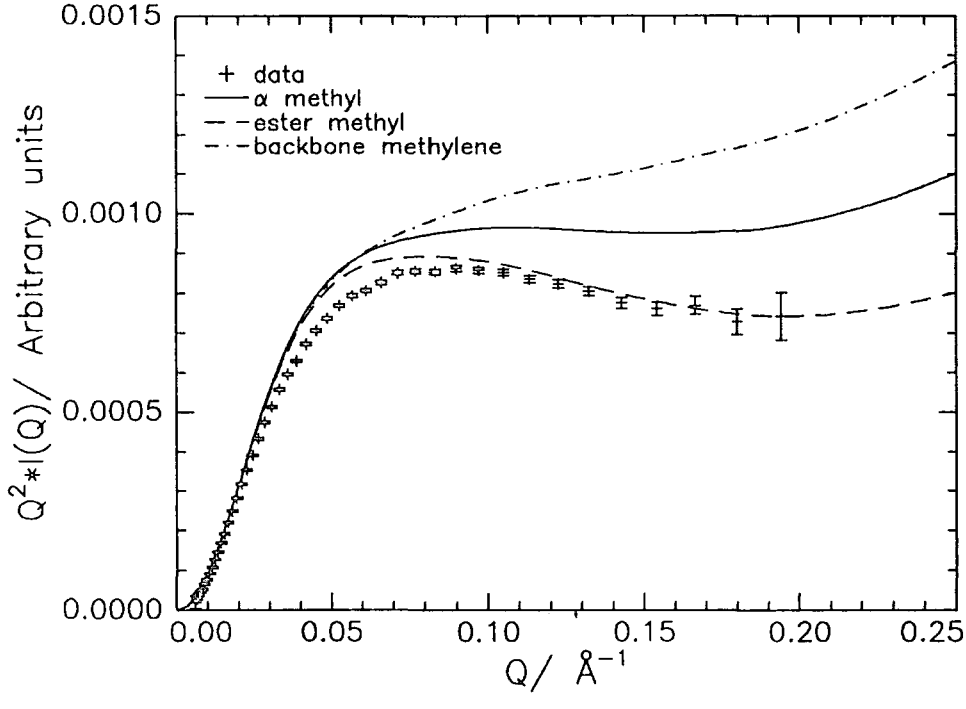

Figure 5.11b: Comparison between scattering from blend B, ϕ = 0.486 at 453K and RIS calculations from the scattering centres of the MMA monomer.

5.1.4 Conclusions

The effective interaction parameter, χ, of three d-PMMA/h-PMMA blends has been measured. For the isotactic blend I the results are rather tentative because of the large polydispersity of the polymers used, in addition clear signs of crystallinity were observed at lower temperatures and at higher temperatures unusual scattering is observed at low Q that may indicate the continued presence of crystallinity, possibly invalidating the use of the RPA.

The values of χ measured for blend D (an intermediate molecular weight d-PMMA blended with a high molecular weight h-PMMA) are comparable in magnitude to values of χ obtained for other isotopic blends. Blend B, where the molecular weight of the d-PMMA is low, exhibits relatively large negative values of χ and a much larger temperature coefficient than has been observed for other isotopic blends. This behaviour is attributed to entropic contributions arising from the strong asymmetry of the blend. This conclusion is supported qualitatively by theory, although the magnitude of the theoretical prediction is far smaller than the effect seen. Both blend B and blend D exhibit an upturn in χ at low volume fractions of d-PMMA. This upturn has the same magnitude for both blends and is comparable to that observed in other isotopic blends. The cause of such behaviour is not entirely clear, but it may well be a result of the failure of the incompressible RPA caused by non-ideal volume changes on mixing.

Some RIS molecular modelling has been done to examine the deviation of the observed scattering from that expected from polymers obeying Gaussian statistics. These models show the importance of the substituent groups of PMMA in determining the observed scattering.

5.1.5 References for Section 5.1

1 . J. Brandrup, E.H. Immergut, 'Polymer Handbook 3rd ed.', (New York: John Wiley & Sons, 1989), pp VII/36.

2 . F.S. Bates, S.B. Dierker, G.D. Wignall, *Macromolecules*, 19, **1986**, 1938.

3 . A. de Boer, G.O.R Alberda van Ekstein, G. Challa, *Polymer*, 16, **1976**, 930.

4 . C. Booth, C. Price, 'Comprehensive Polymer Science (vol. 2)', (Oxford: Pergamon Press, 1989) pp385.

5 . C. Booth, C. Price, 'Comprehensive Polymer Science (vol. 1)', (Oxford: Pergamon Press, 1989) pp294-296.

6 . F.S. Bates, G.D. Wignall, *Macromolecules*, 19, **1986**, 932.

7 . D. Schwann, K. Hahn, J. Streib, T. Springer, *Journal of Chemical Physics*, 93(11), **1990**, 8383.

8 . A. Lapp, C. Picot, H. Benoit, *Macromolecules*, 18, **1985**, 2437.

9 . M.D. Gehlsen, J.H. Rosedale, F.S. Bates, G.D. Wignall, L. Hansen, K. Almdal, *Physical Review Letters*, 68(16), **1992**, 2452.

10 . W.W. Graessley, R. Krishnamoorti, N.P. Balsara, L.J. Fetters, D.J. Lohse, D.N. Schulz, J.A. Sissano, *Macromolecules*, 26, **1993**, 1137.

11 . F.S. Bates, M. Muthukumar, G.D. Wignall, L.J. Fetters, *Journal of Chemical Physics* , 89(1), **1988**, 535.

12 . F.S. Bates, G.D. Wignall, *Physical Review Letters*, 57(12), **1986**, 1429.

13 . R.C. Weast, 'CRC Handbook of Chemistry and Physics 68th ed.', CRC Press, 1988.

14 . M.G. Bawendi, K.F. Freed, *Journal of Chemical Physics*, 88(4), **1988**, 2741.

15 . A. Sariban, K. Binder, *Macromolecules*, 21, **1988**, 711.

16 . S.K. Kumar, *Macromolecules*, 27, **1994**, 260.

17 . A. Yethiraj, K.S. Schweizer, *Journal of Chemical Physics*, 98(11), **1993**, 9080.

18 . M. Muthukumar, *Journal of Chemical Physics*, 85(8), **1986**, 4722.

19 . F.S. Bates, personal communication.

20 . I. Hopkinson, F.T. Kiff, R.W. Richards, S.M. King, H. Munro, *Polymer*, 35(8), **1994**, 1722.

21 . H. Tang, K.F. Freed, *Macromolecules*, 24, **1991**, 958.

22 . D.Y. Yoon, P.J. Flory, *Macromolecules*, 9, **1976**, 299.

23 . Computational results obtained from Biosym Technologies (San Diego) Polymer Module, version 5.1.

24 . P.R. Sundararajan, P.J. Flory, *Journal of the American Chemical Society*, 96(16), 1974, 5025.

5.2 Surface Enrichment

5.2.1 Experimental

The aim of this set of experiments was to study the surface enrichment behaviour of syndiotactic d-PMMA/h-PMMA blends as a function of the molecular weight of the d-PMMA and the annealing time. To this end four blends were prepared, in each case the h-PMMA 'matrix' had a molecular weight of 994,000 and the volume fraction of d-PMMA in the blend was ~0.17. This volume fraction of d-PMMA was chosen because such a blend will have a nuclear scattering length density equal to that of the silicon substrate, the intention was that this would make the presence of surface enrichment more apparent in the reflectivity profiles. The molecular weight of the d-PMMA was varied between 12,400 and 417,000. The exact volume fraction of d-PMMA in each blend and the glass transition temperatures, T_g, of the five polymers used are shown in Table 5.7. Further details of the polymers used can be found in the section 4.1, the 'global' labels for the five polymers used are also given in Table 5.7. The blends will be referred to in this section as blend A for the blend containing the lowest molecular weight d-PMMA through to blend D containing the highest.

	M_w	$\phi_{d\text{-PMMA}}$	T_g/K
h-PMMA (TK21)	994,000	0	397.6
Blend A (TK24)	12,400	0.174	392.6
Blend B (TK25)	25,200	0.171	376.7
Blend C (TK26)	136,000	0.178	403.1
Blend D (TK23)	417,000	0.174	403.7

Table 5.7: Details of polymers and blends

Thin films of each of these blends were spun cast onto silicon blocks from 5% w/w toluene solution, the spinning speed was 4000 rpm. No attempt was made to remove the native silicon oxide layer from the surface of the silicon. The thicknesses of the films obtained were measured using contact profilometry, the variation in thickness over the

area of any one film was small, being less than 100Å, and the film thicknesses were in the range 3000Å - 4000Å.

Unannealed samples of each film blend were retained, in addition films were annealed, under vacuum, over a wide range of 'effective' annealing times. This was done by annealing the samples over a range of temperatures, T and then converting the actual annealing times, t_{actual}, to 'effective' annealing times, t_{ref}, at a single reference temperature, T_{ref}, using the Williams - Landel - Ferry (WLF) equation[1] :

$$t_{ref} = \frac{t_{actual}}{a_T}$$

Equation 5.9

where

$$\log_{10} a_T = \frac{-C_1^0 (T - T_{ref})}{C_2^0 + (T - T_{ref})}$$

Equation 5.10

T_{ref} was chosen to be 423K, and $C_1{}^0 = 32.2$, $C_2{}^0 = 80.0$ (see reference 1)

The minimum annealing time, t_{actual}, used was ~1 hour and samples were annealed by placing them on large preheated metal blocks in the oven. Similarly annealed samples were 'quenched' by removal from the oven and placing on large metal blocks at room temperature. This was to ensure that the heating and cooling times were small compared to the actual annealing times. Table 5.8 shows details of the annealing program.

Temperature/K	Actual Annealing time/min	Effective Annealing time/min	Blends
411	1585	3.3×10^{-3}	A, D
418	140	0.1	B, C
418	270	1.9	A,D
418	1390	9.9	A, D
418	1430	10	A, B
423	60	60	A, D
423	100	100	A, B, C, D
423	500	500	A, D
423	800	800	A
423	1000	1000	A, B, C, D
423	3000	3000	A, D
428	64	5000	A, D
428	102	8000	A, D
428	191	15000	A
428	255	20000	D
428	640	50000	D
428	1420	1.1×10^{5}	B
433	270	1.0×10^{6}	A, B, C, D
438	80	1.0×10^{7}	C
438	1030	1.3×10^{8}	A, B, C, D
443	360	9.9×10^{8}	C
448	207	9.6×10^{9}	B, C, D
457	4230	1.7×10^{13}	A, B, C, D

Table 5.8: Annealing program for d-PMMA/h-PMMA blends

5.2.2 Results

A representative selection of the reflectivity profiles obtained are shown in Figure 5.12, for clarity only the data from the unannealed samples are shown as points with error bars, the number of points has also been reduced. The errors are calculated from Poisson counting statistics. The reflectivity profiles were all very similar, they were all smooth, all had very similar critical edges and only small differences were observed at higher Q.

The reflectivity data were analysed in two ways: firstly the values for the air/polymer interface volume fraction of d-PMMA were calculated from the asymptote at high Q of the RQ^4 vs Q plot; this was done for all the data collected. Figure 5.13 shows a typical RQ^4 vs Q plot, the asymptote was calculated over the Q range 0.03-0.048$Å^{-1}$, and over this range the data appears to have reached a constant value. The data in the region 0.048-0.06$Å^{-1}$ were excluded due to the larger statistical error seen in this region. Statistical error in the surface volume fraction calculated from such asymptote values was in the range of 0.01-0.03. To evaluate the influence that surface roughness and the silicon/polymer interface have on the values of surface volume fraction calculated in this way, apparent surface volume fractions were calculated using the asymptote method from simulated data derived from the optical matrix methods. Model profiles were calculated for a series of volume fractions in the range 0.17-0.18 and the asymptotic values were measured for these profiles using the same procedure that was used for the experimental data. These measurements showed that there was a systematic over estimation of the surface volume fraction of 0.014, but this over estimate was constant over the range of bulk volume fractions used. This error probably arises from the Q range used to calculate the asymptote being slightly too low, i.e. the RQ^4 vs Q plot has not yet reached its asymptote value, but increasing the Q range to higher Q leads to a larger statistical error.

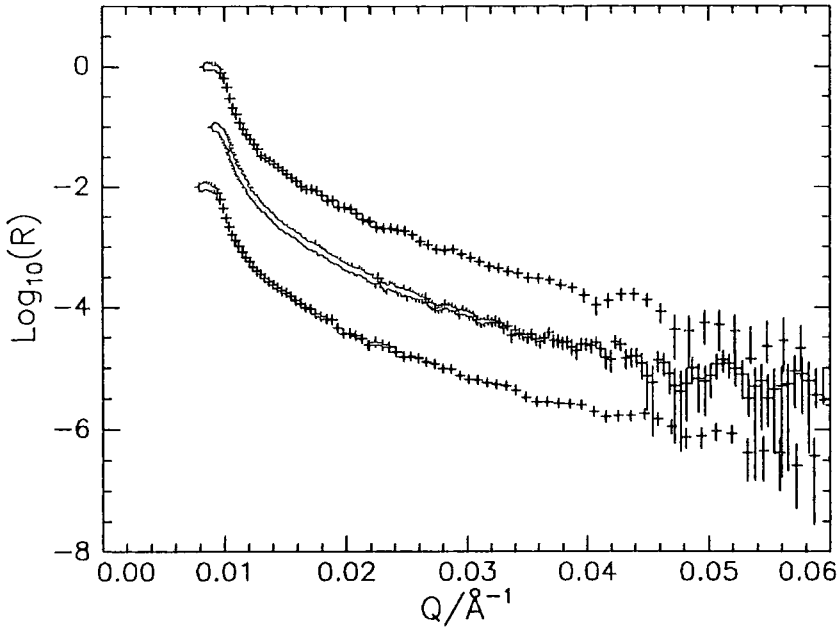

Figure 5.12a:Reflectivity profiles ($Log_{10}(R)$ vs. Q) for blend C Samples. (top) unannealed sample, (middle) annealed for 3000 minutes effective time and (bottom) 1×10^{13} minutes (effective time). The latter have been offset by -1 and -2 units, for clarity. Error bars are those arising from Poisson counting statistics.

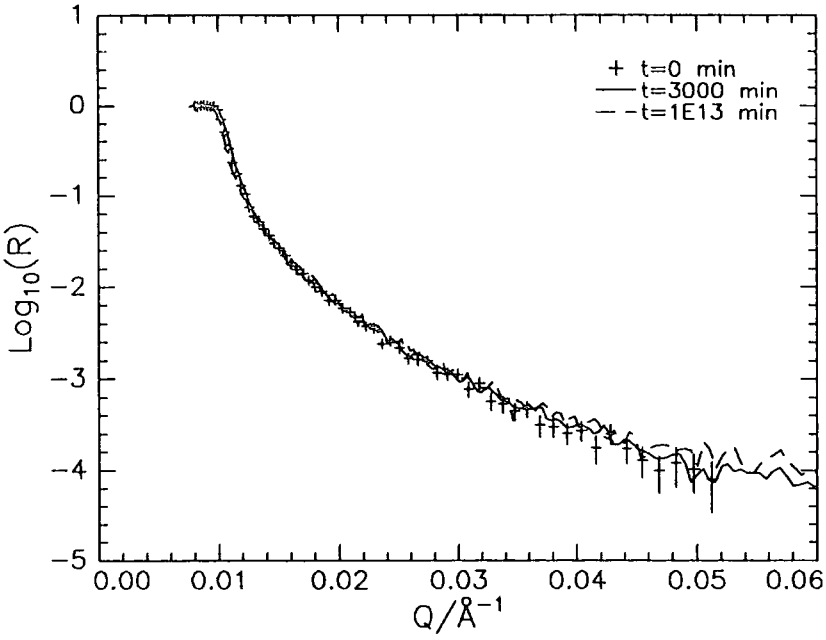

Figure 5.12b: Reflectivity profiles ($Log_{10}(R)$ vs. Q) from blend D samples. Over laid to show high degree of similarity between data.

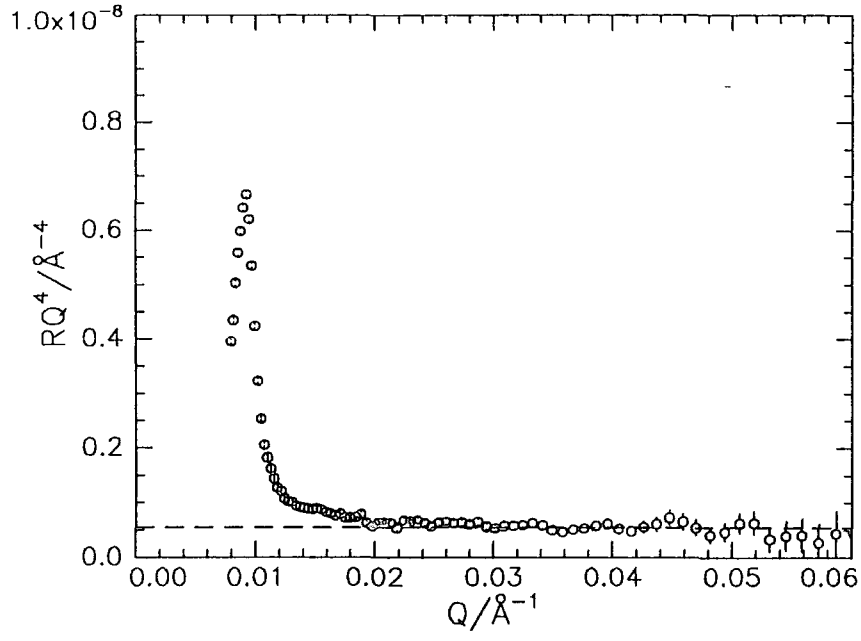

Figure 5.13: RQ^4 vs. Q plot for blend C sample, annealed for 1×10^{13} minutes (effective time) broken line shows value of asymptote, used to calculate surface volume fraction of d-PMMA. Error bars show error arising from Poisson statistics.

The effect of surface roughness is rather larger, increasing the surface roughness at the air/polymer interface from 0Å to 10Å causes the surface volume fraction obtained from an RQ^4 vs Q plot to fall below that used to simulate the data, a surface volume fraction of 0.158 is obtained for a film with nominal bulk volume fraction of 0.187 and an air surface roughness of 10Å. The surface roughness of spun cast PMMA films was measured using X-ray reflectivity and it was found that the air surface root mean square roughness is around 5Å. The combined effect of the silicon/polymer interface, surface roughness effects and the slight over-estimate due to the Q range used on the measured value of the surface volume fraction obtained from RQ^4 vs Q plots is likely to be a slight (<0.01) over estimate of the surface volume fraction. Figure 5.14 shows the values of the surface volume fraction calculated using the asymptote method, values for the unannealed films are shown at effective time = 10^{-4} minutes. Clearly for blends A, B and C no enrichment of d-PMMA to the air surface is observed. It would seem possible that a very small amount of surface enrichment is observed in blend D, using the asymptotic method of calculating the surface volume fraction of the d-PMMA, but the 'enriched'

surface volume fraction observed is only slightly outside the error range derived from the sources discussed.

Secondly a large subset of the data were analysed via optical matrix methods utilising a maximum entropy procedure[2] to fit a free form model of 150 layers of fixed thickness. Figure 5.15 shows examples of composition profiles obtained in this way, the data have been offset by a factor of 0.1 for clarity. Figure 5.16 shows a selection of the fits obtained using maximum entropy. Mis-fitting is almost exclusively in the critical edge region. Figure 5.14 shows the values of the minimum and maximum volume fraction of d-PMMA found in the top 250Å, obtained from these free form fits. The uncertainty in the minimum and maximum volume fraction d-PMMA in the top 250Å, arising purely from the Poisson counting statistics of the data, is in the range 0.005-0.01.

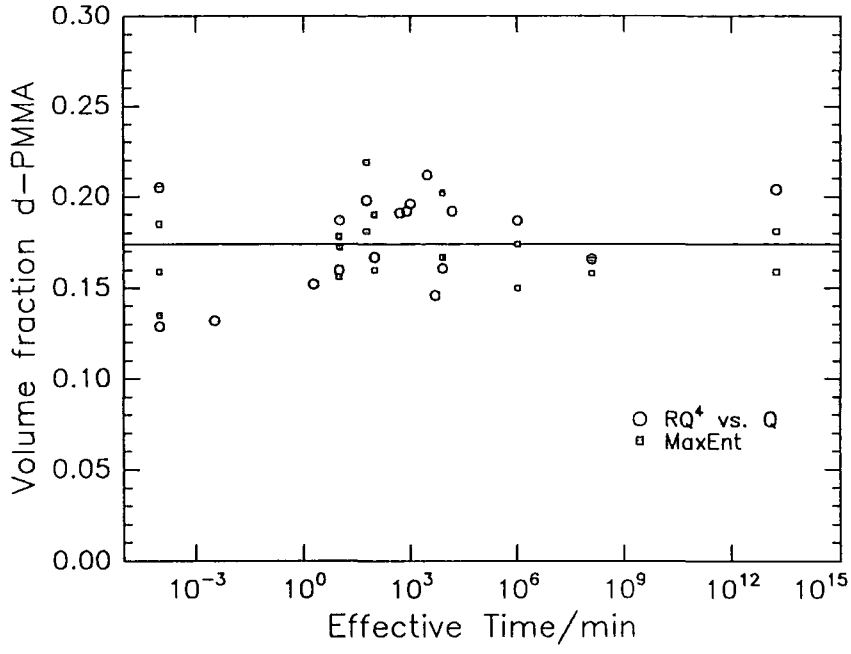

Figure 5.14a:Air surface volume fraction for blend A. Open circles are data from RQ^4 vs. Q asymptotes. Closed squares are from maximum entropy fitted profiles and indicate the range of volume fractions of d-PMMA found in the top 250Å of the profile. Data from unannealed samples is placed at Log(effective time) = -4.

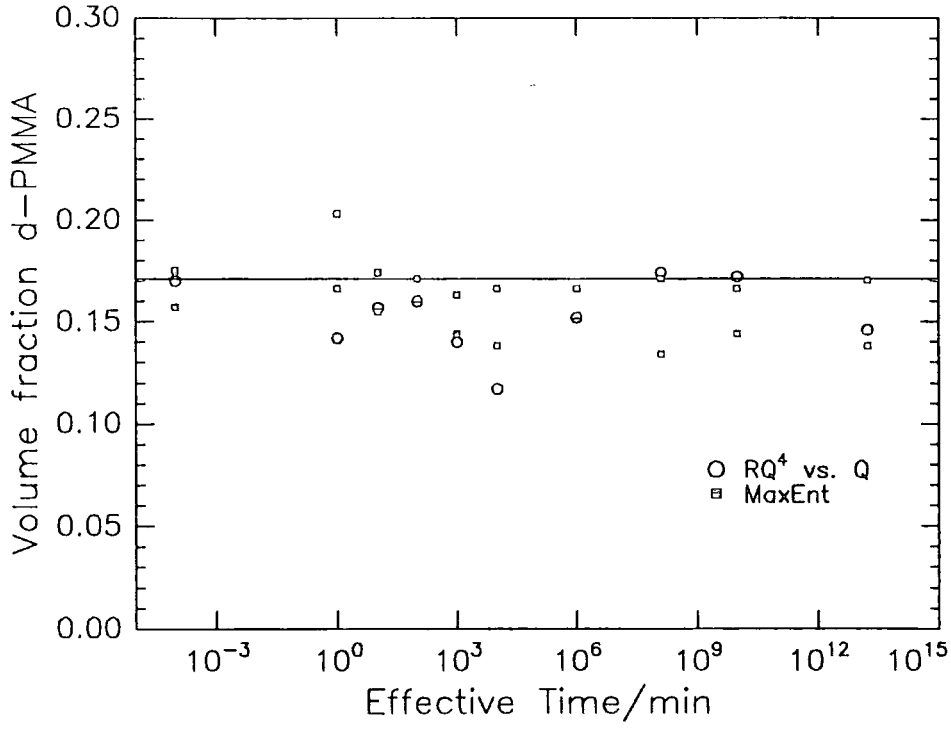

Figure 5.14b: Air surface volume fractions of d-PMMA for blend B. For details see Figure 5.14a above.

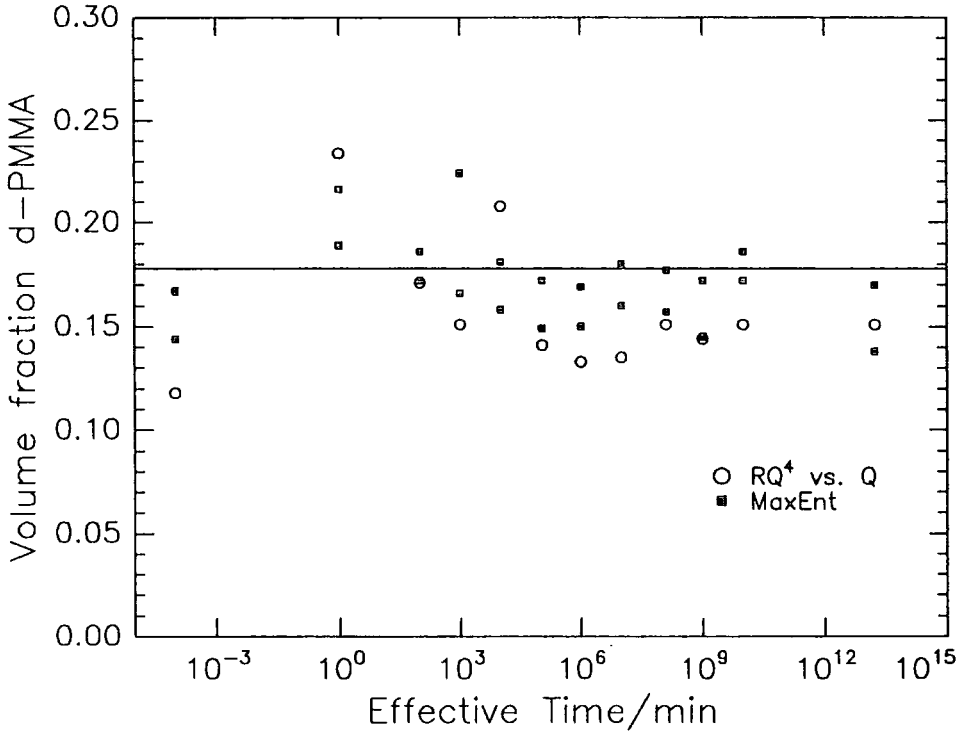

Figure 5.14c: Air surface volume fractions of d-PMMA for blend C. For details see Figure 5.14a above.

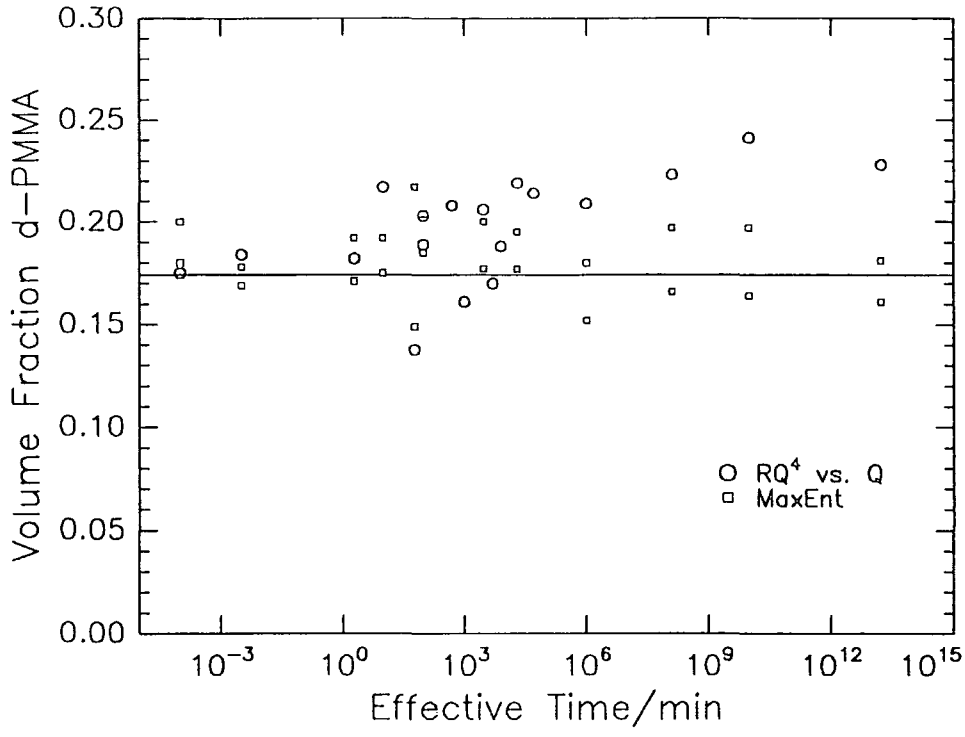

Figure 5.14d: Air surface volume fractions of d-PMMA for blend D. For details see Figure 5.14a above.

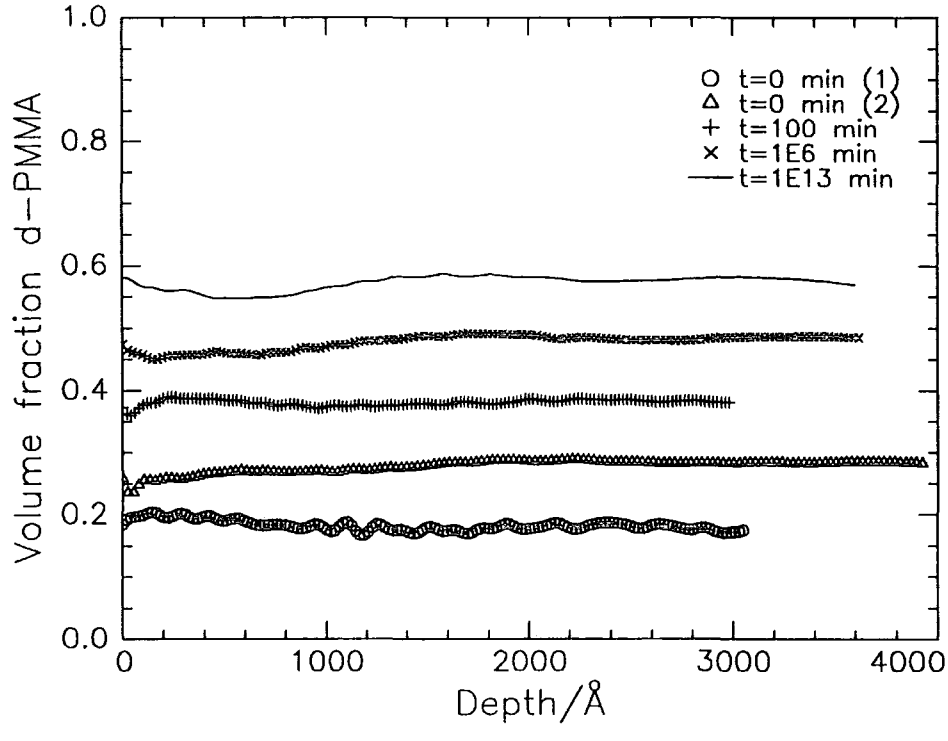

Figure 5.15a: Selected volume fraction vs. depth profiles from blend A, obtained using maximum entropy methods. Profiles are offset by 0.1 for clarity.

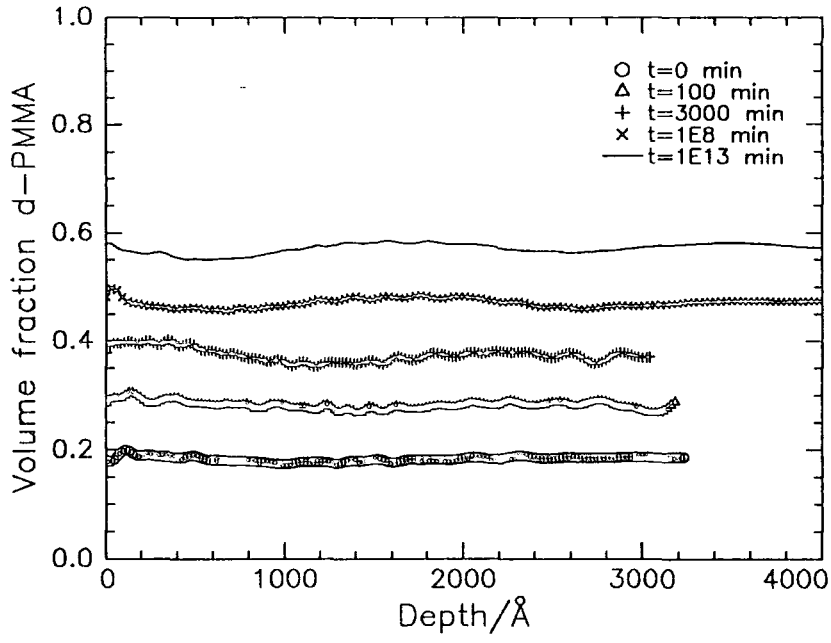

Figure 5.15b: Selected volume fraction vs. depth profiles from blend D, obtained using maximum entropy methods. Profiles are offset by 0.1 for clarity.

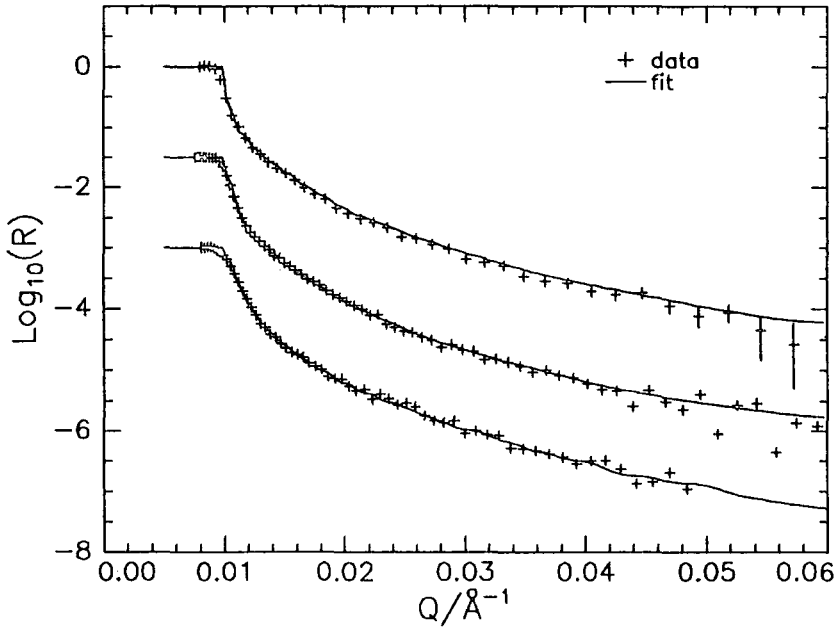

Figure 5.16: Maximum entropy model fits to data, (top) blend C t = 1×10^{13} min, (middle) blend A, t = 0 min., (bottom) blend D, t = 20000 min. these last two offset by -1.5 and -3 respectively for clarity - errors in blend C data are from Poisson statistics.

These maximum entropy fits appear to show weak concentration gradients in all the films, even the unannealed films. The variation in the volume fraction profile between the two different unannealed blend A films is as large as the variation between an unannealed film and an annealed film. There are two explanations for this behaviour, either these composition gradients really exist in the films and they arise during the spin casting process or they are an artefact of the data analysis. If the gradients arose from the spin casting it would be expected that during annealing the gradients in the bulk of the sample would be removed. Free energy is required to maintain concentration gradients and so the free energy of the system is reduced by removing the bulk concentration gradients. Several of the composition profiles show very similar variations in composition through the bulk of the specimen, characterised by a small amplitude, low frequency spatial variation in volume fraction. A similar pattern appears in different blends and for different annealing times which would suggest that it is an analysis artefact rather than actual structure, such a low spatial frequency artefact could arise from a small systematic mis-fitting near the region of total reflection. Model reflectivity profiles incorporating absorption effects show that, even if the absorption term for h-PMMA is 10× the predicted value, the effect of absorption is negligible. However if model reflectivity data are generated using a range of 'simulated' resolutions (8-13%) and these data are presented to the maximum entropy analysis program which in this case assumes a fixed value for the experimental resolution of 7% then structures similar to those seen in the fitted profiles are seen in the volume fraction profiles (see Figure 5.17). The artefacts in the volume fraction profiles are thus explained by an experimental resolution rather poorer than that calculated from the nominal slit geometry. This poorer resolution could be due to alignment of the samples, sample quality (i.e. macroscopically uneven samples) or slit setting. The most probable source of the reduced resolution is the slit setting, the data presented here were collected before the new computer controlled slit packages were installed on the CRISP beam line, the previous slit packages were showing signs of physical deterioration. In conclusion, both asymptote and maximum entropy analysis are in agreement and show no clear evidence for surface enrichment in any of the blends over a wide range of annealing times and temperatures. This conclusion is supported by SIMS work on blends A and D done by collaborators at the University of Strathclyde.

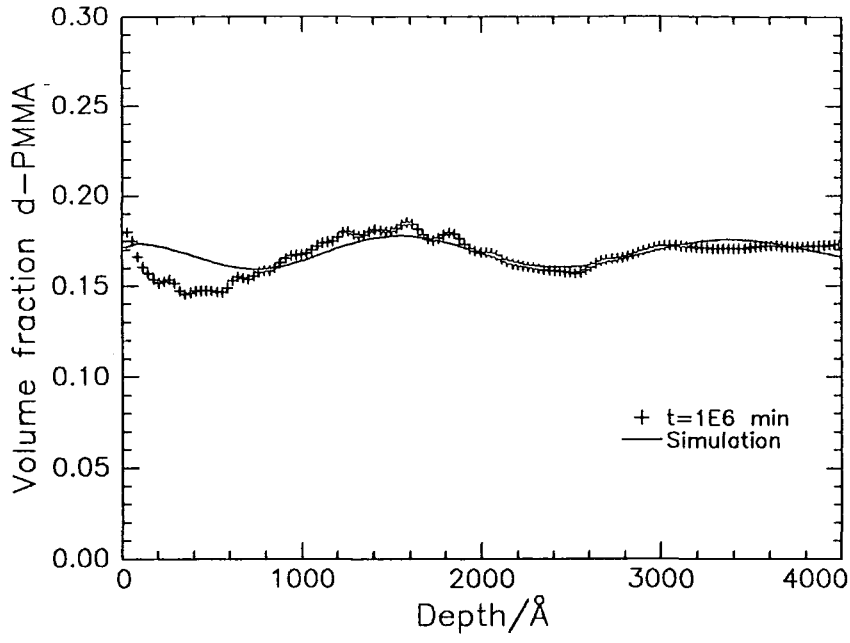

Figure 5.17: Volume fraction vs. depth profile extracted using maximum entropy methods. The crosses are from real data and the line is from simulated data - designed to show the effect of unaccounted resolution reductions.

5.2.3 Discussion

There are a number of possible explanations as to why no surface enrichment was observed in the d-PMMA/h-PMMA systems studied here:

(1) insufficient annealing time was allowed for the surface enriched layer to form.

(2) Flory-Huggins interaction parameter, χ, is such that the blends are too distant from the coexistence curve for enrichment to occur.

(3) there is insufficient surface energy difference between the d-PMMA and h-PMMA to drive surface enrichment.

The WLF equation has been used by other workers[3,4] to increase the 'effective' annealing time domain. Use of the WLF equation (i.e. annealing at different temperatures) implies the belief that the polymer specimen under consideration is effectively ideal i.e. there are no excess thermodynamic interactions. It was shown earlier in this chapter (reference) that the interaction parameter, χ, for h-PMMA/d-PMMA blends is not zero and varies with temperature, this will be discussed further when item 2 is considered.

An alternative method of normalising the annealing data is by consideration of self diffusion coefficient, D_s, of the low molecular weight component. Recently Liu *et al*[5] published such data for blends of a series of d-PMMA molecular weights in a matrix of h-PMMA (M_W = 980,000). These polymers were ~40-50% syndiotactic and as such had glass transition temperatures consistently lower than those of the polymers we used, which are 70-80% syndiotactic. Liu *et al* find that:

$$D_s = kM_w^{-\alpha}$$

Equation 5.11

where $k = 1.8\times10^{-6}$ cm^2 s^{-1} g^{-1} mol

$\alpha = 2.0$

The data from which this expression was derived was collected at 418K, the temperature dependence of the diffusion coefficient is described by an Arrhenius type expression:

$$D_s = D^o \exp(-E_D / RT)$$

Equation 5.12

where E_D is an activation energy, Van Alsten and Lustig[6] have measured this to be 109 kJ mol^{-1}, combining these two expressions for the diffusion coefficient we find:

$$D_s = k' M_w^{-\alpha} \exp(-E_D / RT)$$

Equation 5.13

where k' = 7.14×10^6 cm^2 s^{-1} g^{-1} mol.

This expression allows us to estimate the diffusion coefficient for a probe d-PMMA in a h-PMMA matrix with $M_W \approx 10^6$ M_W over a range of temperatures and d-PMMA molecular weights. In an attempt to allow for the effect of the differing tacticities of the polymers used in Liu's work and in this work the diffusion coefficients will be calculated using T_g as a reference. Table 5.9 shows variation of the diffusion coefficients, over the range of temperatures used in the annealing program, estimated using Equation 5.13.

	Diffusion coefficients/cm^2s^{-1}			Diffusion length range/Å	
Blend	418K	433K	457K	Low	High
A	4.7×10^{-15}	1.5×10^{-14}	7.8×10^{-14}	520	14100
B	1.1×10^{-15}	3.6×10^{-15}	1.9×10^{-14}	310	6940
C	3.9×10^{-17}	1.2×10^{-16}	6.5×10^{-16}	60	1290
D	4.1×10^{-18}	1.3×10^{-17}	6.9×10^{-17}	15	420

Table 5.9: Diffusion coefficients and diffusion lengths

The quantity of interest when determining how far towards equilibrium the system has been annealed is the diffusion length $(D_s t)^{1/2}$, where t is the actual annealing time, these diffusion lengths are also included in Table 5.9. By this measure the range of 'effective' annealing times used is far smaller than the range calculated by the WLF equation and shown in Table 5.8.

Jones and Kramer[7] have studied the kinetics of enrichment for the d-PS/h-PS system and they derive several approximate expressions for the rate of growth of the surface excess z^*, in particular the characteristic time, t_c, of the approach to equilibrium is given by:

$$t_c = \left(\frac{z^*_{eq}}{\phi_B} \right)^2 \frac{1}{D_s}$$

Equation 5.14

So the 'diffusion length' for equilibrium to be achieved is of order $(D_s t_c)^{1/2}$ and this can be calculated from the surface excess and the bulk volume fraction of d-PMMA. The phenomenological theory of surface enrichment predicts that the surface enrichment composition profile will be approximately exponential in form and that the decay length of the exponential will be of the order of the radius of gyration of the enriching polymer. The radii of gyration of the deuterated polymers used in this work are approximately 30Å, 40Å, 95Å and 165Å for blends A to D respectively. The surface volume fraction of d-PS observed in the d-PS/h-PS blends is around 0.6. Using these values a 'diffusion length' of the order of 75Å for blend A and 410Å for blend D for surface equilibrium to be reached. The characteristic 'diffusion length' for equilibrium is proportional to the surface excess and so for smaller surface excesses proportionally smaller equilibrium 'diffusion lengths' are required. Comparing these estimates of equilibrium diffusion lengths with the range explored by the annealing program then by these criteria some surface enrichment should be observable in all of the blends examined. Therefore insufficient annealing is not responsible for the lack of observable surface enrichment.

The value of χ for a binary blend and the difference between the surface energies of the two components both affect the expected surface volume fraction. Earlier in this chapter the following expressions for χ were obtained:

$$\chi = -0.12 + \frac{54}{T} \qquad \text{(Blend B)}$$

Equation 5.15

$$\chi = \frac{1.6}{T} \qquad \text{(Blend D)}$$

Equation 5.16

These data indicate that the higher molecular weight blends were annealed rather closer to the phase boundary than the lower molecular weight blends, given these values

for χ and assuming that the surface energy difference between h-PMMA and d-PMMA is the same as that between d-PS and h-PS (i.e. 0.078mJ m^{-2}) insignificant amounts of enrichment for the low molecular weight blends (A and B) are expected but significant amounts of enrichment for the highest molecular weight blend (D) and possibly blend (C). Surface enrichment profiles for blend D, calculated using the expressions derived by Jones and Kramer are shown in Figure 5.18, these expressions assume that the two components of the blend have the same degree of polymerisation. The χ parameters used in Figure 5.18a are the extremes of the range of values calculated for the annealing program, this figure shows how the surface enriched layer becomes much thicker as the coexistence curve is approached i.e. χ increases. The differences in surface tension, used in Figure 5.18b, range from the value found in the d-PS/h-PS system downwards. For the systems modelled here the surface enrichment is virtually zero when the surface energy difference is 0.02 mJ m^{-2}. Entropic forces, favouring the low molecular weight species at the surface, will enhance the surface enrichment slightly, this effect will be largest for blend A an smallest for blend D.

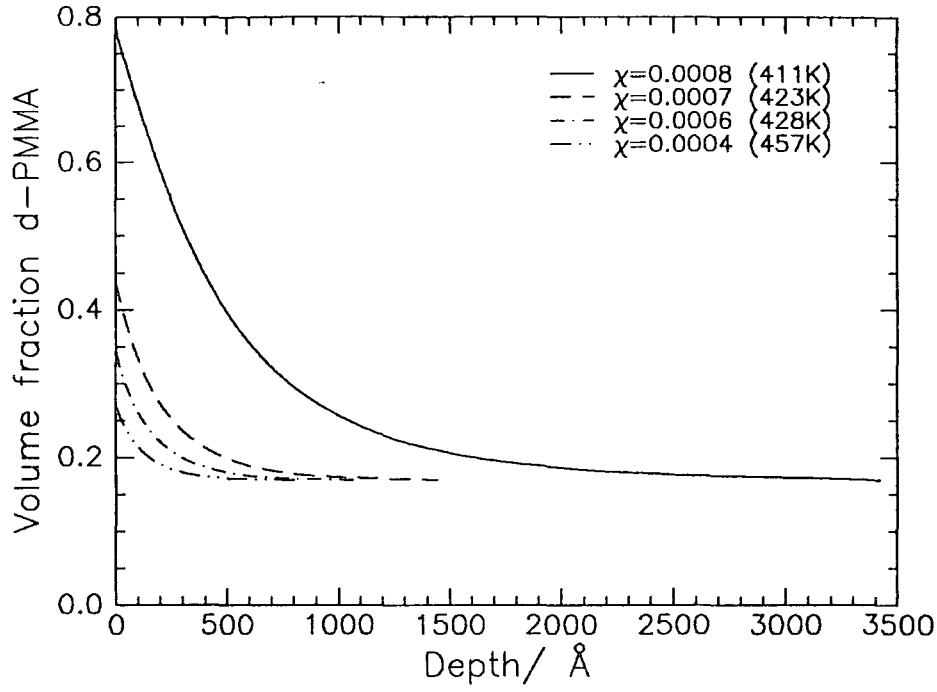

Figure 5.18a: Theoretical composition profiles calculated from the expressions of Jones and Kramer for blend D. Surface energy fixed at 0.08 mJ m^{-2} and χ varied over the range for blend D (temperature in brackets is that at which the value of χ is found.

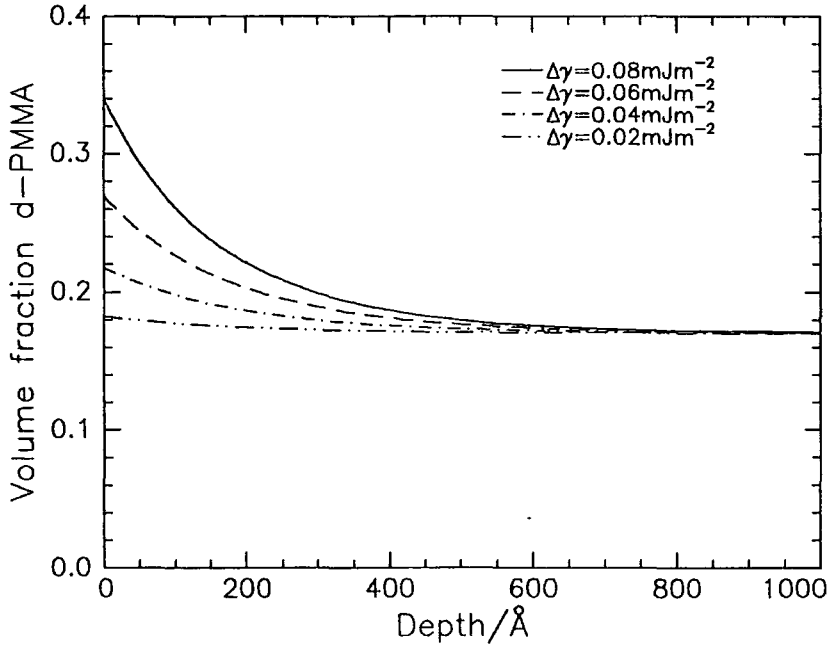

Figure 5.18b: χ = 0.0006, the surface energy difference is varied.

Surface enrichment can be driven by surface energy differences too small to measure directly. Experiments on the competitive adsorption[8] of d-PS and h-PS from solution onto SiO_2 show an isotope effect (with the d-PS adsorbing preferentially), in contrast similar experiments[9] using PMMA show no isotope effect. Granick attributes this difference to the fact that PMMA interacts with the SiO_2 surface via the carbonyl bond, which is not subject to the effects of deuterium isotope substitution. An attempt was made to calculate the surface energy of d-PMMA relative to that of h-PMMA using the parachor[10]. The parachor predicts surface energy by adding terms from the atomic composition and structural features such as double bonds and rings together. No data are available for the contribution of the deuterium atom. The deuterium contribution was estimated from the known difference in surface energy between h-PS and d-PS and then this deuterium term was used to calculate the surface energy of d-PMMA, the surface energy for h-PMMA was also calculated using the parachor. The difference between these calculated surface energies is 0.06mJ m^{-2}, about 75% of the difference between d-PS and h-PS. Clearly this is a fairly crude calculation, but it does indicate that the expected surface energy difference between d-PMMA and h-PMMA is rather less than that between d-PS and h-PS. The neutron reflectivity data presented here suggest that the surface energy difference between d-PMMA and h-PMMA is in the range 0.0 to 0.04mJ m^{-2}.

Tasaki *et al*[11] have published neutron reflectivity data that indicate enrichment of d-PMMA does occur in blends of d-PMMA and h-PMMA, where M_w (h-PMMA) ≈ 330,000 and M_w (d-PMMA) varies from 12,000 to 330,000. The degree of enrichment is very high (almost 100% d-PMMA at the surface), but the surface excess is very small because the characteristic length of the enriched layer is very small (~10Å). The authors make no mention of the background subtraction they have used and the reflectivity profiles they show are characteristic of data from which no background has been subtracted, the enrichment they observe may well be an artefact arising from incorrect background subtraction. In addition the authors do not state the tacticity of their polymers, but the annealing temperature used was 120°C, approximately 10°C below the glass transition temperature of the polymers used here, but slightly above that of the polymers used by Liu *et al.*

5.2.4 Conclusions

The surface enrichment behaviour of various low molecular weight probe d-PMMA in a high molecular weight matrix h-PMMA has been studied; over a range of probe molecular weights and annealing times. Neutron reflectometry has been used to determine the surface and near surface composition. No significant enrichment of either the h-PMMA or the d-PMMA to the air interface has been observed, this is attributed to an insufficient surface energy difference between the hydrogenous and deuterated polymers. This is in contrast to the behaviour observed by other workers in the d-PS/h-PS system where deuteration does produce a large enough change in surface energy to drive considerable amounts of d-PS to the air surface.

5.2.5 References for Section 5.2

1 . J. D. Ferry, 'Viscoelastic Properties of Polymers 3rd ed.', Wiley, 1980.

2 . D. S. Sivia, W. A. Hamilton, G. S. Smith, *Physica B*, 173, 1991, 121.

3 . T.P. Russell, *Material Science Reports*, 5, 1990, 171.

4 . G. Reiter, U. Steiner, *Journal de Physique II*, 1, 1991, 659.

5 . Y. Liu, G. Reiter, K. Kunz, M. Stamm, *Macromolecules*, 26, 1993, 2134.

6 . J. G. Van Alsten, S. R. Lustig, *Macromolecules*, 25, 1992, 5069.

7 . R. A. L. Jones, E. J. Kramer, *Philosophical Magazine B*, 62(2), 1990, 129.

8 . P. Frantz, D. C. Leonhardt, S. Granick, *Macromolecules*, 24, 1991, 1868.

9 . H. E. Johnson, S. Granick, *Macromolecules*, 23, 1990, 3367.

10 . D.W. Van Krevelen, 'Properties of Polymers 3rd edition', Elsevier, 1990.

11 . S. Tasaki, H. Yamaoka, F. Yoshida, *Physica B*, 180 & 181, 1992, 480.

This page left intentionally blank

6. Poly (ethylene oxide) / poly (methyl methacrylate) blends

6.1 Thermodynamics

6.1.1 Experimental

The small angle neutron scattering from blends of d-PEO with syndiotactic h-PMMA and h-PEO with syndiotactic d-PMMA have been measured at temperatures of 423K, 438K, 458K and 473K to determine the effective Flory - Huggins interaction parameter, χ, and hence the phase behaviour of these blends. These temperatures were chosen to be well above the melting point of PEO/PMMA at ~333K. The samples for neutron scattering were prepared in the manner described in the Section 4.2, the solvent used for re-precipitation was hexane. The pure PEO samples, used to make background measurements, were pressed at 373K, all other samples were pressed at 423K. The pure PEO samples were found to flow out of the sample press at the higher pressing temperature. Four different volume fractions of PEO for each of the two blends were used. Details of the blend compositions, the molecular weights of the polymers used and the 'global' codes for the polymers are shown in Table 6.1.

Label		M_w	M_w/M_n	Code	Volume fraction PEO, ϕ			
DPEO	d-PEO	102,200	1.2	TK77	0.101	0.151	0.199	0.247
	h-PMMA	147,600	1.3	TK76				
HPEO	h-PEO	124,300	1.1	TK74	0.126	0.186	0.239	0.272
	d-PMMA	117,900	1.2	TK22				

Table 6.1: Details of blends used in small angle scattering experiments.

All data were collected on single occasion in July 1993. Elastic coherent scattering I(Q) vs Q were obtained by the methods outlined in the 4.2 section. The quartz windows of the h-PMMA sample cell cracked early in the experiment, for this reason scattering from pure h-PMMA measured on a previous occasion was used in the background subtraction.

6.1.2 Results

Figure 6.1 shows examples of the elastic scattering, I(Q), for both the DPEO and HPEO blends. At 423K the data show the trends in overall intensity that would be expected for such blends, i.e. scattering increases as the volume fraction of PEO is increased. The $\phi = 0.126$ HPEO blend exhibits much higher scattering at very low Q values than the other HPEO blends, which show a downturn in this region. This is probably caused by incorrect subtraction of the direct beam, at higher Q values the relative intensities are as expected. There is generally no regular trend in the scattering intensity for a single blend as a function of increasing temperature. Broadly the intensity drops as the temperature increases, but the decrease between consecutive measurements is not uniform. For the $\phi = 0.101$ and $\phi = 0.151$ DPEO blends negative apparent scattering is observed at high Q values for the higher measurement temperatures (458K and 473K), clearly this is unphysical and must arise from the over subtraction of the incoherent background. The $\phi = 0.199$ DPEO blend exhibits scattering considerably less intense at 458K and 473K than at 423K and 438K, this may well indicate a less extreme manifestation of the over subtraction of the background. The background scatter from the blend is not necessarily the simple sum of the scatter from the pure components of the blend, as has been commented upon in the section 4.2.4. Table 6.2 gives a broad indication of the 'quality' of the I vs. Q data obtained, three categories have been used to classify the data: (✓) the data conform with expectation in terms of the shape of the I vs Q profile and the overall intensity compared to the scattering of the same sample at lower temperatures, (✗) the data exhibit negative apparent scattering in some parts of the Q range. (?) the data do not exhibit negative apparent scattering, but the overall intensity is low in comparison with scattering from the same sample at lower temperatures. It was noted that air bubbles formed in nearly all the samples during the course of the experiment, an estimate of the degree of bubble formation at the end of the experiment is shown in Table 6.3. The extent of the bubbles increased with increasing temperature. The presence of air bubbles in the sample will have two consequences, firstly the flat incoherent background will be over subtracted because more material will have been accounted for in the background calculation than is 'seen' by the neutron beam, this effect will be independent of Q. Secondly the intensity of the elastic coherent scattering will be reduced, again because the amount of material 'seen' by the neutron beam is

reduced from the expected value; this will result in an observed elastic scatter that is some fraction of the actual elastic scatter. The data will initially be analysed assuming only a correction in the incoherent background, subsequently an attempt will be made to account for the expected scaling of the elastic scatter caused by the presence of air bubbles.

Blend	423K	438K	458K	473K
DPEO (ϕ = 0.101)	✓	✓	✗	✗
DPEO (ϕ = 0.151)	✓	✓	✗	✗
DPEO (ϕ = 0.199)	✓	✓	?	?
DPEO (ϕ = 0.247)	✓	✓	✓	✓
HPEO (ϕ = 0.126)	✓	?	?	?
HPEO (ϕ = 0.186)	✓	?	?	?
HPEO (ϕ = 0.239)	✓	✓	?	?
HPEO (ϕ = 0.272)	✓	?	?	?

Table 6.2: Evaluation of the quality of the I vs Q obtained for the blends

Blend	Rank	Comments
DPEO (ϕ = 0.101)	4	A number of large bubbles
DPEO (ϕ = 0.151)	2	Several small bubbles near edges
DPEO (ϕ = 0.199)	3	Several large bubbles
DPEO (ϕ = 0.247)	1	No bubbles
HPEO (ϕ = 0.126)	4	A number of large bubbles
HPEO (ϕ = 0.186)	2	Several small bubbles near edges
HPEO (ϕ = 0.239)	4	A number of large bubbles
HPEO (ϕ = 0.272)	4	A number of large bubbles

Table 6.3: Ranking of samples, as regards bubble formation, at experiment end.

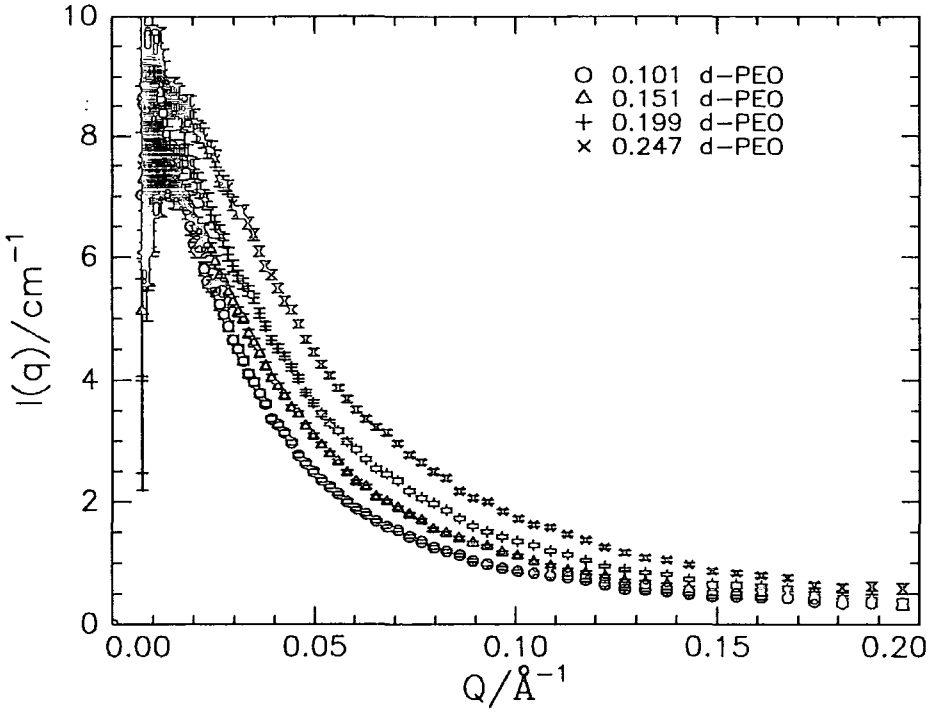

Figure 6.1a: I(Q) vs Q for the DPEO blend at 423K with errors from Poisson statistics, as a function of composition.

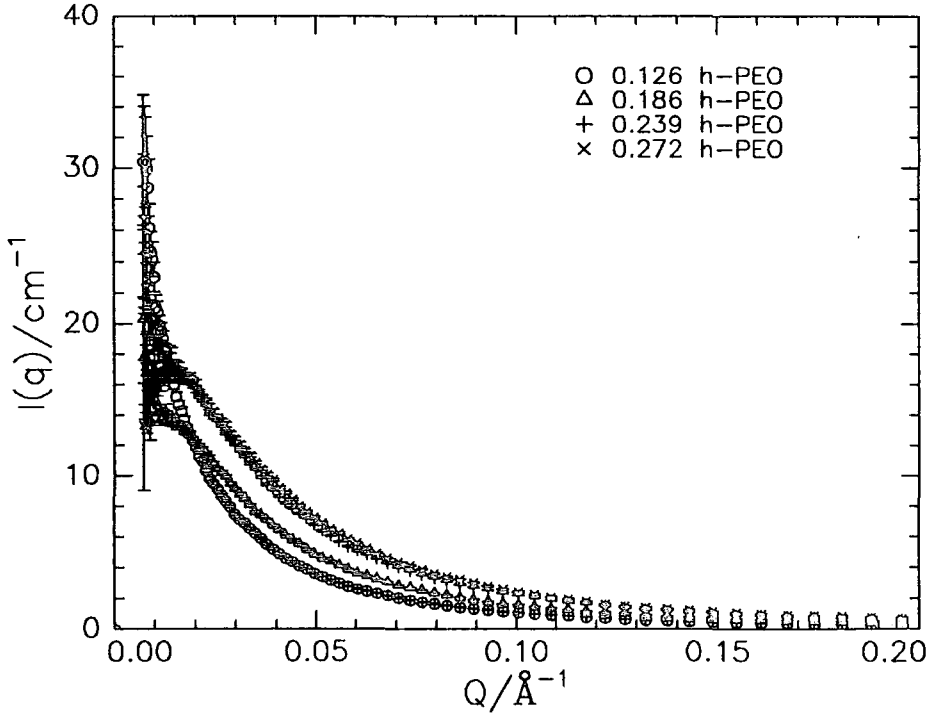

Figure 6.1b: I(Q) vs Q data for the HPEO blend at 423K, as a function of composition

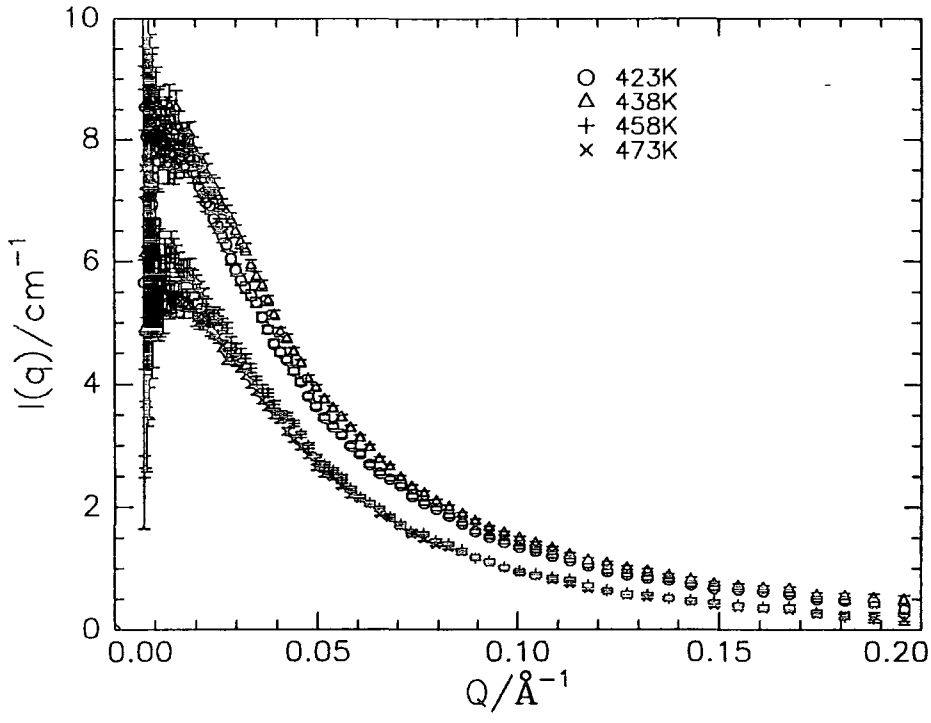

Figure 6.1c: I(Q) vs Q data for the DPEO blend ϕ = 0.151, as a function of temperature.

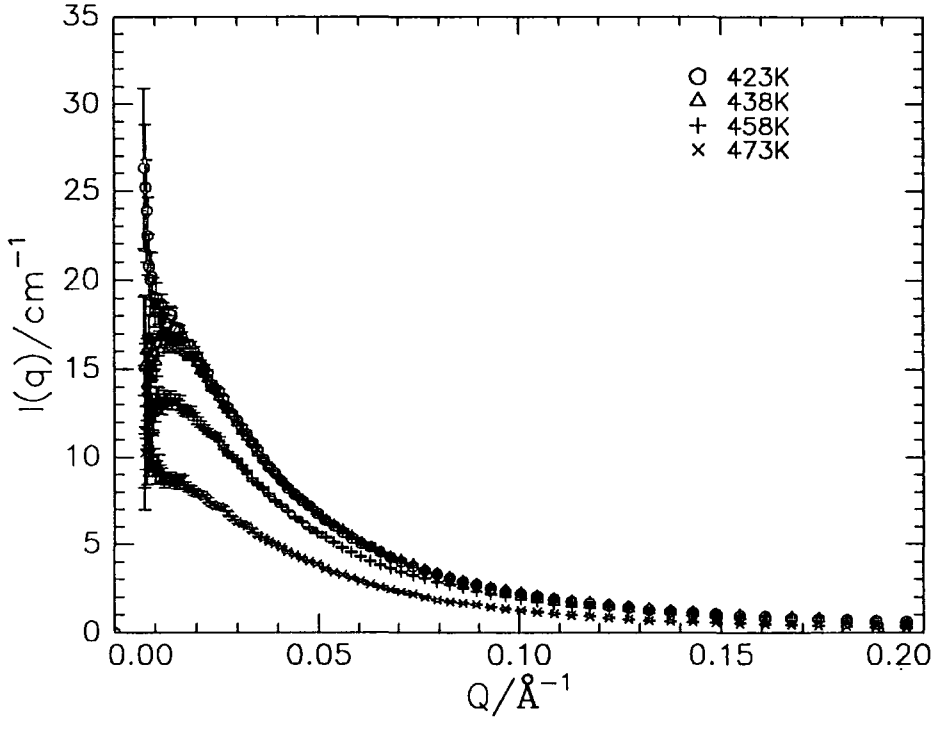

Figure 6.1d: I(Q) vs Q data for the HPEO blend ϕ = 0.239, as a function of temperature.

Values in the literature[1] for $<S_o/M_w^{1/2}>$ indicate that the low Q limit of the Debye function is not probed by the LOQ diffractometer for these blends. For this reason the data were fitted using the FORTRAN program Pullet4, which fits the random phase approximation allowing for the different volumes of the PEO and PMMA repeat units, also included is a flat 'residual' background to allow for possible errors in the initial background subtraction procedure. The data were fitted over the full Q range $0.008Å^{-1} < Q < 0.21Å^{-1}$. χ, the 'residual' background and the radii of gyration of both blend components were fitted. The χ data obtained using these fits are shown in Figure 6.2. There are quite large variations in χ with temperature and composition, in the HPEO blends these trends are fairly uniform, whereas for the DPEO blend there is a discontinuity between values obtained for the samples at 423K and 438K (the 'good' samples) and those obtained at 458K and 473K (the 'poor' samples). Representative fits to the data are shown in Figure 6.3, in the form of Kratky plots. The fits to the data were generally of a high quality and replicated the negative scattering at high Q observed for some of the blends. The fit to the low Q region of the $\phi = 0.126$ HPEO blends, which exhibited unusual scattering at low Q compared to the other HPEO blends, was rather poor. It was found to be impossible to fit the radii of gyration of both components of the blends simultaneously, the scattering is not sensitive to both of these parameters but rather the combination of the two.

Figure 6.4 shows values of the residual background fitted for the HPEO and DPEO blends. The residual background fitted to the DPEO correlate well with the evaluations of the data in Table 6.2, those samples deemed to be of the expected intensity are fitted with a positive residual background and those with lower than expected intensity are fitted with a negative residual background. The positive values could indicate either that the incoherent background is initially under subtracted or the residual background could be fitting deviations from the Debye function exhibited by the scattering polymers. The HPEO blends were all fitted with negative values for the residual background. The residual backgrounds fitted were up to 20% of the measured incoherent background in magnitude, because the 'best' samples are fitted with positive values and the worst with negative values of the residual background the incoherent background subtracted could be as much as $\times 1.4$ the correct magnitude in the worst case.

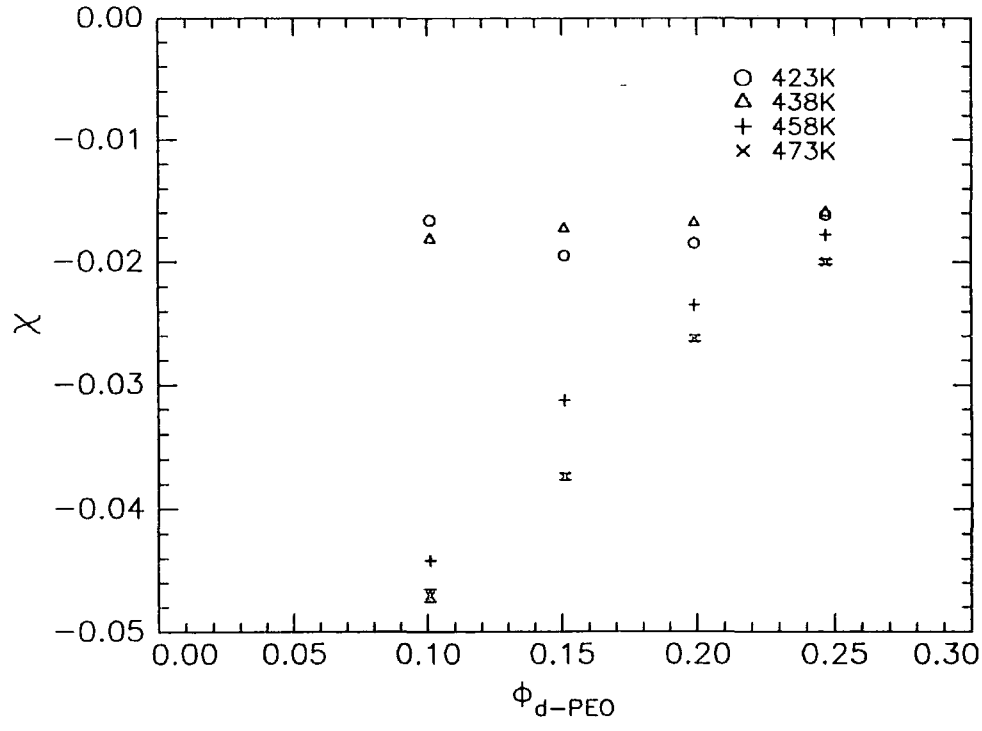

Figure 6.2a: χ vs ϕ for the DPEO blend, fitted using fixed normalisation constant and varying radii of gyration of the blend components.

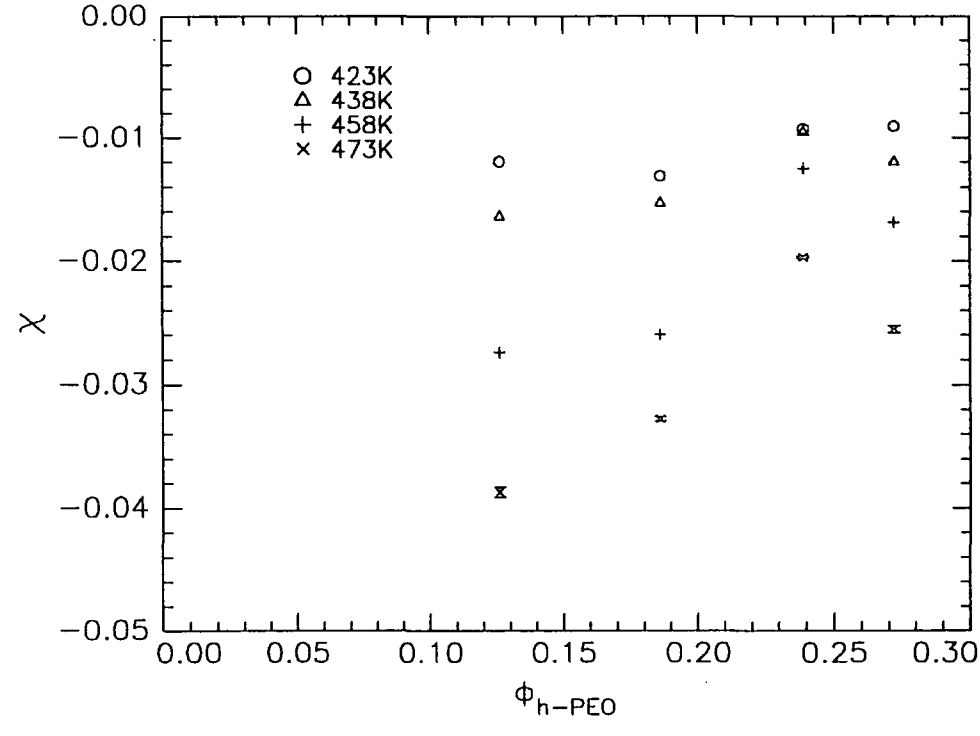

Figure 6.2b: χ vs ϕ for the HPEO blend, fitted using fixed normalisation constant and varying radii of gyration of the blend components.

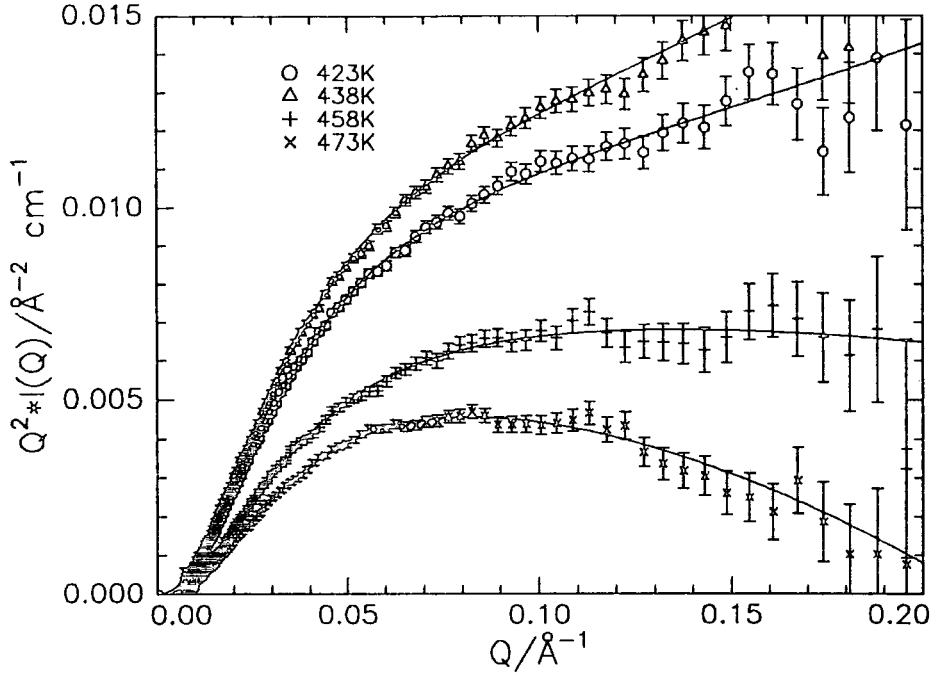

Figure 6.3a: Representative fits to the DPEO data (ϕ = 0.151), using the Kratky plot $Q^2I(Q)$ vs Q. Data fitted using fixed normalisation constant and varying radii of gyration.

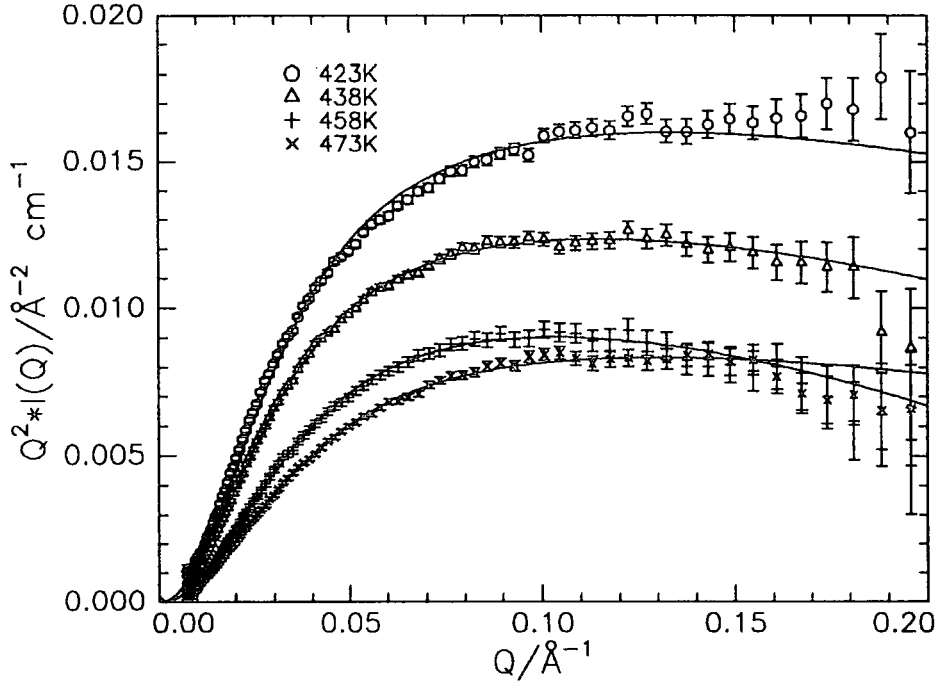

Figure 6.3b: Representative fits to the HPEO data (ϕ = 0.186), using the Kratky plot $Q^2I(Q)$ vs Q. Data fitted using fixed normalisation constant and varying radii of gyration.

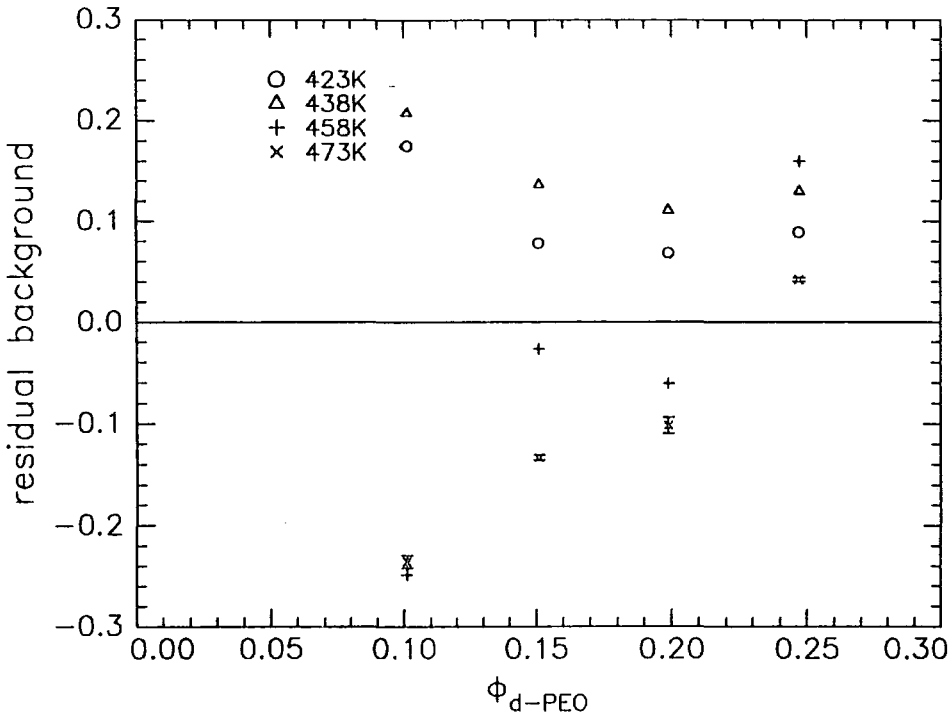

Figure 6.4a: Values fitted for the residual background to the DPEO blend data, normalisation constant fixed, radii of gyration of the blend components varied.

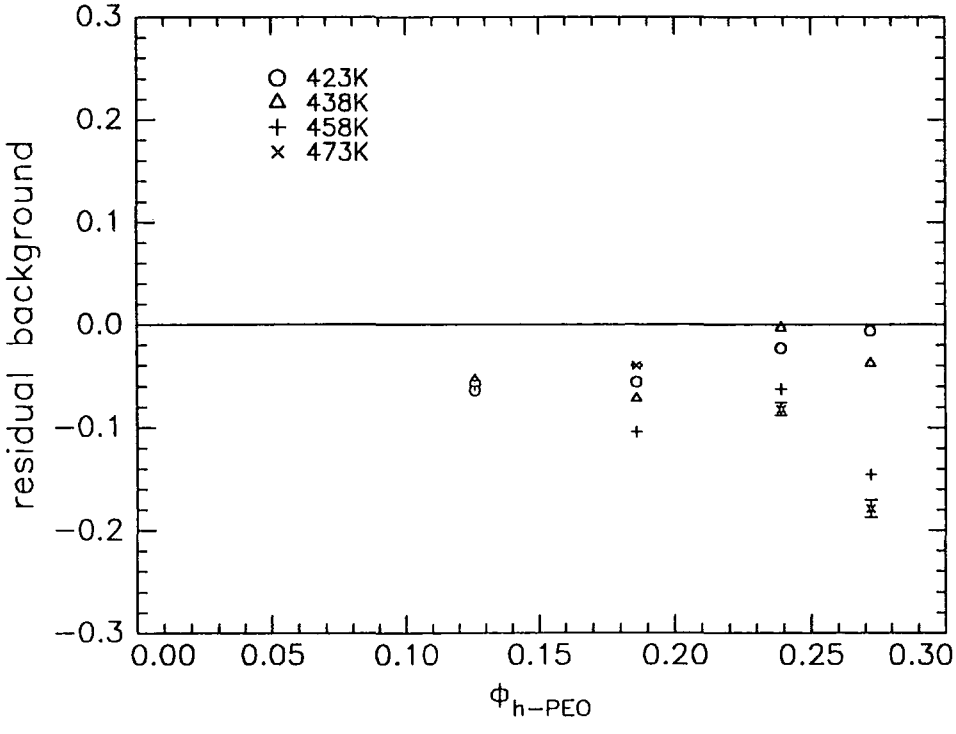

Figure 6.4b: Values fitted for the residual background to the DPEO blend data, normalisation constant fixed, radii of gyration of the blend components varied.

This over subtraction of background should be associated with an equally large fractional change in the coherent scatter, this would result in apparent χ values that were considerably more negative than the actual χ values. To account for this reduction in the coherent scattering the data were fitted using a varying value for the normalisation constant. This was done using Pullet4, the values for the radii of gyration of the components were fixed at the values calculated from the molecular weights of the polymers and literature values for $<S_o/M_w^{½}>$. These were for the d-PEO = 98Å, 108Å for the h-PEO, 86Å for the d-PMMA and 104Å for the h-PMMA. χ, the residual background and the normalisation constant were allowed to vary. Clearly the fitting of the normalisation constant is somewhat undesirable and results obtained in this way should be considered as tentative. The values of χ fitted using this procedure are shown in Figure 6.5. The three parameters fitted were found to reach well defined values quite rapidly. The quality of the fits was good, in fact the fit index's generated by Pullet4 were identical for both methods of data analysis for any particular sample, this would suggest that the model profiles are identical using these two fitting methods it is simply the parameters used to generate the fit that are different. The expected value of the normalisation constant for these data, in the absence of bubbles is 0.95, fitted values ranged from very slightly above this value down to around 0.5 for some of the data collected at 473K.

Comparing the values of χ obtained using these two different methods of data analysis, it was found that for the 'good' DPEO samples the fitted values of χ are very similar, see Table 6.4. Given this agreement for the 'best' samples and the fact that the analysis fitting the normalisation constant represents a solution to an expected inadequacy in measured data the remaining analysis and discussion in this section will be centred on the χ values obtained using the method involving the fitting of the normalisation constant.

There are several possible sources of error in the χ values presented, excluding the relatively small error that is indicated by the fitting procedure. Firstly there is the possibility of a calibration error, this will effect both DPEO and HPEO blends equally and so will not effect the conclusions drawn from the data. Secondly there is the uncertainty arising from the values of the radii of gyration that have been calculated from literature values of $<S_o/M_w^{½}>$ and the molecular weights of the polymers. The uncertainty in $<S_o/M_w^{½}>$ is around 4% for PEO and 10% for PMMA. The uncertainty in

the molecular weights is around 10%, the square root of M_w is used in the calculation of the radii of gyration and so the error from this source is around 5%. Errors in $<S_\alpha/M_w^{½}>$ will effect both DPEO and HPEO blends equally, so relative differences in the χ values for these two sets of blends should be preserved, if this is the only source of error. Uncertainties in the molecular weight may result in changes in the relative differences in χ between the DPEO and HPEO blends. In summary, the systematic error in the absolute value of χ, arising from uncertainties in $<S_\alpha/M_w^{½}>$ and the calibration constant are of the order of 10-15%. Relative statistical errors in χ between the DPEO and HPEO blends are of the order of 10%.

ϕ (DPEO)	T/ K	χ (normalisation constant fixed)	χ (normalisation constant fitted)	Difference
0.101	423	-0.0166	-0.0169	0.0003
0.151	423	-0.0195	-0.0181	-0.0014
0.199	423	-0.0185	-0.0181	-0.0004
0.247	423	-0.0162	-0.0188	-0.0026
0.101	438	-0.0182	-0.0178	-0.0004
0.151	438	-0.0173	-0.0182	0.0009
0.199	438	-0.0168	-0.0175	0.0007
0.247	438	-0.0160	-0.0178	0.0018
0.247	458	-0.0178	-0.0184	0.0006
0.247	473	-0.0200	-0.0200	0.0000

Table 6.4: Comparison of the 'good' DPEO data fitted using the two methods presented in the text.

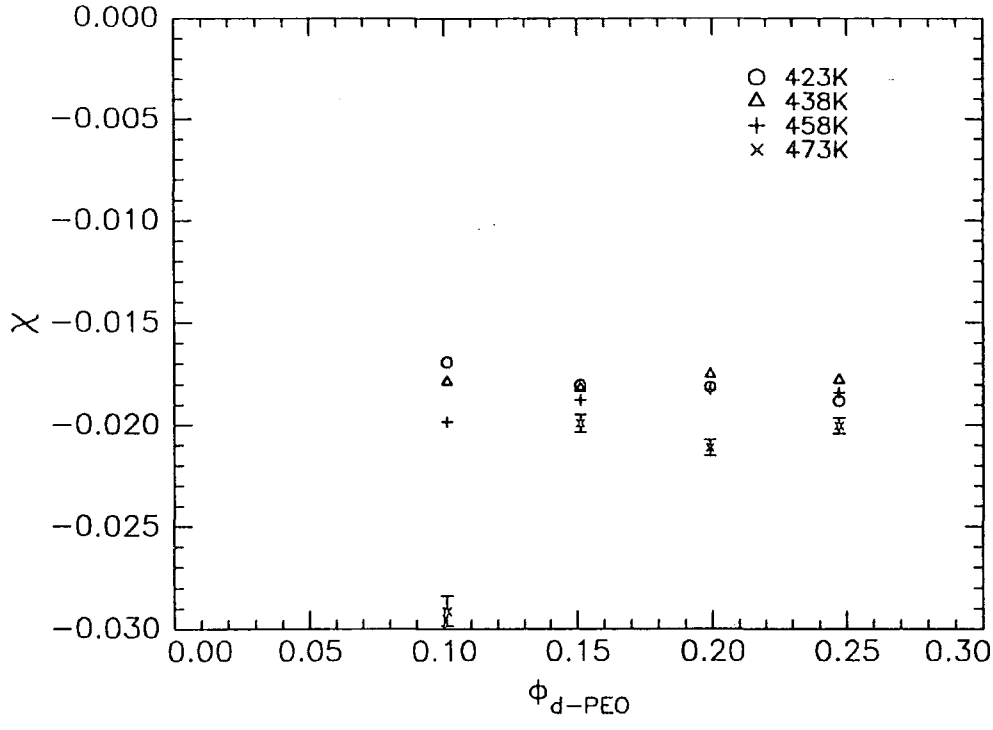

Figure 6.5a: χ vs ϕ for the DPEO blend, fitted using a varying normalisation constant and fixed radii of gyration for the blend components.

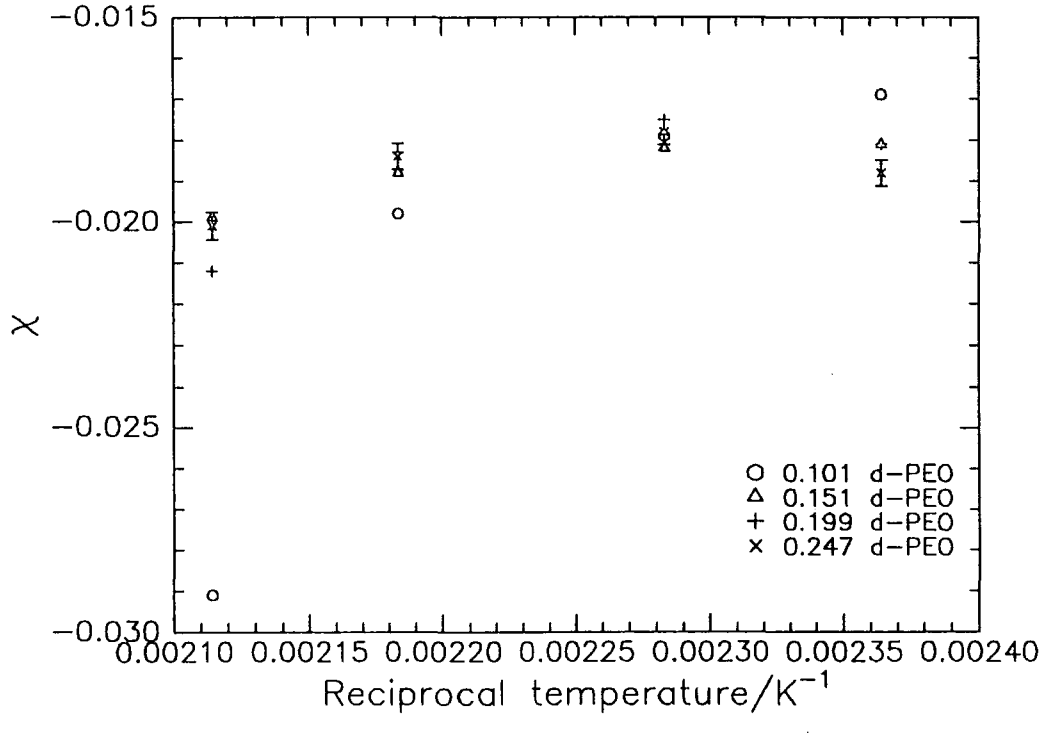

Figure 6.5b: χ vs 1/T for the DPEO blend, fitted using a varying normalisation constant and fixed values for the radii of gyration for the blend components.

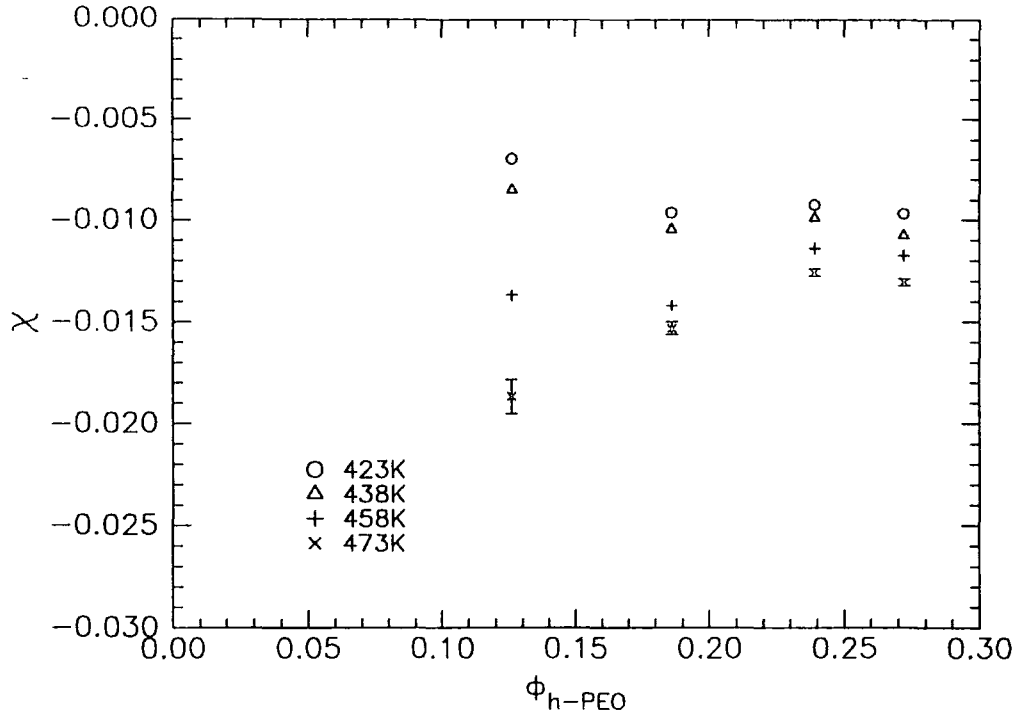

Figure 6.5c: χ vs ϕ for the HPEO blend, fitted using a varying normalisation constant and fixed radii of gyration for the blend components.

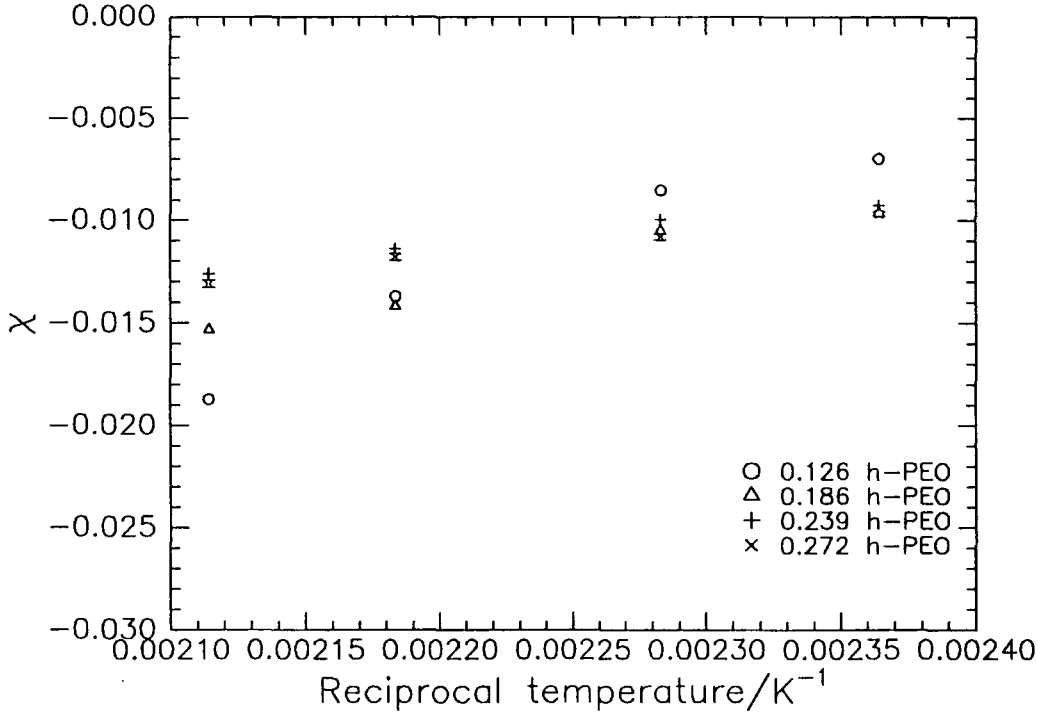

Figure 6.5d: χ vs 1/T for the HPEO blend, fitted using a varying normalisation constant and fixed values for the radii of gyration for the blend components.

	ϕ(PEO)	A	B /K^{-1} -	T_s/K
DPEO	0.101	-0.12(4)	44(18)	360(190)
	0.151	-0.034(4)	7(2)	190(60)
	0.199	-0.04(2)	11(8)	240(240)
	0.247	-0.03(1)	5(5)	150(150)
HPEO	0.126	-0.12(2)	47(8)	390(90)
	0.186	-0.068(8)	25(4)	360(70)
	0.239	-0.041(3)	14(1)	320(30)
	0.272	-0.040(3)	13(1)	310(30)

Table 6.5: A and B parameters fitted to the DPEO and HPEO blend data according to Equation 6.1

Table 6.5 shows parameters of fits of the form shown in Equation 6.1 along with the spinodal temperature calculated from these fits.

$$\chi = A + \frac{B}{T}$$

Equation 6.1

A is the entropic contribution to χ and B is the enthalpic contribution to χ. The reciprocal temperature dependence of the χ values for the DPEO blends is non-linear, this is reflected in the large errors in the fitted parameters. The variation in χ with composition is quite weak, except for the $\phi = 0.101$ blend where the χ value measured at 473K is rather more negative than the values measured at lower temperatures. The variation of χ with reciprocal temperature for HPEO is rather more linear as is indicated by the smaller values for the errors in the fitting parameters. There is a weak decrease in χ as ϕ is decreased, again the $\phi = 0.136$ data are anomalous when compared to the data at higher ϕ values.

Although literature values of $<S_o/M_w^{1/2}>$ indicate that the low Q limit of the Debye function is not reached for these blends, when the data are plotted in the Ornstein - Zernike mode (see Figure 6.6), they are found to be linear at low Q which is the behaviour expected in the low Q limit of the Debye function. When linear fits to this

region are made and χ values extracted from the intercept at Q = 0 the values of χ obtained are very similar to those obtained using the full random phase approximation. There are larger deviations where negative values for the residual background have been fitted using Pullet4, this is expected because this linear fit takes no account of errors in the background subtraction.

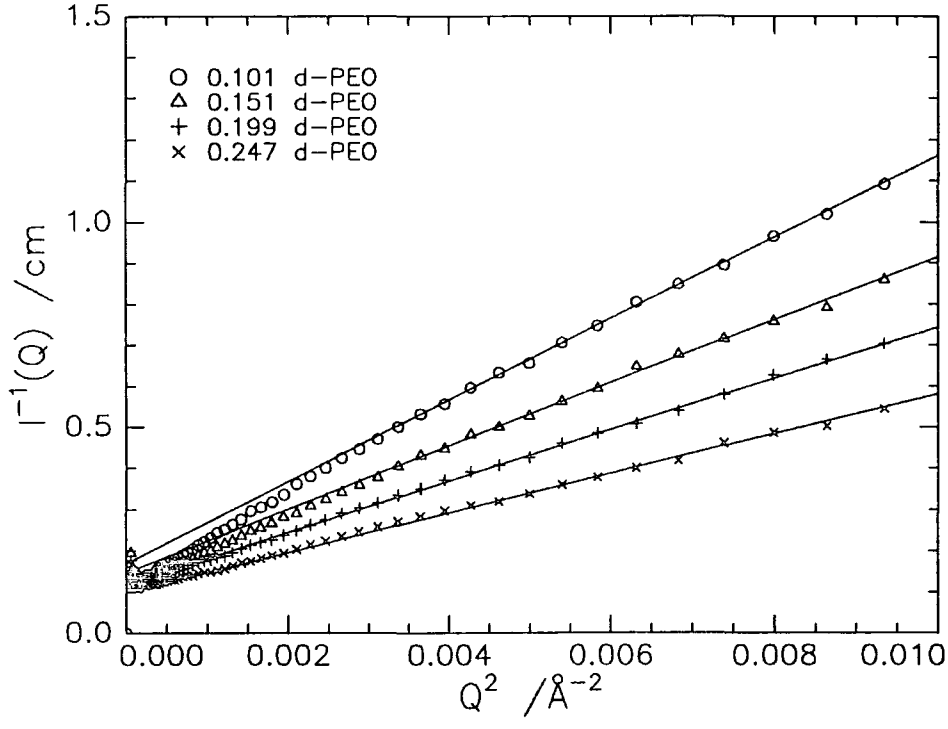

Figure 6.6: Ornstein - Zernike plots for DPEO blends at 423K, illustrating the linearity at low Q.

6.1.3 Discussion

The values of χ determined in this work can be compared to those which have been obtained for other polymer blends. This discussion will concentrate on χ values determined using small angle neutron scattering, the systems for which χ values have been measured in this way can be divided into three categories:

(1) The very simplest 'homopolymer' blends, where a hydrogenous polymer is blended with its deuterated counterpart, these systems have been discussed in this thesis in relation to the h-PMMA/d-PMMA blends.

(2) Systems where the two blend components are chemically very similar, such as deuterated polystyrene (dPS) / poly (α methylstyrene) (PαMS)[2], poly (ethylene-co-propylene)(PEP) / poly (ethylene -co-butene-1)(PEB)[3], polystyrene (PS) / Poly (bromo-styrene) (PBrS)[4 §] and blends of poly (ethylene-co-butene)[3] with various proportions of ethylene and butene (dPEBx/dPEBy).

(3) Blends of chemically quite different polymers, these include deuterated polystyrene (dPS) / poly (vinyl methyl ether) (PVME)[5,6,7] , deuterated poly (methyl methacrylate) (d-PMMA) / poly (styrene-co-acrylonitrile) (PSAN)[8], deuterated polystyrene (dPS) / poly (butadiene) (PB)[9], partially deuterated methoxylated poly (propylene glycol) (d PPGM) / methoxylated poly (propylene glycol) (PEGM)[9], deuterated polystyrene (d-PS) / poly (phenylmethylsiloxane) (PPMS)[7], the interaction parameter for PEO/PMMA has also been measured by Ito *et al*[10]. Table 6.6 shows values of χ obtained for systems in these second two categories, in addition to small angle scattering measurements χ has also been measured for some of these blends using equation of state (PVT) measurements (PEO/PMMA[11], d-PS/PVME[7], d-PS/PPMS[7]) or by cloud point measurements (PS/PαMS[12], PS/PVME[12]). Values of the interaction parameter, from all sources, for PEO/PMMA blends can be found in Table 6.7

Examining the values of χ in Table 6.6, it can be seen that the blends of chemically similar components are characterised by a small ($\sim 10^{-3}$) positive interaction parameter. For the blends of more dissimilar components, d-PS/PVME has a relatively large negative interaction parameter, this arises from specific interactions between the styrene ring and the PVME[13]. Other systems (d-PS/PPMS, d-PS/PB, d-PPGM/PEGM),

§ Small Angle X-ray Scattering

exhibit equally large positive values of χ suggesting unfavourable interactions between the blend components.

	χ	Temperature /K	Composition
d-PS/PαMS	0.005	503	0.5
PS/PBrS	0.003	403	0.5
DPEB/PEP	0.0013	353	0.5
dPEBx/hPEBy	0.001	440	0.5
d-PS/PVME[5]	-0.0368	298	0.5
d-PS/PVME[6]	-0.0359	298	0.5
d-PS/PVME[7]	-0.0598	298	0.31
d-PMMA/PSAN	-0.0164	413	0.5
PEO/PMMA[10]	-0.0010	353	0.3
PEO/d-PMMA	-0.004(6)	353	0.272
d-PS/PPMS	0.099	353	0.13
d-PS/PB	0.076	353	0.5
d-PPGM/PEGM	0.064	353	0.5

Table 6.6: Values of χ obtained for various blends using small angle scattering, key to abbreviations and literature sources in the text above.

Finally, there are the values of χ from the d-PMMA/PSAN and PEO/PMMA blends, these values are negative and not as large in magnitude as the values obtained for d-PS/PVME. These relatively small χ values are probably the result of a combination of favourable and unfavourable interactions, PMMA and PS are known to be incompatible and are characterised by a positive interaction parameter[14] of around 0.03. This unfavourable interaction must be balanced and indeed exceeded by the dipole-dipole interactions that would be expected to exist between PMMA and poly (acrylonitrile) in the d-PMMA/PSAN system. Similarly it has been proposed that in the PEO/PMMA system favourable interactions between the electronegative oxygen in PEO and the electropositive carbonyl carbon in PMMA are opposed by repulsive forces between the electronegative oxygens in both PEO and PMMA[15], leading to a weak overall interaction.

Moving on to the χ values for PEO/PMMA in Table 6.7, the values of χ measured using melting point depression and equation of state measurements are rather larger in magnitude than the values obtained using SANS.

ϕ (PEO)	Temperature /K	χ	Method, reference
-	347	-0.35	MP, 16
-	333	-0.139	MP, 17
-	333	-0.157	MP, 18
-	337	-0.08	MP, 19
0.10	393	-0.16	PVT, 11
0.82	353	-0.0067	SANS, 10
0.54	353	-0.0058	SANS, 10
0.33	353	-0.0029	SANS, 10
0.18	353	-0.0010	SANS, 10
0.05	353	0.0083	SANS, 20
0.272 (h-PEO)	353	$-0.004(6)^{ex}$	SANS, this work
0.126 (h-PEO)	353	$0.02(2)^{ex}$	SANS, this work
0.272 (h-PEO)	423	-0.0097(2)	SANS, this work
0.126 (h-PEO)	423	-0.0070(2)	SANS, this work
0.247 (d-PEO)	353	$-0.02(2)^{ex}$	SANS, this work
0.101 (d-PEO)	353	$0.01(9)^{ex}$	SANS, this work
0.247 (d-PEO)	423	-0.0188(2)	SANS, this work
0.101 (d-PEO)	423	-0.0169(2)	SANS, this work

Table 6.7: Values of χ obtained for PEO/PMMA from all techniques, included are values from this work. MP - melting point depression, ex - extrapolated from higher temperatures. PVT - equation of state measurements.

In the case of the equation of state data this difference can be attributed to a difference in definition of the 'interaction parameter, the 'χ' value measured by Privalko[11] is actually X defined by Sanchez and Lacombe[21]. (see equations 38 and 39 and Appendix B in reference 21). In principle it should be possible to calculate the Flory - Huggins interaction parameter from the equation of state data in the Privalko paper, unfortunately the data are not presented clearly enough to extract the parameters with the required

accuracy. Although melting point depression measurements give an indication of the degree of polymer-polymer miscibility, through the medium of an interaction parameter, there are both experimental and theoretical difficulties[22] which make the values of χ obtained somewhat inaccurate when compared to the absolute values measured using small angle neutron scattering.

Turning to the other SANS data on the PEO/PMMA blends there are areas of agreement and disagreement between this work and the work of Ito *et al*[10]. Extrapolating the values of χ obtained in this work to the temperature at which Ito *et al* made their measurements (353K), it is found that the values of χ obtained are the same, within the substantial error which arises from the extrapolation. In addition the variation in χ over the composition range used here is the same as that measured by Ito. The only difference this work and that of Ito is the measured temperature dependence of χ; Ito *et al* report that there is no temperature dependence in χ over an 80K range for a ϕ_{PEO} = 0.54 blend, this is not in agreement with the behaviour observed here for blends with a lower volume fraction of PEO. It is not clear from Ito *et al* which temperatures the 80K range covers, but the implication is that Ito *et al* would expect values of χ at 423K considerably smaller than those measured here. There are a number of experimental differences between the work of Ito *et al* and this work, firstly the system being measured is somewhat different, Ito *et al* studied blends of PEO/h-PMMA/d-PMMA, varying the ratio of h-PMMA to d-PMMA in order to calculate the particle scattering function, rather than assuming the Debye function used in this work. This approach ignores any differences in χ for h-PEO/d-PMMA and h-PEO/h-PMMA and assumes that χ for h-PMMA/d-PMMA is zero, other results in this work indicate that this second assumption is invalid and work in this section strongly suggests that the first assumption is also invalid. In discussing the influence of these effects on their measured χ values Ito *et al* do quote values for PEO/d-PMMA calculated using the apparent radius of gyration for $\phi_{h\text{-}PEO}$ = 0.25, they find $\chi = -9.5\times10^{-4}$, again this is within the error of the values obtained here extrapolated to 353K, this suggests that the effect of deuteration on is exceedingly small. Ito *et al* do not take account of the different segmental volumes of PEO and PMMA in calculating χ, re-calculating their values using the experimental values for the segment volumes leads to small corrections, typically ~0.0002.

The final observation to make of the work of Ito *et al* is the proximity of the temperature at which measurements were made to the melting point of the blend;

measurements were made only 20K above melting point of these blends and were started a relatively short time (20 minutes) after the measurement temperature was achieved, this may mean that the samples had not reached equilibrium.

Deuteration is known to effect the phase behaviour of polymer mixtures, this is shown in blends of hydrogenous polymers and their deuterated counterparts, the effect of deuteration is to change χ from zero (for a homopolymer) to $\sim 10^{-4}$. Graessley *et al*[3] have studied the effect of swapping the locus of deuteration in blends of poly (ethylene-co-butene) with differing proportions of ethylene, this leads to changes in χ of $(2\text{-}5)\times 10^{-4}$, it should be noted that the polymers used by Graessley *et al*[3] were only partially deuterated (30-50%). Russell[23] has reported values of χ for poly (styrene(S)-b-methyl methacrylate(MMA)) block copolymers with either the styrene or the methyl methacrylate or both partially deuterated (~50%), differences in χ as large as 5×10^{-3} were observed between poly (d-S-b-MMA) and poly (d-S-b-d-MMA) and differences as large as 9×10^{-3} when compared to values of χ for poly (S-b-MMA) calculated from cloud point curves[14]. Shifts in the cloud point of 30K between d-PS/PVME compared with PS/PVME[12], imply a change in χ of $\sim 5\times 10^{-3}$, estimated using expressions for χ as a function of ϕ and T that Han *et al*[6] have calculated for d-PS/PVME, and simply calculating the χ values at 433K (the cloud point for h-PS/PVME) and 463K (the cloud point for d-PS/PVME). This is a crude estimate that assumes that the change in χ is due entirely to changes in the entropic part of χ, (the parameter A in fits of the form of Equation 6.1). Over the range of temperatures and conditions used in this work the mean change in χ between d-PEO/h-PMMA and h-PEO/d-PMMA blends was $8(2)\times 10^{-3}$, this compares well with values from the poly (S-b-MMA) and PS/PVME systems.

Examining the values of A and B fitted to the χ values according to Equation 6.1, it can be seen that for the lowest volume fraction of PEO (either deuterated or hydrogenous) A and B are rather larger than for higher volume fractions of PEO. This behaviour arises from the downturn in χ observed for the lowest volume fraction PEO data, Kumar[24] has pointed out that simply allowing for a non-ideal volume change on mixing will lead to a downturn in χ at the limits of the composition range. The behaviour of this blend is characteristic of an attractive blend, i.e. where there is a decrease in volume on mixing the components, the size of the effect observed is in general agreement with the results in Kumar's paper. The relationship between χ and the

'true' Flory - Huggins interaction parameter is given in Kumar's paper by Equation 6.2, but attempts to replicate the effect quantitatively using this equation have failed:

$$\chi = -\frac{1}{2N\phi(1-\phi)}\left[\frac{1}{4\bar{\rho}^2}\left(\frac{1}{\bar{V}_D}+\frac{1}{\bar{V}_H}\right)^2 - 1\right] + \frac{\chi_{FH}}{4\bar{\rho}^2}\left(\frac{1}{\bar{V}_D}+\frac{1}{\bar{V}_H}\right)^2$$

Equation 6.2

(this is equation 29 from Kumar's paper). $\bar{V}_D$ and $\bar{V}_H$ are the partial volumes of the two components, N is the degree of polymerisation. $\bar{\rho}$ is the molar density. Equation 6.2 suggest that a plot of χ versus $1/(\phi\ (1 - \phi)$ should be linear and Figure 6.7 shows that if the data for the DPEO and HPEO blends are plotted in this manner there is indeed some evidence for linearity (the symbols on this plot are the experimental data and the lines least squares fits). It is interesting to note that the gradient of these lines changes from positive to negative as the temperature increases. Clearly this analysis is rather tentative given the limited ϕ range over which χ values were measured. It is not clear why the HPEO χ data should be fitted relatively well using Equation 6.1 whilst the DPEO data are fitted rather poorly, this could be due to the DPEO blend being further from a phase boundary than the HPEO blend or a result of the air bubble formation that was observed for these samples. For both blends the A and B parameters fitted to χ for the blends with the lowest volume fraction are the same, for the other compositions it appears that the A parameters (the entropic part of χ) approximately the same, but the B parameters (the enthalpic part) are different, with the DPEO blend having significantly lower values for B than the HPEO blend. The implication of this is that swapping the locus of deuteration has changed the measured χ values through the enthalpic contribution whilst the entropic contribution remains unaltered, this result could be anticipated because simply reversing the labelling in a blend should not change the entropy, but it is known that deuteration changes the polarisability of the C-D bond (relative to the C-H bond) and this could lead to changes in the enthalpic interactions, most probably via a change in the partial charge of the ether oxygen in PEO.

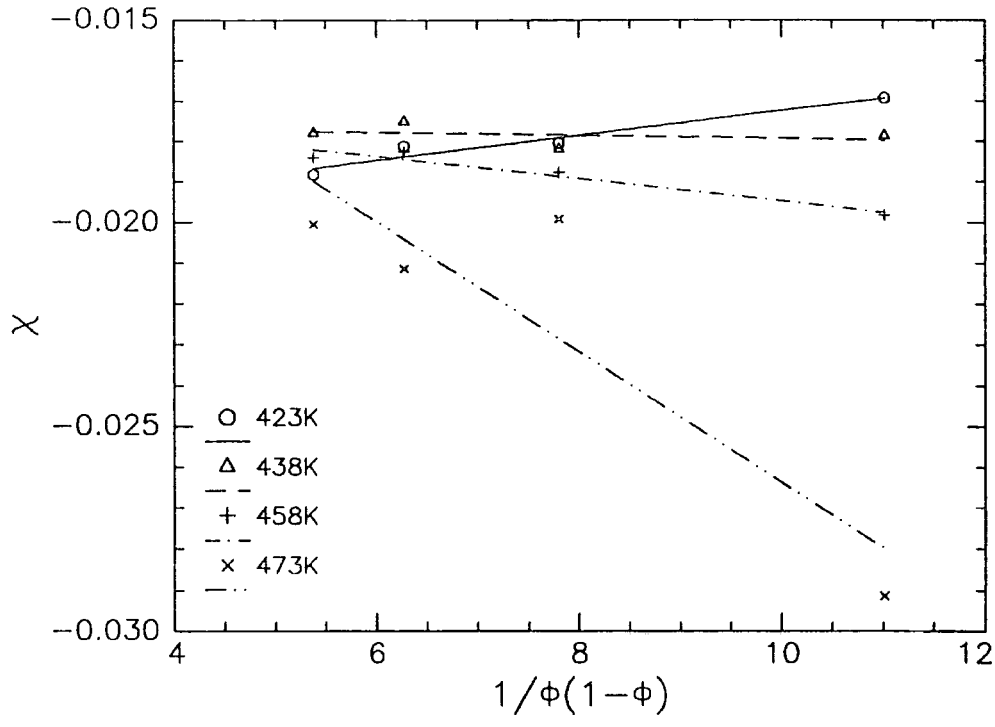

Figure 6.7a: DPEO χ data (symbols) plotted versus 1 / ϕ(1 - ϕ), along with linear fits (lines) to these data.

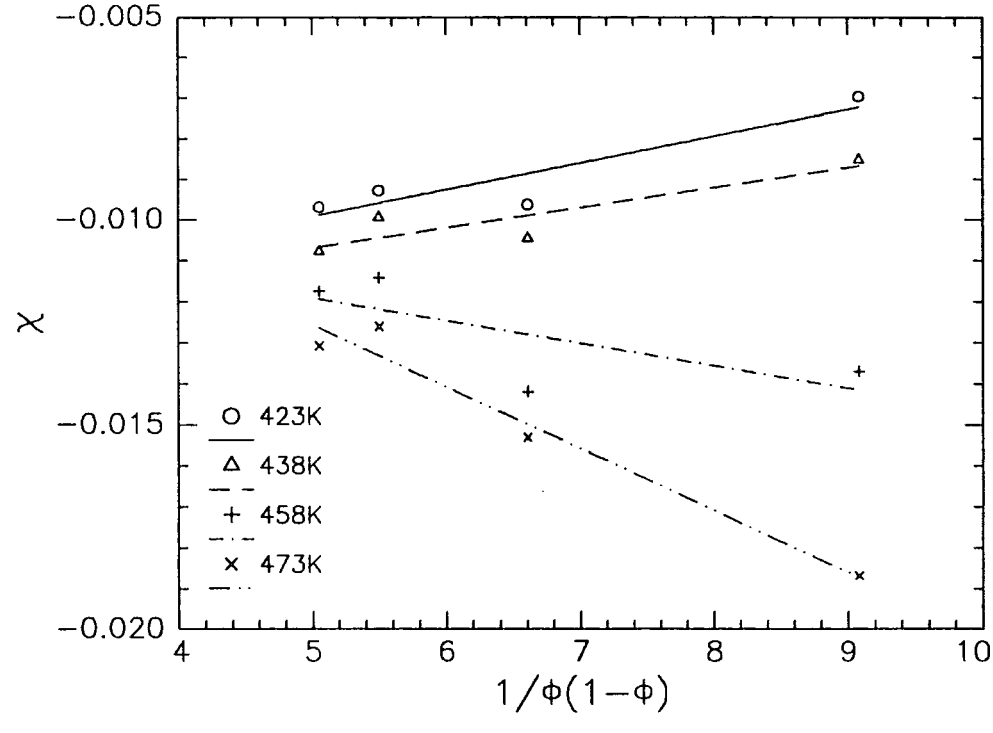

Figure 6.7b: HPEO data (symbols) plotted versus 1 / ϕ(1 - ϕ), along with linear fits (lines) to these data.

6.1.4 Conclusions

This work on d-PEO/h-PMMA and h-PEO/d-PMMA blends has emphasised the need to exclude air from samples rigorously in order to determine χ with the minimum of known parameters. In spite of the flaws in the experimental procedure χ values were obtained, these values are negative and of intermediate magnitude, indicating that there are weak attractive interactions in the blends, leading to miscibility over a wide temperature range. Values of χ for the DPEO blend lie in the range -0.017 to -0.029, values for the HPEO blend lie in the range -0.007 to -0.019. These values are in agreement with values measured by Ito *et al*[10], using small angle neutron scattering, for PEO/PMMA. The change in χ on switching the deuteration from PEO to PMMA is $8(2)\times10^{-3}$ and is similar in magnitude to the change seen in other systems on changing the locus of deuteration.

The variation of χ with composition is small except for the lowest PEO concentration for which χ is often significantly more negative than for the higher volume fractions of PEO, this phenomenon can be attributed to non-ideal volume changes on mixing. Fitting the χ data for each blend and each composition with functions of the form $\chi = A + B/T$, where A and B are entropic and enthalpic contributions to χ respectively, it is found that the HPEO data are fitted well with functions of this form, whereas the DPEO data are not. The values for the entropic part are broadly similar for the two blends whilst the values fitted for the enthalpic part differ between the DPEO and HPEO blends. This can be attributed to changes in the partial charges of ether oxygen in the PEO, arising from the difference in polarisability between C-H and C-D bonds.

6.1.5 References for Section 6.1

1 . J. Brandrup, E.H. Immergut, 'Polymer Handbook 3rd ed.' (New York: John Wiley & Sons,1989), pp VII/36.

2 . A. Rameau, Y. Gallot, P. Marie, B. Farnoux, *Polymer*, 30, 1989, 386.

3 . W.W. Graessley, R. Krishnamoorti, N.P. Balsara, L.J. Fetters, D.J. Lohse, D.N. Schulz, J.A. Sissano, *Macromolecules*, 26, 1993, 1137.

4 . T. Koch, G.R. Strobl, *Journal of Polymer Science Part B: Polymer Physics*, 28, 1990, 343.

5 . M. Shibayama, H. Yang, R.S. Stein, C.C. Han, *Macromolecules*, 18, 1985, 2179.

6 . C.C. Han, B.J. Bauer, J.C. Clark, Y. Muroga, Y. Matsushita, M. Okada, Q. Tran-cong, I.C. Sanchez, *Polymer*, 29, 1988, 2002.

7 . S. Janssen, D. Schwahn, K. Mortensen, T. Springer, *Macromolecules*, 26, 1993, 5587.

8 . K. Hahn, B.J. Schmitt, M. Kirschey, R.G. Kirste, H. Salié, S. Schmitt-Strecker, *Polymer*, 33(24), 1992, 5150.

9 . P.E. Tomlins, J.S. Higgins, *Macromolecules*, 21, 1988, 425.

10 . H. Ito, T.P. Russell, G.D. Wignall, *Macromolecules*, 20, 1987, 2213.

11 . V.P. Privalko, K.D. Petrenko, Y.S. Lipatov, *Polymer*, 31, 1990, 1277.

12 . J-L. Lin, R-J. Roe, *Macromolecules*, 20, 1987, 2168.

13 . F. Ben Cheikh Larbi, S. Leloup, J.L. Halary, L. Monnerie, *Polymer Communications*, 27, 1986, 23.

14 . T.A. Callaghan, D.K. Paul, *Macromolecules*, 26, 1993, 2439.

15 . G.Ramana Rao, C. Castiglioni, M Gussoni, G. Zerbi, E. Martuscelli, *Polymer*, 26, 1985, 811.

16 . E. Martuscelli, M. Pacella, W. P. Yue, *Polymer*, 25, 1984, 1097.

17 . M.M. Cortazar, M.E. Calahorra, G.M. Guzmán, *European Polymer Journal*, 18, 1982, 165.

18 . S.A. Liberman, A. de S. Gomes, E.M. Macchi, *Journal of Polymer Science: Polymer Chemistry*, 22, 1984, 2809.

19 . P. H. Richardson, Ph. D. Thesis, Durham University, 1993.

20 . J.M. Lefebvre, R.S. Porter, G.D. Wignall, reported in reference 10.

21 . I.C. Sanchez, R.H. Lacombe, *Macromolecules*, 11(6), 1978, 1145.

22 . J. Runt, K.P. Gallagher, *Polymer Communications*, 32(6), 1991, 180.

23 . T.P. Russell, *Macromolecules*, 26, 1993, 26.

24 . S.K. Kumar, *Macromolecules*, 27, 1994, 260.

6.2 Surface Enrichment

6.2.1 Experimental

The surface composition profiles of thin films of d-PEO/h-PMMA and h-PEO/d-PMMA were studied using neutron reflectometry and nuclear reaction analysis, where the PMMA was syndiotactic. Table 6.8 shows the molecular weights and global codes for these polymers, these are the same polymers that were used for the SANS work in the previous section.

	M_w	Code
d-PEO	102,200	TK77
h-PMMA	147,600	TK76
h-PEO	124,300	TK74
d-PMMA	117,900	TK22

Table 6.8: Molecular weights and global codes for the polymers used in this section.

The blends were each co-dissolved in chloroform and then spun cast onto silicon substrates, the total weight percentage of polymer in the solutions was fixed at 2%. The films were cast with a spinning speed of 4000rpm for 60 seconds, this produces films around 2000Å thick.

Three sets of experiments were done:

'NRA' experiments on two d-PEO/h-PMMA blends, containing different volume fractions of d-PEO. These blends were annealed for a series of times at 423K. Details of the bulk volume fractions of d-PEO in these blends, ϕ_B, the annealing times, t, and the labels used to designate these blends are shown in Table 6.9 (overleaf). PMMA is sensitive to damage by the incident $^3He^+$ in the NRA experiment and for this reason the samples were cooled with liquid nitrogen during the experiment. The NRA data were all collected on a single occasion in March 1994.

Label	ϕ_B	t /hrs	Thickness /Å
DPEO10u	0.09	0	1660 ± 70
DPEO10a1	0.09	1	-
DPEO25u	0.24	0	2730 ± 70
DPEO25a1	0.24	1	-
DPEO25a4	0.24	30	-
DPEO25a6	0.24	97	-

Table 6.9: Blend labels, annealing times, compositions and thicknesses for the d-PEO/h-PMMA blends used in the NRA experiments.

'NR equilibrium' studies on the composition profiles for unannealed films and films annealed for 70 hours at 423K. This was done for both d-PEO/h-PMMA and h-PEO/d-PMMA blends. Details of the bulk volume fractions of PEO, the sample codes and the film thicknesses can be found in Table 6.10. The bulk volume fraction of PEO was kept below 0.30 in order to avoid bulk crystallisation. Suffixes are 'u' for unannealed samples and 'a5' for annealed samples.

	Label	Volume fraction PEO, ϕ_B	Thickness /Å
d-PEO/h-PMMA	DPEO5	0.05	1830 ± 40
	DPEO10	0.09	1830 ± 70
	DPEO15	0.14	2000 ± 120
	DPEO20	0.19	2120 ± 90
	DPEO25	0.24	2190 ± 200
h-PEO/d-PMMA	HPEO5	0.06	1470 ± 50
	HPEO10	0.11	1660 ± 90
	HPEO15	0.16	1910 ± 120
	HPEO20	0.22	1930 ± 150
	HPEO25	0.27	1960 ± 90

Table 6.10: Film thicknesses, bulk compositions and sample codes for blends used in the *NR Equilibrium* experiments.

These experiments were done on a single occasion in December 1992. The multidetector was used and data were collected at incident angles of 0.25° and 0.6°, giving a Q range of 0.005-0.06Å^{-1}. Details of the experimental procedure can be found in Section 4.3.

'NR Kinetics' experiments were carried out to study the development of the composition profiles with annealing time, t. This was done for d-PEO/h-PMMA blends with bulk volume fractions d-PEO 0.19 and 0.23. Table 6.11 shows the annealing program used. These blends will be referred to as DPEO20 and DPEO25 followed by the suffixes shown in Table 6.11. Experiments were carried out on a single occasion in March 1994, and the procedure was identical to that for the ***NR equilibrium*** studies.

Suffix	Annealing time /hours
u	0
a1	1
a2	5
a3	16
a4	30
a5	70
a6	99

Table 6.11: Annealing program for the samples used in the *NR Kinetics* experiments.

6.2.2 Results

Before presenting the results of the NR and NRA experiments some brief comments will be made on the thin film samples prepared for this work. The films of h-PMMA/d-PMMA and h-PS/d-PS used elsewhere in the this work were very smooth; the root mean square roughness over length scales of 100's of microns was around 20Å - as measured by contact profilometry, X-ray reflectivity results show that over smaller length scales the roughness is even less (~ 5Å). The PEO/PMMA films prepared for this work are far rougher, with root mean square roughness of between 50Å and 170Å. A comparison of typical contact profilometry profiles of distance across sample versus height are shown in Figure 6.8 for the annealed and unannealed DPEO25 blends and an annealed d-PS/h-PS blend. There is no reduction in the roughness of the DPEO25 blend on annealing the sample. It was noted that before annealing films of the DPEO20 and DPEO25 blends exhibited an iridescent violet hue when viewed at a low angle. This coloration was quite different to the colours normally seen in thin polymer films on optically polished silicon substrates, which arise from interference effects. On annealing the samples the iridescence disappears.

NRA

Figure 6.9 shows composition profiles derived from the NRA data for the DPEO10 and DPEO25 blends. These show a uniform distribution of DPEO in both the unannealed and annealed films. The air-polymer interface is broader than that observed in the polystyrene films, this is due to the larger roughness of these films. The apparent thicknesses of the films are rather smaller than the values measured by contact profilometry, this is because the stopping distances for polystyrene were used in the analysis of the data, instead of those for PEO/PMMA. It would be relatively straightforward to re-analyse the data using the correct stopping distances but since this would not effect the shape of the profiles this has not been done.

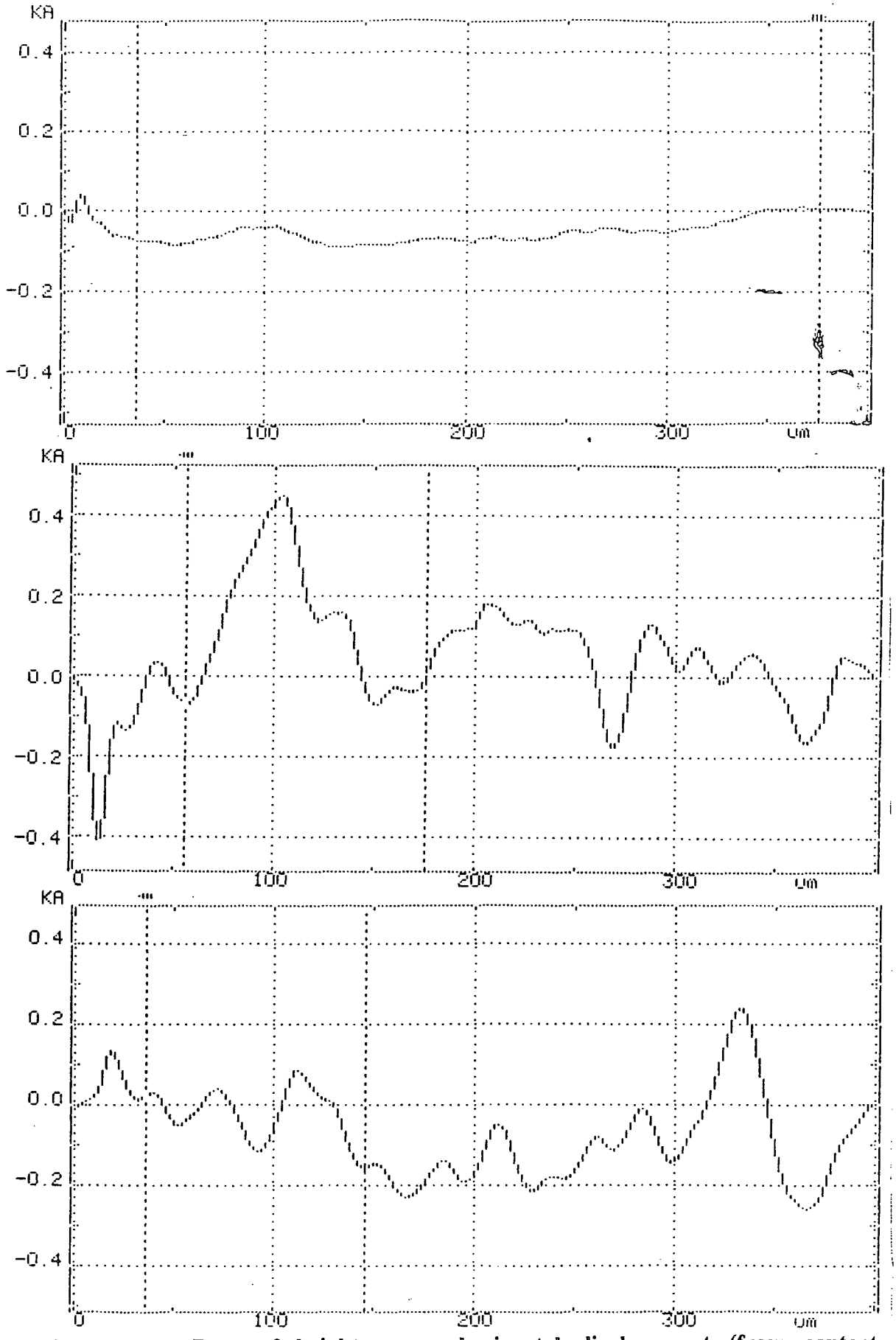

Figure 6.8: Plots of height versus horizontal displacement (from contact profilometry) for (top) polystyrene, (middle) unannealed DPEO25 and (bottom) DPEO25a5 - annealed 70 hours. Vertical axes in kÅ, horizontal axes in μm.

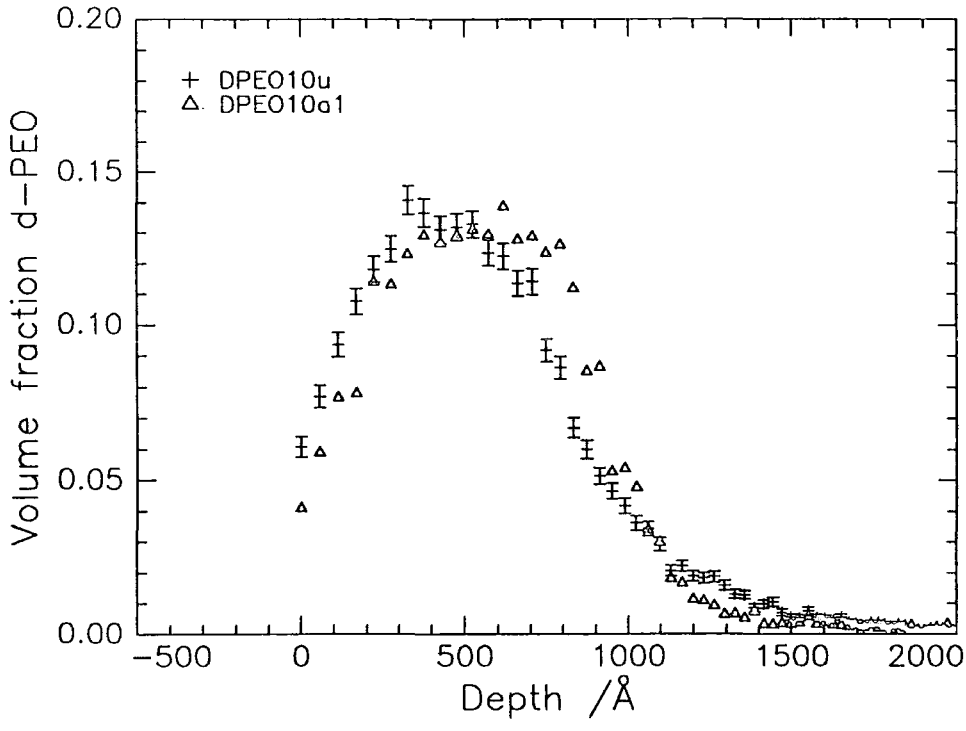

Figure 6.9a: DPEO10 composition profiles obtained using nuclear reaction analysis.

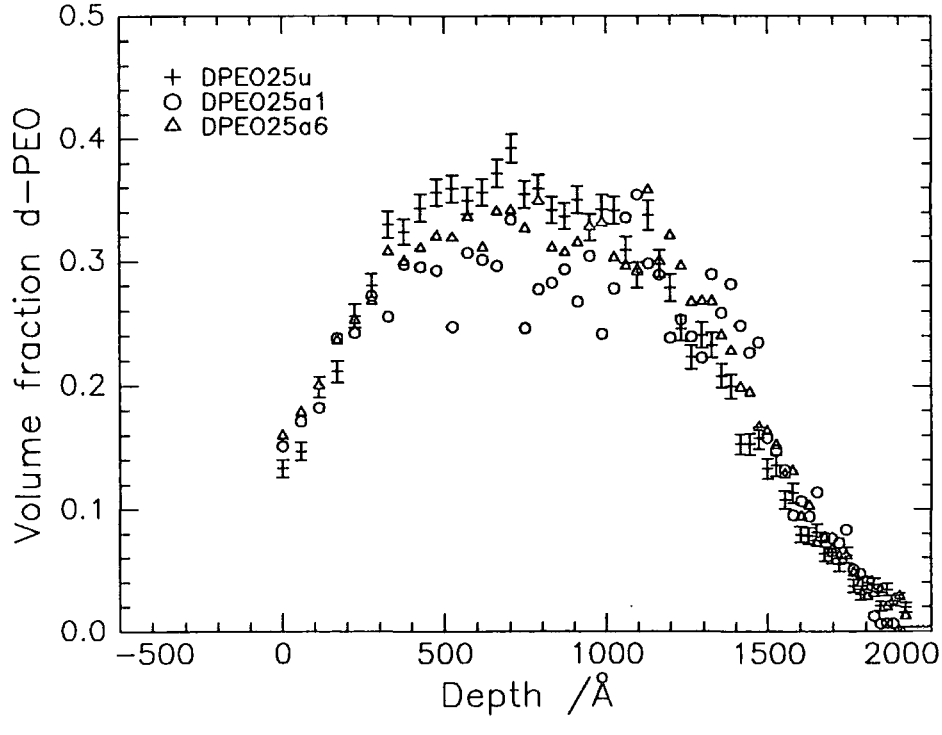

Figure 6.9b: DPEO25 composition profiles obtained using nuclear reaction analysis.

NR Equilibrium

Figure 6.10 shows sample reflectivity data for the DPEO and HPEO blends, before annealing and after annealing at 423K for 70 hours. For the blends with volume fractions of PEO 0.15, 0.20 and 0.25 there is an increase in the reflectivity on annealing, this increase is largest for the DPEO25 blend. These blends exhibit more off specular scatter than the h-PS/d-PS and h-PMMA/d-PMMA blends, there is more off specular scatter in the 0.6° data than in the 0.25° data. This off specular scatter is illustrated in Figure 6.11, these are graphs of incident total neutron intensity versus position on the multidetector. The data have been normalised such that the maximum of specular peak has the same value and small shifts (+1 or +2) have been applied such that the specular peak positions are identical, these are essentially cosmetic changes. As well as data from d-PEO/h-PMMA Figure 6.11 includes data from a typical d-PS/h-PS sample which exhibits virtually no off specular scatter, these data were all collected on a single occasion. This implies that the behaviour observed for the DPEO blends is a property of the blends rather than an artefact arising from, for example, inadequate shielding of the straight through beam. The reflectivity data were analysed using two methods:

(1) Free form fits using the VOLFMEM program with a pixel size of 15Å and incorporating a 15Å SiO_2 layer.

(2) Two layer fits using the PHOENIX program, also incorporating an SiO_2 layer.

A resolution of 6% was used in both these analysis methods, the reflectivity data is essentially smooth and thus contains no information on the film thickness, for this reason the film thickness was generally fixed at 2000Å in the analysis programs except where there was evidence for fringes arising from the film thickness.

Initially VOLFMEM fitted the annealed DPEO blend with an excess of d-PEO at the air - polymer interface, this excess was quite large for the DPEO25 blend and rather small for the other blends, volume fraction profiles $\phi(z)$ for this initial fit are shown in Figure 6.12. However this excess of DPEO at the air - polymer interface is at odds with SIMS data[1] collected from this system by collaborators at the University of Strathclyde and XPS data[2] for blends containing higher fractions of PEO, these workers both show an excess of PMMA at the air-polymer interface.

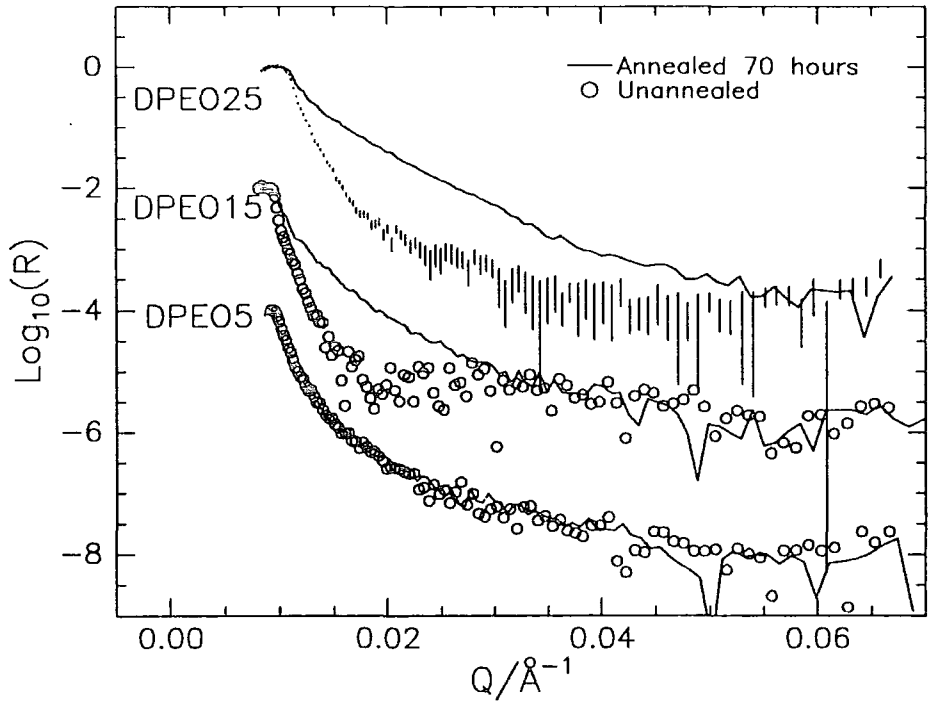

Figure 6.10a: Neutron reflectivity data for selected DPEO blends. Symbols or error bars - unannealed, lines annealed for 70 hours. DPEO15 and DPEO5 data offset by -2 and -4 respectively for clarity.

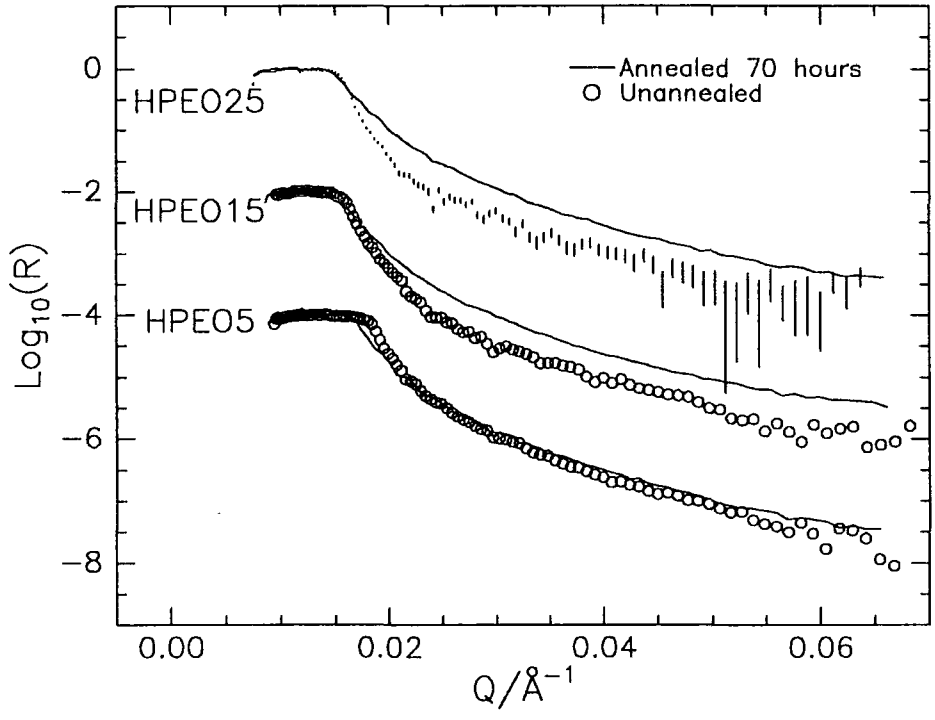

Figure 6.10b: Neutron reflectivity data for selected HPEO blends. Symbols or error bars - unannealed, lines annealed for 70 hours. HPEO15 and HPEO5 data offset by -2 and -4 respectively for clarity.

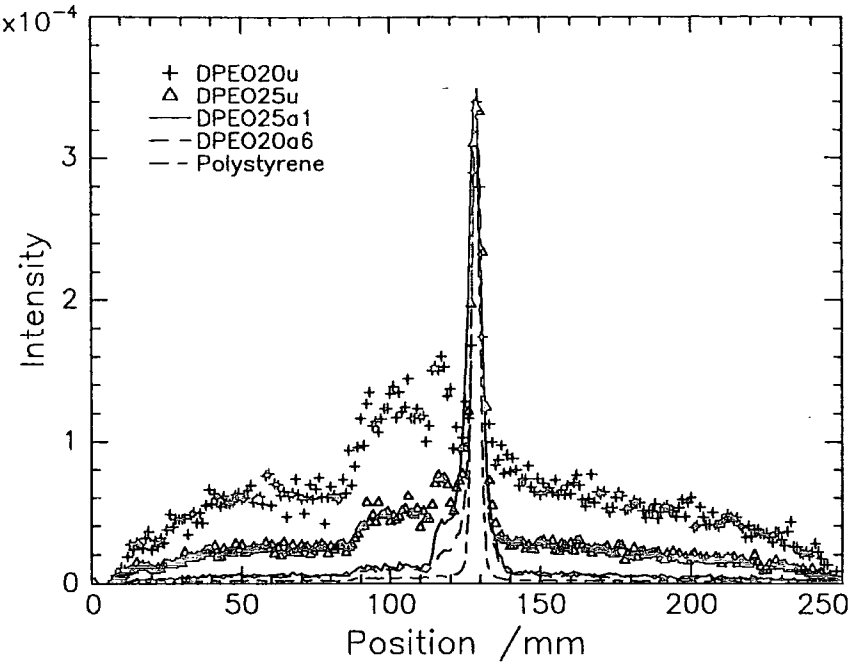

Figure 6.11a: Plot of intensity versus position on multidetector for a typical polystyrene blend and a selection of DPEO blends. Incident angle is 0.60°. Data have been normalised to the same height at the specular peak.

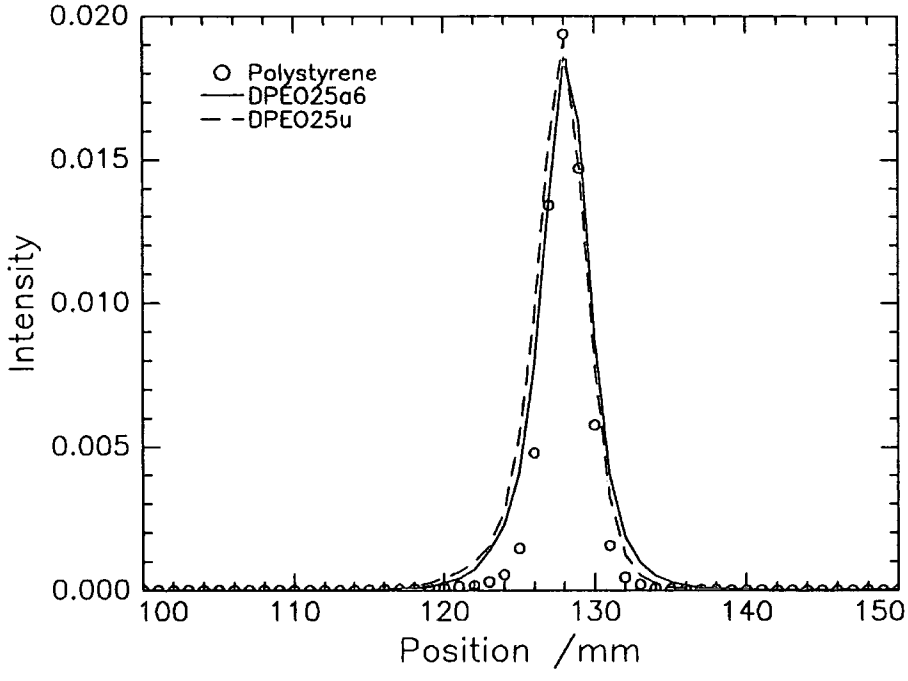

Figure 6.11b: Plot of intensity versus position on multidetector for a typical polystyrene blend and DPEO25u and DPEO25a6. Incident angle is 0.25°. Data have been normalised to the same height at the specular peak.

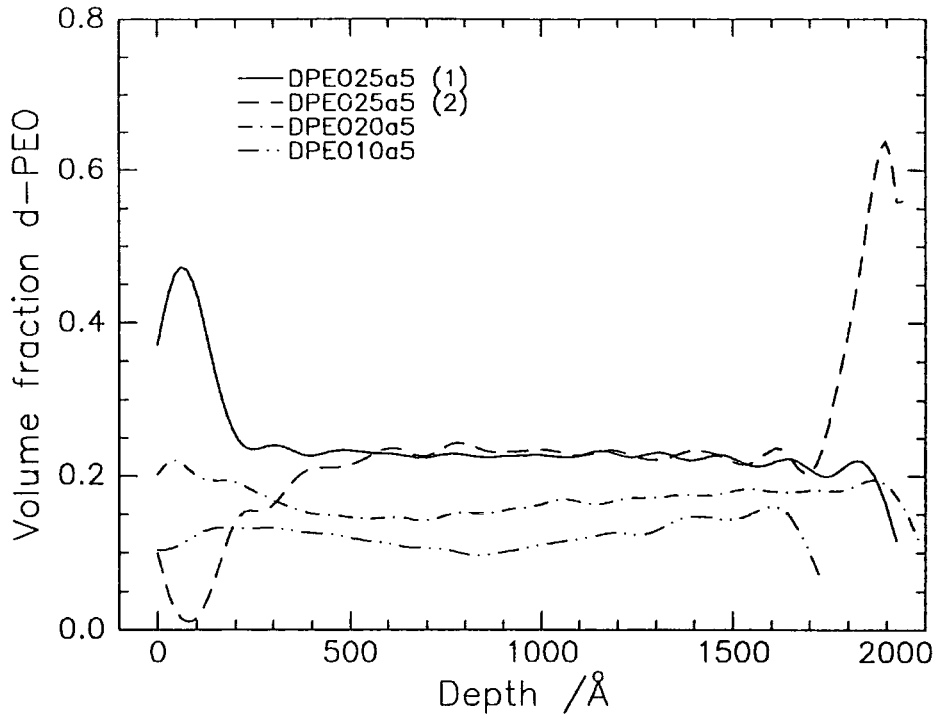

Figure 6.12: Composition versus depth profiles for selected annealed DPEO blends, obtained using VOLFMEM. For the DPEO25 blend models with an excess of d-PEO at the (1) air or (2) substrate interface are obtained.

In addition it has already been observed that the surfaces of these blends are very rough and the effect of this will be to reduce the apparent volume fraction of d-PEO at the air-polymer interface fitted by the program VOLFMEM, which does not explicitly include the effects of surface roughness. Returning to the data it was found that another model could be fitted to the annealed DPEO25 data using VOLFMEM, in this case there is a depletion of d-PEO from the air-polymer interface (corresponding to surface roughness and possibly an enrichment of PMMA) and an excess of d-PEO at the SiO_2-polymer interface. This profile is also illustrated in Figure 6.12. The normalised χ^2 parameters for these fits are 0.8 and 3.0 for d-PEO excesses at the air-polymer and SiO_2-polymer interfaces respectively. The fits of these two models to the reflectivity data are shown in Figure 6.13. The model with an excess of d-PEO at the air-polymer interface gives the better fit, although the model with the d-PEO excess at the SiO_2-polymer interface also gives a very good fit. However given the XPS and SIMS data and the likely effect of a large surface roughness it is probable that the model with a d-PEO excess at the SiO_2-polymer interface is the correct physical description. Attempts were made to encourage VOLFMEM to fit similar compositions to the other annealed DPEO data, but these

proved unsuccessful. However two layer models, with an excess of d-PEO at the SiO_2-polymer interface and a large air-polymer interfacial roughness, were fitted to all the annealed DPEO data using PHOENIX.

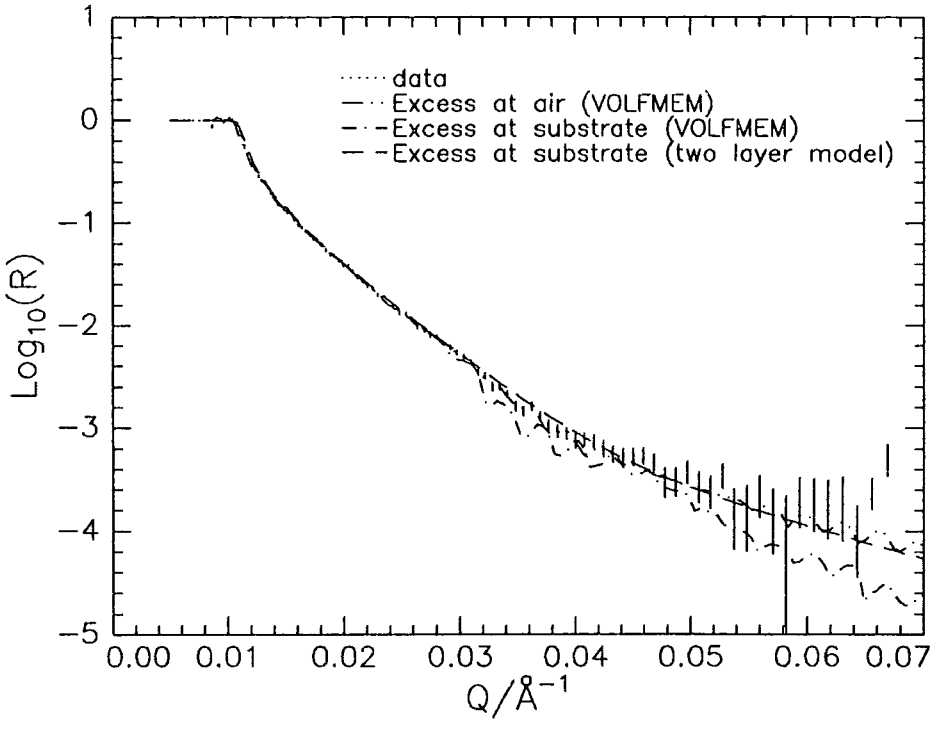

Figure 6.13: Neutron reflectivity data for DPEO25a5, with fits using VOLFMEM models with d-PEO excesses at the air or substrate interface and a two layer model with d-PEO at the substrate interface.

The parameters of these fits are shown in Table 6.12, where z_n, ϕ_n and σ_n are the thickness, volume fraction d-PEO and roughness of the n^{th} layer, the air-polymer interfacial roughness is σ_0. Also included in Table 6.12 is the fit index, which is not identical to the normalised χ^2 parameter more commonly used to indicate fit quality. Tables of the correspondence between fit index and normalised χ^2 parameter can be found in Section 7.2 (Table 7.7) and Section 8.2 (Table 8.3). Briefly fit indices of 0.06, 0.12 and 0.16 correspond to normalised χ^2 parameters of 4, 8 and 19 respectively. The surface excesses at the polymer - SiO_2 interface $z^*_{Si} = z_2*(\phi_2 - \phi_1)$, are also shown in Table 6.12.

	σ_0/Å	ϕ_1	z_1 /Å	σ_1/Å	ϕ_2	z_2/ Å	Fit Index	excess, z^*_{Si}/Å
DPEO5a5	429	0.05	1870	55	0.42	41	0.18	15
DPEO10a5	660	0.10	1700	78	0.41	61	0.12	19
DPEO15a5	641	0.15	2000	108	0.48	80	0.13	27
DPEO20a5	336	0.16	2000	88	0.51	82	0.13	29
DPEO25a5	674	0.24	2000	56	0.72	95	0.06	46

Table 6.12: Fit parameters for two layer PHOENIX fits to the annealed DPEO blend data.

Figure 6.14 shows a selection of the composition profiles shown obtained using these parameters. The polymer - SiO_2 interface is at the left of this graph.

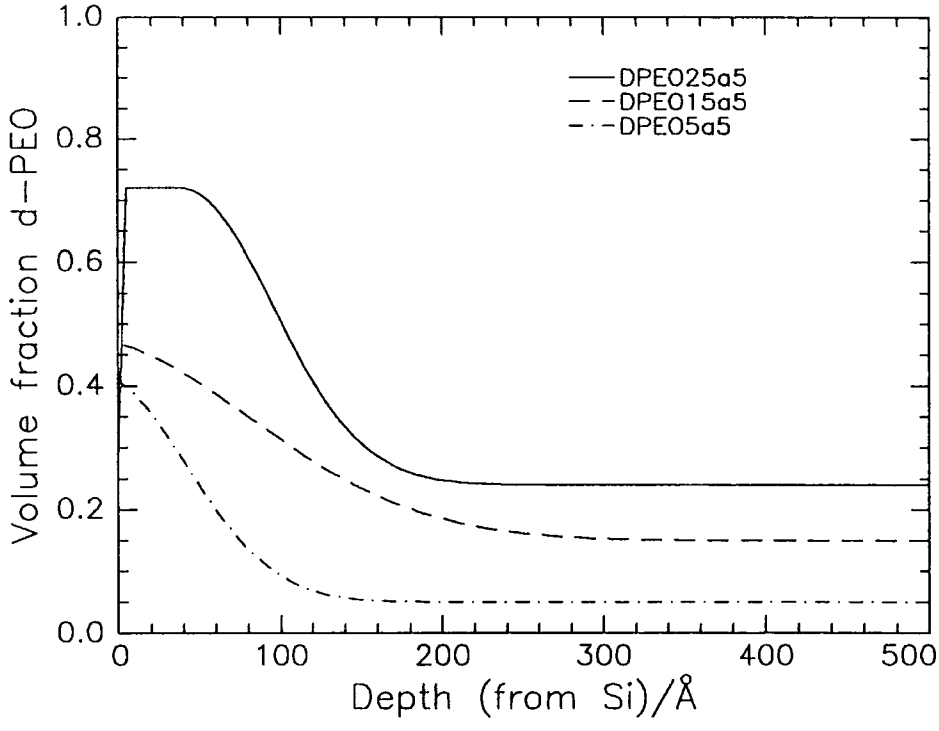

Figure 6.14: Selected composition vs depth profiles for the annealed DPEO blends, obtained using two layer model fits with roughness. Horizontal axis has substrate interface on the left.

The air-polymer interfacial roughness fitted to these data is very large, larger even than the value obtained from the contact profilometry data, but the reflectivity profile is

insensitive to increases in roughness beyond a certain value, this is illustrated in Figure 6.15. These are simulated data for a 2000Å layer of 'd-PEO/h-PMMA' with a volume fraction of d-PEO = 0.25. The polymer - SiO_2 interfacial roughness is fixed at 5Å but the air-polymer interfacial roughness is varied from 50Å to 300Å. Increasing the roughness above ~150Å produces no further changes in the reflectivity data.

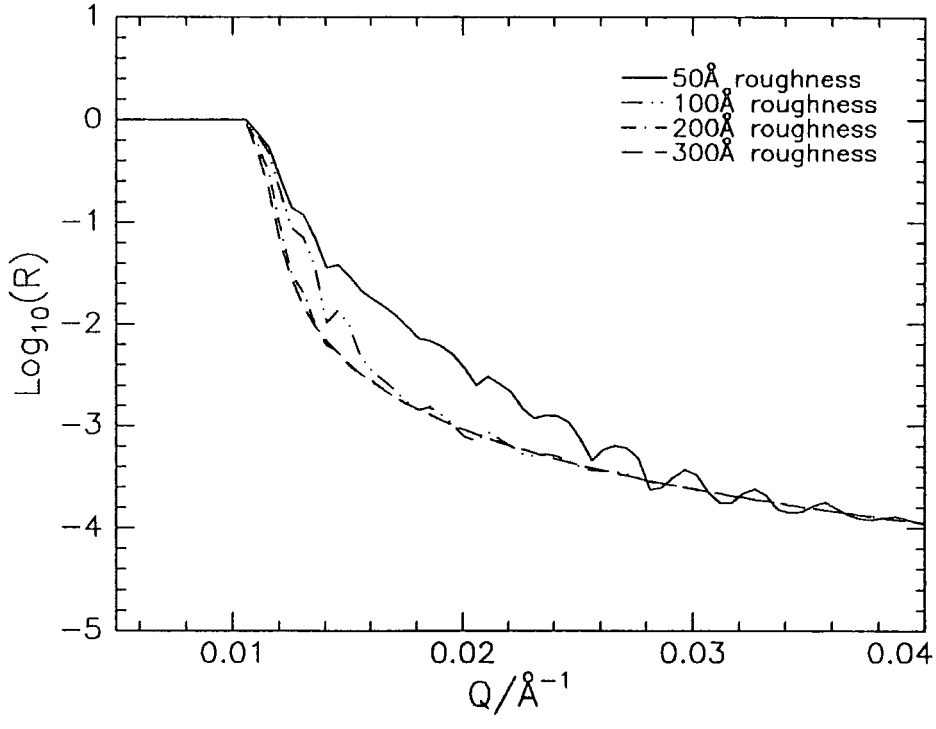

Figure 6.15: Model reflectivity data, illustrating the effect that increasing roughness at the air-polymer interface has on the reflectivity.

Table 6.13 shows the fit parameters for two layer fits to the unannealed DPEO blend data; these data exhibit small depletions of the d-PEO from the SiO_2-polymer interface for the DPEO20u and DPEO25u blends and largish excesses for the DPEO5u, DPEO10u and DPEO15u although the fitted values for the bulk volume fraction of d-PEO are rather larger than expected for the DPEO5u blend and rather smaller than expected for the DPEO15u blend.

	σ_0/Å	ϕ_1	z_1 /Å	σ_1/Å	ϕ_2	z_2/Å	Fit Index	excess, z^*/Å
DPEO5u	198	0.10	2000	142	0.36	90	0.07	23
DPEO10u	166	0.11	2000	90	0.30	148	0.13	28
DPEO15u	145	0.12	2000	128	0.21	137	0.19	12
DPEO20u	71	0.19	2000	59	0.13	134	0.06	-8
DPEO25u	73	0.25	2000	83	0.24	98	0.15	-1

Table 6.13: Fit parameters for two layer models for unannealed DPEO blend data

Some problems were encountered in fitting the HPEO data using the geometric resolution of 6%, it was not possible to fit the data without obtaining a value for the bulk volume fraction of h-PEO far above the nominal value. However by relaxing the resolution to 13% fairly good two layer fits were obtained using PHOENIX. A comparison of fits to the HPEO25 data using the same model with either 6% or 13% resolution is shown in Figure 6.16, the difference in resolution produces a substantial change in the modelled reflectivity near the critical edge. The parameters of these fits shown in Table 6.14, along with the 'excess' of h-PEO at the polymer - SiO_2 interface. In contrast to the DPEO blend data, these data for HPEO show a depletion of h-PEO from the polymer - SiO_2 interface. The fits appear to show a volume fraction h-PEO of less than zero - clearly this is unphysical, this could arise from simply using incorrect values for the nuclear scattering length densities of the h-PEO and d-PMMA. Note also that the bulk volume fractions of h-PEO obtained for the HPEO10 and HPEO15 blends are rather different from the nominal bulk volume fractions for these blends.

	σ_0/Å	ϕ_1	z_1 /Å	σ_1/Å	ϕ_2	z_2/Å	Fit Index	excess, z^*/Å
HPEO5a5	105	0.05	2000	49	-0.21	71	0.10	-19
HPEO10a5	166	0.22	2000	41	-0.09	91	0.21	-28
HPEO15a5	145	0.24	2000	39	-0.07	88	0.12	-27
HPEO20a5	71	0.20	2000	27	-0.06	91	0.13	-24
HPEO25a5	73	0.24	2000	29	-0.06	89	0.13	-27

Table 6.14: Fit parameters for two layer models for annealed HPEO blend data

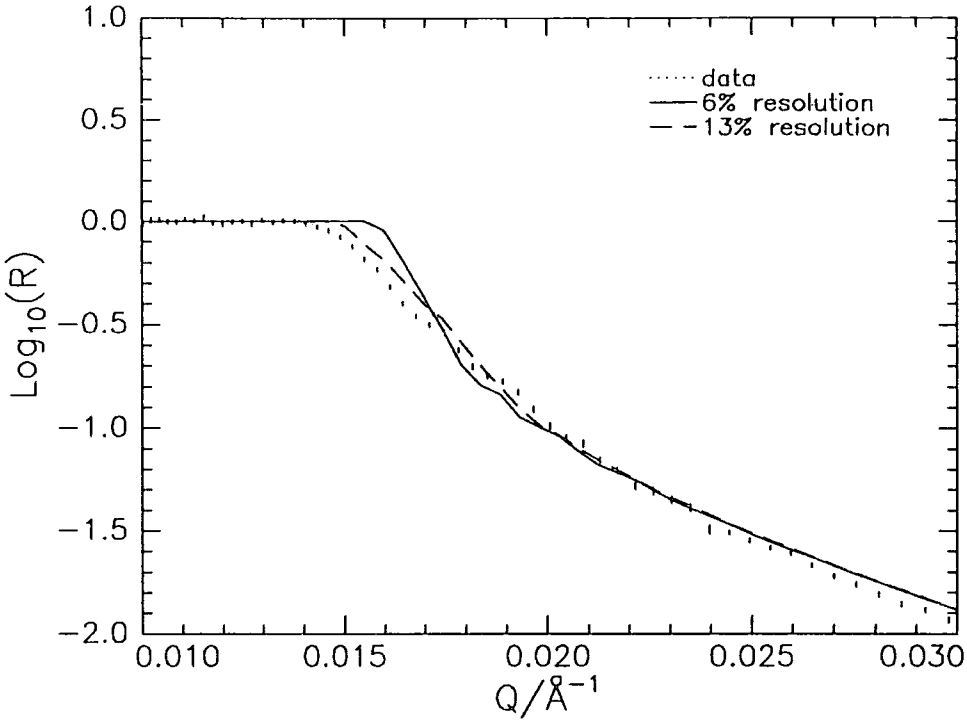

Figure 6.16: Two layer model fits to HPEO25 data, these are the same model with two different resolutions (6% and 13%).

NR Kinetics

Figure 6.17 shows reflectivity data collected from the blends DPEO25(u-a6) and DPEO20(u-a6). There is no trend in the reflectivity data with increasing annealing time , although the unannealed samples exhibit the lowest reflectivity the reflectivity does not increase monotonically for the subsequently annealed samples. These reflectivity data were analysed in the same way as the ***NR Equilibrium*** data, again it was found that for the DPEO25 blends VOLFMEM fits with an excess of d-PEO at the air-polymer or SiO_2 - polymer interface could be obtained.

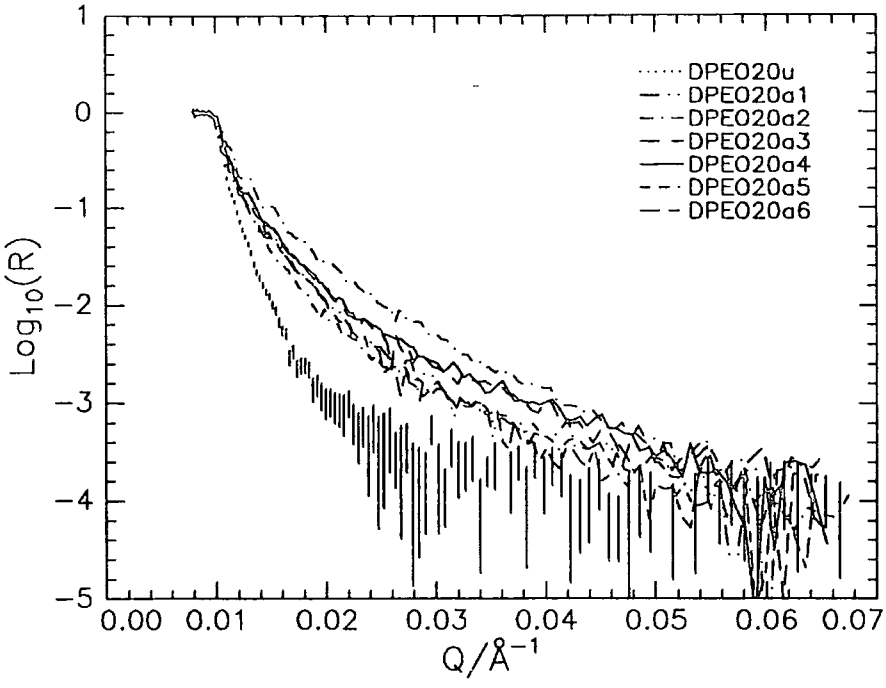

Figure 6.17a: Reflectivity data for the DPEO20 blends, as a function of annealing time. Error bars from Poisson statistics included for the unannealed data.

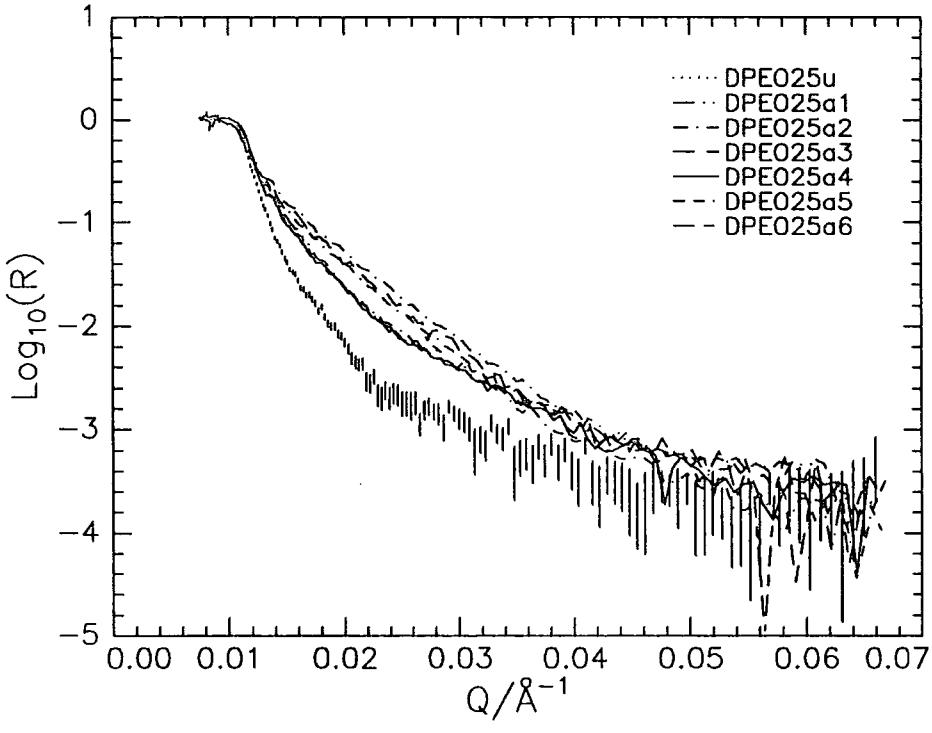

Figure 6.17b: Reflectivity data for the DPEO25 blends, as a function of annealing time. Error bars from Poisson statistics included for the unannealed data.

Two layer models were fitted to the data, using PHOENIX, with an excess of d-PEO at the SiO_2 - polymer interface and a large air-polymer interfacial roughness. The parameters of these two layer fits can be found in Table 6.15 along with fit index and the surface excess, z^*_{Si}, of d-PEO at the SiO_2-polymer interface. For the DPEO20 blends the value of the SiO_2-polymer surface excess reaches an equilibrium value of 32(5)Å after 1 hour annealing. There surface excess for the DPEO25 varies rather more as a function of annealing time but there seems to be no pattern in the variation, so this may be the result of unusually large errors in these values. The average value of the surface excess for the annealed DPEO25 is 45(6)Å.

	σ_0/Å	ϕ_1	Z_1 /Å	σ_1/Å	ϕ_2	Z_2/ Å	Fit Index	excess, z^*_{Si}/Å
DPEO20u	71	0.19	2000	59	0.13	133.6	0.06	-8
DPEO20a1	322	0.19	2000	89	0.52	88	0.08	29
DPEO20a2	82	0.19	1764	60	0.77	70	0.08	41
DPEO20a3	148	0.19	1773	63	0.62	74	0.11	31
DPEO20a4	134	0.19	1773	62	0.63	72	0.10	31
DPEO20a5	336	0.16	2000	88	0.51	82	0.13	29
DPEO20a6	346	0.19	1773	101	0.52	89	0.05	30
DPEO25u	73	0.25	2000	83	0.24	98	0.15	-1
DPEO25a1	300	0.25	2000	77	0.67	102	0.13	43
DPEO25a2	324	0.24	2000	66	0.88	82	0.05	53
DPEO25a3	231	0.24	2000	70	0.83	82	0.07	48
DPEO25a4	298	0.28	2000	72	0.69	86	0.09	35
DPEO25a5	674	0.24	2000	56	0.72	95	0.06	46
DPEO25a6	400	0.25	2000	90	0.68	100	0.13	43

Table 6.15: Fit parameters for two layer models obtained using PHOENIX for the *NR Kinetics* data.

6.2.3 Discussion

Although it is possible that swapping the locus of deuteration changes the relative surface energies of PEO and PMMA to SiO_2 sufficiently to reverse the enrichment behaviour. The expectation must be that the effects of deuteration would be far smaller than the chemical effect. This leads to the conclusion that the composition profiles obtained from either the DPEO or HPEO blends are incorrect. Tentatively it will be assumed that the DPEO results are correct for the following reasons:

(1) More data has been collected for the DPEO blends and the results are all consistent.

(2) It was not necessary to relax the resolution for DPEO in order to obtain good fits.

(3) The NR data for the HPEO blends intrinsically contain less information than for the DPEO blends because the critical edge fall at higher Q.

(4) The negative values for the volume fraction of h-PEO at the polymer - SiO_2 interface.

Clearly this discrepancy also casts some doubt on the validity of the DPEO data and the solution to this would be to collect more data using other techniques.

Figure 6.18 shows the variation of the excess of d-PEO at the SiO_2 - polymer interface, z^*_{Si}, as a function of the bulk volume fraction of d-PEO. The thickness of the adsorbed layer is of the order of the radius of gyration for the d-PEO (~100Å). This is far thicker than the thickness predicted by mean field theory, using the values of χ obtained in Section 6.1 of this thesis. A selection of theoretical predictions of the surface composition profile are shown in Figure 6.19, these were calculated using the Jones and Kramer approximation to the theory of Binder with a value of $\phi_B = 0.25$ and a range of values for $\Delta\gamma$ and χ. Data in the literature indicates that $\Delta\gamma$, relative to air is quite small for PEO and PMMA[3], around 2 mJ m^{-2}, and it would seem reasonable to assume that the difference relative to SiO_2 would also be small. However even if the surface energy difference were much larger than that used for the calculations shown in Figure 6.19 the predicted surface enrichment profile would still be thin compared to the experimental measurement.

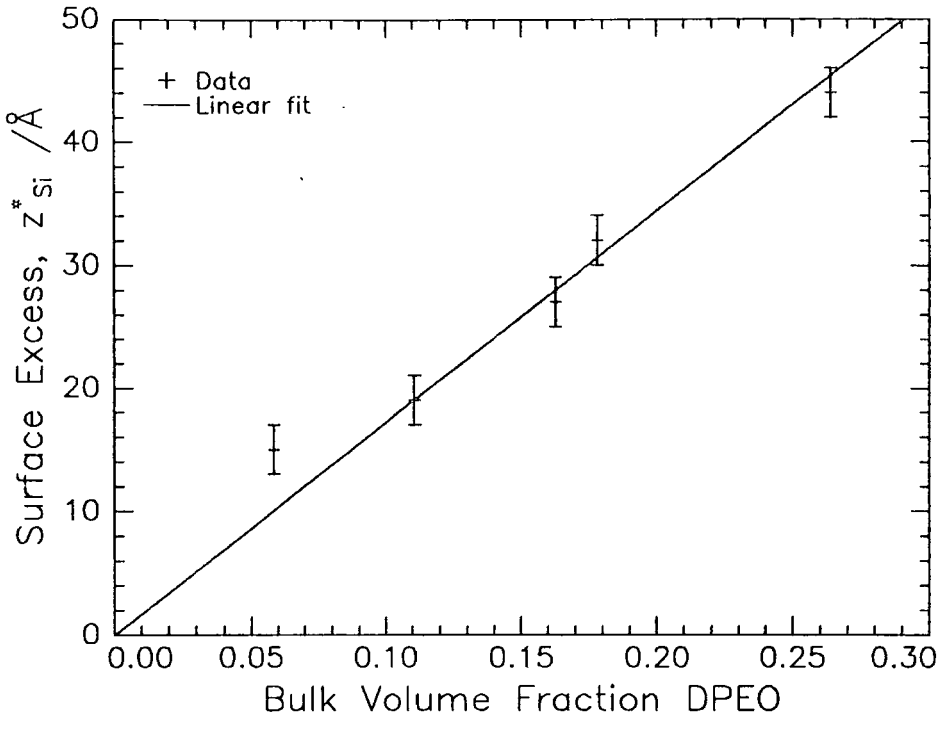

Figure 6.18: Surface excess of d-PEO at the polymer - SiO_2 interface as a function of the bulk volume fraction of d-PEO.

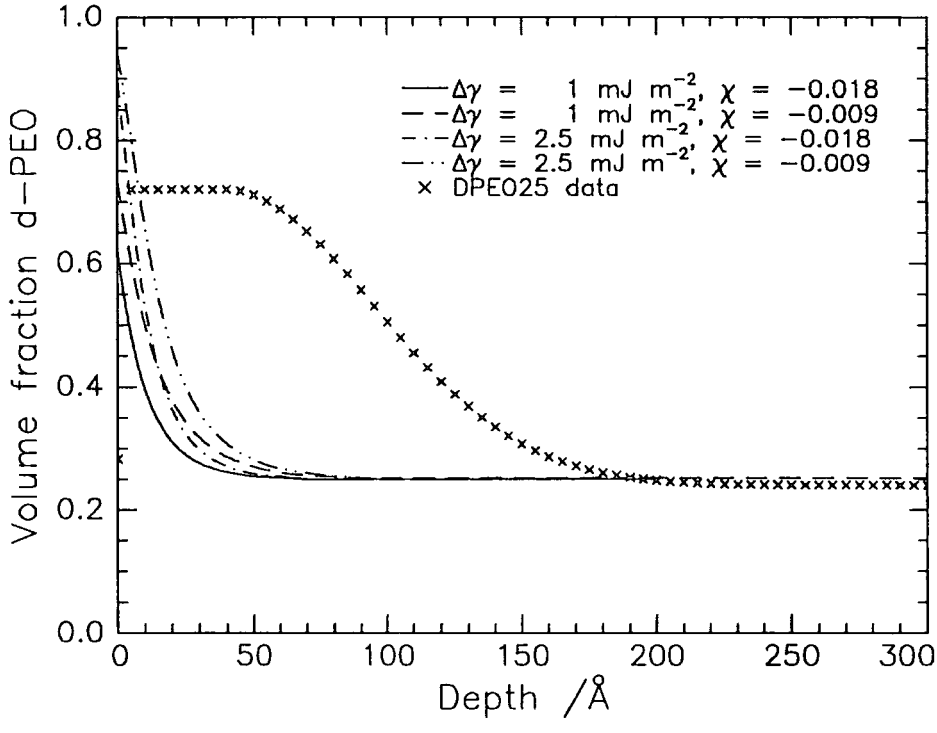

Figure 6.19: Model composition versus depth profiles calculated using mean field theory, with a selection of χ and $\Delta\gamma$ values.

There are two explanations as to why the layer enriched with d-PEO at the SiO_2 interface is so much thicker than predicted:

(1) There is a failure in the mean field theory such that it does not predict the thickness of the surface enriched layer accurately for all systems, there is already some evidence that this may be the case - it has been observed[4] that the shape of the near surface enrichment profile in d-PS/h-PS deviates slightly from the mean field prediction near the surface. Deviations from the profile shape predicted by a mean field theory have been observed in this work for brush formation in d-PS(F)/h-PS blends. Kramer[5] reports that in the d-PEP/h-PEP system a shallow plateau, ~50Å wide, is observed in the near surface composition profile.

(2) There may be physical processes that occur in PEO/PMMA blends that are not accounted for by the mean field theory used here, such as a difference in segmental volume between the blend components or surface induced crystallisation. However the blends used in this work were deliberately chosen such that there was no bulk crystallisation of the of the PEO. The volume fraction of d-PEO at the SiO_2 does rise to values rather higher than those required for bulk crystallisation, but x-ray diffraction measurements[6] show no signs of crystallinity in these thin film samples. However this absence of observed crystallinity may be because x-ray diffraction is not sensitive enough to detect the very small fraction of crystallisation that would be required to produce the observed effect.

One would expect both the PEO and PMMA to interact with the SiO_2 surface via hydrogen bonding to silanol groups on the surface[7,8], the PMMA interacting via the carbonyl oxygen and the PEO via the ether oxygen. The fact that the PEO is found in excess at the SiO_2 surface implies that the ether oxygen has a more negative partial charge than the carbonyl oxygen.

The large surface roughness of these blends has rendered the analysis of these data difficult, since it introduces a further unknown parameter in the data analysis and removes the Kiessig fringes that are useful in fitting the data. Ideally it would be desirable to repeat these experiments with smoother samples. It was observed during preliminary experimental work that spun cast films of h-PMMA/d-PMMA were rougher when cast from chloroform than those cast from toluene, changing the casting solvent could improve the sample roughness, although the blends are still quite rough even after annealing. This would suggest that the roughness arises when the films make the transition from being in the melt or solution state - where the sample would be smooth -

to the glassy state, whether it arises from further loss of solvent or from cooling to below the glass transition temperature of the blend. Therefore it may be possible to produce smoother samples either by slow cooling from the melt or by using a less volatile casting solvent - the difficulty here is to find a suitable solvent for both PEO and PMMA. Alternatively these blends could be studied in the melt state using neutron reflectometry, in order to determine the composition profile near the air-polymer interface, the assumption being that in the melt state the blends will be smooth. This would need to be done under an inert atmosphere to prevent sample oxidation, at present equipment is not available to do this at CRISP, however there are no difficulties in principle with such an experiment. An experiment of this sort offers a new line of study; the surface energies of PEO and PMMA are reported[3] to vary at a different rate with temperature, this is illustrated in Figure 6.20. This means that the difference in surface energy between the two components of the blend varies as a function of temperature, it would be interesting to study the surface enrichment behaviour of these blends and probe the effect of this varying surface energy difference.

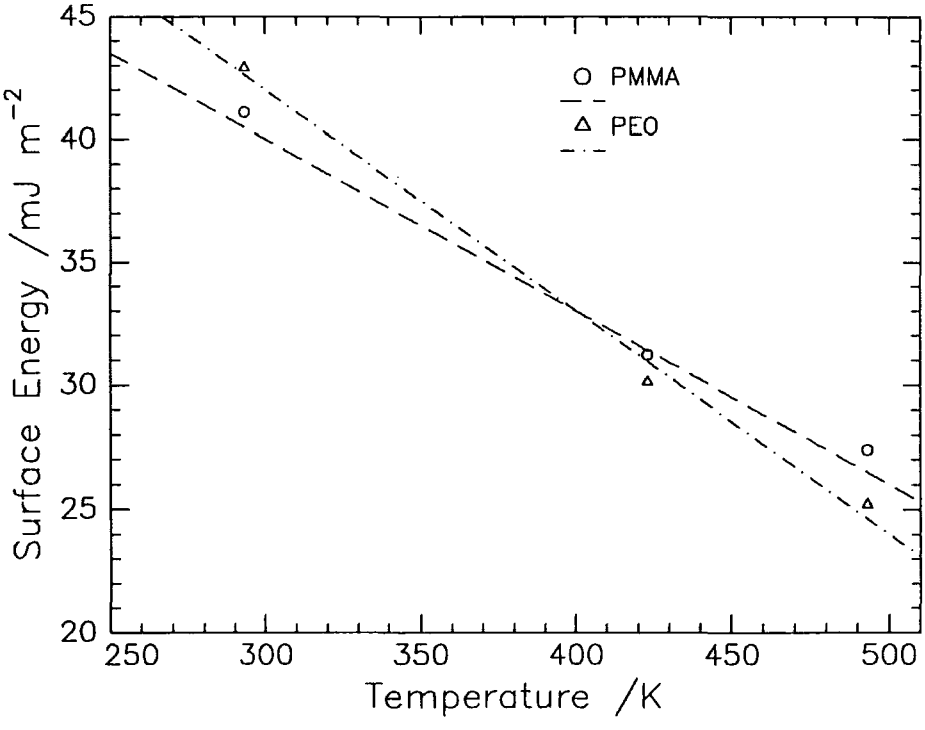

Figure 6.20: Values of surface energy (from the literature) for PEO and PMMA, as a function of temperature.

Another advantage of a study at elevated temperature is that, provided the temperature is kept high enough, bulk crystallinity can be avoided even at higher volume fractions of d-PEO.

The blends used in this work exhibited a substantial amount of off specular reflectivity, it is possible that this arises from the large roughness of the samples however the expected off specular reflectivity for such a situation would tend to be more symmetric about the specular peak[9], in addition the length scale of the roughness - as measured by contact profilometry is probably rather larger than the coherence length of the neutrons. Another source of off specular scattering is Yoneda scatter[10] which occurs when incident neutrons although not totally reflected at the sample surface are refracted on entering the sample such that they are totally reflected just below the sample surface, again this would tend to lead to an off specular scattering pattern somewhat more symmetric about the specular peak. The most likely explanation is that the behaviour observed is due to small angle scattering[11]. This must arise from composition fluctuations, however it is not due to the crystallisation of the d-PEO since no characteristic peaks are seen in the x-ray diffraction from these films. The violet iridescence observed in the unannealed DPEO20 and DPEO25 could also be attributed to scattering from composition fluctuations, although in this case the length scale of the composition fluctuations must be much larger (since light has a longer wavelength than the neutrons used in this work). These concentration fluctuations are much smaller in the annealed blends, since after annealing the off-specular scatter is much reduced, although still present and the violet iridescence has gone.

6.2.4 Conclusions

The surface composition profiles of annealed d-PEO/h-PMMA blends have been studied as a function of the bulk volume fraction, ϕ_B, of d-PEO (with $\phi_B < 0.30$ to avoid bulk crystallisation). NRA indicated that the distribution of d-PEO in thin films of d-PEO/h-PMMA was uniform, within the resolution of the technique (~300Å). Neutron reflectometry showed an excess of d-PEO at the SiO_2-polymer interface. The surface composition reached a maximum value of 0.70 d-PEO for a blend with $\phi_B = 0.25$, the characteristic length scale of the profile was around 80Å, which is similar in size to the radius of gyration of the d-PEO. The equilibrium surface excess was reached in less than one hour annealing at 423K. The form of the enrichment profile could not be described accurately by mean field theory, the theory predicts a very thin region of surface excess for blends such as this, with large negative χ parameters which are measured elsewhere in this work for these blends.

The analysis of the neutron reflectometry data was made substantially more difficult by the presence of a large amount of surface roughness at the air-polymer interface (~100Å), for this reason no definitive statement can be made on the surface composition profile of these blends at the air-polymer interface.

This system also provided an excellent practical example of the non-uniqueness of neutron reflectometry data, initially a model with an excess of d-PEO at the air-polymer interface was fitted, but this model was discounted on the basis of SIMS results on the same system and the fact that the extreme roughness of the air-polymer interface will produce a large reduction of the apparent surface volume fraction of d-PEO.

Neutron reflectometry experiments were also done on analogous h-PEO/d-PMMA blends, but it is was not possible to fit the data with physically reasonable models.

6.2.5 References for Section 6.2

1 . M. Hartshorne, S. Affrossman, unpublished data.

2 . P. Sakellariou, *Polymer*, 34(16), 1993, 3408.

3 . J. Brandrup, E.H. Immergut, 'Polymer Handbook 3rd ed.' J. Wiley & Sons, 1989.

4 . R.A.L. Jones, L.J. Norton, E.J. Kramer, R.J. Composto, R.S. Stein, T.P. Russell, A. Mansour, A. Karim, G.P. Felcher, M.H. Rafailovich, J. Sokolov, X. Zhao, S.A. Schwarz, *Europhysics Letters*, 12(1), 1990, 41.

5 . E.J. Kramer, unpublished data.

6 . R.W. Richards, unpublished data.

7 . J. Rubio, J.A. Kitchener, *Journal of Colloid and Interface Science*, 57(1), 1976, 132.

8 . H.E. Johnson, S. Granick, *Macromolecules*, 23, 1990, 3367.

9 . C.A. Lucas, *Faraday Disscussion*, 89, 1990, 928.

10 . Y. Yoneda, *Physical Review B*, 131, 1963, 2010.

11 . C.J. Clarke, private communication.

This page left intentionally blank

7. End capped perdeuterated polystyrene / polystyrene blends

7.1 Experimental

The composition depth profiles, $\phi(z)$, of a series of mixtures of end functionalised deuterated polystyrene with hydrogenous polystyrene have been determined. The deuterated polystyrene was end capped with a small perfluorinated group at one (d-PS(F)) or both (d-PS(F2)) ends or had no fluorinated end caps (d-PS). Details of the end group can be found in Section 4.1.1. The molecular weights and 'global' sample codes of the polymers used in this section can be found in Table 7.1. Both Nuclear Reaction Analysis (NRA) and Neutron Reflectometry (NR) were used in this work, details of the experimental procedure can be found in sections 4.3 and 4.4 respectively. NR data were collected using the multidetector (April 1994) and the single detector (November 1993).

	Global Code	M_w
d-PS(F)	TK92	658,000
h-PS	TK58	1,710,000
d-PS	TK93	816,000
d-PS(F)	TK89	30,700
h-PS	TK79	44,700
d-PS(F2)	TK145	56,000

Table 7.1: Details of the polymers used in this section.

The experiments carried out on these blends can be divided into six parts, these can be summarised as follows:

(1) High M_w d-PS(F)/h-PS blends, equilibrium behaviour - '***Equilibrium (1)***'

(2) High M_w d-PS/h-PS blends, equilibrium behaviour - '***Equilibrium (2)***'

(3) Low M_w d-PS(F)/h-PS blends, equilibrium behaviour - '***Equilibrium (3)***'

(4) Low M_w d-PS(F)/h-PS blends, influence of casting solution concentration on initial composition gradients - '***Casting Concentration***'

(5) Low M_w d-PS(F)/h-PS blends, development of the air surface excess with time - '*Kinetics*'

(6) Low M_w d-PS(F2)/h-PS blends, equilibrium behaviour- '***Double End Capped***'

This scheme will be used as a framework to describe the experiments done and the results obtained, although the discussion will deviate somewhat from this arrangement. Below is a summary of the codes used to describe the blends used in this section:

FL	Single end capped d-PS(F) low molecular weight blends
2FL	Double end capped d-PS(F2) low molecular weight blends
FH	Single end capped d-PS(F) high molecular weight blends
H	'Plain' high molecular weight d-PS/h-PS blend
u	unannealed sample
a	annealed sample - for the kinetics experiment a1, a2, etc.
A, B, C ,D	FL blends cast from 10%, 7.5%, 5.0% and 2.5% total weight polymer solutions.
...35..	A blend with nominally for example 35% deuterated polymer

Equilibrium (1)

High molecular weight blends of d-PS(F)/h-PS (TK92/TK58) were prepared with a range of bulk volume fractions of d-PS(F), shown in Table 7.2 along with the labels used to identify these blends. Thin films of these blends were spun cast onto silicon blocks (for NR work) and silicon wafers (for NRA work) from 2% total weight polymer toluene solution.

High Mw (TK92/TK58)	Volume fraction d-PS(F)
FH5	0.048
FH15	0.144
FH25	0.235
FH35	0.310
FH50	0.475

Table 7.2: Nominal bulk volume fractions of d-PS(F), ϕ_B, used in *Equilibrium (1)*, along with the labels used to identify these blends.

The average thickness of the films used for NRA was 2000±250Å and for NR samples the average thickness was 1400±100Å, measured by contact profilometry. This difference in thickness arises from a difference in the spinning speed used in casting (2000 rpm and 4000 rpm respectively). Thinner films were prepared for the NR work in order that Kiessig fringes, characteristic of the sample thickness, could be seen in the reflectivity data. Slightly thicker films were prepared from for the NRA work in order the air and silicon interfaces could be clearly resolved. Unannealed films were retained and films annealed under vacuum for 10.8 days at 428K were also prepared. Secondary ion mass spectrometry (SIMS) by collaborators at Strathclyde University has shown that after this annealing programme the surface volume fraction of d-PS(F) has reached an equilibrium value[1]. NRA measurements were made on blends FH5, FH15, FH25, FH35 and FH50 on a single occasion in November 1993, NR measurements were made on FH5, FH25, FH35 and FH50 on a single occasion in November 1993.

Equilibrium (2)

High molecular weight blends of d-PS/h-PS (TK93/TK58) were prepared with compositions shown in Table 7.3. Thin films of these blends were spun cast onto silicon wafers from ~4% total weight polymer toluene solution (spinning speed 4000 rpm). The average film thickness measured by contact profilometry was 2500±500Å. These samples were annealed for 9.9 days at 428K. NRA measurements were made on a single occasion in March 1994. The intention of these experiments was to obtain a measure of the contribution that surface enrichment made to the behaviour seen in '***Equilibrium (1)***'.

High Mw (TK93/TK58)	Volume fraction d-PS
H5	0.045
H15	0.141
H25	0.233

Table 7.3: Nominal bulk volume fractions of d-PS, ϕ_B, used in *Equilibrium (1)*, along with the labels used to identify these blends.

Equilibrium (3)

Low molecular weight blends of d-PS(F)/h-PS (TK89/TK79) were prepared with a range of bulk volume fractions of d-PS(F), see Table 7.4. Thin films of these blends were spun cast onto silicon blocks (for NR) and silicon wafers (for NRA), from 7.5% solution of total polymer in toluene (spinning speed 2000 rpm). The average thicknesses of the films produced were 3900±200Å and 3750±250Å respectively, measured by contact profilometry. Thicker films were used for the low molecular weight blends in this experiment than the high molecular weight blends in ***Equilibrium (1)*** because it was found that for thinner films (annealed at higher temperatures) the film completely dewetted from the silicon substrate, such dewetting behaviour has been investigated by other workers[2]. Unannealed films were retained and films annealed under vacuum for 2 days at 403K were also prepared, SIMS results have shown that after this annealing programme the surface volume fraction of d-PS(F) has reached an equilibrium value.

Low Mw (TK89/TK79)	Volume fraction d-PS(F)
FL5	0.046
FL10	0.091
FL15	0.138
FL20	0.190
FL25	0.248
FL35	0.331
FL50	0.504

Table 7.4: Nominal bulk volume fractions of d-PS(F), ϕ_B, used in *Equilibrium (3)*, along with the labels used to identify these blends.

NRA measurements were made on a single occasion in November 1993. NR measurements were made on two occasions, in November 1993 (FL5, FL25, FL50) and April 1994 (FL10, FL15, FL20 and FL35).

Casting Concentration

To observe the effect that the concentration of the casting solution had on the near surface composition profile of unannealed samples four solutions of a low molecular weight d-PS(F)/h-PS (TK89/TK79) blend were prepared. The volume fraction of d-PS(F) was fixed at 0.331, solutions with weight percentage of total polymer 10%, 7.5%, 5% and 2.5% were made. These samples will be referred to as A35u, B35u, C35u and D35u respectively. These solutions were spun cast onto silicon blocks, spinning speed was 2000rpm. Film thickness for these samples, measured using contact profilometry were: 5820±30Å, 3870±20Å, 1430±10Å and 620±30Å respectively. NR experiments were carried out on these films on a single occasion in April 1994.

Kinetics

To evaluate the kinetics of the formation of the air surface excess of d-PS(F) observed for the low molecular weight d-PS(F)/h-PS (TK89/TK79) a series of samples were prepared, all with bulk volume fraction of d-PS(F) of 0.331. The sample preparation procedure was identical to that used in ***Equilibrium (3)***. Average film thicknesses for these sample was 3870±20Å. An unannealed sample was retained and samples annealed under vacuum at 403K were prepared, the annealing times used and the corresponding sample labels are shown in Table 7.5.

	Annealing time /hours
FL35u	0
FL35a1	0.33
FL35a2	1
FL35a3	3
FL35a4	5
FL35a5	48

Table 7.5: Annealing times and sample labels for the low molecular weight blends used in the *Kinetics*.

NR measurements were made in April 1994, one sample (FL35a2) was measured on a different date by the CRISP instrument scientists using the single detector.

Double End Capped

Low molecular weight blends of the double end capped d-PS(F2) with h-PS (TK145/TK79) were prepared, the compositions of the blends used can be found in Table 7.6.

Low Mw TK145/TK79	Volume fraction d-PS(F2)
2FL10	0.094
2FL35	0.335
2FL50	0.486

Table 7.6: Nominal bulk volume fractions of d-PS(F2), ϕ_B, used in *Double End Capped*, along with the labels used to identify these blends.

Thin films of these blends were spun cast onto silicon blocks (for NR) from 5% total weight polymer toluene solution (spinning speed 2000 rpm). The average thickness of these blends, measured using contact profilometry, was 2220±40Å. An unannealed sample (2FL35u) was retained, in addition samples of all three blends were annealed under vacuum for 2 days at 403K. NR data were collected on a single occasion in April 1994.

7.2 Results

Before presenting the results a number of general observations regarding data analysis will be made.

Comments on Neutron Reflectometry

Three methods of data analysis were used on the reflectivity data:

(1) VOLFMEM, described in Section 4.3.3., was used to fit 'free form' composition profiles, $\phi(z)$, with a pixel resolution in the range 10Å - 15Å and internal smoothing of 100Å.

(2) PHOENIX, described in Section 4.3.3., was used to fit multilayer models (up to 3 layers) with Gaussian roughness between the layers.

(3) PHOENIX was used to fit profiles with a Tanh function (see Equation 7.1) to describe composition profiles at the air and/or silicon interface.

$$\phi(z) = \phi_B + \frac{(\phi_1 - \phi_B)}{2}\left\{1 + Tanh\left(\frac{2(z_{off} - z)}{w}\right)\right\}$$

Equation 7.1

ϕ_1 corresponds crudely to a 'surface composition', z_{off} and w approximate to the offset of the decay to bulk composition, ϕ_B, and the sharpness of the decay, respectively. For the fits using PHOENIX the roughness at the air and silicon interfaces was fixed at 5Å and a 15Å SiO_2 layer was included, although this improved the quality of the fits for the thinner samples (in line with the calculation presented in section 3.1.2), the parameters fitted were essentially the same as those obtained with no SiO_2 layer. The experimental resolution used in the fitting procedures was fixed at the geometric value (3.5% and 4.4% for the November 1993 and April 1994 experiments respectively). The fit parameters from the PHOENIX fits are quoted along with the 'Fit Index', which is <u>not</u> identical to the normalised χ^2 parameter traditionally used. The Fit Index is defined in section 4.3.3. As a guide the normalised χ^2 parameter was calculated for a limited number of multilayer fits to the reflectivity data, comparisons of these values with the equivalent fit index can be found in Table 7.7.

Blend	Fit Index	normalised χ^2
2FL10a	0.06	4
FL35u	0.10	8
FL50a	0.16	17
FH35a	0.15	19

Table 7.7: Correspondence between the Fit Index and the normalised χ^2 parameter for selected blends (multilayer fits).

The $\phi(z)$ profiles generated using VOLFMEM all show a sharp decrease in the volume fraction of d-PS(F) in the top 30Å of the films (see Figure 7.1). This behaviour was particularly noticeable in the low molecular weight blends. This decrease in $\phi(z)$ is an artefact of the maximum entropy data analysis.

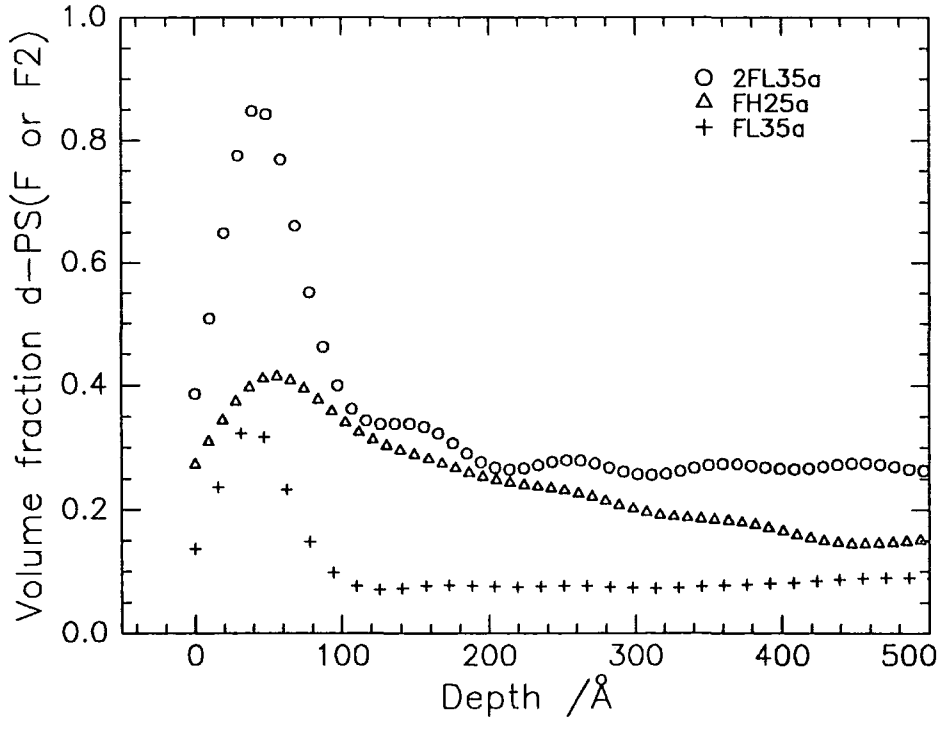

Figure 7.1: A selection of $\phi(z)$ profiles, generated using VOLFMEM, illustrating the downturn in ϕ at the surface.

Firstly VOLFMEM does not include a value for the air/surface roughness. To compensate for this it would be expected that the maximum entropy algorithm would

reduce the volume fraction of the surface layers to mimic the effect of roughness. Secondly the truncation of the R(Q) data at finite values of Q introduces further artefacts. To evaluate the influence of these effects 'simulated' R(Q) data were created from a Tanh profile (ϕ_1 = 0.63, ϕ_B = 0.25, z_{off} = 33.5 and w = 120, film thickness 4000Å, 'experimental' resolution = 4.4%), with air - polymer and polymer - silicon roughness' of 5Å, simulated error values were included. The simulated reflectivity data were analysed by VOLFMEM in a manner identical to that used for real data. A comparison of the 'real' profile and the profiles extracted using VOLFMEM and PHOENIX (Tanh model) are shown in Figure 7.2.

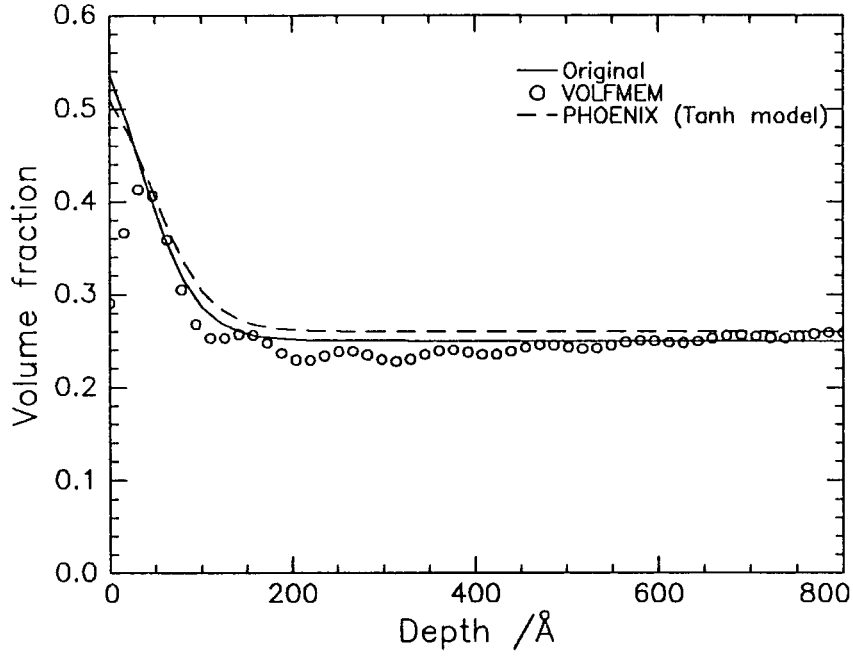

Figure 7.2: Comparison of composition profiles produced by PHOENIX (Tanh model) and VOLFMEM from simulated data.

The simulated data were also fitted with multilayer and Tanh models. A comparison of the surface excess, z^*, (given by Equation 7.2) and surface volume fraction of d-PS(F), ϕ_{air}, obtained using these three methods and from the original $\phi(z)$ profile are shown in Table 7.8.

$$z^* = \int (\phi(z) - \phi_B) dz$$

Equation 7.2

These results show that VOLFMEM considerably under estimates the values of z^* and ϕ_{air}. Further modelling showed that this effect occurs even in the absence of roughness, although it is considerably enhanced for rougher films. The Tanh function fit provided the best predictions of z^* and ϕ_{air}.

	z^*/Å	ϕ_{air}
Original	16.0	0.53
VOLFMEM	10.5	0.40
Multilayer (3 layers)	13.5	0.50
Tanh profile	15.5	0.51

Table 7.8: Parameters derived from fits to simulated reflectivity data and the parameters derived from the 'original' profile used to generate the data.

It was found that, in the ***Kinetics*** experiment, an equilibrium value of the surface excess was reached after only one hour. Assuming therefore that the subsequent samples (FL35a2-a5) have essentially identical composition profiles since they have reached equilibrium, this provides an opportunity to check the reproducibility of the derived parameters z^*_{air} and $(\phi_{air} - \phi_B)$ under real experimental conditions. Table 7.9 shows a comparison of these parameters, along with their average values, for the four samples (FL35a2-FL35a5) obtained using the three different methods of data analysis. It can be seen that the multilayer and VOLFMEM methods fit systematically lower values of z^*_{air} and $(\phi_{air} - \phi_B)$ compared to the values obtained using the Tanh profile. The standard deviations in the results from VOLFMEM are larger than for the other two methods, the standard deviations in z^*_{air} and $(\phi_{air} - \phi_B)$ calculated for the Tanh and multilayer methods are of similar magnitude to the statistical errors in these values arising from uncertainty in the fitting process. It can be seen in Table 7.9 that the fitted value of ϕ_B varies quite considerably. This does not effect the derived parameters z^*_{air} and $(\phi_{air} - \phi_B)$.

		FL35a2	FL35a3	FL35a4	FL35a5	Average
VOLFMEM	z^*_{air}	40	27	23	30	30 ± 7
	ϕ_B	0.36	0.35	0.36	0.35	0.36 ± 0.01
	$\phi_{air} - \phi_B$	0.48	0.38	0.35	0.40	0.40 ± 0.06
Multilayer	z^*_{air}	32	29	31	28	30 ± 2
	ϕ_B	0.37	0.32	0.29	0.36	0.34 ± 0.04
	$\phi_{air} - \phi_B$	0.39	0.41	0.43	0.35	0.40 ± 0.03
Tanh	z^*_{air}	35	36	33	38	36 ± 2
	ϕ_B	0.35	0.28	0.28	0.30	0.34 ± 0.03
	$\phi_{air} - \phi_B$	0.45	0.52	0.43	0.47	0.47 ± 0.04

Table 7.9: Comparison of parameters obtained using the three methods of data analysis, from four identical samples. Errors are standard deviations.

The average volume fraction of d-PS(F), ϕ_{av}, is defined below:

$$\phi_{av} = \frac{1}{l}\int \phi(z)dz$$

Equation 7.3

(where l is the film thickness).

ϕ_{av} was calculated using all three methods of data analysis for all the films used and it was found that the values obtained were up to 0.05 below the nominal value of ϕ_{av}, calculated from the masses of d-PS(F) and h-PS used in making the blends. The cause of this discrepancy is not clear, but it may be due to errors in the values of the nuclear scattering length densities used for h-PS and d-PS or to a mixture of systematic and random errors in determining Q. Since the effect is small and does not effect the values of z^*_{air} and ($\phi_{air} - \phi_B$), which will be used in the discussion, it was not investigated further.

The data were initially analysed using VOLFMEM, and Tanh profiles were subsequently fitted to the reflectivity data using starting parameter values derived from the $\phi(z)$ profiles generated by VOLFMEM. It is the parameters derived from the Tanh profiles that most accurately represent the probable distribution of d-PS(F) in the films and will be used in the discussion. The exception to this is the analysis of the unannealed

samples, where a depletion layer was seen below the surface excess, see Figure 7.3 for a schematic illustration, in this case multilayer fits were used to evaluate the extent of the depletion z^*_{dep}. Statistical errors in the surface excess (measured by neutron reflectometry) and the surface volume fraction are ±2Å and ±0.02, respectively.

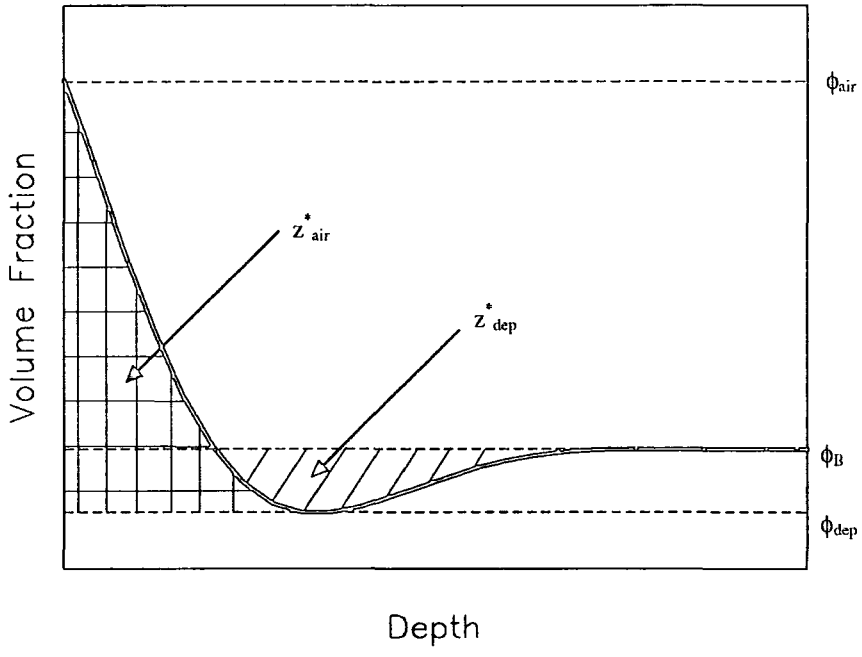

Figure 7.3: Schematic diagram of structure observed in unannealed films, with definitions of terms used.

Comments on Nuclear Reaction Analysis

The surface excesses z^* were calculated from the NRA data using GENPLOT; the average bulk volume fraction, ϕ_B, was subtracted from the normalised data. This 'bulk subtracted' data was then numerically integrated to give the surface excess. This value of the excess was found to be significantly lower than the value measured using neutron reflectometry, this discrepancy arises from resolution effects, which will be discussed here. Figure 7.4 illustrates the effect of convoluting a Gaussian resolution function (Full Width Half Maximum (FHWM = 350Å), with a series of step functions.

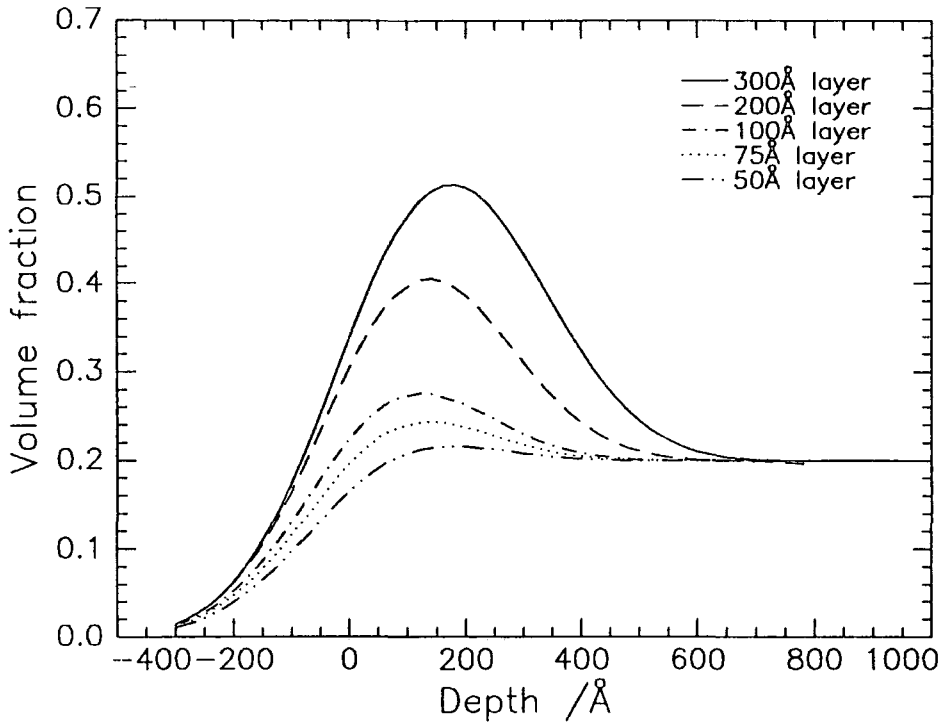

Figure 7.4: Several step functions with varying thickness (ϕ_{air} = 0.7) convoluted with a Gaussian resolution function (FWHM = 350 Å).

These step functions have a thin layer with a volume fraction 0.7 sandwiched between 'air' and a thick layer with bulk volume fraction = 0.2. The thickness of the overlayer is varied from 50Å - 300Å, i.e. 0.15 FWHM to 0.85 FWHM. The values of z^* and the 'surface volume fraction', ϕ_{air} measured for these simulated profiles using the methods applied to the experimental data are shown in Table 7.10, along with the excess calculated for the original step function. For the NRA data ϕ_{air} is taken to be the maximum measured value of ϕ in the region near the surface.

Overlayer thickness/ Å	original z^*/Å	measured z^*/Å	measured ϕ_{air}
300	150	113	0.51
200	100	65	0.41
100	50	20	0.28
75	38	10	0.24
50	25	3	0.22

Table 7.10: Reduction in the value of z^* measured by NRA compared to the original z^*.

The resolution effect causes decreases in the measured z^* and ϕ_{air} that are of the magnitude required to explain the differences in values obtained using neutron reflectometry and nuclear reaction analysis. In real experiments the measured value of z^* would also depend to a certain extent on the shape of the near surface composition profile. There are a number of procedures which could be adopted in order to extract the 'true' z^* from the NRA data:

(a) In principle Fourier transform deconvolution of the NRA data could be performed, this would involve Fourier transforming the measured $\phi(z)$ and dividing by the Fourier transform of the resolution function and then Fourier transforming the resulting function to obtain a deconvoluted $\phi(z)$ from which the 'true' z^* could be extracted. More details of this procedure can be found in reference 3 . This procedure would be sensitive to statistical errors in the measured $\phi(z)$ and inadequate knowledge of the resolution function.

(b) The experimental data could be fitted with a model $\phi(z)$ convoluted with a resolution function. This would be computationally demanding, but rather more robust than (a).

(c) The measured z^* could be multiplied by a 'correction factor' derived from data such as that in Table 7.10, although the correction factor would be somewhat arbitrary because it depends on the profile shape.

Rather than using these procedures on the NRA data, it can be shown that the NR and NRA data are comparable by taking the Tanh function profiles fitted to the NR data and convoluting them with a Gaussian resolution function and then comparing these convoluted NR data with the NRA data. The comparisons between ϕ_{air} and the surface excess, z^*, obtained in this way can be found in Figure 7.5 for the FH (***Equilibrium (1)***) blends and Figure 7.6, the FL (***Equilibrium (3)***) blends. The Gaussian resolution function for these data had a FWHM of 300Å for both sets of data, this value was found to give the best fit and is in line with the expected value. The agreement between the ϕ_{air} obtained using NRA and convoluted NR is very good, but there is rather more scatter in the z^* values. This is because the z^* calculated using NRA is quite sensitive to the value of ϕ_B chosen when making the integration. (These data will be fully introduced shortly).

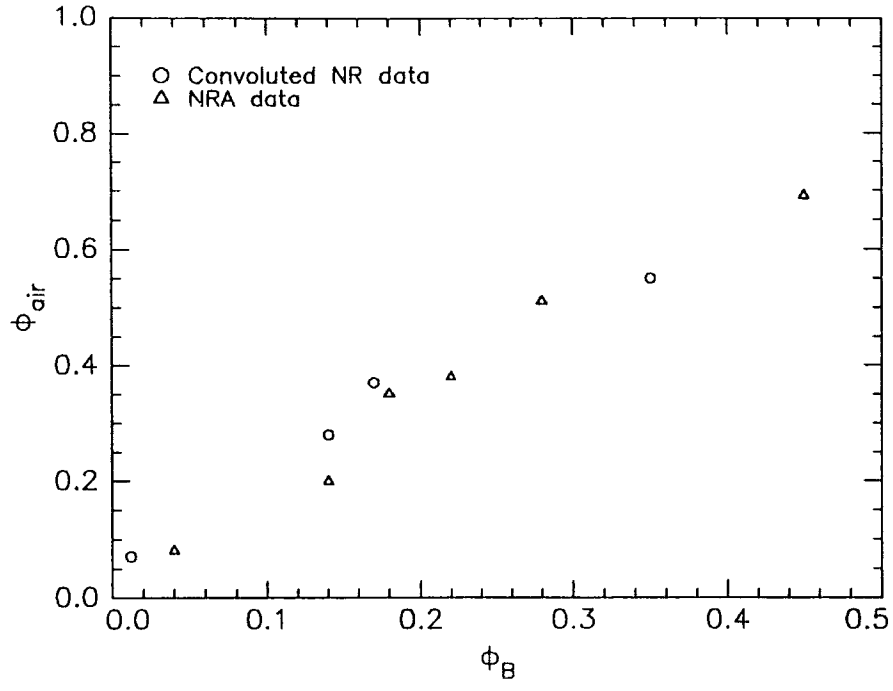

Figure 7.5a: Comparison between ϕ_{air} values obtained for the FH blends using NRA and NR Tanh profiles convoluted with a Gaussian resolution function (FWHM = 300Å).

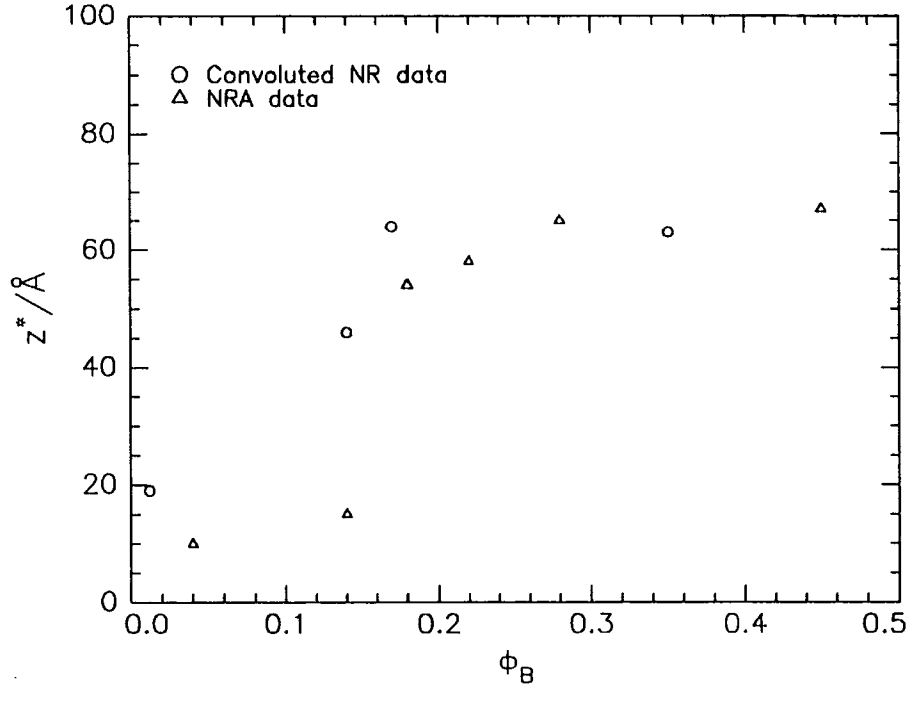

Figure 7.5b: Comparison between z^* values obtained for the FH blends using NRA and NR Tanh profiles convoluted with a Gaussian resolution function (FWHM = 300Å).

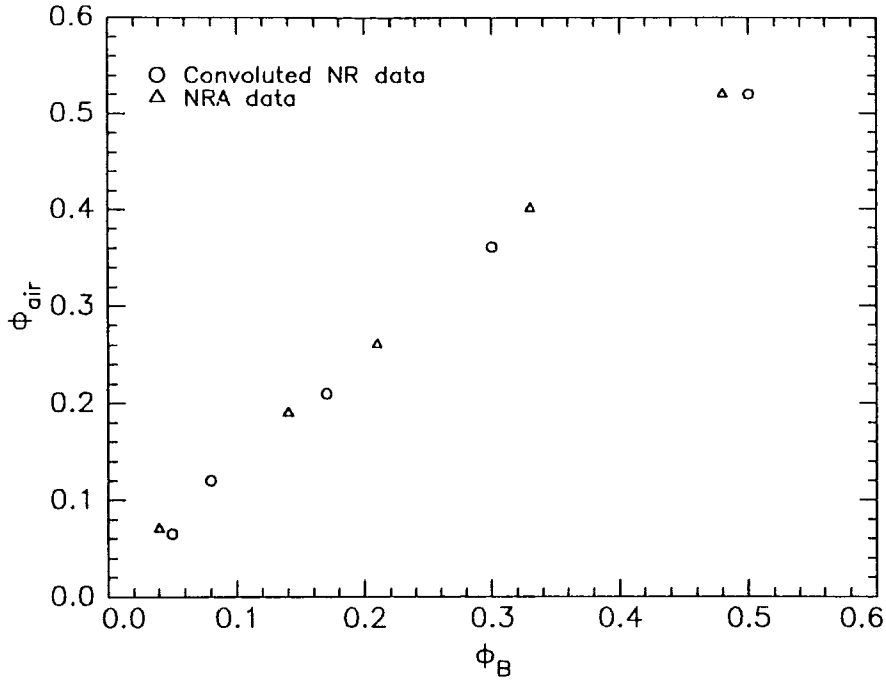

Figure 7.6a: Comparison between ϕ_{air} values obtained for the FL blends using NRA and NR Tanh profiles convoluted with a Gaussian resolution function (FWHM = 300Å).

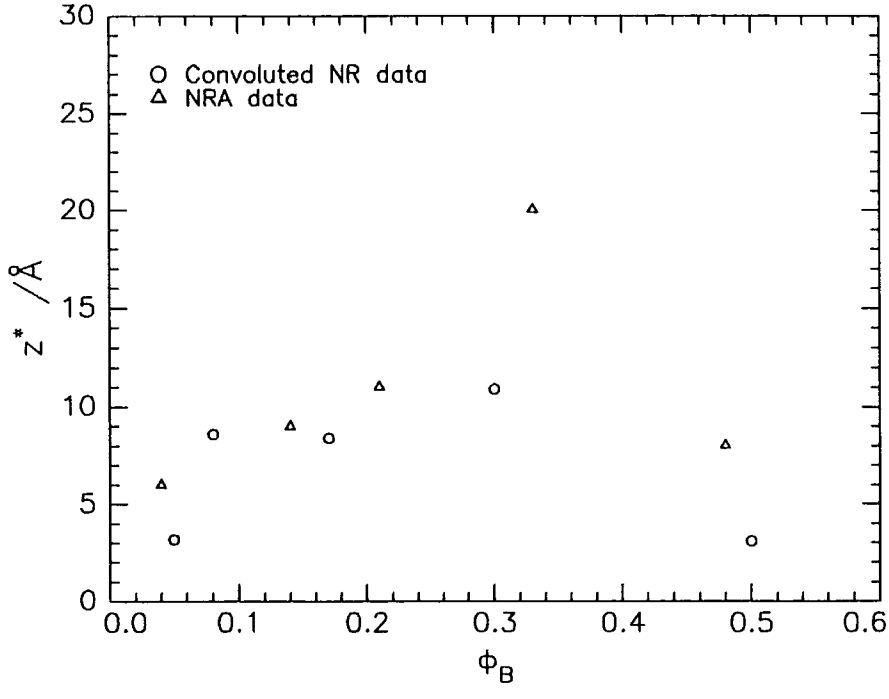

Figure 7.5a: Comparison between z^* values obtained for the FL blends using NRA and NR Tanh profiles convoluted with a Gaussian resolution function (FWHM = 300Å).

Equilibrium (1)

Composition versus depth profiles for the high molecular weight d-PS(F)/h-PS blends were obtained from the NRA data using the methods outlined in section 4.4. The average value for the film thickness, calculated for all these films is 1980±160Å, which is in good agreement with the value obtained by contact profilometry. Figure 7.7 shows these profiles for samples (a) before annealing and (b,c) after annealing.

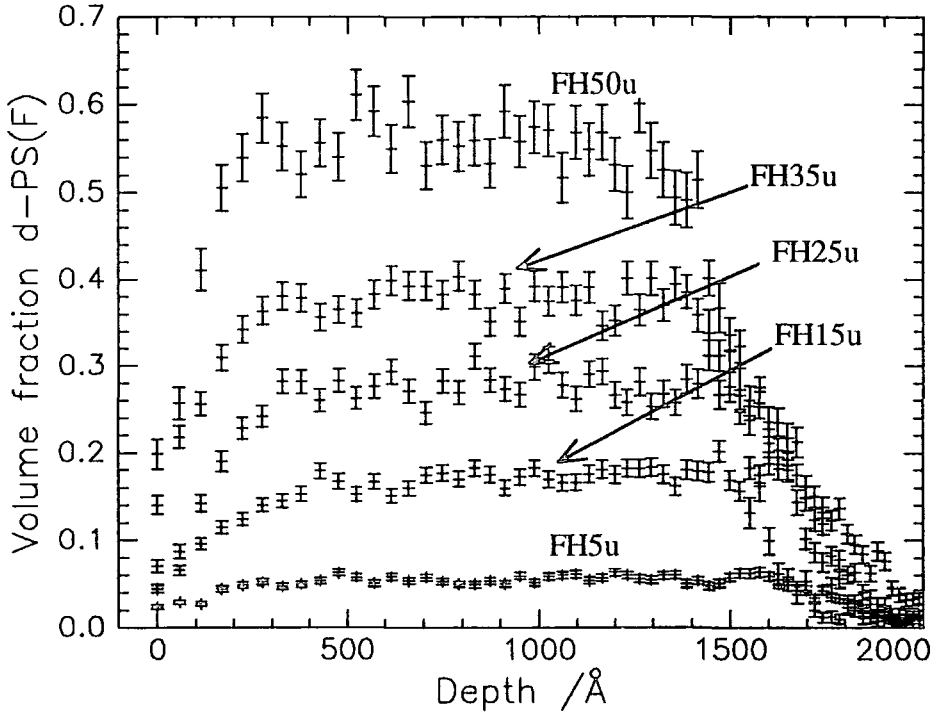

Figure 7.7a: Compositions profiles $\phi(z)$ for unannealed FH blends, obtained using NRA, error bars from Poisson statistics.

These data show that before annealing the d-PS(F) is distributed uniformly in the films. After annealing d-PS(F) is found to segregate to both the air and silicon interfaces. The values of z^*_{air}, z^*_{si} and ϕ_B calculated from the NRA data using GENPLOT are shown in Table 7.11, the experimental error in the surface excesses is 10Å.

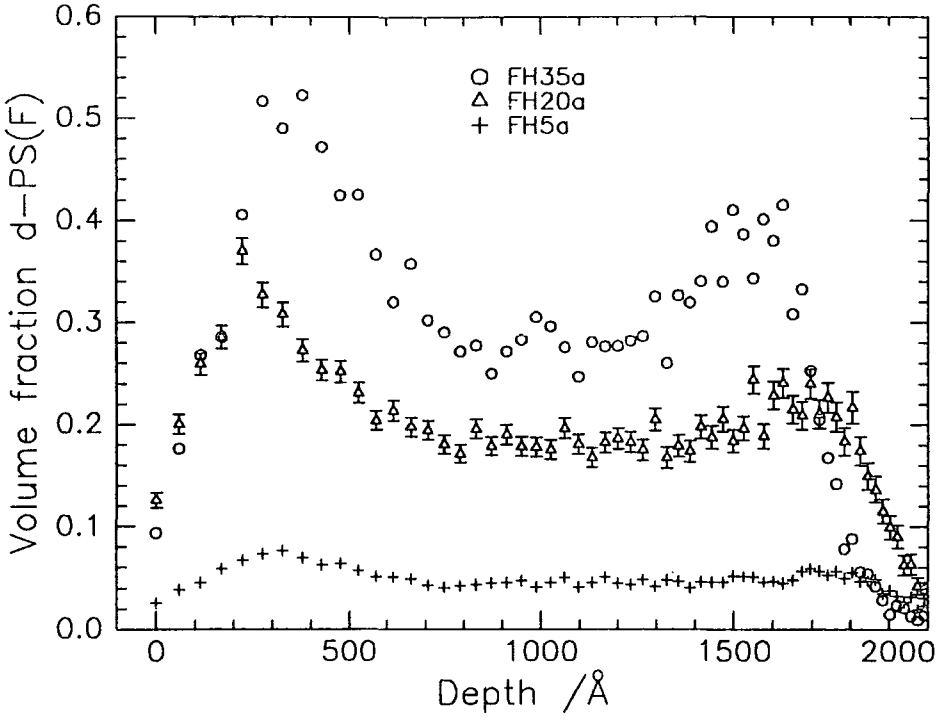

Figure 7.7b: Composition profiles for annealed FH blends, obtained using NRA. Error bars from Poisson counting statistics for a representative dataset.

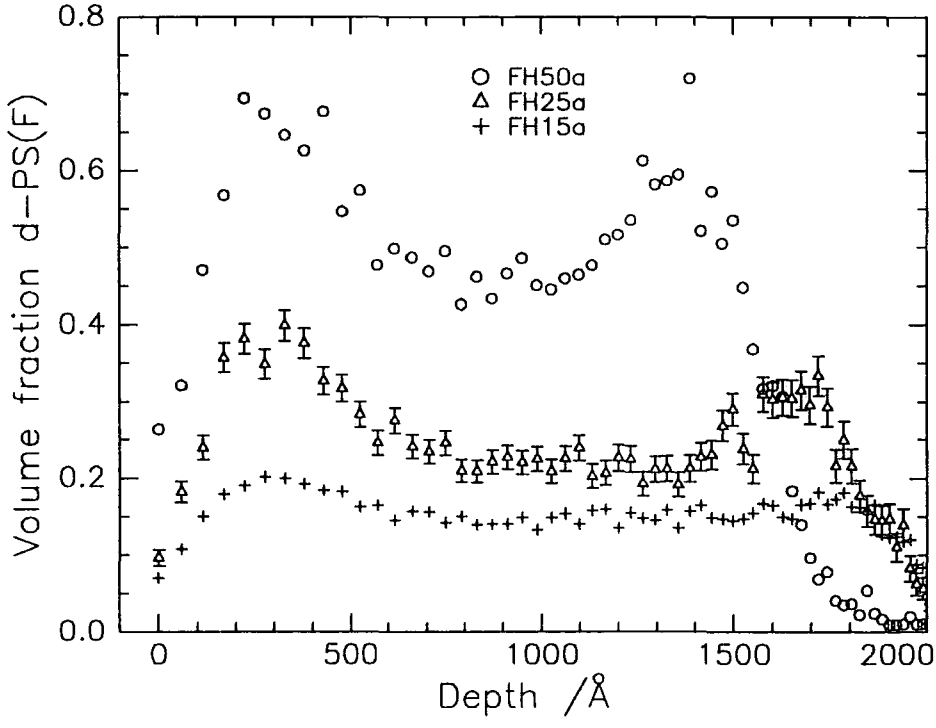

Figure 7.7c: Composition profiles for annealed FH blends, obtained using NRA. Error bars from Poisson statistics for a representative dataset.

Blend	ϕ_B	z^*_{air}/Å	z^*_{si}/ Å	ϕ_{air}	ϕ_{si}
FH5a	0.04	10	5	0.08	0.06
FH15a	0.14	15	9	0.20	0.18
FH20a	0.18	54	12	0.35	0.49
FH25a	0.22	58	22	0.38	0.31
FH35a	0.28	65	28	0.51	0.40
FH50a	0.45	67	44	0.69	0.60

Table 7.11: Parameters for the FH annealed blends from NRA measurements

The ratio z^*_{si} / z^*_{air} is 0.5 ± 0.2 for these blends. Values of the maximum volume fraction of d-PS(F) observed at air (ϕ_{air}) and silicon (ϕ_{si}) interfaces are also shown in Table 7.11, the ratio ϕ_{si} / ϕ_{air} is 0.9 ± 0.2.

Turning to the NR data, examples of the reflectivity data, R(Q), are shown in Figure 7.8a along with fits obtained using PHOENIX (Tanh model), the data exhibit Kiessig fringes which give an indication of the film thickness. For the blends FH25, FH35 and FH50 there is a significant increase in the overall reflectivity on annealing, the FH5 blend shows only small changes in reflectivity on annealing. This is illustrated in Figure 7.8b. The average value of the film thickness fitted was 1430±100Å which is in good agreement with the values obtained using contact profilometry. Figure 7.9a shows the composition profiles obtained for the unannealed FH blends using VOLFMEM, Tanh function profiles were not fitted to these data. Figure 7.9b shows the $\phi(z)$ profiles obtained for the annealed blends using VOLFMEM and PHOENIX (Tanh model) fits. The blends FH50u and FH25u showed a small depletion of d-PS(F) from the air interface and the blends FH35u and FH5u showed a small excess of d-PS(F) at the air interface. These deviations from uniformity are very small when compared with the excesses observed after annealing. The annealed blends all show substantial excesses of d-PS(F) at both the air and silicon interfaces, the film thickness is small so these excesses lead to a significant reduction of the volume fraction of d-PS(F) in the middle of the film from the nominal 'bulk' value. For the NRA experiments the films were thicker and so a weaker effect of this sort was observed.

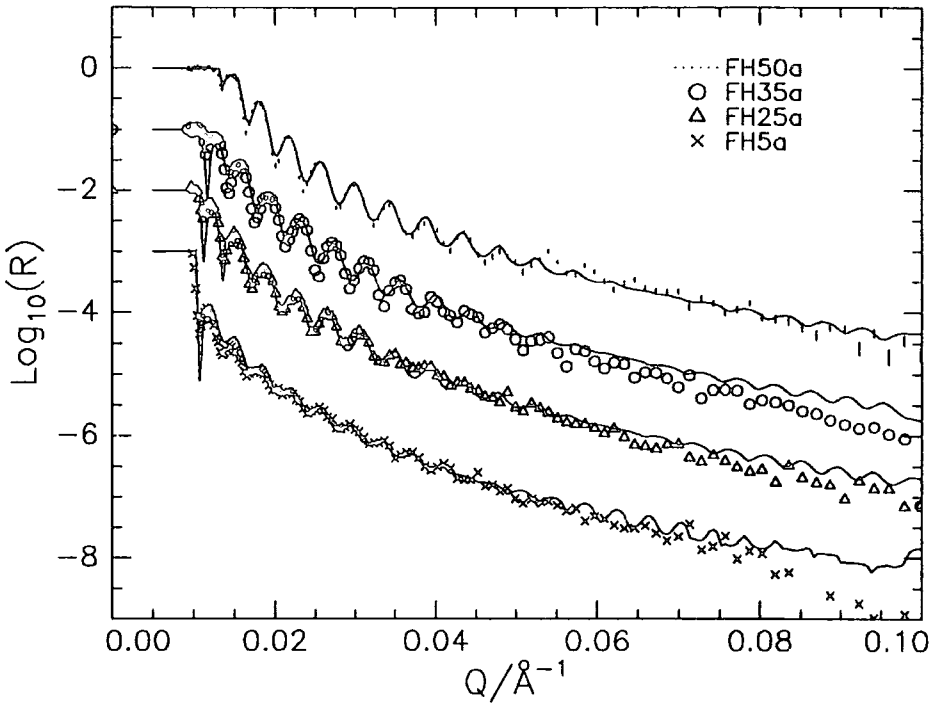

Figure 7.8a: Neutron reflectivity data for annealed FH blends (symbols), with fits from PHOENIX (Tanh model). Error bars for FH5a from Poisson statistics. Successive profiles offset by -1 for clarity.

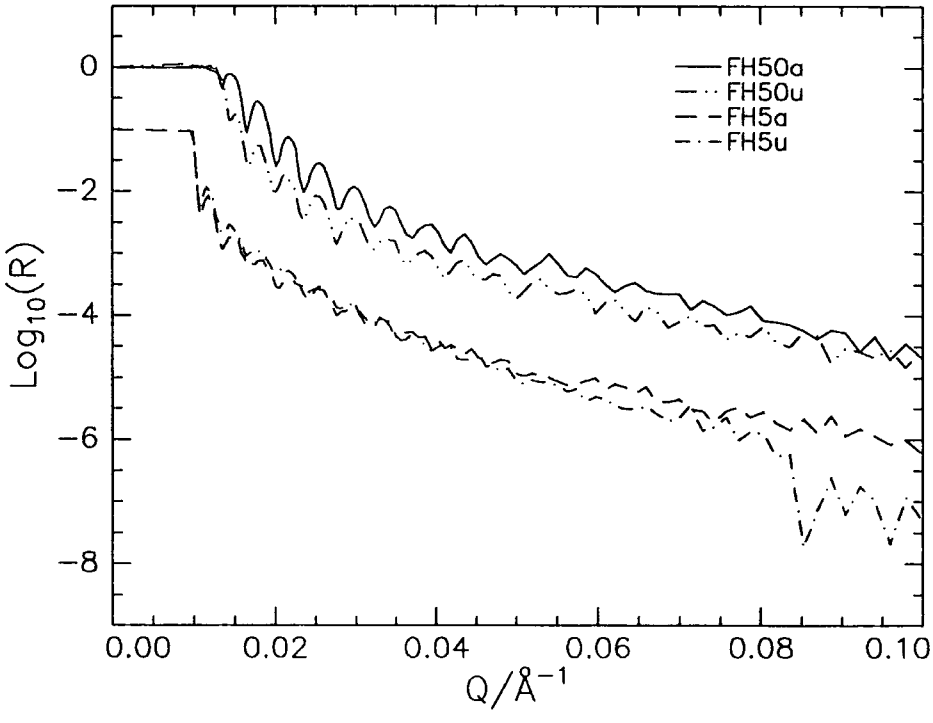

Figure 7.8b: Neutron reflectivity data for unannealed and annealed FH5 and FH50 data, FH5 data offset by -1 for clarity.

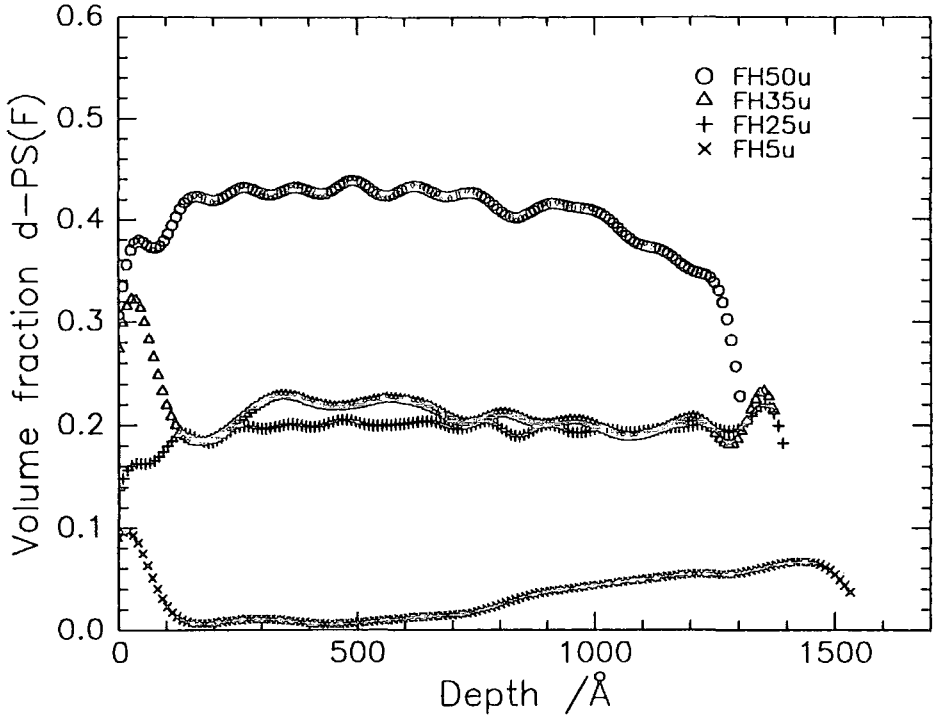

Figure 7.9a: Composition profiles for unannealed FH blends obtained using VOLFMEM analysis of neutron reflectivity data.

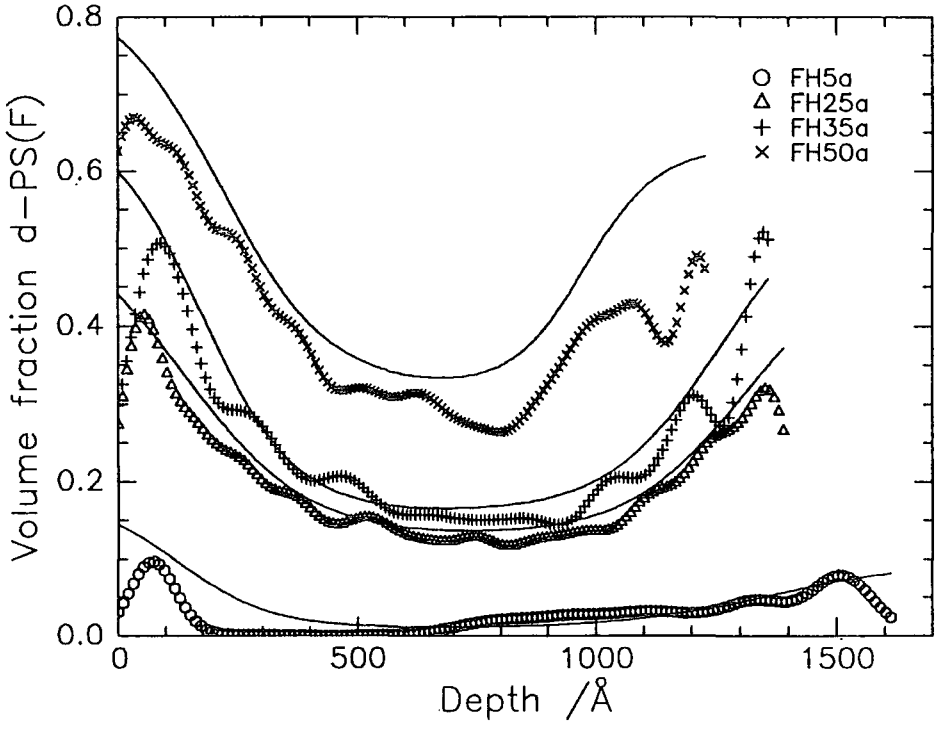

Figure 7.9b: Composition profiles for annealed FH blends, calculated from reflectivity data, VOLFMEM (symbols) and PHOENIX (Tanh model) (solid lines) fits.

Table 7.12 shows the values of the surface excesses z^*_{air} and z^*_{si} and surface volume fractions of d-PS(F), ϕ_{air} and ϕ_{si}, obtained using Tanh profile fits. The ratio z^*_{si} / z^*_{air} is 0.75 ± 0.07 and the ratio ϕ_{si} / ϕ_{air} is 0.7 ± 0.2. The parameters for the Tanh profile fits are in Table 7.13.

Blend	ϕ_B	z^*_{air} /Å	z^*_{si} /Å	ϕ_{air}	ϕ_{si}
FH5a	0.01	29	23	0.16	0.08
FH25a	0.13	73	51	0.44	0.38
FH35a	0.16	97	67	0.60	0.48
FH50a	0.32	109	90	0.77	0.62

Table 7.12: Parameters derived for the FH annealed blends from Tanh profile fits to NR data.

			Air			Silicon			
Sample	ϕ_B	1/Å	ϕ_1	z_{off} /Å	w /Å	ϕ_1	z_{off} /Å	w /Å	Fit Index
FH5a	0.01	1600	0.20	129	386	0.095	241	591	0.19
FH25a	0.13	1400	0.54	142	500	0.5	89	489	0.13
FH35a	0.16	1380	0.67	175	387	0.59	120	464	0.13
FH50a	0.32	1304	0.84	214	445	0.63	326	304	0.15

Table 7.13: Parameters for Tanh fits to FH annealed blends.

Equilibrium (2)

Figure 7.10 shows composition profiles obtained from NRA data for the blends H5a, H15a and H25a. The average thickness measured from these data is 1900±200Å, which is lower than the average value obtained from contact profilometry, this discrepancy is due mainly to the H5a sample. In common with the high molecular weight d-PS(F)/h-PS blends segregation is observed at both the air and silicon interfaces. Values z^*_{si}, z^*_{air}, ϕ_{air} and ϕ_{si} for these blends can be found in Table 7.14. The ratio z^*_{si} / z^*_{air} is 0.5 for these data and ϕ_{si} / ϕ_{air} is 0.5 (excluding the H5a blend). The surface excesses for these blends are approximately half that of the equivalent end labelled (FH) blends.

Blend	ϕ_B	z^*_{air} /Å	z^*_{si} /Å	ϕ_{air}	ϕ_{si}
H5a	0.05	2	0	0.06	0.05
H15a	0.15	11	5	0.44	0.19
H25a	0.25	21	12	0.60	0.32

Table 7.14: Parameters derived for the annealed H blends from NRA data

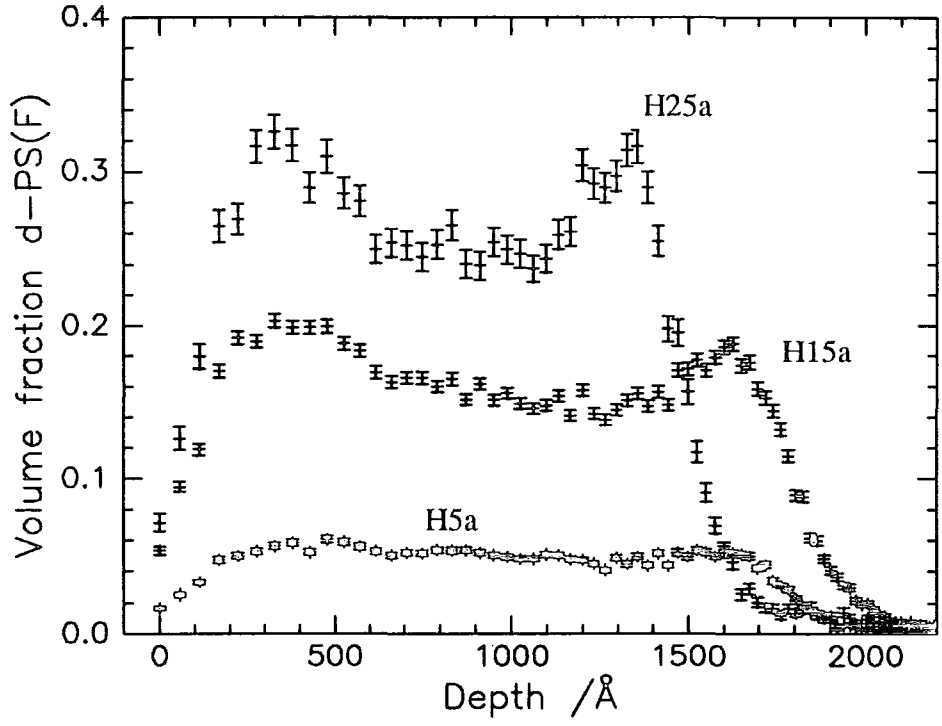

Figure 7.10: Compositions profiles for annealed H blends, obtained using NRA, error bars from Poisson statistics.

Equilibrium (3)

Figure 7.11 shows $\phi(z)$ profiles for the low molecular weight d-PS(F)/h-PS blends, obtained using NRA (a) before and (b) after annealing. The average film thickness indicated by these data appears to be around 2500Å, this is significantly less than the 3750±250Å measured using contact profilometry, but there is no clear 'back edge' visible in the data as there was for the thinner films used for the high molecular weight blends. This suggest that the incident $^3He^+$ did not penetrate to the silicon interface, the path length to the silicon interface for the incident angle used is around 1.5μm, which is similar in magnitude to the expected stopping distance for $^3He^+$ in polystyrene. This means no information is available on the composition profile at the silicon interface.

The NRA data shows the d-PS(F) to be distributed uniformly in the unannealed films, in the annealed films there is a small excess of d-PS(F) at the air interface. The air surface excess, z^*_{air}, and the surface volume fraction of d-PS(F), ϕ_{air}, for these blends can be found in Table 7.14.

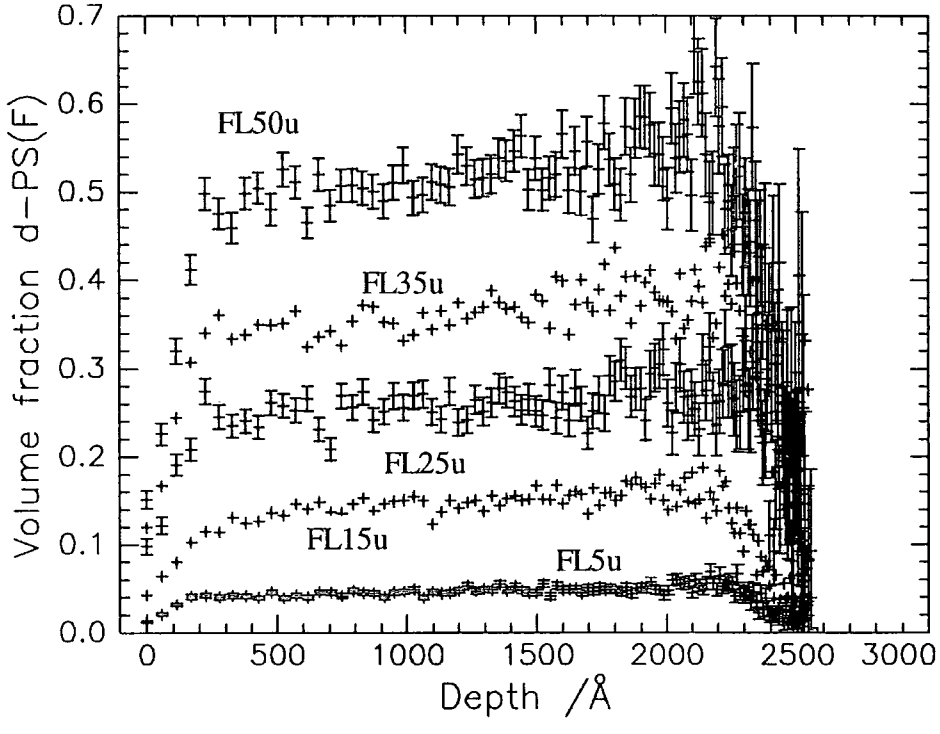

Figure 7.11a: Composition profiles for unannealed FL blends, obtained using NRA, error bars from Poisson statistics for representative datasets.

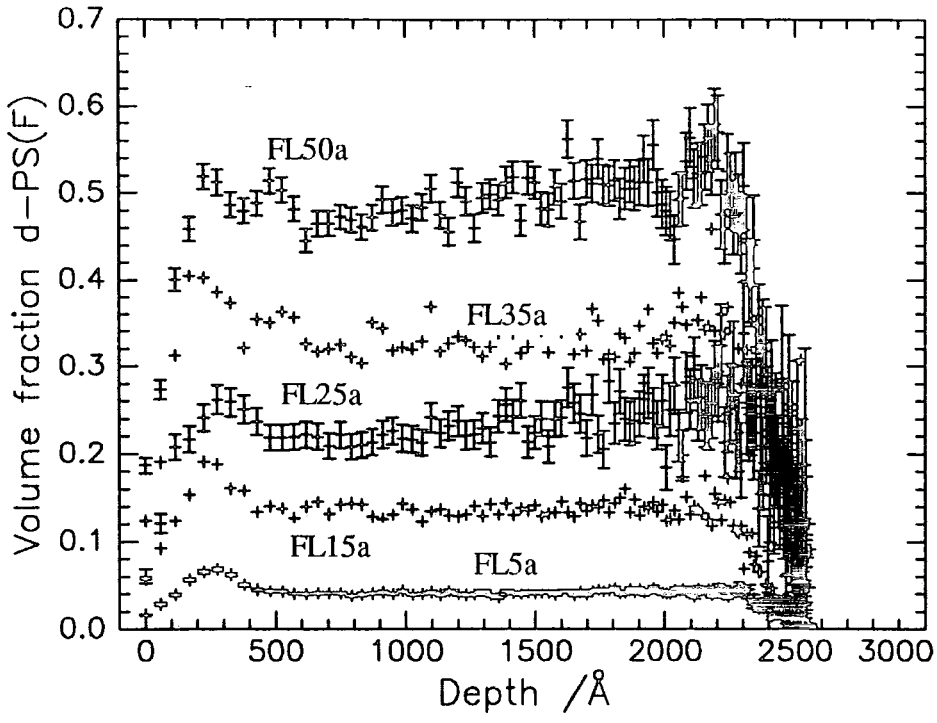

Figure 7.11b: Composition profiles for annealed FL blends, obtained using NRA. Error bars from Poisson statistics for representative datasets.

	ϕ_B	z^*_{air} /Å	ϕ_{air}
FL5a	0.04	6	0.07
FL15a	0.14	9	0.19
FL25a	0.21	11	0.26
FL35a	0.33	20	0.40
FL50a	0.48	8	0.52

Table 7.14: Parameters derived for annealed FL blends from NRA data

Figure 7.12a shows examples of the reflectivity data obtained for these samples along with fits obtained using PHOENIX (Tanh model). For all but the FL5 blend there is an increase in reflectivity for the annealed samples, this is shown in Figure 7.12b. None of the data exhibit fringes characteristic of the film thickness, because the film thickness is sufficiently large that the fringes are too closely spaced to be resolved. This means that the reflectivity is insensitive to the film thickness and for this reason the thickness of the films was set at the value indicated by the contact profilometry.

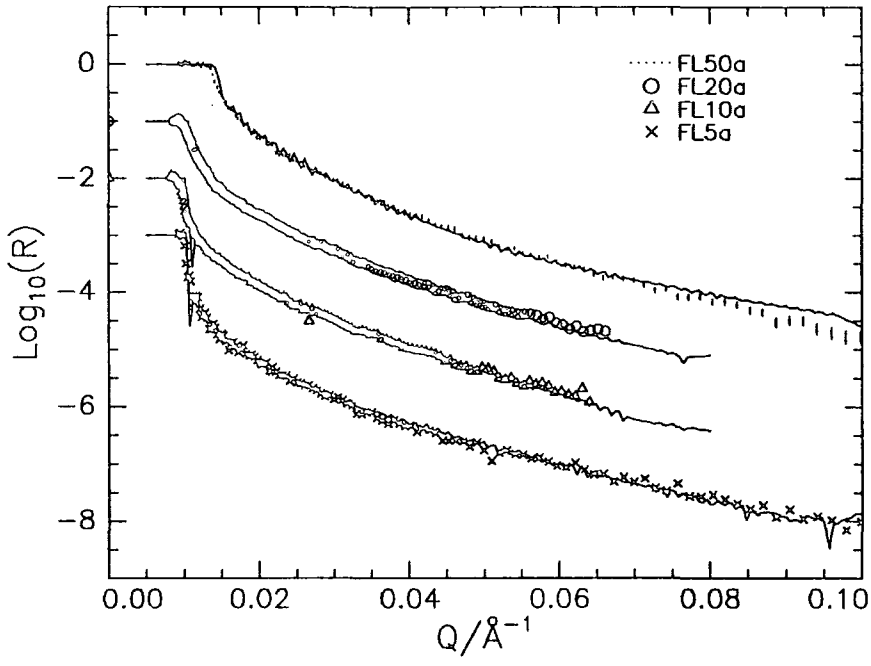

Figure 7.12a: Neutron reflectivity profiles for selected annealed FL blends. Experimental data (symbols) and PHOENIX (Tanh model) (solid line) fits. Successive datasets offset by -1 for clarity. Error bars for FL5a from Poisson statistics.

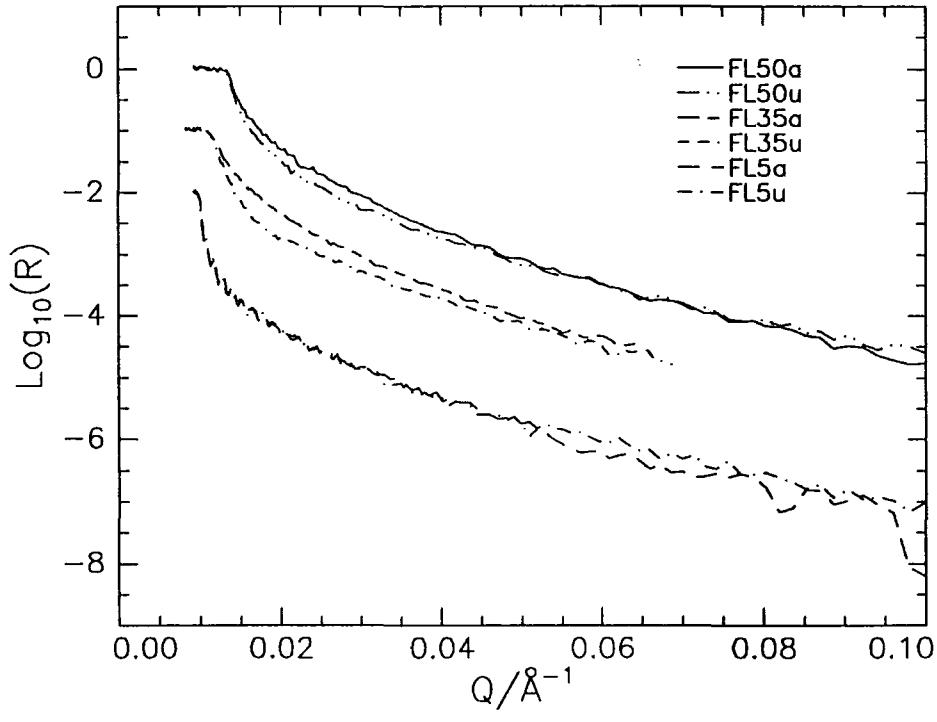

Figure 7.12b: Neutron reflectivity profiles for the FL5, FL35 and FL50 blends before and after annealing, FL5 and FL35 data offset by -2 and -1 respectively.

Figure 7.13 shows composition depth profiles, $\phi(z)$, extracted from the reflectivity data using VOLFMEM and PHOENIX (Tanh model). Table 7.15 shows values for z^*_{air} and ϕ_{air} obtained using the Tanh profile fits, (both before and after annealing). Table 7.16 shows the parameters of the Tanh profile fits.

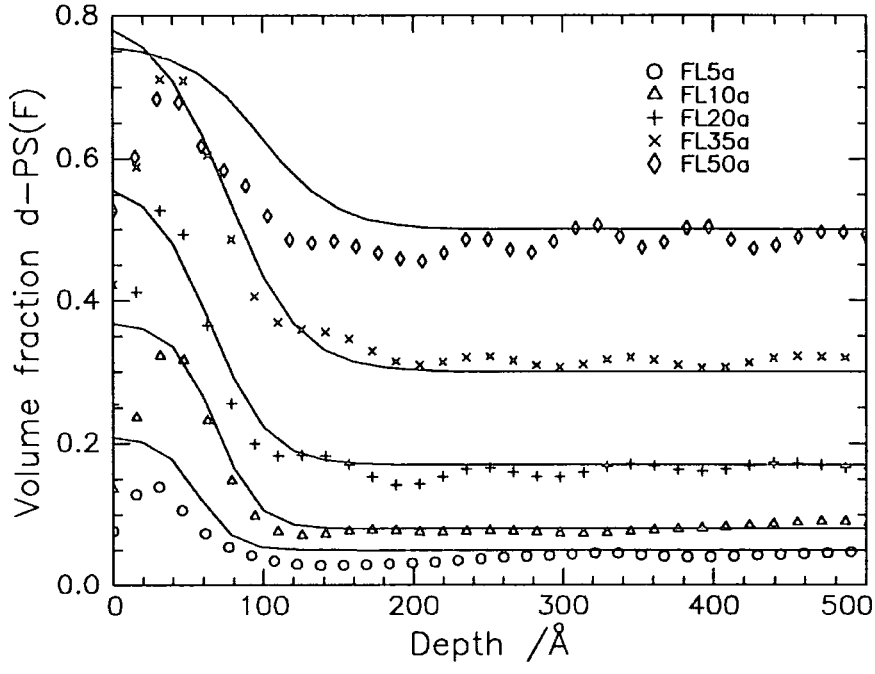

Figure 7.13: Composition profiles for annealed FL blends, obtained from NR. Symbols - VOLFMEM fits, solid lines - corresponding PHOENIX (Tanh model) fit.

	Unannealed			Annealed		
	ϕ_B	z^*_{air}/Å	ϕ_{air}	ϕ_B	z^*_{air}/Å	ϕ_{air}
FL5	0.05	9	0.21	0.05	9	0.21
FL10	-	-	-	0.08	20	0.36
FL15	-	-	-	0.11	21	0.46
FL20	-	-	-	0.17	27	0.56
FL25	0.18	15	0.43	0.18	30	0.54
FL35	0.29	17	0.60	0.30	36	0.77
FL50	0.50	12	0.63	0.50	26	0.75

Table 7.15: Parameters derived for FL blends using Tanh models to NR data.

	ϕ_B	l/Å	ϕ_1	z_{off}/Å	w /Å	Fit Index
FL5u	0.05	4000	0.21	58	50	0.13
FL5a	0.05	4000	0.21	56	49	0.15
FL10a	0.08	4000	0.37	68	55	0.13
FL15a	0.11	4000	0.49	55	85	0.10
FL20a	0.17	4000	0.57	64	78	0.08
FL25u	0.18	3818	0.45	52	79	0.15
FL25a	0.18	3822	0.57	119	73	0.11
FL35u	0.29	4000	0.61	54	41	0.09
FL35a	0.30	4000	0.80	76	96	0.10
FL50u	0.50	3892	0.64	81	93	0.19
FL50a	0.50	3748	0.76	99	99	0.13

Table 7.16: Fit parameters for Tanh profiles for the FL blends

There were no signs of an excess of d-PS(F) at the silicon interface using the VOLFMEM analysis or the three layer models and for this reason no attempt was made to fit a Tanh profile at the silicon interface. The reflectivity is relatively insensitive to the volume fraction of d-PS(F) at the silicon interface for such thick films and these results do not rule out the possibility of an excess of d-PS(F) at the silicon interface. Three layer (multilayer) model fits were used to calculate the near surface depletion, observed only in the unannealed films. The derived parameters z^*_{air}, z^*_{dep}, ϕ_{air}, ϕ_{dep} and ϕ_B for these multilayer models can be found in Table 7.17 and the parameters of the three layer fits can be found in Table 7.18. The parameters ϕ_n, z_n and σ_n refer to the volume fraction d-PS(F), thickness and interfacial roughness of the n^{th} layer respectively. The air/polymer interfacial roughness, σ_0, and polymer/silicon interfacial roughness, σ_3, were fixed at 5Å. Fitting was relatively insensitive to σ_2 and so the value of σ_2 was fixed at 40Å. The excesses z^*_{air} and z^*_{dep} were calculated as $(\phi_1 - \phi_2)*z_1$ and $(\phi_3 - \phi_2)*z_2$ respectively. In contrast to the high molecular weight d-PS(F)/h-PS blends these low molecular weight blends show consistent surface segregation behaviour in the unannealed films. For the FL5 blend the equilibrium composition profile is apparently reached in the unannealed films.

	ϕ_{air}	z^*_{air}/Å	ϕ_{dep}	z^*_{dep}/Å	ϕ_B
FL5u	0.20	9	0.05	0	0.05
FL25u	0.50	15	0.17	3	0.19
FL35u	0.77	22	0.27	4	0.29
FL50u	0.68	12	0.49	6	0.53

Table 7.17: Parameters derived from multilayer fits for unannealed FL blends

	ϕ_1	z_1/Å	σ_1/Å	ϕ_2	z_2/Å	σ_2/Å	ϕ_3	z_3/Å	Fit Index
FL5u	0.20	58	22	0.05	170	40	0.05	3672	0.16
FL25u	0.50	45	31	0.17	125	40	0.19	3730	0.10
FL35u	0.77	44	18	0.27	155	40	0.29	3701	0.06
FL50u	0.68	65	25	0.49	130	40	0.53	3705	0.13

Table 7.18: Parameters for multilayer fits to unannealed FL blend NR data

Figure 7.14 shows the effect that the interfacial roughness has on the composition profile for the three layer model.

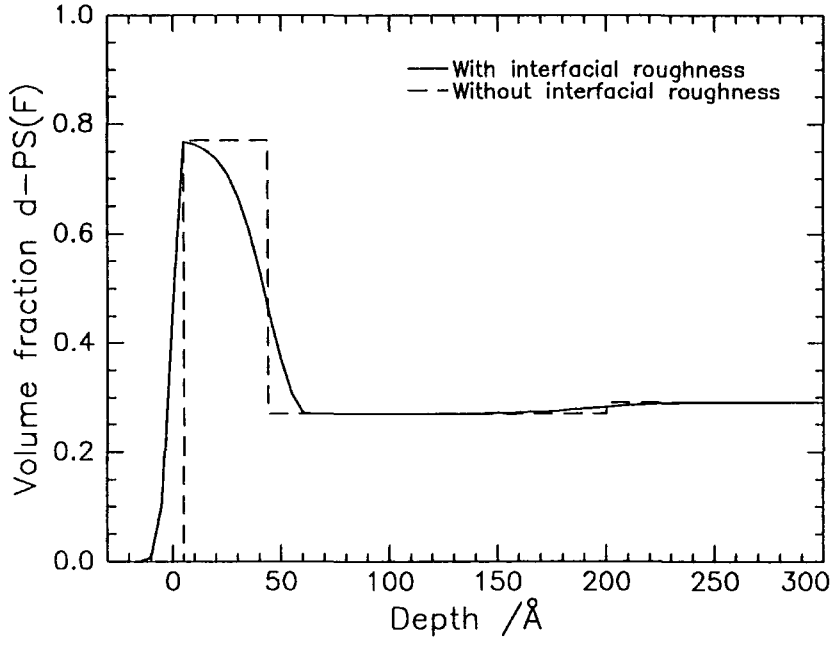

Figure 7.14: Three layer model profile for the FL35u data, with and without interfacial roughness.

Casting Concentration

Figure 7.15 shows the reflectivity data collected from the samples A35u, B35u, C35u and D35u, the series of samples cast from solutions with different total concentrations of polymer, also included in this figure are the fits obtained using PHOENIX (multilayer model). The reflectivity profiles of C35u and D35u show the fringes characteristic of the film thickness. The thickness' fitted to these two films are 1579Å and 678Å respectively, slightly larger than the values measured contact profilometry. The VOLFMEM fits to these data showed the existence of a depletion zone below the initial surface excess (see Figure 7.16), as would be expected from the results of ***Equilibrium (3)***. Since the Tanh profiles do not model this depletion and are computationally intensive only three layer multilayer fits (which allow for the depletion layer) were made to the data. The values for the z^*_{air}, z^*_{dep}, ϕ_{air}, ϕ_{dep} and ϕ_B calculated from these models are shown in Table 7.19. The parameters of these multilayer fits can be found in Table 7.20. The results from the multilayer fits indicate small decreases in z^*_{air} and ϕ_{air} as the casting solution concentration is decreased and a simultaneous small increase in z^*_{dep}.

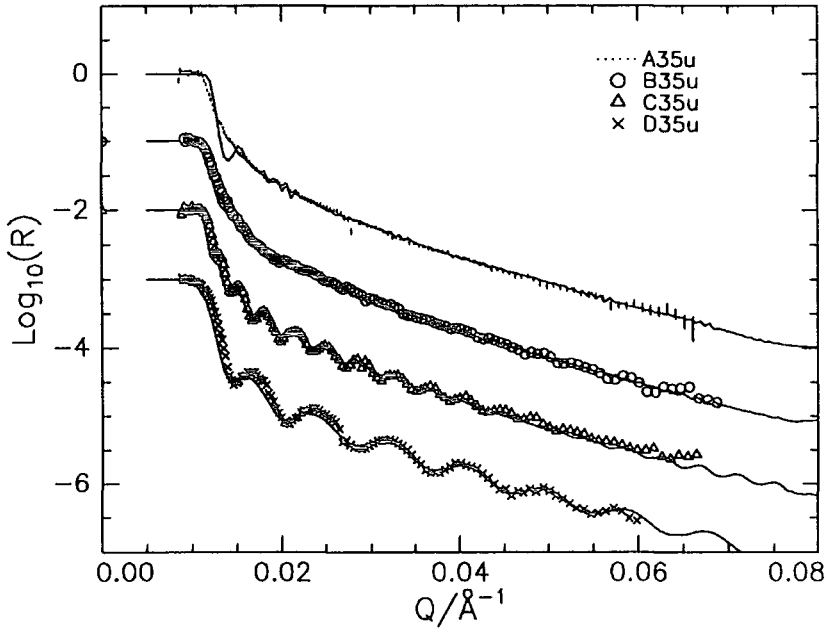

Figure 7.15: Reflectivity data for A35u, B35u, C35u and D35u blends (symbols) with fits using PHOENIX (multilayer models). Error bars for A35u data from Poisson statistics.

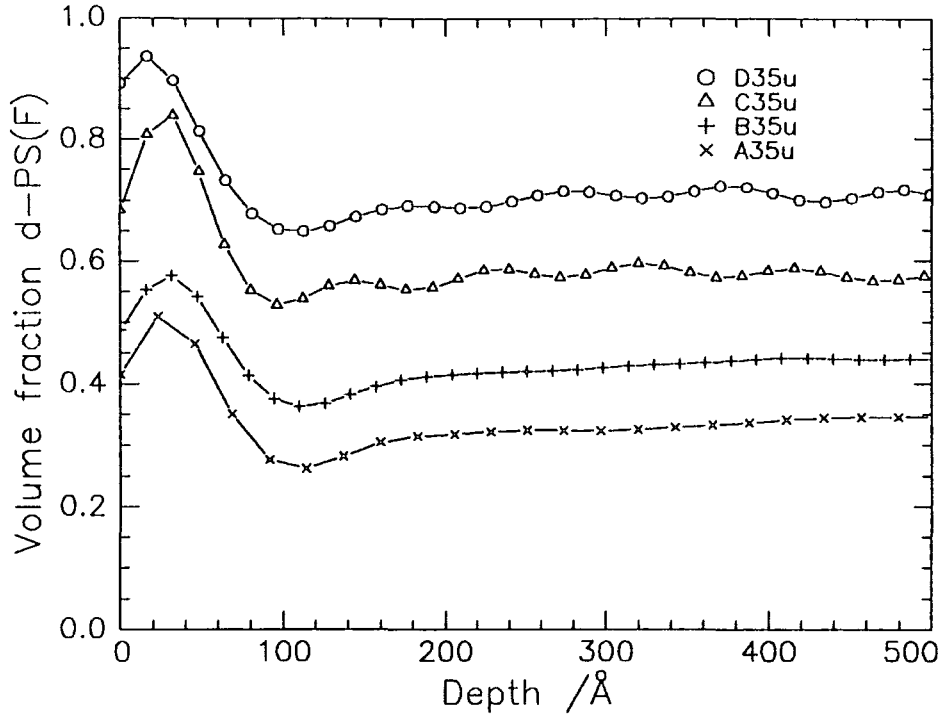

Figure 7.16: Composition profiles for the blends A35u, B35u, C35u and D35u, obtained using VOLFMEM fits to NR data.

	ϕ_{air}	z^*_{air}/Å	ϕ_{dep}	z^*_{dep}/Å	ϕ_B
A35u	0.64	20	0.27	3	0.29
B35u	0.61	19	0.27	3	0.29
C35u	0.64	19	0.25	4	0.29
D35u	0.50	16	0.22	6	0.27

Table 7.19: Parameters derived from multilayer fits for unannealed A35, B35, C35 and D35 data.

	ϕ_1	z_1/Å	σ_1/Å	ϕ_2	z_2/Å	σ_2/Å	ϕ_3	z_3/Å	Fit Index
A35u	0.64	55	18	0.27	160	40	0.29	5700	0.09
B35u	0.61	56	23	0.27	140	40	0.29	3700	0.10
C35u	0.64	50	32	0.25	134	40	0.29	1315	0.10
D35u	0.50	58	10	0.22	131	40	0.27	489	0.04

Table 7.20: Parameters for three layer fits to A35, B35, C35 and D35 data.

Figure 7.17 shows the reflectivity data collected for the samples FL35u, FL35a1, FL35a2 and FL35a5, measured to determine the kinetics of the formation of the surface excess, also included are selected fits to the data obtained using PHOENIX (Tanh model). The parameters z^*_{air} and ϕ_{air} extracted from the Tanh profile fits can be found in Table 7.21.

	ϕ_B	z^*_{air}/Å	ϕ_{air}
FL35u	0.29	17	0.60
FL35a1	0.28	23	0.63
FL35a2	0.35	35	0.80
FL35a3	0.28	36	0.80
FL35a4	0.28	33	0.71
FL35a5	0.30	38	0.77

Table 7.21: Parameters from Tanh profile fits to FL35u-FL35a5 data.

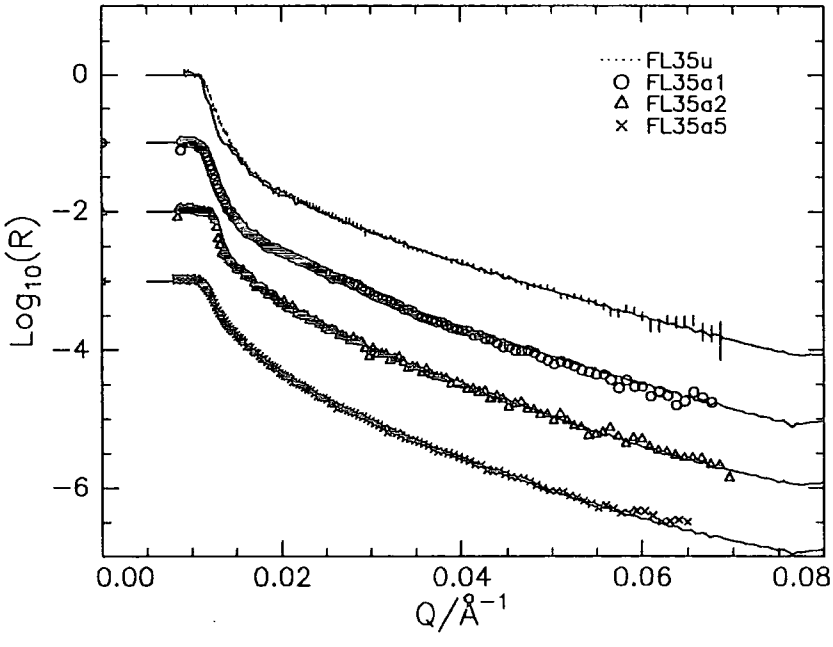

Figure 7.17: Reflectivity data (symbols) for selected FL blends (*kinetics* experiments). Lines are fits using PHOENIX (Tanh model). Error bars for FL35u are from Poisson statistics.

Parameters of the Tanh fits to these data can be found in Table 7.22. Table 7.23 shows the values of z^*_{air}, z^*_{dep}, ϕ_{air}, ϕ_{dep} and ϕ_B obtained for these blends using multilayer fits, the parameters of which can be found in Table 7.24.

	ϕ_B	l/Å	ϕ_1	z_{off}/Å	w /Å	Fit Index
FL35u	0.29	4000	0.61	54	41	0.09
FL35a1	0.28	4000	0.63	65	53	0.10
FL35a2	0.35	4000	0.82	75	67	0.09
FL35a3	0.28	4000	0.87	58	110	0.05
FL35a4	0.28	4000	0.72	75	78	0.05
FL35a5	0.30	4000	0.80	76	96	0.10

Table 7.22: Fit parameters for Tanh profiles for the FL blends

	ϕ_{air}	z^*_{air}/Å	ϕ_{dep}	z^*_{dep}/Å	ϕ_B
FL35u	0.61	19	0.27	3	0.29
FL35a1	0.63	26	0.25	4	0.28
FL35a2	0.76	32	0.37	-	0.33
FL35a3	0.73	29	0.32	-	0.26
FL35a4	0.72	31	0.29	-	0.26
FL35a5	0.71	28	0.36	-	0.26

Table 7.23: Parameters derived from multilayer model fits to FL35u-FL35a5 data

	ϕ_1	z_1/Å	σ_1/Å	ϕ_2	z_2/Å	σ_2/Å	ϕ_3	z_3/Å	Fit Index
FL35u	0.61	56	23	0.27	140	40	0.29	3700	0.10
FL35a1	0.63	68	32	0.25	135	40	0.28	3700	0.10
FL35a2	0.76	82	12	0.37	108	40	0.33	3700	0.09
FL35a3	0.73	71	27	0.32	107	40	0.26	3700	0.08
FL35a4	0.72	73	31	0.29	116	40	0.26	3700	0.08
FL35a5	0.71	80	15	0.36	101	40	0.26	3700	0.08

Table 7.24: Fit parameters to multilayer fits to FL35u-FL35a5 data

These data show that after 1 hour annealing the samples reach equilibrium values of the surface excess, z^*_{air} and surface composition, ϕ_{air}, in addition the depletion zone that is present below the initial surface excess in the unannealed sample (FL35u) and the sample annealed for 20 minutes (FL35a1) is not present in the sample annealed for 1 hour (FL35a2) or any of the samples annealed for longer times.

Double End Capped

Figure 7.18 shows reflectivity data collected from the blends containing the double F capped d-PS(F2), with fits using PHOENIX (Tanh model). Figure 7.19 shows the VOLFMEM and PHOENIX (Tanh model) composition profiles generated for these data. In common with the single end capped FL blends, these samples show no surface excess at the silicon interface in the VOLFMEM generated composition profiles; for this reason the Tanh profile was only fitted at the air/polymer interface.

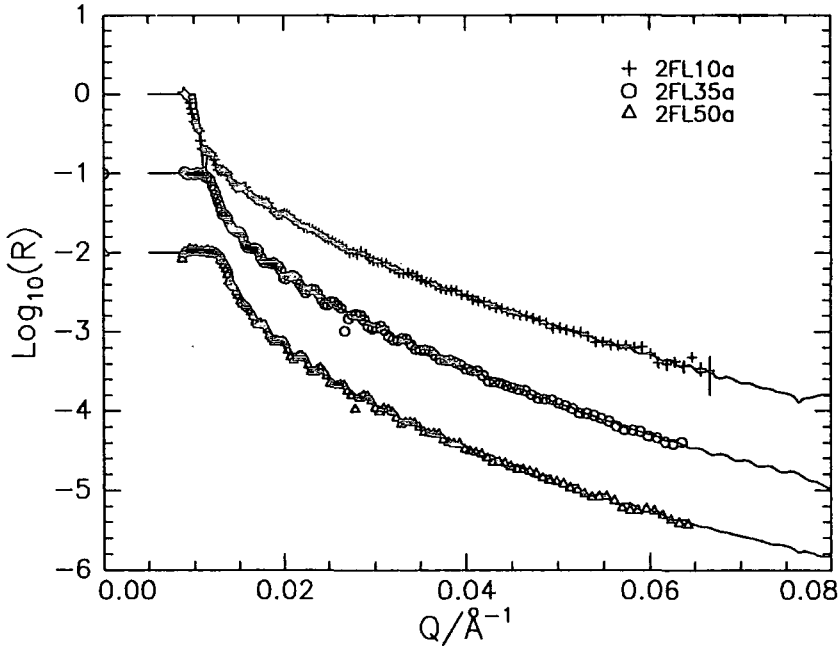

Figure 7.18: Reflectivity data (symbols) for annealed 2FL blends, with fits from PHOENIX (Tanh model) (solid line). Successive datasets offset by -1.5 for clarity. Error bars for 2FL10a data from Poisson statistics.

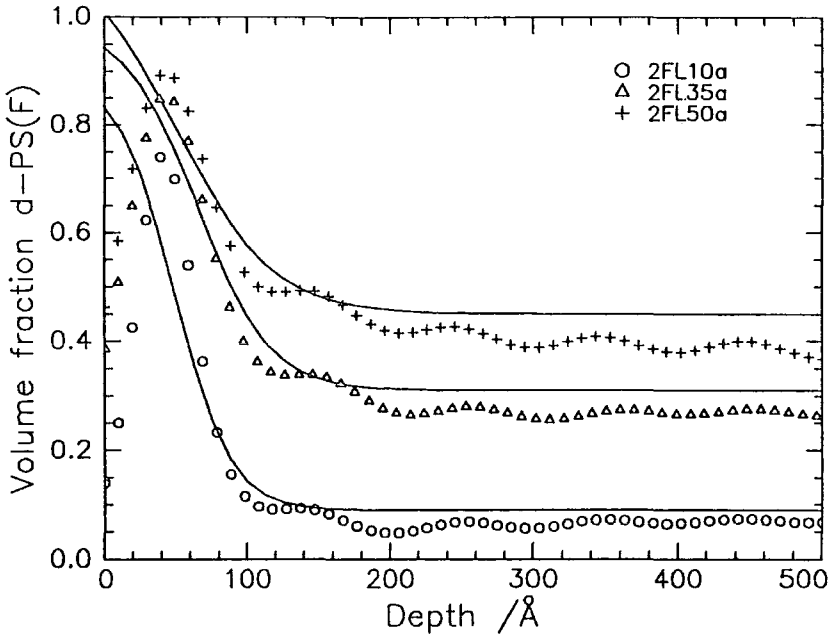

Figure 7.19: Composition profiles for annealed 2FL blends, obtained from NR data using VOLFMEM (symbols) and PHOENIX (Tanh model) (solid line).

Table 7.25 shows the values of ϕ_B, z^*_{air} and ϕ_{air} that were obtained. The parameters of the Tanh functions fitted can be found in Table 7.26.

	ϕ_B	z^*_{air}/Å	ϕ_{air}
2FL10a	0.09	40	0.81
2FL35a	0.31	44	0.92
2FL50a	0.45	39	0.99
2FL35u	0.28	27	0.81

Table 7.25: Parameters derived from Tanh fits to the 2FL blend data, including the unannealed sample 2FL35u.

	ϕ_B	l/Å	ϕ_l	z_{off}/Å	w /Å	Fit Index
2FL10a	0.09	2787	0.89	49	78	0.10
2FL35a	0.31	2380	0.98	65	101	0.10
2FL50a	0.45	2000	1.13	51	138	0.11
2FL35u	0.28	2380	0.81	50	36	0.11

Table 7.26: Parameters of Tanh fits to double F capped blends, including the unannealed sample 2FL35u.

Only one unannealed sample was run (2FL35u), multilayer fits were carried out on this blend and the values of z^*_{air}, z^*_{dep}, ϕ_{air}, ϕ_{dep} and ϕ_B obtained can be found in Table 7.27, the parameters of the multilayer fit can be found in Table 7.28.

	ϕ_{air}	z^*_{air}/Å	ϕ_{dep}	z^*_{dep}/Å	ϕ_B
2FL35u	0.89	32	0.22	6	0.29

Table 7.27: Parameters derived from a multilayer fit to the 2FL35u data.

	ϕ_1	z_1/Å	σ_1/Å	ϕ_2	z_2/Å	σ_2/Å	ϕ_3	z_3/Å	Fit Index
2FL35u	0.89	48	30	0.22	95	40	0.46	2679	0.10

Table 7.28: Fit parameters of multilayer model for the 2FL35u data.

7.3 Discussion

It has been shown[4] that surface enrichment occurs in high molecular weight blends of d-PS/h-PS, driven by a surface energy difference of, $\Delta\gamma$ = 0.078 mJ m^{-2}, between the hydrogenous and deuterated polymers. The theory of Schmidt and Binder[5] gives a good description of the surface enrichment behaviour observed such in high molecular weight polymers blends. Using this theory it can be shown that virtually no surface enrichment is expected in the low molecular weight d-PS(F)/h-PS (FL) blends studied here. This prediction has been confirmed by workers at the University of Strathclyde[1] using Secondary Ion Mass Spectrometry (SIMS), the absence of surface enrichment in the low molecular weight d-PS/h-PS arises because the phase boundary in the low molecular weight system is at a much lower temperature than in the high molecular weight blend and surface enrichment is strongly enhanced close to the phase boundary. Therefore the substantial surface excesses observed in the low molecular weight d-PS(F)/h-PS must be caused by the perfluorohexane end group end attaching the d-PS(F) to the air interface, forming a brush. The self consistent field (SCF) theory of polymer brushes in polymer matrices, developed by Shull[6], was outlined in section 2.3.1. The predictions of this theory will be compared to the results described above.

In order to compare the results of theoretical calculations made using relatively small 'polymers' with the experimental results, a number of procedures will be adopted to normalise the results of both theory and experiment. Firstly the normalised surface excess z^*/R_g will be used, where R_g is the radius of gyration of the d-PS(F), this will also facilitate comparisons between high and low molecular weight blends. The radii of gyration of the d-PS(F) used in this work are 46Å and 212Å for the FL and FH blends, respectively. These values are calculated from the molecular weights of the polymers measured by size exclusion chromatography and literature values of $\langle S_\alpha/M_w^{1/2}\rangle$[7]. These radii of gyration will also be used to normalise the depth into the sample normal to the surface, z/R_g. Values of the Flory - Huggins interaction parameter, χ, used in the model were fixed such that the value of χN was equal to the value of χN calculated for the experimental system, where N is the geometric mean of the degrees of polymerisation. This ensures that the model system is the same 'distance' from the phase boundary as the experimental system, for the low molecular blend χN is effectively zero (and so χ was set to zero for these models). The degrees of polymerisation of the two components in

the Shull model were set to 160 and 100 for the non-adsorbing (≡ h-PS) and absorbing (≡ d-PS(F)) polymers. This preserves the ratio $N_H/N_D = 1.6$, found in the low molecular weight blends. Finally the surface free energy difference, β, defined below, is used.

$$\beta = \chi_e^b - \chi_e^s + 1.1 \ln \sqrt{\frac{6}{N_D}}$$

Equation 7.4

where χ_e^b is the energy of interaction between the perfluorohexane end group and the bulk blend and χ_e^s is the difference in surface energy between the end group and the bulk. Model calculations were made with values of the bulk volume fraction of d-PS(F), ϕ_B, fixed at the values determined experimentally using PHOENIX (Tanh model). The only variable that is available to fit is $(\chi_e^b - \chi_e^s)$, the model is only sensitive to the combination of χ_e^b and χ_e^s, not separately. The aim of this modelling was to fit the form of the composition profile, $\phi(z/R_g)$, the quality of this fit can be evaluated by comparing z^*/R_g vs ϕ_B and $(\phi_{air} - \phi_B)$ vs ϕ_B. The fit of predicted values of z^*/R_g to experimental values of z^*/R_g will be the principal criterion because z^*/R_g is less susceptible to experimental error than $(\phi_{air} - \phi_B)$. The nature of the SCF theory calculations means it is not possible to perform an automatic least squares fit of the theoretical prediction to the experimental data. So the best fit value of $(\chi_e^b - \chi_e^s)$ was obtained by eye, this value corresponds to $\beta = 1.9$. The fitted value of $(\chi_e^b - \chi_e^s)$ is for a system where $N_D = 100$, in the experimental system $N_D = 274$, putting this value and $\beta = 1.9$ into Equation 7.4 we find that $(\chi_e^b - \chi_e^s) = 4.0$ in the experimental system. Figure 7.20 shows a comparison of selected experimental $\phi(z/R_g)$ profiles with theoretically predicted $\phi(z/R_g)$. To obtain units of z/R_g in the lattice model, z in lattice units is divided by 4.082 (this is because $R_g = a\sqrt{(N_D/6)}$, and a = 1 for the model and $\sqrt{(N_D/6)} = 4.082$ for $N_D = 100$). Figure 7.21 shows the theoretical calculations for z^*/R_g vs ϕ_B, with $\beta = 1.9$, compared to the experimental values. The broken lines are the theoretical values calculated using $\beta = 1.7$ and $\beta = 2.1$. Similarly Figure 7.22 is a comparison of the $(\phi_{air} - \phi_B)$ vs ϕ_B values. These fits were all done using the values of ϕ_B obtained from the PHOENIX (Tanh model) fits, if the nominal values were used then a slightly lower value of β would be obtained.

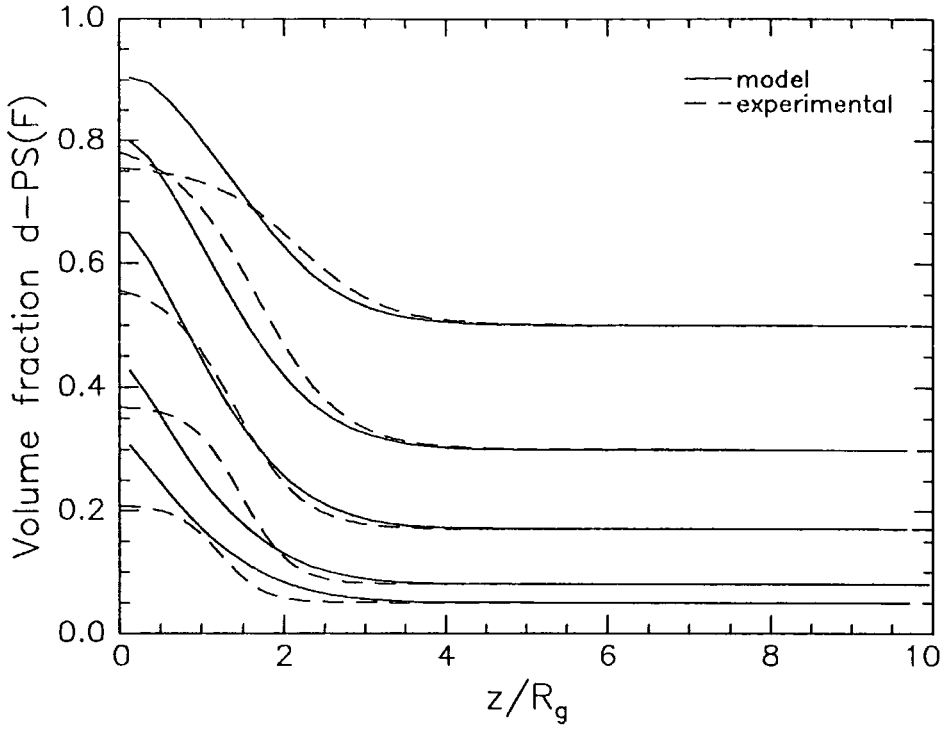

Figure 7.20: Comparison between selected experimental $\phi(z/R_g)$ from PHOENIX (Tanh model) and theoretical $\phi(z/R_g)$ from SCF theory for FL blends

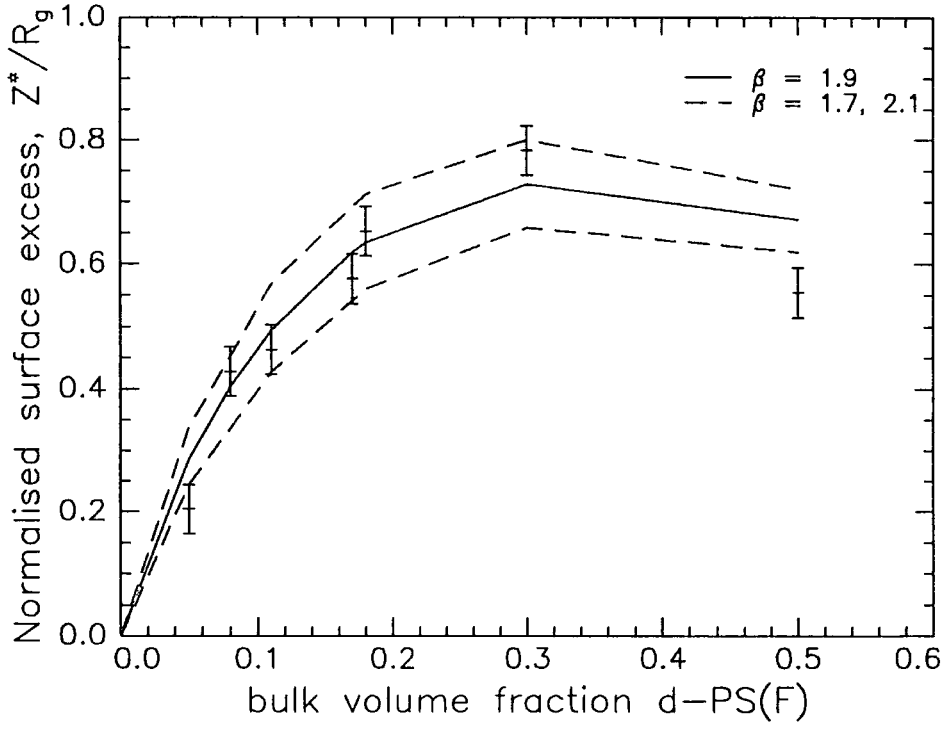

Figure 7.21: Comparison between experimental z^*/R_g and z^*/R_g from SCF theory for the FL blends. Solid line is best fit (β = 1.9).

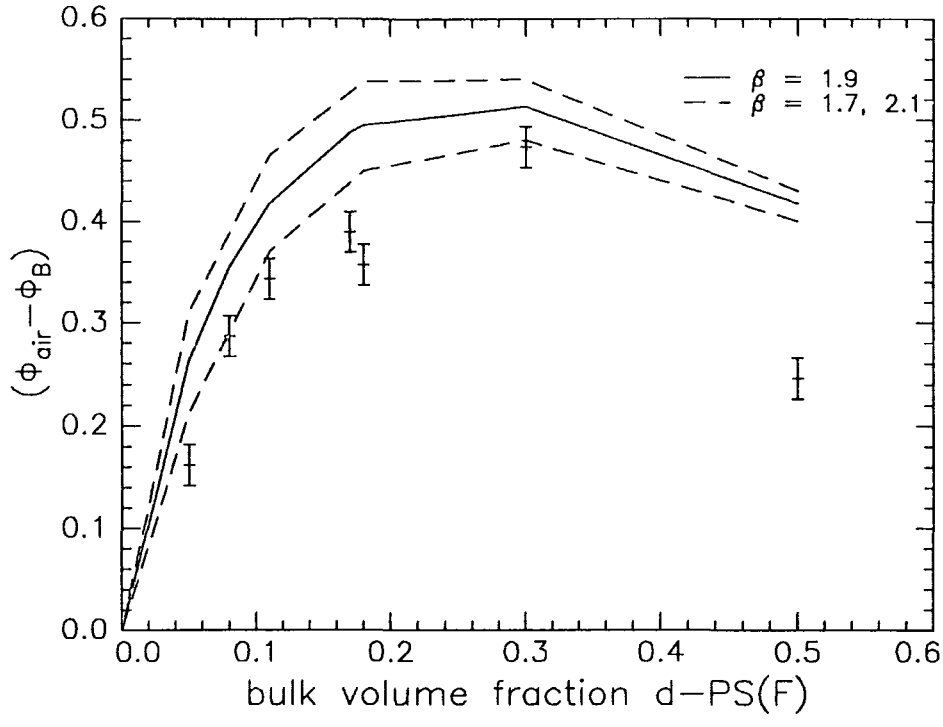

Figure 7.22: Comparison between experimental (ϕ_{air} - ϕ_B) and theoretical prediction from SCF theory. Solid line is from best fit to z^*/R_g (β = 1.9).

The fit to z^*/R_g vs ϕ_B is good, the only significant deviation from the theory is for the blend with ϕ_B = 0.50, however Figure 7.22 shows that the theory systematically over estimates the surface volume fraction, ϕ_{air}, this is also apparent in the composition profiles shown in Figure 7.20. Such deviations have been observed[8] between theoretical predictions based on mean field theories and the surface enrichment in high molecular weight d-PS/h-PS and can be explained by assuming that the surface attraction is not limited solely to the first layer of segments at the surface.

In principle it should be possible to estimate β using data in the literature and the measured value of N_D for the low molecular weight d-PS(F) . χ_e^b is the interaction parameter of perfluorohexane / styrene for a single lattice cell, in units of k_BT. This can be estimated from the solubility parameters of polystyrene, δ_{PS}, and poly (tetrafluoroethylene), δ_{PTFE}, making the assumption that the perfluorohexane can be treated as a short piece of PTFE. χ_e^b is calculated as follows[9]:

$$\chi_e^b = \frac{V_L}{k_B T}\left(\delta_{PS} - \delta_{PTFE}\right)^2$$

Equation 7.5

Where V_L is the volume of a lattice cell, in Shull's program $V_L = a^3$, where a is the statistical segment length, for polystyrene a = 6.7Å, hence $V_L = 3.01\times10^{-22}$ cm^3. Values of δ_{PS} and δ_{PTFE} can be found in reference 7, they are δ_{PS} = 20.2 J cm^{-3} and δ_{PTFE} = 12.7 J cm^{-3}. Using Equation 7.5 (T = 400K) this gives a value of χ_e^b = 3.1. χ_e^s is the surface energy difference per lattice cell, again in units of k_BT. Values for the surface energies of polystyrene and a short chain perfluorinated hydrocarbon ($C_{21}F_{44}$) can be also be found in reference 7, these values are 32.8 mJ m^{-2} and 14.4 mJ m^{-2} for PS and $C_{21}F_{44}$, respectively - interpolated to 400K. The difference in surface energies, $\Delta\gamma$ = 18.4 mJ m^{-2}. This corresponds to a value of χ_e^s = -1.50, calculated using Equation 7.6, below:

$$\chi_e^s = \frac{\Delta\gamma}{n_L k_B T}$$

Equation 7.6

where n_L is the number of lattice cells per metre square, the area of one lattice cell = a^2 = 45Å^2. Positive values of β favour brush formation, hence the sign of χ_e^s is negative because it occurs as $-\chi_e^s$ in Equation 7.4. The value of (χ_e^b - χ_e^s) calculated using these estimated values is 4.6 which compares with a value of 4.0 which is obtained experimentally, i.e. by using data readily available in the literature a good estimate of the β parameter and hence the brush formation behaviour of this blend could be obtained.

The scaling theory, outlined in section 2.3.2, can be used to gain a physical insight into the behaviour of the d-PS(F) polymers which are end attached at the air surface. The parameter of interest is the dimensionless grafting density, σ, defined as the product of the area occupied by one segment, b^2, multiplied by the number of end attached chains per unit area, for polystyrene b = 5.5Å. It can be shown that σ is given by:

$$\sigma = \frac{z^*}{N_D b}$$

Equation 7.7

This gives values of σ in the range 0.006 - 0.022 for the low molecular weight FL blends, the average distance between graft points, D_G, can be calculated from:

$$D_G = \frac{b}{\sqrt{\sigma}}$$

Equation 7.8

For this system D_G ranges from 37Å to 71Å. These values of σ lie above the limit $\sigma = N_D^{-6/5}$ (=0.0012) which is where chains change from being independent 'mushrooms' to overlapping brushes, but the values are below the limit $\sigma = N_H N_D^{-3/2}$ (= 0.095) where the brush becomes strongly stretched. In this case the chains are in the 'screened brush' regime where the end attached chains are only weakly stretched and the brush is still penetrated by the h-PS matrix chains. Scaling theory will fail to predict the form of the near surface composition profile, because for brush systems such as those studied here where the matrix is a relatively high molecular weight (when compared to the solvent molecules typically used in scaling theory) the loss in entropy that the matrix polymer suffers on being confined to the surface is not accounted for so that scaling will predict a maximum in the concentration of the end attached polymer at a finite distance from the surface, with matrix polymers 'filling in' the near surface region to maintain constant density. SCF theory accounts for this reduction in matrix entropy and shows a maximum in the end attached polymer density at the surface which decreases monotonically into the bulk.

Turning to the blends, containing d-PS(F2) where there are perfluorohexane end caps at both ends of the deuterated polymer, for which N_D = 500 and R_g = 61Å. Again mean field calculations show that the amount of surface enrichment occurring in these blends is negligible. SCF theory calculations can be used to predict the degree of brush formation, in common with the single end capped low molecular weight blends $\chi = 0$ was used in the model because the product χN is effectively zero for these blends. The ratio $N_H/N_D = 0.86$ for the 2FL blends so the degrees of polymerisation for the non-adsorbing (≡h-PS) and absorbing (≡d-PS(F2)) polymers were set to 86 and 100 respectively. The

results from the FL blends show that $(\chi_e^b - \chi_e^s) = 4.0$, inserting this value and $N_D = 500$ into Equation 7.4 a value of $\beta = 1.5$ is obtained. This is the free energy of sticking for each end of the d-PS(F2) polymer. Model profiles with $(\chi_e^b - \chi_e^s) = 3.1$ were generated using SCF theory, this value corresponds to $\beta = 1.5$ in a model with $N_D = 500$. A comparison of the model and experimentally determined $\phi(z/R_g)$ are shown in Figure 7.23. Figure 7.24 shows a comparison of theoretical and experimental values of z^*/R_g vs ϕ_B for the 2FL blends, similarly Figure 7.25 shows a comparison of $(\phi_{air} - \phi_B)$ vs ϕ_B.

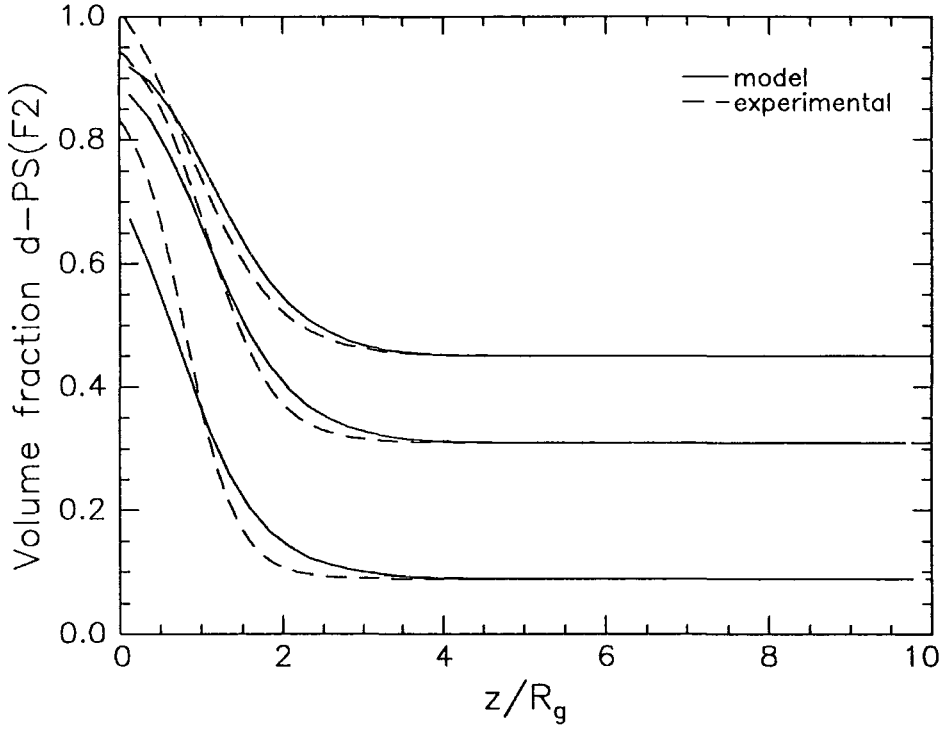

Figure 7.23: Comparison of experimental $\phi(z/R_g)$ from PHOENIX (Tanh model) and theoretical $\phi(z/R_g)$ from SCF theory model for 2FL blends.

It is apparent that, with the parameters extracted from the single end capped FL blends an accurate prediction of the z^*/R_g vs ϕ_B behaviour in the 2FL blends can be obtained. However, in contrast to FL blends, the SCF theory under estimates (rather than over estimates) the values of $(\phi_{air} - \phi_B)$ that are observed in the experimental system. Examining Figure 7.23 it can be seen that this corresponds to the experimental system exhibiting near surface composition profiles that are 'taller' and 'thinner' than the modelled profiles.

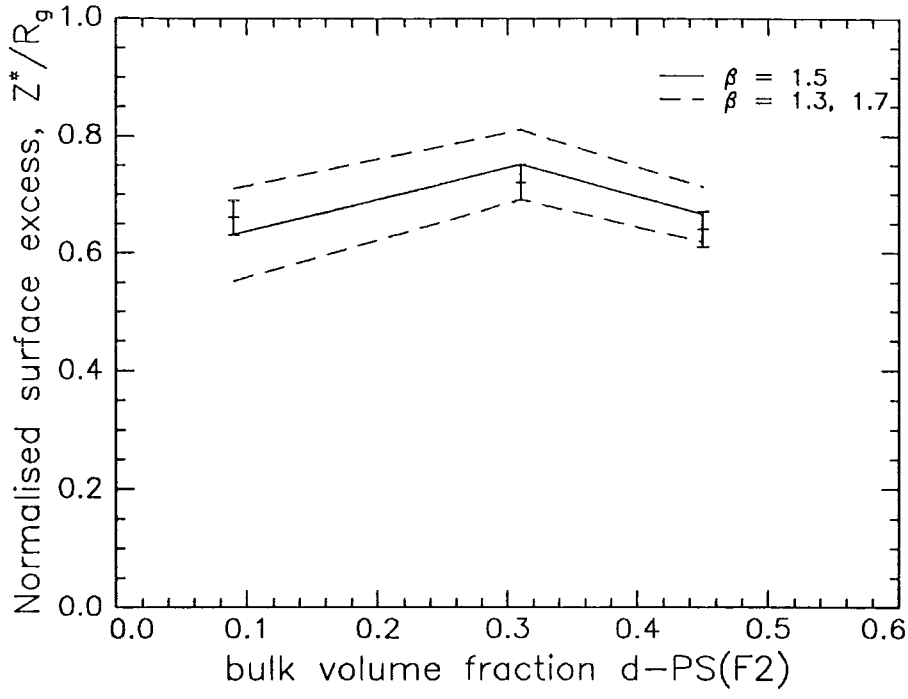

Figure 7.24: Comparison of experimental z^*/R_g and z^*/R_g from SCF theory model for the 2FL blends. Solid line is fit using the value of $(\chi_e^b - \chi_e^s)$ from the FL blends equivalent to $\beta = 1.5$.

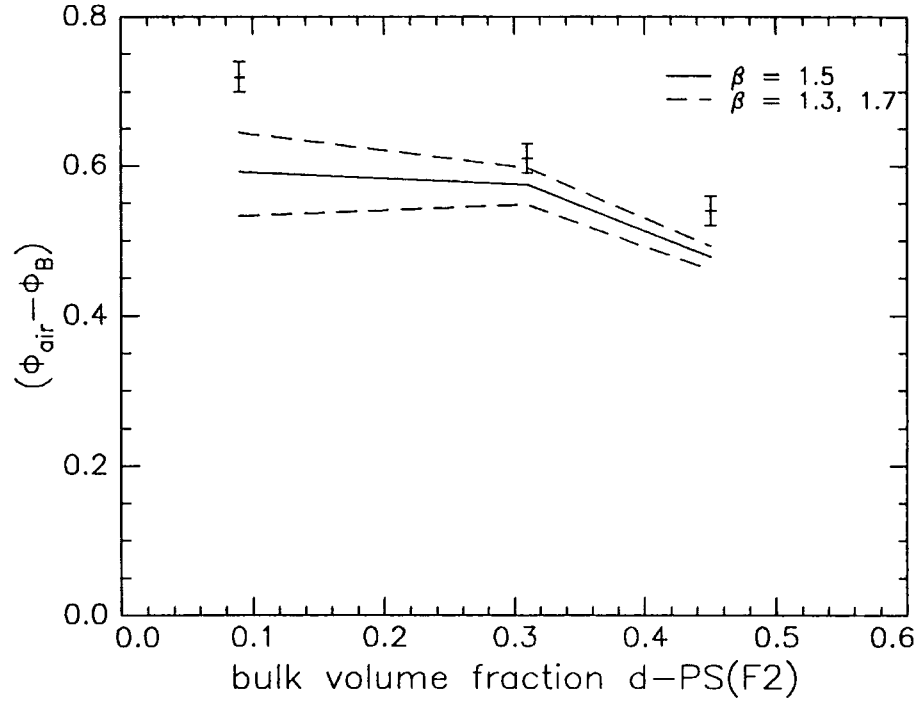

Figure 7.25: Comparison between experimental (ϕ_{air} - ϕ_B) and theoretical prediction from SCF theory model. Solid line is from best fit to z^*/R_g for the FL blends equivalent to $\beta = 1.5$.

Further calculations with the SCF theory show that this difference is not driven by the tiny difference in surface energies (≡ $0.006k_BT$) between d-PS and h-PS segments, i.e. this is not opportunistic surface enrichment arising in chains that have been brought close to the surface by being attached at both ends. An insight into this behaviour can be obtained by examining the grafting densities, σ, for these blends. For the 2FL blends each polymer absorbed at the air surface represents up to two graft points. Therefore:

$$\sigma \leq \frac{2z^*}{Nb}$$

Equation 7.9

The values of σ calculated for these blends lie between 0.028 and 0.030, which is in the same 'screened brush' regime as the single end capped FL blends. The limits of this regime are at $N_D^{-6/5}$ (=0.0006) and $N_H N_D^{-3/2}$ (= 0.038), so the 2FL blends lie rather closer to the stretched brush limit than the FL blends. Calculating the average separation of graft points, D_G, we find values >32Å. This is substantially less than the root mean square end to end distance(= $R_g\sqrt{6}$) for the d-PS(F2) polymer, which is 115Å. It may be that the initial distribution of end groups in the plane of the air - polymer interface is not at equilibrium and that over a period of time the surface volume fraction of d-PS(F2) will relax to the expected value, however one would expect the relaxation to occur relatively rapidly since the attachment energy of the end group to the surface is quite small.

The high molecular weight d-PS(F)/h-PS blends exhibited surface excesses at both the air and silicon interfaces, the 'normal' high molecular weight d-PS/h-PS blends also exhibited surface excesses at both interfaces. On the whole surface enrichment has not been observed at the polymer-substrate interface for d-PS/h-PS blends, the difference with this work would appear to be because this work was done using silicon with it's native silicon dioxide layer intact. This conclusion is supported by the work of Frantz *et al*[10] on the competitive absorption of d-PS and h-PS, from cyclohexane solution onto a silicon attenuated total reflection (ATR) crystal with a silicon oxide layer and the work of Budkowski *et al*[11] on d-PS/h-PS blends on silicon with an intact oxide layer.

The results from the NRA measurements on the 'normal' d-PS/h-PS blends show an excess at the silicon interface around half that observed at the air interface, this suggests that the difference in surface energy between d-PS and h-PS versus silicon

oxide is ~0.04 mJ m^{-2}, this is at the low end of the wide range of values that Frantz *et al* have observed but is larger than the value obtained by Budkowski *et al.* This difference is smaller than the difference of 0.078 mJ m^{-2} that is observed between d-PS and h-PS at the air interface.

In principle it should be possible to predict the parameters, z^*/R_g and $(\phi_{air} - \phi_B)$, of the near surface composition profiles observed in the high molecular weight blends by adding together the contributions from surface enrichment and brush formation. Calculations of the expected surface enrichment behaviour were done using the Jones and Kramer[12] simplifications to the mean field theory of Schmidt and Binder. The values of the parameters used were: $\Delta\gamma$ = 0.078 mJ m^{-2}, $\chi = 1.77\times10^{-4}$ (from Bates and Wignall[13]) and the degree of polymerisation, N = 9800. The calculations were done assuming a symmetric blend with $N_H = N_D$ and the value of N used here is the geometric mean of the values N_H and N_D of the polymers used, this is the scheme suggested for asymmetric blends in reference 12. These calculations produce values for the surface excess that are significantly larger than the measured values, where it is suspected that both surface enrichment and brush formation are taking place. One explanation for this could be that the blends have had insufficient annealing time to reach equilibrium, although this is unlikely because SIMS data on these polymers has shown that an equilibrium in the surface volume fraction of d-PS(F) has been reached. Putting aside this possibility a further attempt to calculate the expected surface excess from theory was made, collaborators at the University of Strathclyde have found, using SIMS, that the surface volume fraction of d-PS in a d-PS/h-PS blend with similar molecular weights to those used here is 0.45 for a blend with $\phi_B = 0.15$. The molecular weights of the blend components were 816,000 and 1,710,00 for the d-PS and h-PS respectively. Using the parameters $\Delta\gamma$ = 0.078 mJ m^{-2}, and N = 10950 (the geometric mean of the degrees of polymerisation), the value of χ was adjusted until the theoretical prediction of the surface volume fraction matched the experimentally measured value. This was found to occur when $\chi = 0.58\times10^{-4}$. This value of χ was then used to calculate the normalised surface excess and the surface volume fractions expected in the high molecular weight FH blends. The justification for this modification of the χ value is that the asymmetry (i.e. $N_H \neq N_D$) in the blend changes the value of χ from the value measured for symmetric high molecular blends of d-PS/h-PS. Such a change in the χ value has been shown in this work for the d-PMMA/h-PMMA blend. This change in χ will change the position of the

blend on the phase diagram in relative to the phase boundary and hence change the surface enrichment behaviour. Moving on to the brush formation predictions: the value of β calculated for these blends, using Equation 7.4, is 0.16. The ratio of N_H/N_D is 2.8 and to maintain this ratio values of N_H = 140 and N_D = 50 were used in the model calculations, this means that value of $(\chi_e^b - \chi_e^s)$ required in the model is 1.3. The value of χ used was 0.007, corresponding to a value of χN = 0.64, where N is the geometric mean of N_H and N_D, this is equal to the value of χN used in the surface enrichment calculations. Figure 7.26 shows the experimental values of z^*/R_g vs ϕ_B and the values of z^*/R_g obtained from the theoretical calculations of both brush formation and surface enrichment - the sum of these contributions is also included. Similarly Figure 7.27 shows the experimental behaviour and the theoretical predictions for $(\phi_{air} - \phi_B)$ vs ϕ_B.

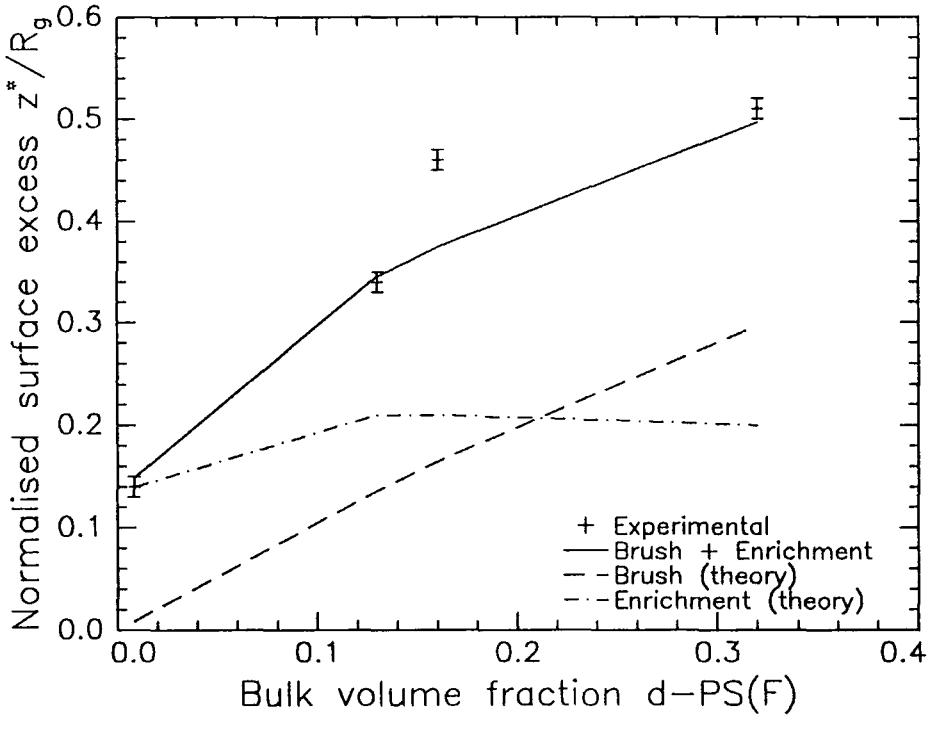

Figure 7.26: Comparison between experimental z^*/R_g and theoretical predictions from the combination of SCF theory models (brush) and mean field theory (enrichment).

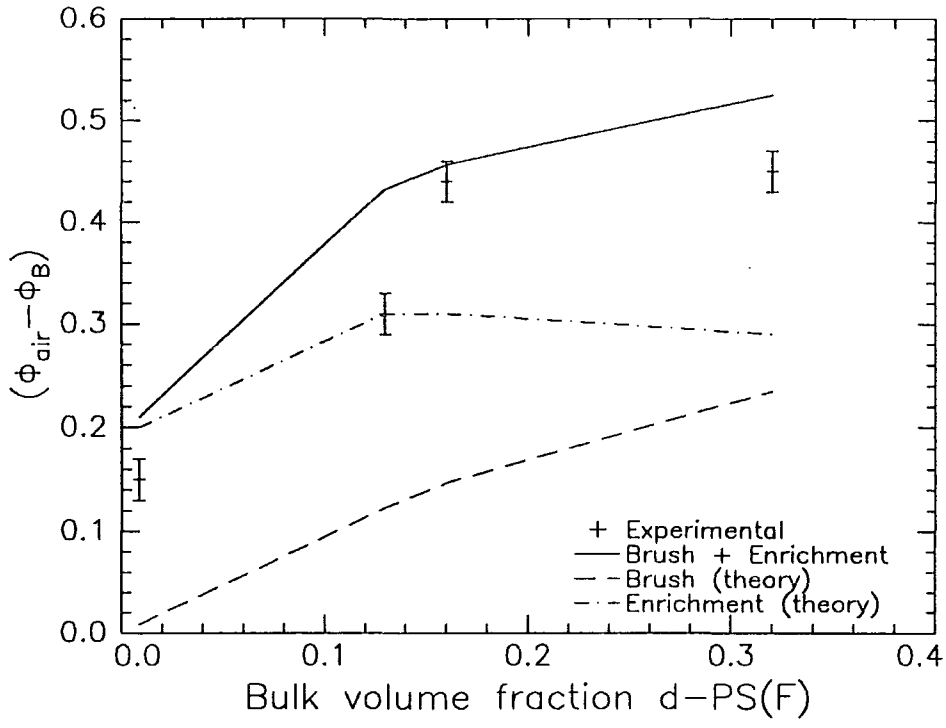

Figure 7.27: Comparison between experimental (ϕ_{air} - ϕ_B) and theoretical predictions from the combination of SCF theory models (brush) and mean field theory (enrichment).

The fit of the combined surface enrichment plus brush formation to z^*/R_g vs ϕ_B is very good and in common with the low molecular weight FL blends (ϕ_{air} - ϕ_B) is slightly over estimated by the theory. Clearly the use of the modified χ parameter makes this result a little less conclusive, but nevertheless it appears that using a single parameter extracted from the low molecular weight FL blends, (χ_e^b - χ_e^s), it is possible to predict the brush formation behaviour in the FL blends, the double F capped 2FL blends and the high molecular weight FH blends.

The final area to cover in this discussion is the non-equilibrium and approach to equilibrium behaviour of these blends. Unannealed films of all the blends exhibit some sort of non-uniform structure. For the FL5 and FH5 blends, structure is essentially unchanged by annealing. The structures in the unannealed FH blends, as revealed by the VOLFMEM fits, are not consistent across the range of bulk compositions, ϕ_B, i.e. the FH25u and FH50u blends exhibit depletion of d-PS(F) from the surface whilst the FH5u and FH35u blends exhibit a surface excess of the d-PS(F). The behaviour in the FL blends, both for varying ϕ_B and varying casting solution concentration, is more uniform. This is despite the fact that these samples were prepared on three separate occasions, as

opposed to the single occasion on which the FH blends were prepared. This suggest that the FH blends are more sensitive to the casting conditions than the FL blends. The same procedure was used to cast films of all the blends: a large aliquot of the casting solution was placed onto the silicon substrate and then the substrate was spun for 60 seconds. However the details of this process are not precisely controlled, i.e. the exact amount of solution, the time between placing the solution on the substrate and starting the spinner, the temperature, the amount of solvent vapour in the immediate vicinity of the forming film, all of these factors could influence the structures observed in the unannealed film. To probe the influence of these factors experiments need to be repeated to establish the degree of variability in unannealed cast in a nominally identical manner. Since the FL blends seem less sensitive to these effects the remainder of this discussion will concentrate on the FL blends.

The three layer models used to fit the composition profiles in the unannealed films indicate a depletion layer below the initial surface excess, but the size of this depletion, z^*_{dep}, is considerably smaller than the corresponding surface excess. This implies that the model is not accurately describing the composition profile in the sample, because if it were then the conservation of mass would force $z^*_{air} = z^*_{dep}$, the reason for this discrepancy probably lies in the relative insensitivity of NR to structures that vary slowly over a long length scale. The measured z^*_{dep} is more an indication of how localised the depletion is to the surface than an accurate measure of the 'true' z^*_{dep}.

Figure 7.28 shows the variation of z^*_{air} as a function of ϕ_B, for both unannealed and annealed FL blends, the measured z^*_{dep} is also included. The surface excess in the unannealed blends has the same behaviour with ϕ_B as the surface excess in the annealed film, but with values of a lower magnitude. The measured z^*_{dep} shows a small increase across the composition range. All these values were calculated from the PHOENIX (multilayer model) fits for consistency. Figure 7.29 shows the variation of z^*_{air} and z^*_{dep} as a function of casting solution concentration for the series of blends A35u, B35u, C35u and D35u. There is a small decrease in the surface excess as the casting solution concentration is decreased accompanied by a small increase in the measured z^*_{dep}, the decrease is largest between the blends cast from 0.05 and 0.025 weight fraction polymer solutions.

There are two stages to the process by which the surface excess develops in the unannealed films:

(1) The equilibrium structure in the casting solution as it lies on the substrate. It has been observed that in polystyrene / toluene solutions[14] that there is a region at the surface of the solution that is depleted in polystyrene. This is driven by two forces, the toluene has a lower surface energy than the polystyrene and it also loses less entropy on being confined to the surface than the polystyrene.

(2) After the spinning process starts the solvent will evaporate until a point is reached where the polymer is the dominant species at the surface.

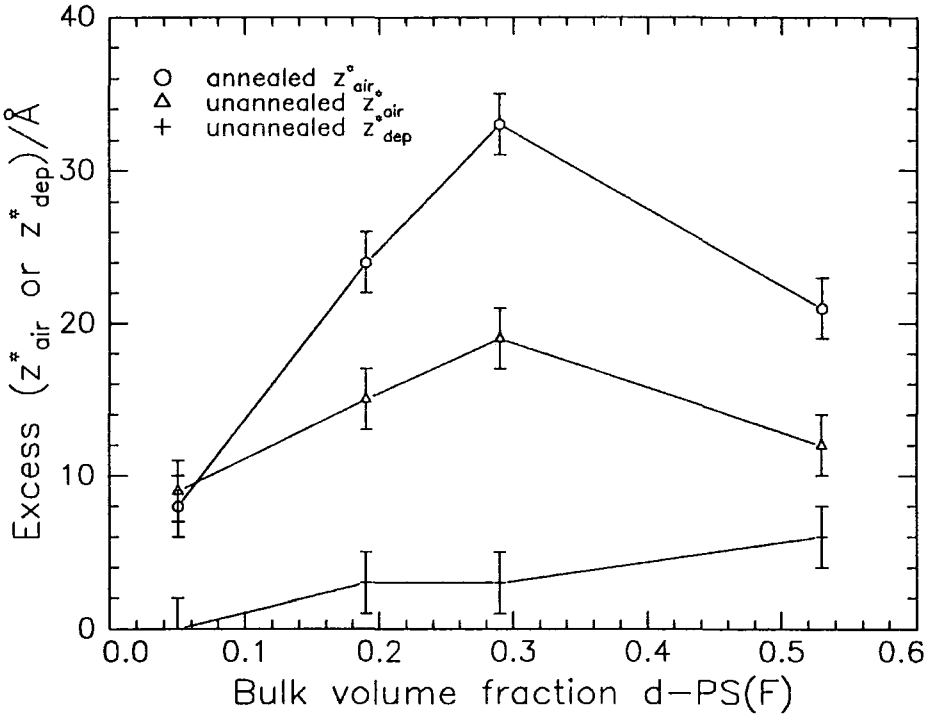

Figure 7.28: The surface excess z^*_{air} for both unannealed and annealed FL blends, along with measured z^*_{dep}. Calculated from PHOENIX (multilayer fits).

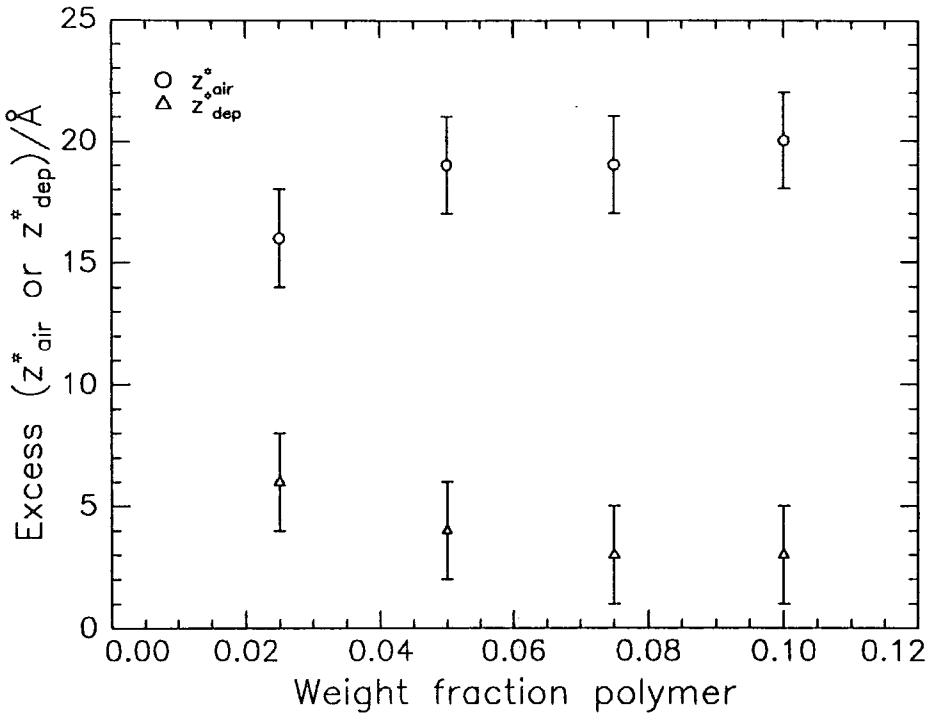

Figure 7.29: The surface excess z^*_{air} and measured z^*_{dep} for the series of FL blends cast from solutions of different concentration.

The blend will still be mobile, plasticised by the presence of the toluene and the polymer in the film will start to move towards the solid state equilibrium structure. This process will be arrested when still more solvent has left the film and the T_g of the blend rises above the casting temperature. The time which this second stage lasts will depend on the thickness of the final film, a thin film will lose a larger proportion of solvent than a similar thicker film and so structure will be frozen into a thin film more rapidly.

These two processes are linked in this experiment because the casting solution concentration, which will have some influence on the equilibrium structure in the casting solution, also controls the film thickness and hence the time it takes for structure to freeze into the film. Surface tension measurements carried out by Wills[15] show that the surface tension of a solution of the pure low molecular weight d-PS(F) polymer was very slightly lower than that of pure toluene, suggesting that there is some excess of the fluorinated end group at the surface of the polymer solution. However there was no measurable change in the surface tension as a function of the solution concentration over the range 2.5% w/w to 10% w/w d-PS(F). Given the very small size of the effect it would be difficult to draw any further conclusions from these data.

An estimate of the self diffusion coefficient, D_s, for the low molecular weight d-PS(F) in h-PS can be made from the surface excesses obtained in experiment (5), where blends containing 0.35 bulk volume fraction d-PS(F) were annealed for periods of up to 2 days. Figure 7.30 shows the development of the surface excess as a function of √(annealing time, t), the equilibrium surface excess is reached after only one hour annealing at 403K. The diffusion coefficient can be obtained from these data using a modified version of the scheme used by Jones and Kramer[16]. The conservation of mass dictates that:

$$z_0^* + z^*(t) = \left[\phi_B - \phi_d(t)\right](D_s t)^{1/2}$$

Equation 7.10

where z^*_0 is the surface excess in the unannealed blend, $z^*_0 + z^*(t)$ is the surface excess at time t, $\phi_d(t)$ is the volume fraction of d-PS(F) in the depletion zone immediately below the surface excess, in this analysis it is assumed that the surface excess is always in equilibrium with this value.

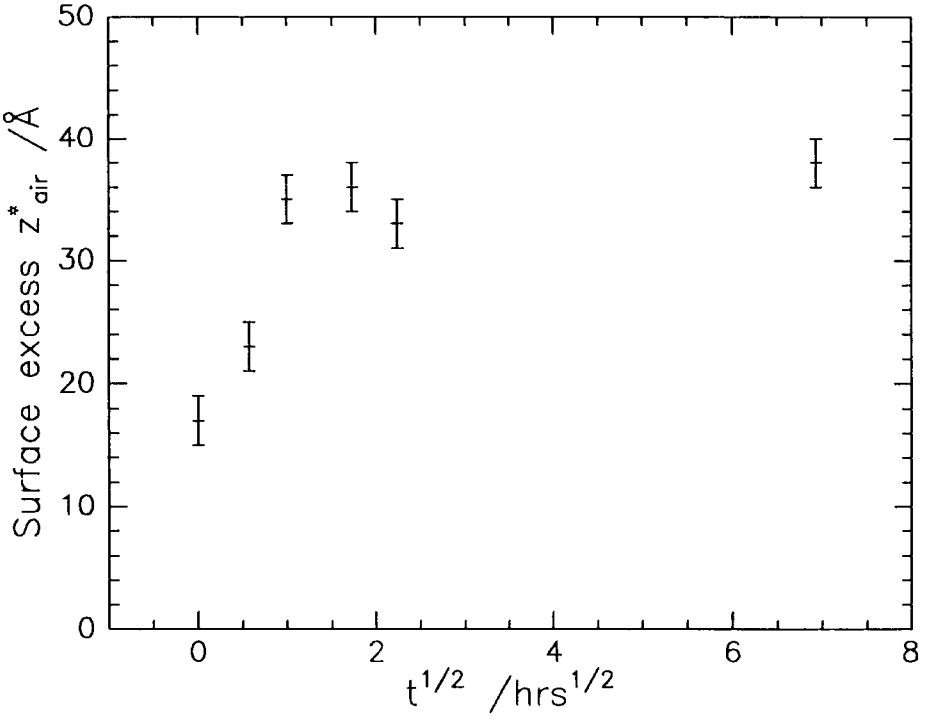

Figure 7.30: Development of the surface excess in FL35 as a function of annealing time. Values are from PHOENIX (Tanh model).

$(D_s t)^{1/2}$ is the diffusion length and it is assumed that the size of the depletion layer is of order $(D_s t)^{1/2}$. For the d-PS/h-PS system studied by Jones and Kramer it was found that $z^*_{eq} = K\,\phi_B$, where z^*_{eq} is the equilibrium value of the surface excess for bulk volume fraction d-PS, ϕ_B, K is a constant. This means that $z^*(t)=K\,\phi_d(t)$ for d-PS/h-PS. In this system the relationship between z^* and ϕ_B is better described by:

$$z^* = A\phi_B + B\phi_B^2$$

Equation 7.11

where A and B are constants. Using this expression would complicate the analysis considerably and so the approximation $z^*_{eq} = K\,\phi_B$ will be used. Substituting for $\phi_d(t)$ in Equation 7.10 we find:

$$z^*(t) = \frac{z^*_{eq}\phi_B (D_s t)^{1/2} - z^*_0}{(z^*_{eq} + \phi_B (D_s t)^{1/2})}$$

Equation 7.12

The characteristic time t_c is defined as the time when the surface excess has reached a value half way between z^*_0 and z^*_{eq}. Substituting this into Equation 7.12 and re-arranging:

$$D_s = \left(\frac{z^*_{eq} + 2z^*_0}{\phi_B}\right)^2 \frac{1}{t_c}$$

Equation 7.13

For the FL blend used $z^*_{eq} = 36$Å, $z^*_0 = 17$Å, $\phi_B = 0.30$ and the halfway point at $z^* = 27$Å is reached after around 30 minutes, hence $D_s \approx 3\times10^{-15}\text{cm}^2\text{s}^{-1}$. Wool and Whitlow[17] have measured the diffusion coefficient of d-PS in h-PS for approximately symmetric blends with molecular weights >100,000 over a range of temperatures spanning the annealing temperature used here. Extrapolating these values to the molecular weights used here using the relationship $D_s \propto M_w^{-2}$ a value for the diffusion coefficient of $\sim1\times10^{-15}$ cm^2 s^{-1} is obtained. Given the numerous approximations in this analysis used here and the paucity of data available between the unannealed and equilibrium state this value is in agreement with the value calculated here.

7.4 Conclusions

The surface composition profiles in a series of d-PS(F)/h-PS blends where the d-PS has been end functionalized with perfluorohexane were determined using NRA and NR. It was found that a SCF theory of polymer brushes could accurately describe the behaviour in low molecular weight single end capped (FL) blends, low molecular weight double end capped (2FL) blends and high molecular weight single end capped (FH) blends. The enthalpic interaction driving the brush formation, $(\chi_e^b - \chi_e^s)$, was fitted with a value of 4.0, using the data from the FL blend. Using this value for the enthalpic interaction and no other free parameters it was possible to obtain good predictions of the behaviour in the 2FL and FH blends. It was found that the SCF theory over estimated the value of $(\phi_{air} - \phi_B)$ for the FL and FH blends but under estimated $(\phi_{air} - \phi_B)$ for the 2FL blends, a possible explanation for this is that the end groups in the 2FL blends not reaching their equilibrium distribution in the plane of the air interface. An estimate of $(\chi_e^b - \chi_e^s) = 4.6$ was obtained from literature values of surface energy and solubility parameters, this value is close to the experimentally determined value. It should be noted that the value of $(\chi_e^b - \chi_e^s) = 4.0$ is likely be the largest that can be obtained for a small end group at the air interface. Crude calculations show that for the FL blends the perfluorohexane end groups produce a surface excess that is equivalent to that produced by a surface energy difference ~0.5 mJ m^{-2}, which is small when compared to the differences in surface energy generally observed between different polymers.

A diffusion coefficient, $D_s \approx 3\times10^{-15}$ cm^2 s^{-1} was obtained for the d-PS(F) in the FL blends, this value of D_s is in broad agreement with values in the literature. It was found that the FL blends reached an equilibrium value for the surface excess after around one hour annealing at 403K.

7.5 References for Section 7

1 . S. Affrossman, M. Hartshorne, T. Kiff, R.A. Pethrick, R.W. Richards, *Macromolecules*, 27(6), 1994, 1588.

2 . G. Reiter, *Langmuir*, 9(5), 1993, 1344.

3 . W.H. Press, S.A. Teukolsky, W.T. Vetterling, B.P. Flannery, 'Numerical Recipes in FORTRAN 2nd ed.', Cambridge University Press, 1992.

4 . R.A.L. Jones, E.J. Kramer, M.H. Rafailovich, J. Sokolov, S.A. Scharwz, *Physical Review Letters*, 62(3), **1989**, 280.

5 . I. Schmidt, K. Binder, *Journal de Physique*, 46, **1985**, 1631.

6 . K.R. Shull, *Journal of Chemical Physics*, 94(8), **1991**, 5723.

7 . J. Brandrup, E.H. Immergut, 'Polymer Handbook 3rd ed. pp VII/36', J.Wiley & Sons, 1989.

8 . R.A.L. Jones, L.J. Norton, E.J. Kramer, R.J. Composto, R.S. Stein, T.P. Russell, A. Mansour, A. Karim, G.P. Felcher, M.H. Rafailovich, J. Sokolov, X. Zhao, S.A. Schwarz, *Europhysics Letters*, 12(1), **1990**, 41.

9 . F.S. Bates, G.D. Wignall, *Macromolecules*, 19, **1986**, 932.

10 . P. Frantz, D.C. Dagmar, S. Granick, *Macromolecules*, 24, **1991**, 1868.

11 . A. Budkowski, U. Steiner, J. Klein, *Journal of Chemical Physics*, 97(7), **1992**, 5229.

12 . (a) R.A.L. Jones, E.J. Kramer, *Polymer*, 34(1), **1993**, 115. (b) R.A.L. Jones, *Polymer*, 35(10), **1994**, 2160.

13 . F.S. Bates, G.D. Wignall, *Macromolecules*, 19. **1986**, 932.

14 . L.T. Lee, O. Guiselin, A. Lapp, B.Farnoux, J. Penfold, *Physical Review Letters*, 67(20), **1991**, 2838.

15 . S. Wills, unpublished results.

16 . R.A.L. Jones, E.J. Kramer, *Philosophical Magazine B*, 62(2), **1990**, 129.

17 . S.J. Whitlow, R.P. Wool, *Macromolecules*, 24, **1991**, 5926.

This page left intentionally blank

8. Perdeuterated dibutyl phthalate / hydrogenous polystyrene blends

8.1 Experimental

The behaviour of perdeuterated dibutyl phthalate (d-DBP) in thin spun cast films of hydrogenous polystyrene (PS) was studied using neutron reflectometry and attenuated total reflection infra-red (ATR-IR) spectroscopy. The molecular weight, M_w, of the h-PS was 891,000 and the global code is TK85. Mixtures of d-DBP and h-PS were co-dissolved in Analar toluene, the total weight percentage of d-DBP plus PS was ~2%, solutions with four different volume fractions of d-DBP were prepared. These solutions were then spun cast (spinning speed 4000rpm) onto a silicon ATR crystal or a silicon block (for the neutron reflectometry work). The average thicknesses of the films are shown in Table 8.1 along with initial volume fractions of d-DBP and the prefixes (W, X, Y and Z) which will be used to designate each blend.

	Volume fraction d-DBP	Thickness/ Å
W	0.09	890 ± 20
X	0.16	850 ± 20
Y	0.23	730 ± 70
Z	0.30	680 ± 70

Table 8.1: Sample prefixes and thickness' measured by contact profilometry after casting.

Experiments were performed on samples held at ambient conditions over a range of times, t, after the films were spun cast. ATR experiments were only done on the W, Y and Z blends; for the W and Y blends the maximum measurement time after casting was ~30 hours and for the Z blend 20 measurements were made for times up to ~600 hours. Details of the experimental procedure for ATR-IR are in Section 4.6. The measurement times for the neutron reflectometry experiments are shown in Table 8.2 in the format days:hours:minutes, where necessary individual datasets will be referred to as [conc][t]

where [conc] is one of W, X, Y and Z and [t] is the nominal time shown in Table 8.2. Gaps in this table indicate that a sample was not run at that time. The reflectometry data were collected on a single occasion in January 1994, using incident angles of 0.25°, 0.6° and 1.2° covering a Q range ~0.005Å^{-1} to 0.10Å^{-1}. The time required to collect the NR data for one sample at all three angles is around 2 hours, this breaks down as around 20 minutes for the 0.25° data, 40 minutes for the 0.6° and 1 hour for the 1.2° data. The data were collected lowest angle first and highest angle last. Details on the experimental procedure for neutron reflectometry can be found in section 4.3. Data collected at nominally 0 hours, 6 hours, 12 hours and 24 hours were obtained using a single sample prepared at the Rutherford Laboratory and run repeatedly. For longer times separate samples were prepared at Durham.

Nominal time, t	W	X	Y	Z
0hrs	0	0	0	0
6hrs	00:05:45	-	0:05:30	00:06:00
12hrs	00:11:15	-	0:11:25	00:11:35
24hrs	-	0:22:55	1:00:25	00:23:00
4days	04:11:20	-	-	04:07:45
11days	11:13:10	11:18:55	11:17:00	11:09:35
17days	17:04:45	18:01:35	17:19:40	16:22:25

Table 8.2: Measurement times for blends W, X, Y and Z in the form days:hours:minutes and the nominal time used to label these samples

8.2 Results

Figure 8.1 shows representative ATR-IR spectra from the Z blends, the contribution from the silicon and other background contributions have been subtracted. Spectra are the average of 64 scans. The atmospheric CO_2 band has been over subtracted and this is the origin of the 'negative band' at ~2350 cm^{-1}. The series of peaks between 3200 cm^{-1} and 2800 cm^{-1} are the C-H stretches of polystyrene. The deuteration results in the equivalent C-D stretches in d-DBP being shifted to the 2000-2300 cm^{-1} region of the spectrum. The strong peak at 1725 cm^{-1} is the carbonyl stretch, which arises solely from the d-DBP.

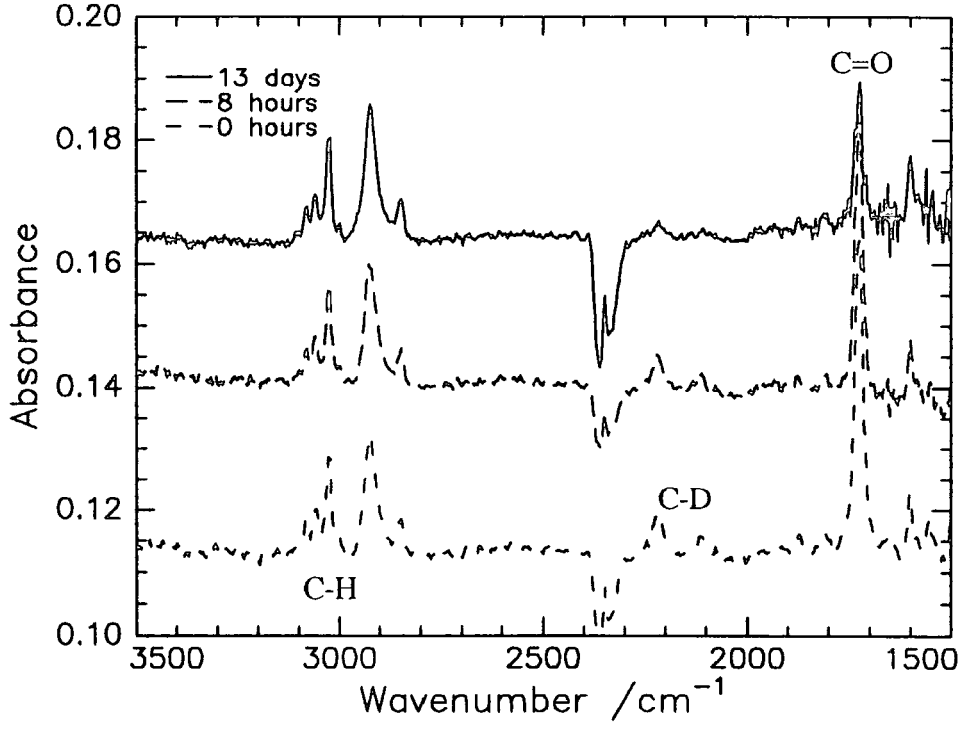

Figure 8.1: Selected ATR-IR spectra for the Z blend collected at the times indicated, data offset for clarity.

The penetration depth, d_p, at IR wavelength, λ, for polystyrene on silicon is given by:

$$d_p = \frac{\lambda}{2\pi\sqrt{n_{Si}^2 \sin^2 \theta_{air} - n_{PS}^2}}$$

Equation 8.1

where n_{Si} = 3.4 is the refractive index of the silicon and n_{PS} = 1.5 is the refractive index of the polystyrene. θ_{atr} is the angle of incidence, which is 45° for all of these experiments.. In this system the penetration depth falls in the range 1.0 μm to 2.0 μm for the polystyrene C-H stretch and d-DBP carbonyl bands respectively. These values are far larger than the film thickness and this means that the absorption peaks are insensitive to the distribution of the d-DBP in the film but they are sensitive to the total amount of d-DBP in the film. The amount of d-DBP in the film will be related to the area, A_{C-X}, under either of d-DBP peaks (A_{C-D} or $A_{C=O}$) normalised by the area under the polystyrene C-H stretch band, A_{C-H}. The areas under these peaks were measured using the peak area function of the PE1600 spectrometer used to make these measurements. The limits of the area integration were 3200-2800 cm^{-1} for the C-H stretch, 2285-2060cm^{-1} for the C-D stretch and 1670-1770 cm^{-1} for the carbonyl stretch. The limits of the baseline were fixed at the same value as the integration limits, this is illustrated schematically in Figure 8.2

The average volume fraction of d-DBP in the films, ϕ_{av}, is related linearly to the ratios A_{C-D}/A_{C-H} and $A_{C=O}/A_{C-H}$, this is a result of the Beer - Lambert Law. To find the constant of proportionality it was assumed that for the first measurements, made at less than 10 minutes after casting, the amount of d-DBP in the film was identical to the nominal amount in the casting solution.

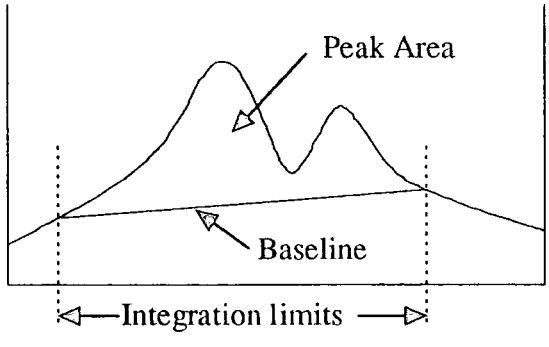

Figure 8.2: Schematic of relationship between baseline and peak area.

Figure 8.3 shows the values of A_{C-D}/A_{C-H} and $A_{C=O}/A_{C-H}$ obtained from the initial measurements on W, Y and Z, also included are values for the area integrals calculated in the same regions using a pure polystyrene sample containing no d-DBP. It was found that for this pure film the values of the area integrals in the C-D and C=O region were

slightly negative. For this reason the data for were fitted with lines of the form $A_{C-X}/A_{C-H} = m\,\phi_{av} + c$. Using the fitted values of m and c, it was found that ϕ_{av} was given by:

$$\phi_{av} = \left(\frac{A_{C-D}}{A_{C-H}} + 0.07(5)\right)\frac{1}{3.0(1)}$$

$$\phi_{av} = \left(\frac{A_{C=O}}{A_{C-H}} + 0.03(3)\right)\frac{1}{1.2(2)}$$

Equation 8.2

The statistical errors in this fitting procedure will introduce a ϕ_{av} independent systematic error in the ϕ_{av} of ±0.02 for values calculated from the C=O band and ±0.03 for the C-D band. In addition there is a ϕ_{av} dependent systematic error of up to ±0.02 for the C=O band and ±0.05 for the C-D band. It can be seen from these values that the values calculated from the C=O will be less prone to error than the values calculated from the C-D band. Figure 8.4 shows values of ϕ_{av} as a function of time calculated from the normalised peak areas using Equation 8.2. The W blend shows no trend in ϕ_{av} as a function of time.

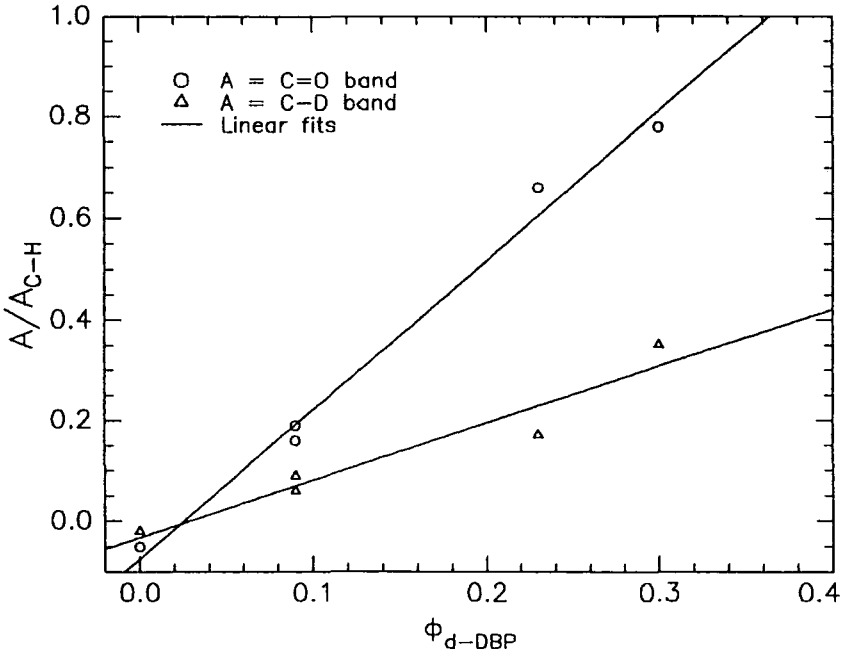

Figure 8.3: Peak area ratios from ATR experiments on t = 0 samples, with nominal average volume fractions d-DBP. Straight line fits are for calibration. Statistical errors in ϕ_{av} are ~0.04 for the C-D band and ~0.01 for the C=O band.

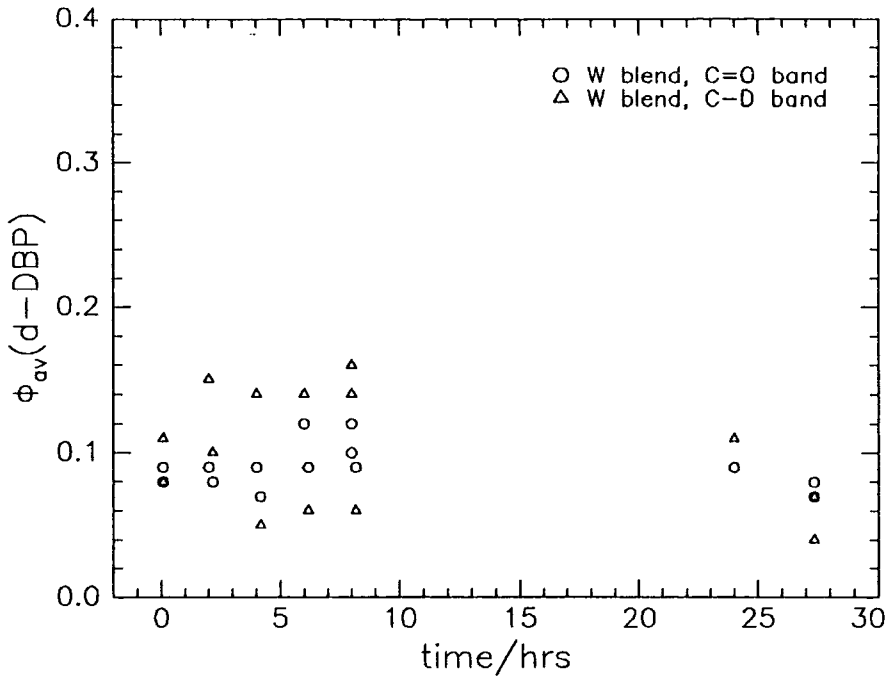

Figure 8.4a: ϕ_{av} vs t/hours for blend W calculated from C=O and C-D band areas. Statistical errors in ϕ_{av} are ~0.04 for the C-D and ~0.01 for the C=O bands.

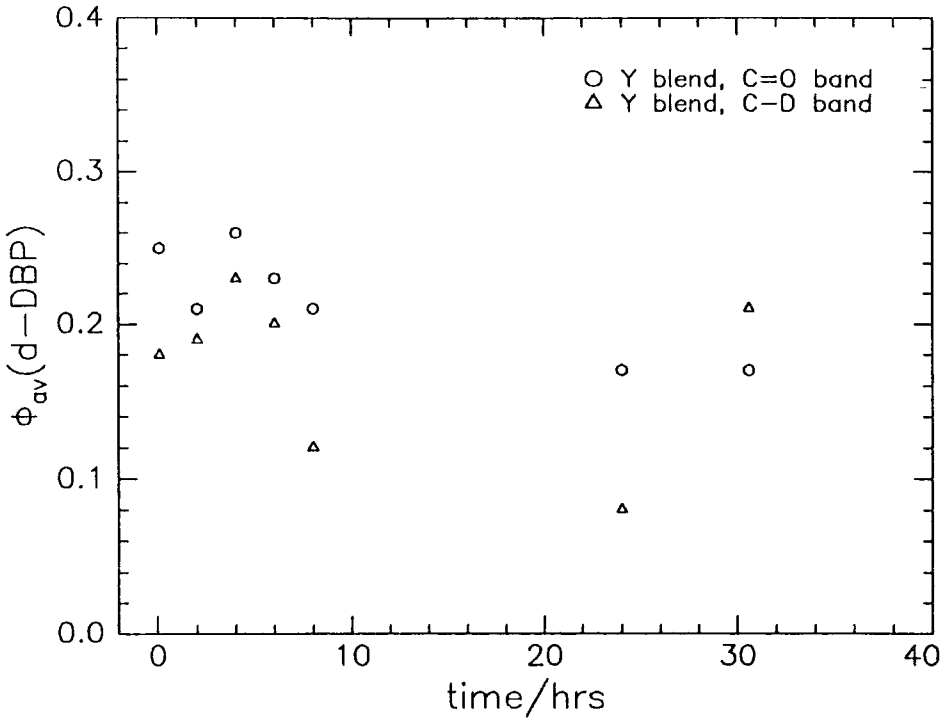

Figure 8.4b: ϕ_{av} vs t/hours for blend Y calculated from C=O and C-D band areas. Statistical errors in ϕ_{av} are ~0.04 for the C-D and ~0.01 for the C=O bands.

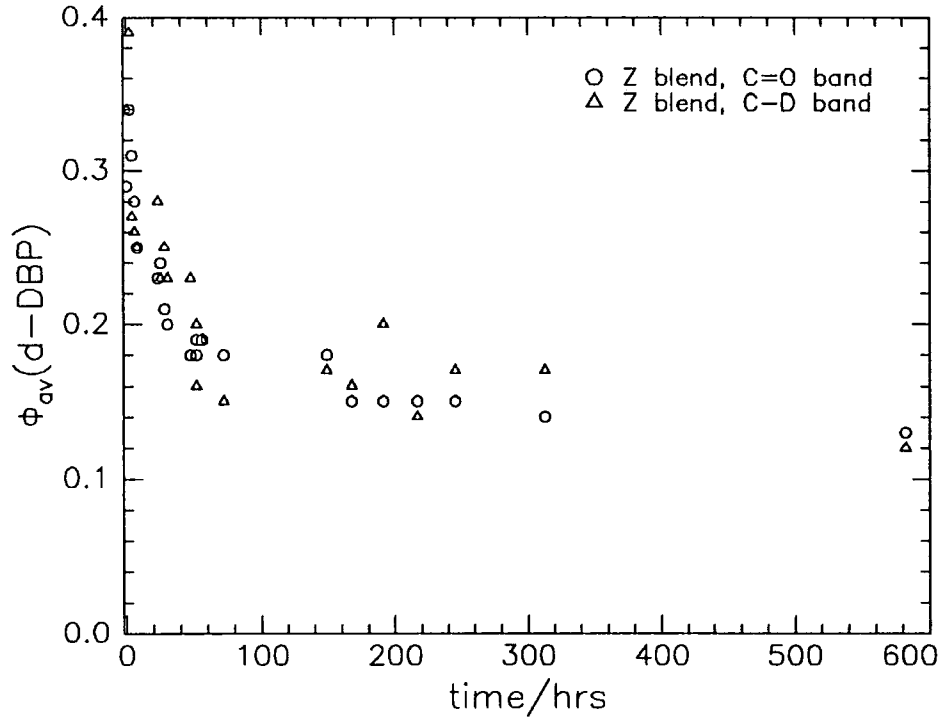

Figure 8.4c: ϕ_{av} vs t/hours for blend Z calculated from C=O and C-D band areas. Statistical errors in ϕ_{av} are ~0.04 for the C-D and ~0.01 for the C=O bands.

Average values of ϕ_{av} calculated over the whole time range from the C-D and C=O bands are 0.10(4) and 0.09(1) respectively, if it is true that there is no underlying variation in the volume fraction of d-DBP then these values give an indication of the random error in the measured ϕ_{av}. Blend Y shows a decrease in ϕ_{av} as a function of time, this is clear in the data from the C=O band but not the C-D band. Finally blend Z, with initially 0.30 volume fraction d-DBP, shows a clear decrease in ϕ_{av} from both C=O and C-D bands over the first ~100 hours subsequently a plateau value of $\phi_{av} = 0.14$ is reached, within the experimental error this level is maintained up to at least ~600 hours (or 25 days).

Figure 8.5 shows a selection of the reflectivity profiles, R vs Q, obtained for the blends W, X, Y and Z as a function of time after spin casting. The reflectivity data generally exhibit Kiessig fringes characteristic of the film thicknesses, the exceptions to this are the data for the X and Y blends for times less than 24 hours. The absence of fringes indicates that the scattering length density of the polymer film (plus d-DBP) is close to that of the silicon substrate, this is expected to occur when then the average volume fraction of d-DBP in the film, ϕ_{av}, is ~0.18.

The reflectivity of the W blend changes very a little as a function of time, in contrast to the Z blend where substantial changes are observed. The clearest of these changes is a shift in the critical edge to lower Q values at longer times, this corresponds to a decrease in the bulk volume fraction of d-DBP. There is also a slight increase in the fringe spacing which suggests that the films are becoming thinner. Trends in the X and Y blend data are more difficult to discern, although there is a slight shift in the location of the critical edge to lower Q values for the Y blend.

The reflectivity data were analysed using two methods, the maximum entropy program VOLFMEM was used to obtain free form fits with a pixel size of ~15Å (this corresponds to ~50 pixels per film) and internal smoothing of 100Å. Secondly a number of multilayer fits were made using PHOENIX. Models with up to three uniform layers on top of a 15Å silicon dioxide layer were fitted. The roughness' at the air-polymer, polymer-SiO_2 and SiO_2-Si interfaces were fixed at 5Å. The fit quality for the PHOENIX multilayer fits will be measured in terms of the fit index, defined in section 4.3.3, which is not identical to the more commonly used 'normalised χ^2 parameter'. Table 8.3 shows the correspondence between the normalised χ^2 parameter and the fit index, obtained for a selection of PHOENIX (multilayer fits).

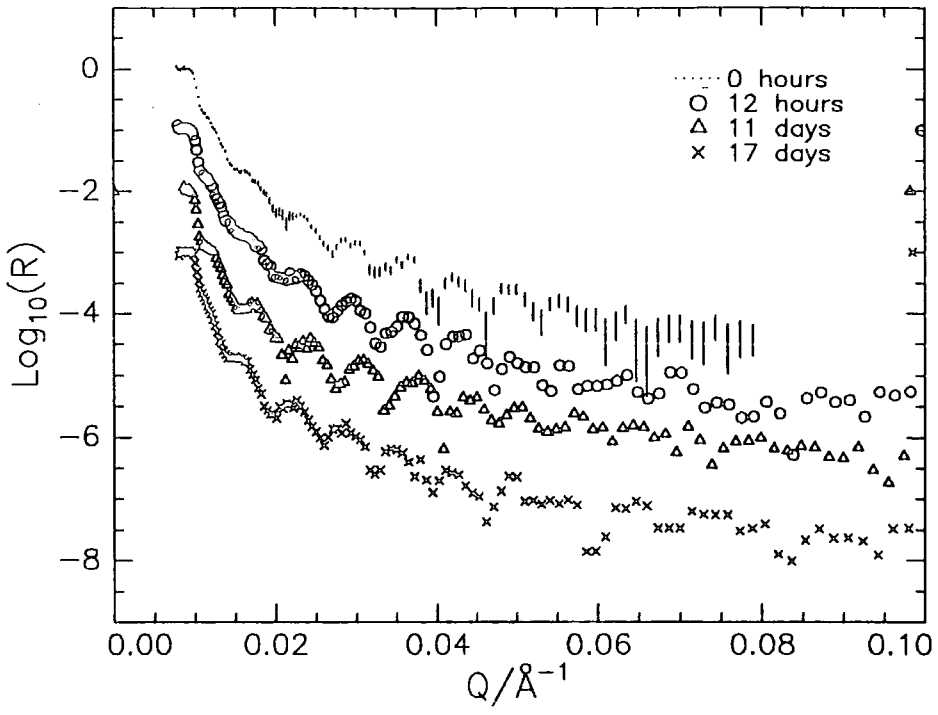

Figure 8.5a: Reflectivity data for selected blend W samples, errors from Poisson statistics shown for W0hrs. Successive datasets offset by -1 for clarity.

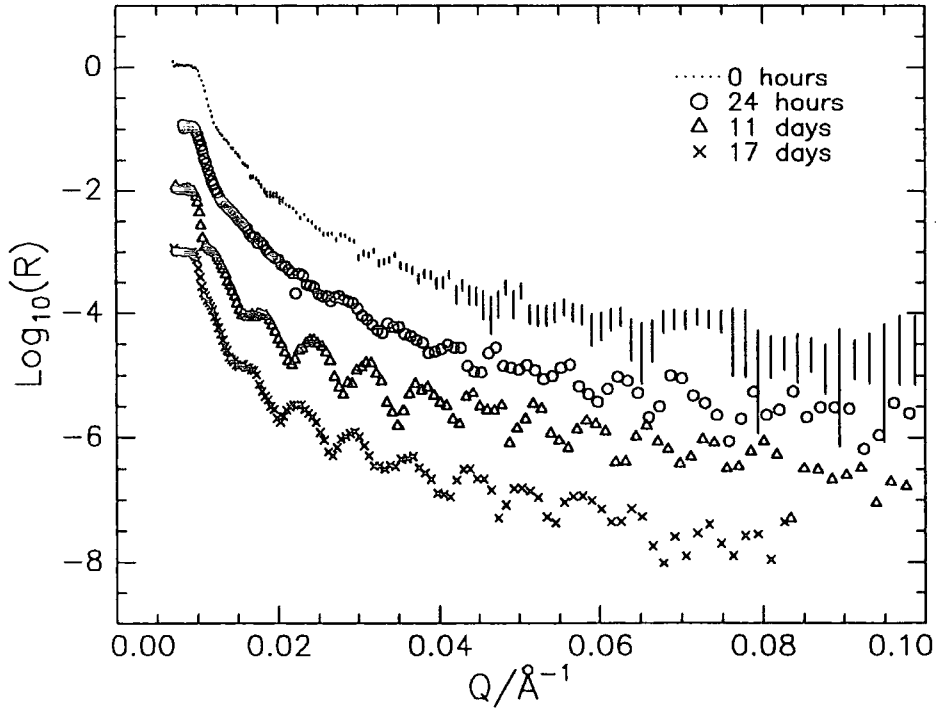

Figure 8.5b: Reflectivity data for blend X samples, errors from Poisson statistics shown for X0hrs. Successive datasets offset by -1 for clarity.

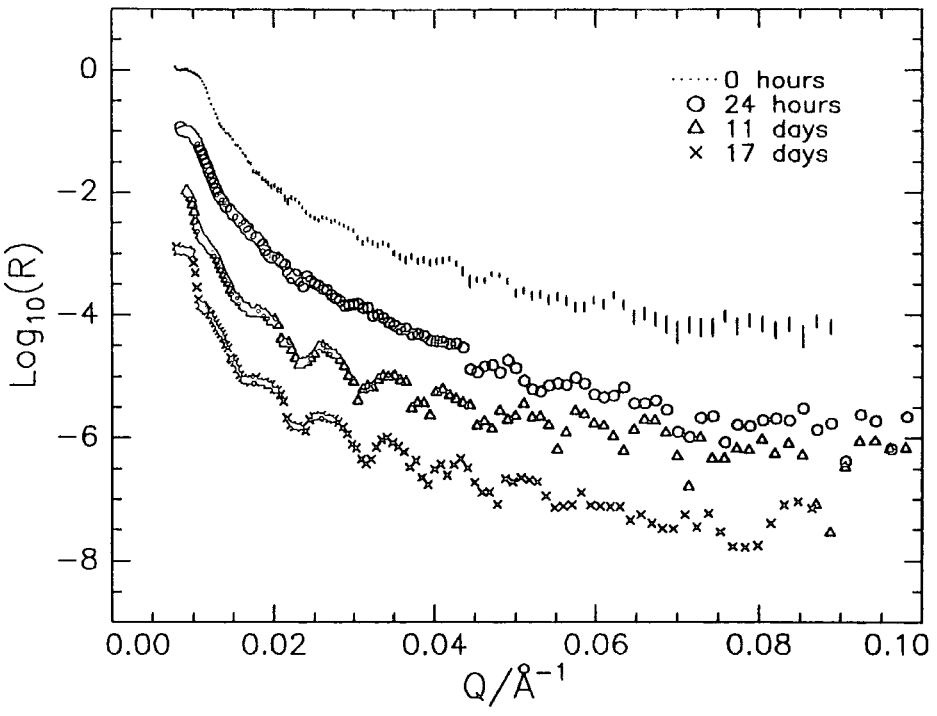

Figure 8.5c: Reflectivity data for selected Y samples, errors from Poisson statistics shown for Y0hrs. Successive datasets offset by -1 for clarity.

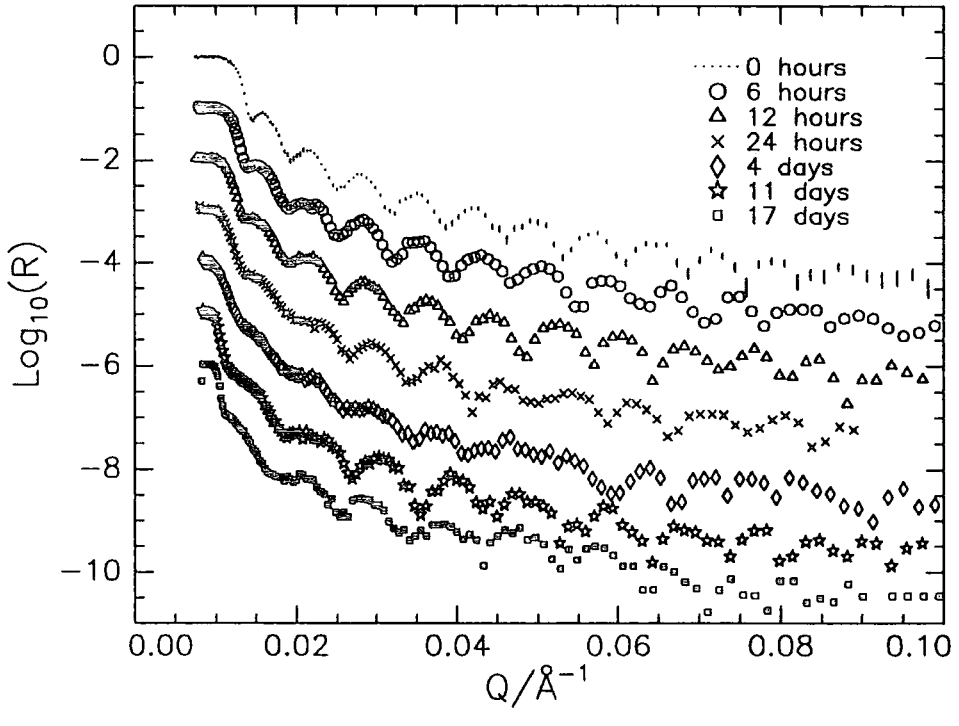

Figure 8.5d: Reflectivity data for selected Z samples, errors from Poisson statistics shown for Z0hrs. Successive datasets offset by -1 for clarity.

The data were initially fitted with single layer models using PHOENIX, in order to obtain a value of the film thickness to be used in VOLFMEM.

Sample	Fit index	Normalised χ^2	Number of layers
z6hrs	0.41	63	1
z12hrs	0.32	42	1
z0hrs	0.23	26	1
z3days	0.15	13	1
z15days	0.12	6	1
z3days	0.09	6	3
z15days	0.06	4	3

Table 8.3: The equivalence between the fit index and the normalised χ^2 parameter, calculated for selected PHOENIX (multilayer fits).

The parameters of these fits are shown in Table 8.4. The average film thicknesses fitted are 890 ± 20Å, 870 ± 120Å, 870 ± 140Å and 750 ± 50Å for the W, X, Y and Z blends respectively. These values compare well with the values obtained using contact profilometry in Table 8.1 The thickness values obtained for the X and Y blends using reflectivity are relatively imprecise because of the absence of fringes in the majority of films of these two blends. Figure 8.6 shows the variation in thickness of the blend Z and blend W samples as a function of time. In addition to thicknesses calculated from neutron reflectometry data, the thickness of a single blend Z film are shown as a function of time, these results have been obtained from x-ray reflectivity data[1]. These data show that there is a reduction in the film thickness as the d-DBP content decreases, this is clearly apparent in the data collected from the samples <24 hours and the x-ray data where a single film is measured repeatedly. The thicknesses of the separate films used at longer times, do not follow this trend but this can be attributed to slightly different casting conditions leading to different original film thicknesses. The blends Y and Z show an improvement in the fit quality as time increases, this suggests that the initial distribution of d-DBP in the films is rather non-uniform and as the experiment progresses the distribution becomes more uniform.

	Sample code	Thickness /Å	$\phi_{d\text{-}DBP}$	Fit index
0.10	w0hrs	953	0.14	0.23
	w6hrs	936	0.08	0.30
	w12hrs	922	0.07	0.38
	w4days	927	0.07	0.21
	w11days	875	0.07	0.33
	w17days	962	0.07	0.17
0.17	x0hrs	768	0.18	0.18
	x24hrs	793	0.17	0.18
	x11days	879	0.12	0.13
	x17days	1034	0.13	0.16
0.24	y0hrs	852	0.27	0.38
	y6hrs	832	0.26	0.40
	y12hrs	1070	0.23	0.36
	y24hrs	660	0.20	0.24
	y11days	802	0.14	0.21
	y17days	974	0.13	0.15
0.30	z0hrs	827	0.35	0.23
	z6hrs	808	0.31	0.41
	z12hrs	771	0.26	0.32
	z24hrs	738	0.23	0.18
	z4days	722	0.18	0.15
	z11days	676	0.13	0.12
	z17days	736	0.13	0.12

Table 8.4: Fit parameters for the one layer fits to the reflectivity data, error in $\phi_{d\text{-}DBP}$ is ~ 0.02

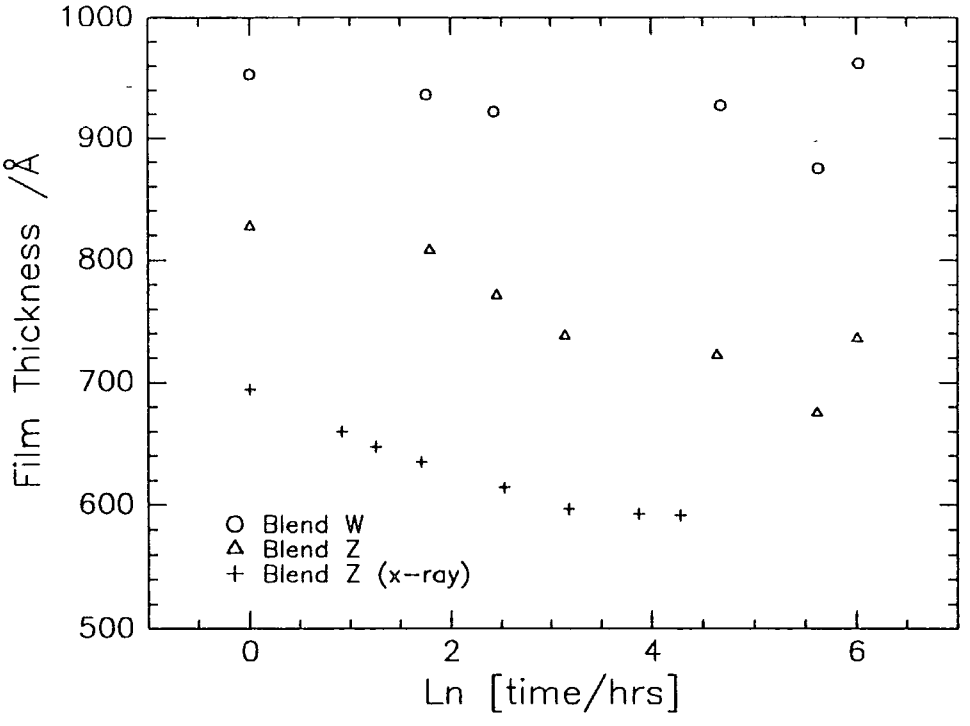

Figure 8.6: Film thicknesses obtained for blends W and Z as a function of time.

Figure 8.7 shows the $\phi(z)$ profiles obtained from the reflectivity data using VOLFMEM, the normalised χ^2 parameters for these fits are shown in Table 8.5. There is a considerable variation in the fit quality but overall the Z blend fits are the best and there is a crude correlation between the fit quality and the average volume fraction of d-DBP in the film.

	W	X	Y	Z
0 hour	18.1	4.2	6.2	5.5
6 hours	21.9	-	6.2	7.1
12 hours	6.1	-	9.5	4.4
24 hours	-	8.8	6.4	3.7
4 days	25.7	-	-	7.3
11 days	15.4	26.5	31.7	13.4
17 days	7.1	18.7	19.3	4.4

Table 8.5: Normalised χ^2 parameters for VOLFMEM fits to reflectivity data.

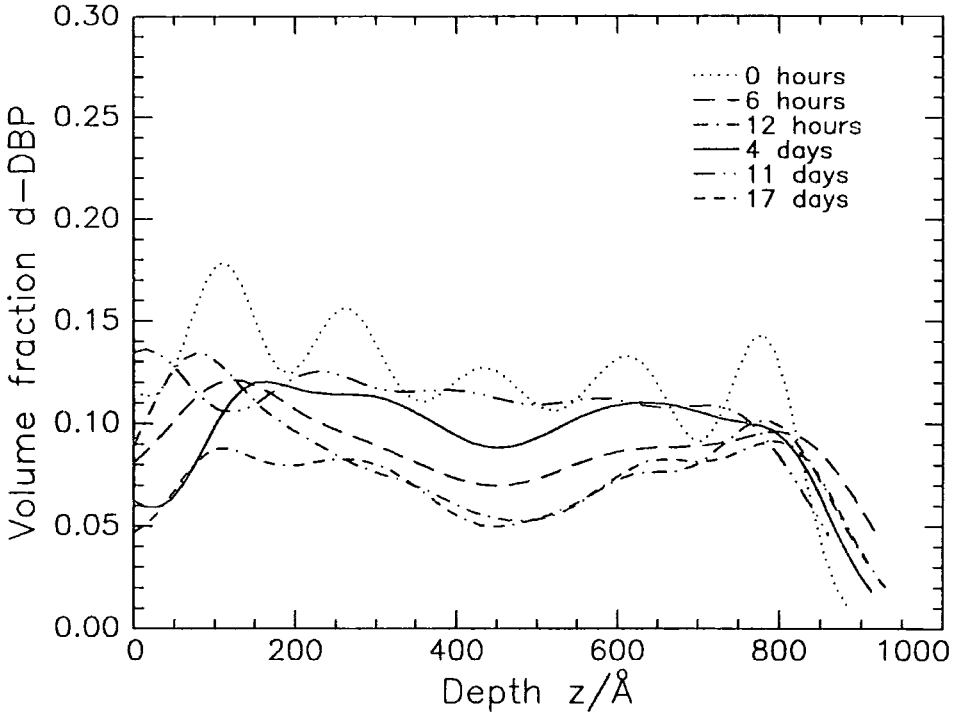

Figure 8.7a: Composition vs depth profiles obtained for blend W samples as a function of time, using VOLFMEM.

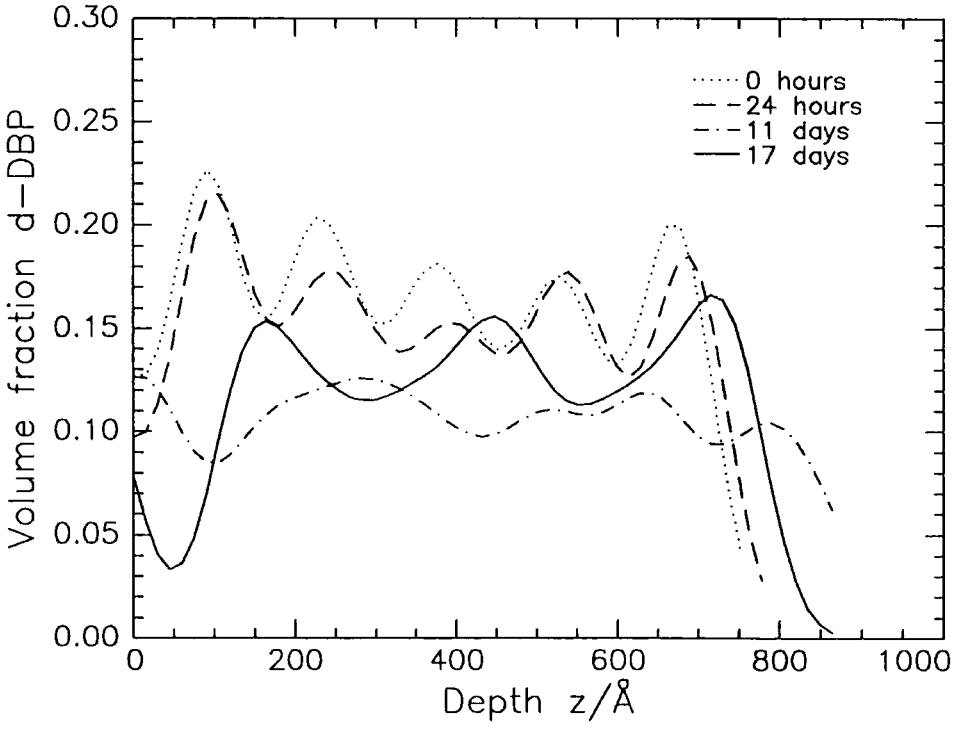

Figure 8.7b: Composition vs depth profiles obtained for blend X samples as a function of time, using VOLFMEM.

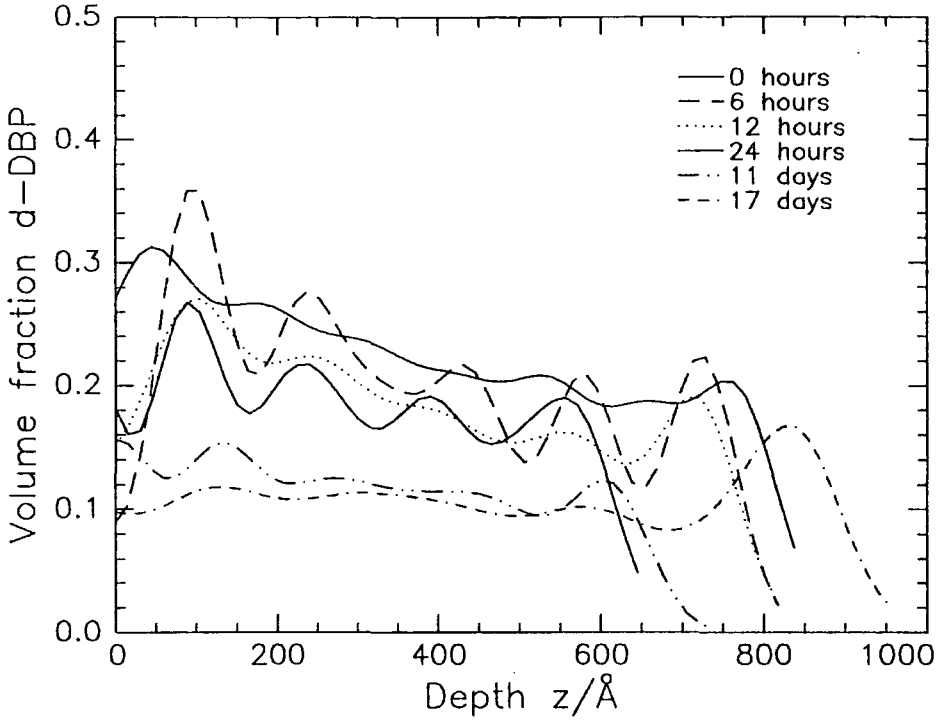

Figure 8.7c: Composition vs depth profiles obtained for blend Y samples as a function of time, using VOLFMEM.

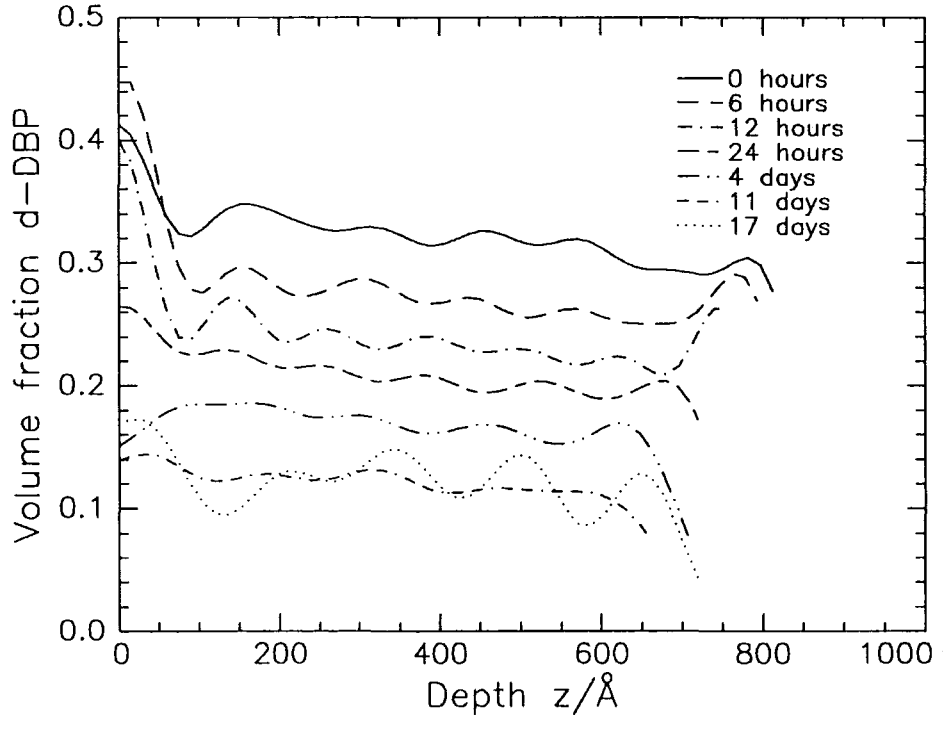

Figure 8.7d: Composition vs depth profiles obtained for blend Z samples as a function of time, using VOLFMEM.

A number of the composition profiles exhibit high frequency ripples that are probably due to truncation errors in the data, these ripples are not correlated with the normalised χ^2 parameter, i.e. do not arise solely in relatively poor or good fits.

The is little evidence for a consistent underlying structure in the $\phi(z)$ profiles, except for the Y and Z blends at shorter times where there appears to be a small excess of d-DBP at the air interface, the normalised χ^2 parameters are, on average, better for these samples than for the other samples. In the light of the VOLFMEM fits all the data were fitted with two layer models using PHOENIX, the parameters of these fits are shown in Table 8.6. The symbols ϕ_n, z_n and σ_n refer to the volume fraction d-DBP, thickness and roughness at the bottom of the n^{th} layer, where the first layer is at the air-polymer interface. The two layer models showed a thin well defined layer of d-DBP at the air-polymer interface, typically ~30Å thick and with a volume fraction d-DBP up to 0.2 higher than the bulk value. The fit indices for these two layer models are better than those for the equivalent one layer models. Examples of the $\phi(z)$ profiles obtained using the two layer models for the Z blend can be found in Figure 8.8.

Figure 8.9 shows a comparison of the fits obtained for selected data using PHOENIX multilayer fits and VOLFMEM free form fits. It can be seen that the one layer models give good fits up to ~0.02Å^{-1}, but beyond this point they under estimate the reflectivity, the two layer and VOLFMEM fits correct this under estimation. The excess scattering at higher Q, above the value predicted by the one layer models, is characteristic of a region of higher scattering length density (i.e. more d-DBP) at the surface.

Table 8.7 shows the values ϕ_{av} obtained using each of the methods of data analysis, there is good agreement between these values and the values obtained using ATR spectroscopy. It is interesting to note that the one layer models give a good estimate of ϕ_{av} when compared to the two layer and VOLFMEM fits. Figure 8.10 shows values of ϕ_{av} obtained using two layer models as a function of time, in common with the ATR data the W blend exhibits no variation in ϕ_{av} within the experimental. The average value is 0.12(3). The X, Y and Z blends exhibit a drop in ϕ_{av} to ~0.12 over the first 100-200 hours then ϕ_{av} remains constant within the experimental error.

	Sample	ϕ_1	z_1/ Å	σ_1	ϕ_2	z_2/ Å	Fit index.
0.10	w0hrs	0.25	22	36	0.14	944	0.15
	w6hrs	0.16	29	33	0.13	959	0.15
	w12hrs	0.23	26	5	0.14	957	0.17
	w3days	0.17	24	5	0.13	958	0.16
	w10days	0.50	20	3	0.12	871	0.11
	w15days	0.20	50	26	0.07	922	0.13
0.17	x0hrs	0.32	32	15	0.18	775	0.16
	x24hrs	0.32	29	13	0.17	705	0.16
	x10days	0.25	32	12	0.12	840	0.10
	x15days	0.14	49	9	0.13	998	0.16
0.24	y0hrs	0.45	38	21	0.26	909	0.33
	y6hrs	0.56	32	16	0.25	685	0.27
	y12hrs	0.42	49	15	0.21	627	0.25
	y24hrs	0.23	333	164	0.14	236	0.09
	y10days	0.41	33	9	0.13	825	0.16
	y15days	0.24	30	14	0.12	791	0.14
0.30	z0hrs	0.55	26	9	0.34	792	0.16
	z6hrs	0.60	41	9	0.29	752	0.15
	z12hrs	0.52	36	7	0.25	722	0.15
	z24hrs	0.42	31	11	0.22	695	0.13
	z3days	0.36	24	12	0.18	700	0.14
	z10days	0.28	33	13	0.13	641	0.09
	z15days	0.44	27	7	0.13	712	0.08

Table 8.6: Fit parameters for PHOENIX (two layer models) fits to the reflectivity data.

		ϕ_{av}			
	Sample	VOLFMEM	1 layer	2 layer	Average
0.10	w0hrs	0.12	0.14	0.14	0.13(1)
	w6hrs	0.09	0.08	0.13	0.10(3)
	w12hrs	0.08	0.07	0.14	0.10(4)
	w3days	0.09	0.07	0.13	0.10(3)
	w10days	0.11	0.07	0.12	0.10(3)
	w15days	0.07	0.07	0.07	0.07(0)
0.17	x0hrs	0.16	0.18	0.18	0.17(1)
	x24hrs	0.15	0.17	0.17	0.16(1)
	x10days	0.11	0.12	0.12	0.12(1)
	x15days	0.11	0.13	0.13	0.12(1)
0.24	y0hrs	0.23	0.27	0.26	0.25(2)
	y6hrs	0.20	0.26	0.25	0.24(3)
	y12hrs	0.18	0.23	0.21	0.21(3)
	y24hrs	0.18	0.20	0.17	0.18(2)
	y10days	0.11	0.14	0.13	0.13(2)
	y15days	0.11	0.13	0.12	0.12(1)
0.30	z0hrs	0.33	0.35	0.34	0.34(1)
	z6hrs	0.30	0.31	0.29	0.3(1)
	z12hrs	0.26	0.26	0.25	0.26(1)
	z24hrs	0.22	0.23	0.22	0.22(1)
	z3days	0.17	0.18	0.18	0.18(1)
	z10days	0.12	0.13	0.13	0.13(1)
	z15days	0.13	0.13	0.14	0.13(1)

Table 8.7: Values of ϕ_{av} obtained using the different methods of data analysis, along with an average value with the standard deviation.

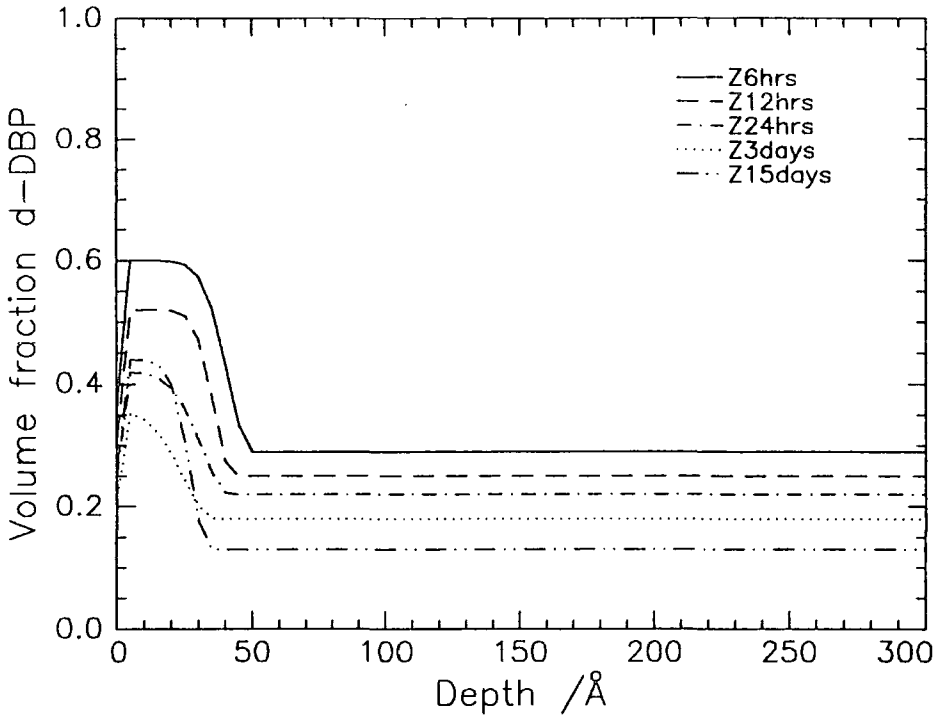

Figure 8.8: $\phi(z)$ profiles for the Z blend, derived from two layer model fit parameters for neutron reflectivity data.

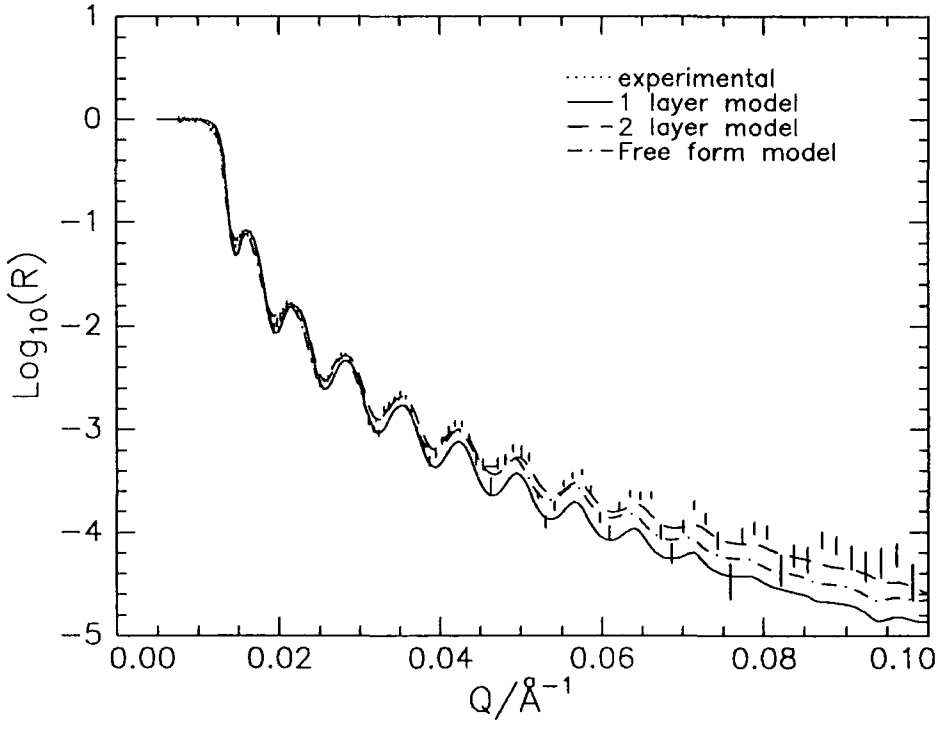

Figure 8.9a: A comparison between the Z0hrs reflectivity data (with errors from Poisson statistics) and model fits from one layer, two layer and free form fits.

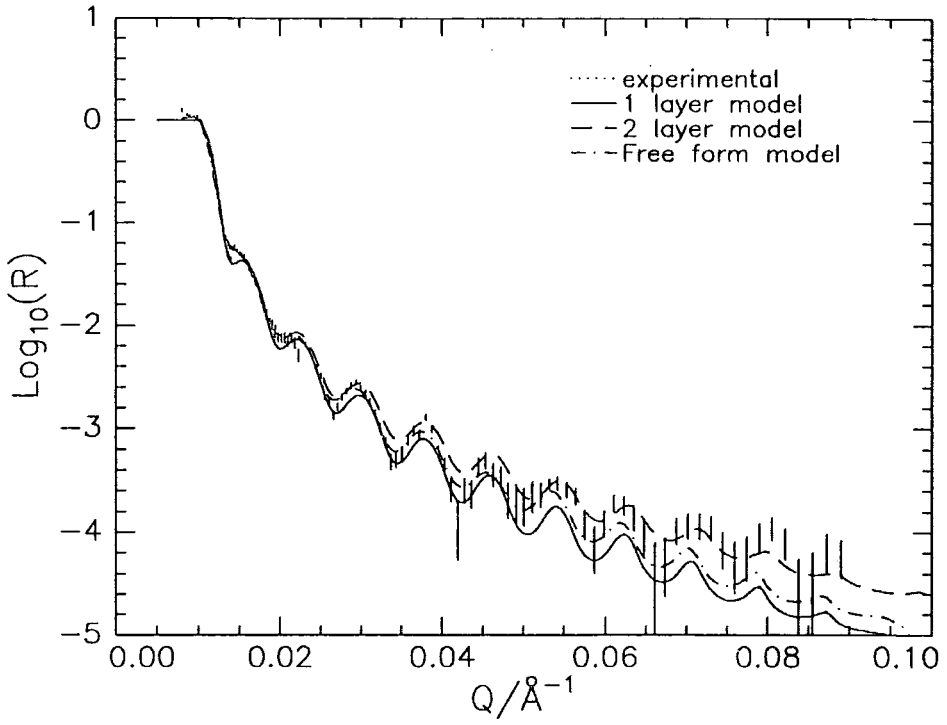

Figure 8.9b: A comparison between the Z24hrs reflectivity data (with errors from Poisson statistics) and model fits from one layer, two layer and free form fits.

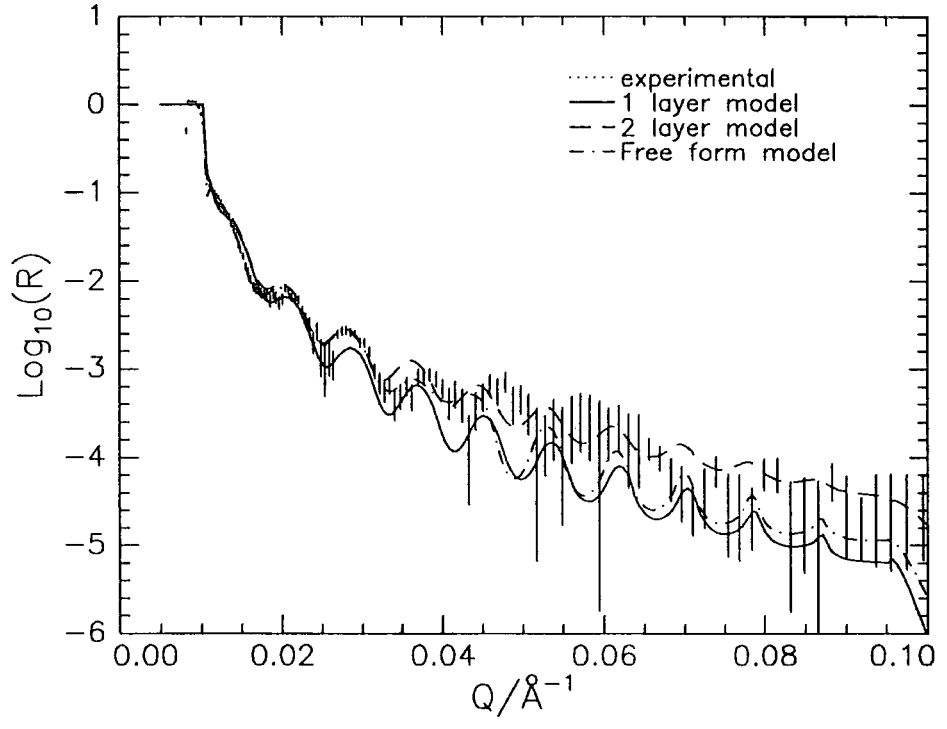

Figure 8.9c: A comparison between the Z17days reflectivity data (with errors from Poisson statistics) and model fits from one layer, two layer and free form fits.

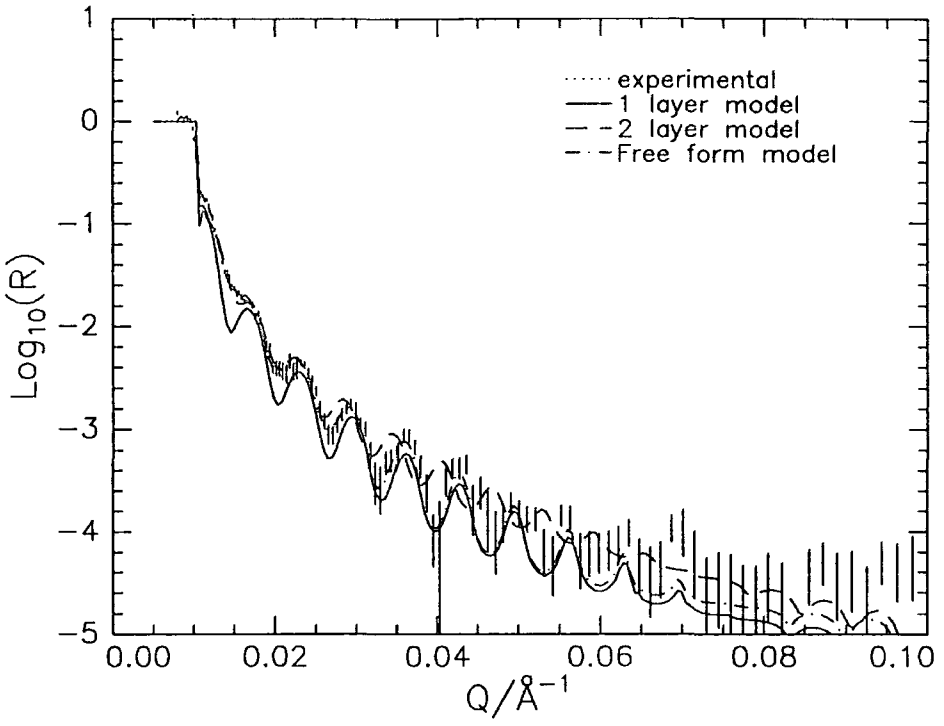

Figure 8.9d: A comparison between the W12hrs reflectivity data (with errors from Poisson statistics) and model fits from one layer, two layer and free form fits.

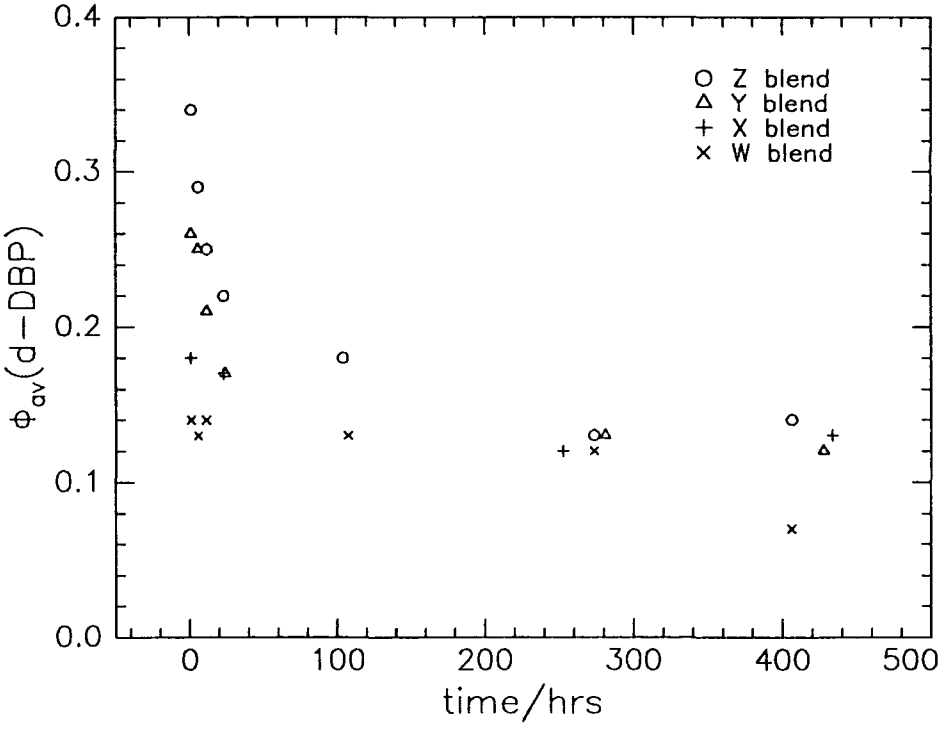

Figure 8.10: ϕ_{av} vs time/hours for the W, X, Y and Z blends, measured using neutron reflectivity data, two layer models. Statistical error in ϕ_{av} is ~0.02.

8.3 Discussion

In the previous section it was found that the average volume fraction of d-DBP, ϕ_{av}, in thin films of polystyrene decreases as a function of time and reaches a constant value of ~0.13. Additionally it was found that a thin layer of d-DBP (~30Å) formed at the air-polymer interface. The relatively large loss of this plasticiser from the substrate polymer is known[2] and is one of the reasons that DBP is no longer used industrially as a plasticiser.

Three factors will be involved in determining the rate at which ϕ_{av} decreases, these are the evaporation rate, α, the mutual diffusion coefficient, D_m, and the film thickness, l. The type of behaviour observed will depend on the relative sizes of these factors. Two regimes arising from the relative sizes of α and D_m can be envisaged:

(i) where the evaporation rate is larger or comparable in size to the diffusion rate.

(ii) where the evaporation rate is small compared to the diffusion.

Intuitively it can be seen that, in the absence of any other factors, films in regime (i) will exhibit some sort of variation in the volume fraction of d-DBP as a function of depth whereas those in regime (ii) will exhibit no such variations because immediately d-DBP is lost from the surface region it is replaced by material from the bulk of the sample. Crank[3] discusses the mathematics of analysing diffusion data in a wide range of situations. The simplest of these is the sorption-desorption case, where it is assumed that the evaporation rate α is large (case (i)) and so the rate of mass loss from the film is determined by the mutual diffusion coefficient, D_m. A crude estimate of D_m can be obtained using the expression below:

$$D_m \approx 0.049\left(\frac{l^2}{t_c}\right)$$

Equation 8.3

where t_c is the characteristic time required for the value of ϕ_{av} to drop half way to it's equilibrium value. Using a value of l = 700Å and t_c = 24 hours this would imply a value of $D_m \approx 3\times10^{-17}$ cm^2 s^{-1}. Such a value of D_m for d-DBP would be far smaller than values for di-octyl phthalate in natural rubber[4] ($D_m = 1.8\times10^{-8}$ cm^2 s^{-1}), toluene in poly (vinyl acetate)[5] ($D_m = 10^{-9}$-10^{-7} cm^2 s^{-1}) and water in poly (styrene-co-acrylonitrile)[6] ($D_m \sim 10^{-}$

^{10} cm^2 s^{-1}) for example. This suggest that the analysis of the data assuming α is large is invalid. A more rigorous attempt to estimate the value of D_m was considered, but methods for estimating D_m for small molecules in polymers apply only to gases or organic vapours[7], although there is some work linking the viscosity of organic liquids to D_m values in natural rubber. In addition to these factors concerning the probable diffusion coefficient, the expectation for d-DBP is that it will be highly involatile, since its boiling point is 613K and thus α will be small.

Crank also discusses the situation of the evaporation of a diffusant from the surface of semi-infinite layer with a range of values of α and D_m values. In this case a region depleted in the diffusant will be found at the surface of the semi-infinite layer - the length scale of this depletion will be of the order $(4D_mt)^{1/2}$, if the value of D_m calculated from Equation 8.3 were correct then the depletion layer at the air -polymer interface would be around 170Å deep after 6 hours. The reflectivity data shows no such depletion of d-DBP from the air -polymer interface. These data indicate that the d-DBP/PS system falls in regime (ii) and that the decrease in ϕ_{av} with time is determined solely by the evaporation rate, α. The rate of mass, M, loss is related to the evaporation rate, α, by:

$$\frac{dM}{dt} = \alpha(C_t - C_\infty)$$

Equation 8.4

where C_t is the surface concentration of d-DBP at time t and C_∞ is the surface concentration at equilibrium. Converting to volume fractions using:

$$dM = lA\rho d\phi$$

Equation 8.5

and

$$(C_t - C_\infty) = \rho(\phi_t - \phi_\infty)$$

Equation 8.6

Where A is a unit area, ρ is the density of d-DBP, ϕ_t is the surface volume fraction of d-DBP at time t and ϕ_∞ is the volume fraction at equilibrium. The following expression is obtained:

$$Al\frac{d\phi}{dt} = \alpha(\phi_t - \phi_\infty)$$

Equation 8.7

This is analogous to first order reaction kinetics. Hence the variation of ϕ_{av} as a function of time is given by:

$$\ln\left(\frac{\phi_t - \phi_\infty}{\phi_o - \phi_\infty}\right) = \frac{\alpha t}{Al}$$

Equation 8.8

where ϕ_o is the volume fraction of d-DBP at t = 0, i.e. the gradient of the plot $\ln\left(\frac{\phi_t - \phi_\infty}{\phi_o - \phi_\infty}\right)$ vs t is α/Al, this will apply until $\phi_t = \phi_\infty$ at which point the ln term becomes indeterminate. Figure 8.11 shows plots these plots for the first 24 hours of the experiments on blend Y and blend Z (nominally 0.24 and 0.30 initial volume fraction of d-DBP), there is insufficient data for these plots for the X blend and the W blend shows no variation in ϕ_{av} with time. Also included in this figure are linear fits to the data. The values of ϕ_o and ϕ_∞ were set at ϕ_∞ = (minimum value of ϕ_{av} - 0.01) and ϕ_o = (first measured value of ϕ_{av} + 0.01). The values of m and the calculated values of α obtained using this procedure are shown in Table 8.5.

Blend	Technique	gradient /hr^{-1}	l/Å	α /cm^{3}s^{-1}
Y	NR	-0.040(2)	865±140	1.0(2)×10^{-10}
	ATR	-0.046(7)	740±50	1.0(2)×10^{-10}
Z	NR	-0.040(2)	750±50	0.83(7)×10^{-10}
	ATR	-0.031(4)	640±40	0.55(8)×10^{-10}

Table 8.9: Values of α calculated from plots after Equation 8.8, along with thickness data used in calculations.

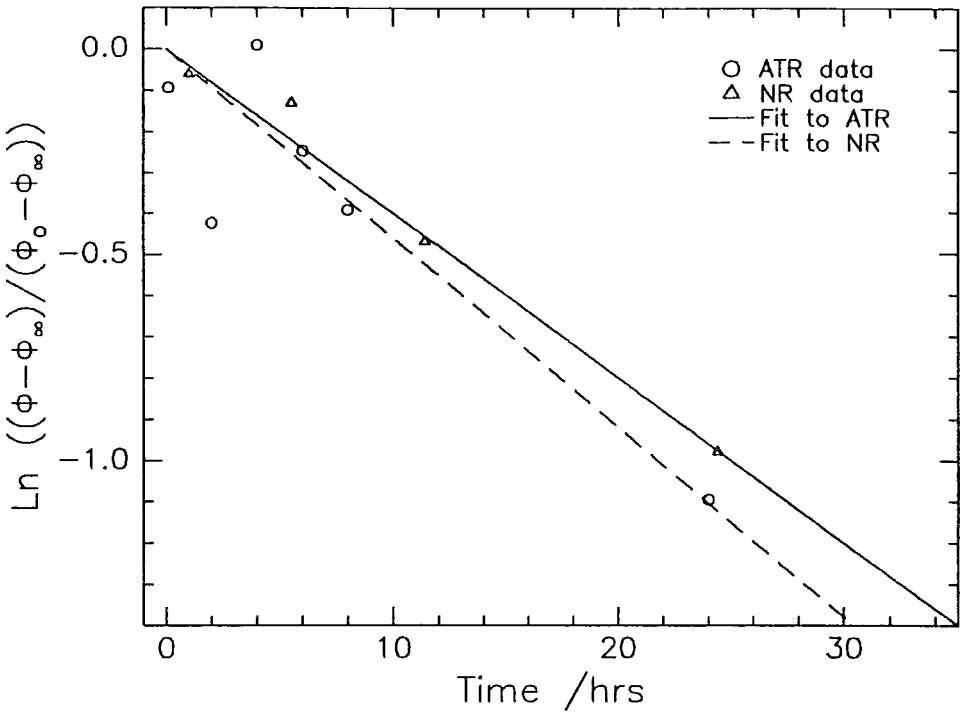

Figure 8.11a: Plots of $\ln\left(\frac{\phi_t - \phi_\infty}{\phi_o - \phi_\infty}\right)$ vs t for the Y blend, using ATR and NR data with linear fits.

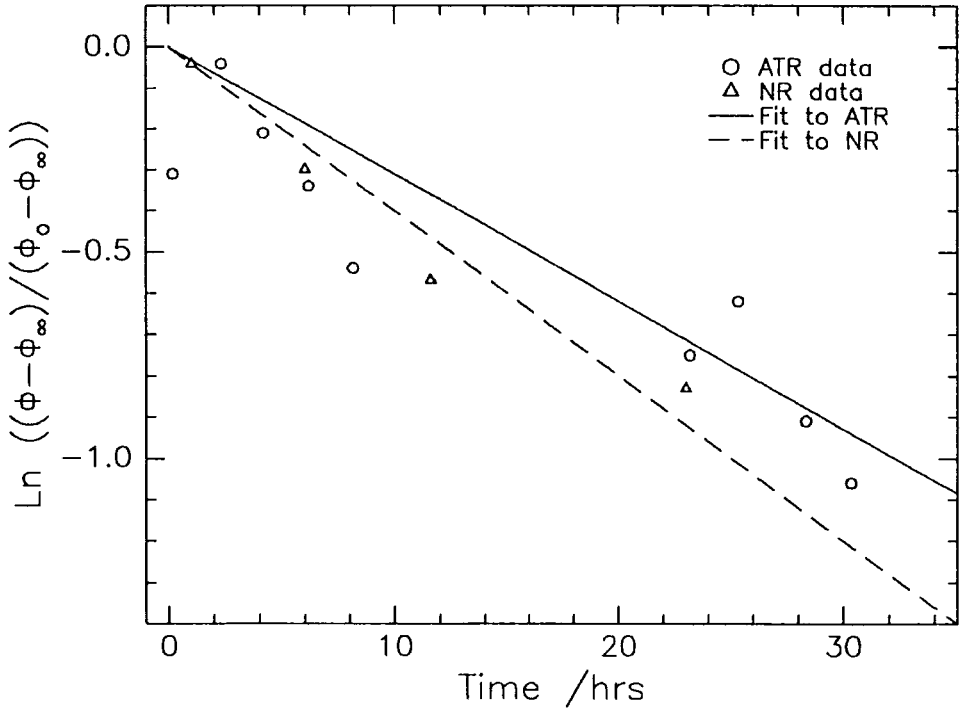

Figure 8.11b: Plots of $\ln\left(\frac{\phi_t - \phi_\infty}{\phi_o - \phi_\infty}\right)$ vs t for the Z blend, using ATR and NR data with linear fits.

To put these values of α in context, one would expect from these results that in an 8cm diameter circular dish with a 1 mm thick layer of d-DBP in the bottom that over a period of one week only 0.07% of the d-DBP would evaporate. This assumes that the evaporation rate of pure d-DBP is the same as that for d-DBP in polystyrene. A further experiment that could be done would be to measure the evaporation rate for pure d-DBP, this is not straight forward since the expected effect is very small and DBP absorbs atmospheric water.

In the preceding analysis it was assumed that the polystyrene + d-DBP film thickness was constant, this is known not to be true but including the effect of a film thickness dependent on ϕ_{av} means that no simple analytical form for $\phi_{av} = f(t)$ is available. Figure 8.12 shows a comparison of ϕ_{av} vs ln [time /hours] for the approximation used above and for a more exact solution which allows for the variation of film thickness with ϕ_{av}. Fitting this expression manually to the Z blend NR data a value of $\alpha = 1.5(2) \times 10^{-10}$ $cm^3 s^{-1}$ is obtained. Neither of these analyses include the effect that a surface composition different from the bulk composition might have.

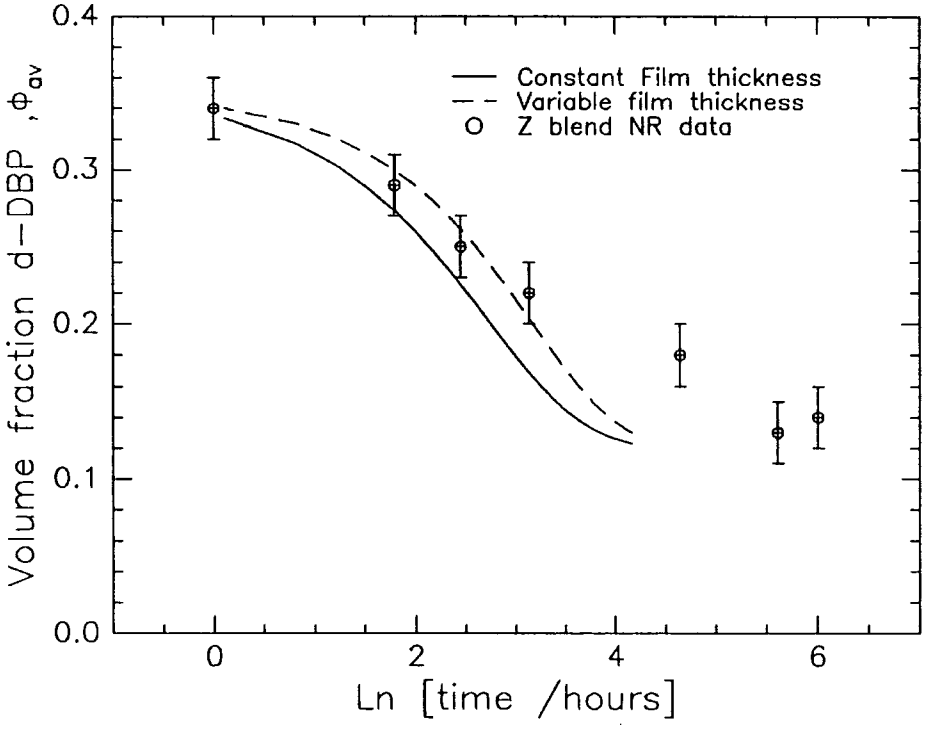

Figure 8.12: ϕ_{av} vs Ln [time /hours] for the Z blend along with theoretical predictions from two models, α parameter is fixed at optimum value for variable thickness model.

These experiments have shown that neutron reflectometry is not an ideal method for determining diffusion coefficients for such small molecules. If the evaporation rate had been large then the diffusion coefficient could have been obtained from the total mass loss from the film using the sorption-desorption equations discussed by Crank, but then this could also have been done using ATR and although the statistical error in ATR is rather larger the measurement time is smaller and so larger diffusion coefficients can be examined. If the diffusion coefficient were to be determined by examining the profile shape at the air interface then again neutron reflectometry would only be suitable for relatively small diffusions coefficients ($<10^{-14}$ cm^3 s^{-1}) because, given the minimum measurement time the length scale of the profile would be such that NR was insensitive to it at larger values of D_m.

It is likely that the mutual diffusion coefficient of DBP in PS would vary markedly with composition. Zhang and Wang[8] have shown that the diffusion coefficient of camphorquinone in polystyrene plus dioctyl phthalate varies markedly with the concentration of di-octyl phthalate for temperatures above the glass transition temperature of the polymer, which is influenced by the concentration of the di-octyl phthalate. Xia, Whang and Li[9] have shown that the diffusion coefficient for camphorquinone in poly (aryl ether ether ketone) exhibits a clear change in behaviour as the temperature drops below T_g. In the system studied here the DBP plasticises the polystyrene. It was found using differential scanning calorimetry (DSC) that for a volume fraction DBP of 0.30 the T_g is ~277K (compared to T_g = 376K for the pure polymer). Data in the literature[2,8] indicate a linear relationship between T_g and volume fraction DBP, so that over the composition range studied here the films change from being above their T_g at room temperature for ϕ_{av} = 0.30 to below T_g with ϕ_{av} = 0.10. The T_g becomes equal to room temperature when $\phi_{av} \approx 0.23$. If diffusion data had been obtained then it could be analysed in the context of the free volume models of Vrentas and Duda[10].

It was found that the d-DBP did not continue to evaporate from the polystyrene film until there was no d-DBP left, instead it was found that for the W blend there was no evaporation and for the other blends the average volume fraction decreased until a constant value of ~0.12 was reached. If this level of ϕ_{av} represents an equilibrium value then it would be expected that at this point the chemical potential of the d-DBP in the

film will be equal to that of the d-DBP vapour above the film. The chemical potential of the d-DBP in the film, μ_f, can be calculated from Flory - Huggins theory:

$$\frac{\mu_f - \mu_f^o}{RT} = \ln\phi + \left(1 - \frac{1}{r}\right)(1-\phi) + \chi_{FH}(1-\phi)^2$$

Equation 8.9

where $r = N/N_s$ is the ratio of the degree of polymerisation of the polymer to the effective degree of polymerisation of the solvent, comparing the segment volume of polystyrene ($= 1.653\times10^{-22}$ cm^3) and the molecular volume of d-DBP ($= 4.33\times10^{-22}$ cm^3) indicates that $r \approx 3400$. R is the gas constant ($= 8.315$ J K^{-1} mol^{-1}) and T is the absolute temperature. ϕ is the volume fraction of d-DBP. χ_{FH} is the Flory - Huggins interaction parameter and is not known. The chemical potential of the d-DBP vapour, μ_v, is given by:

$$\frac{\mu_v - \mu_v^o}{RT} = \ln\frac{p_v}{p_o}$$

Equation 8.10

where p_o is the pressure in the standard state and p_v is the vapour pressure. The vapour pressure can be estimated from the boiling point (or the vapour pressure at another temperature) using the Clausius - Clapeyron equation:

$$\frac{d\ln p_v}{dT} = \frac{\Delta H_{vap}}{RT^2}$$

Equation 8.11

where ΔH_{vap} is the enthalpy of vaporisation of d-DBP, integrating this to give:

$$p_v = p^* e^{-c}$$

Equation 8.12

where:

$$c = \frac{\Delta H_{vap}}{R}\left(\frac{1}{T} - \frac{1}{T^*}\right)$$

Equation 8.13

p^* is a known vapour pressure at temperature T^*. Two possible combinations of T^* and p^* are T^* = 613K and p^* = 760 mmHg (from the boiling point) and T^* = 479K and p^* = 20 mmHg (data in reference 11). The enthalpy of vaporisation can be estimated from Troutons rule ($\Delta H_{vap} \approx 85$ J K^{-1} $mol^{-1} \times T$), for DBP this corresponds $\Delta H_{vap} \approx 52$ KJ mol^{-1}. These values of p^* and T^* indicate a vapour pressure of 0.005 mmHg for dibutyl phthalate at room temperature, this indicates a value of $(\mu_v-\mu_v^o)/RT$ = -12. In principle we should be able to estimate a value of χ_{FH} by setting ϕ = 0.12 in Equation 8.8 and varying χ_{FH} until the chemical potential of matches that of the vapour. This gives a value of χ_{FH} = -13, which is unfeasibly large in magnitude when compared to values of χ_{FH} obtained for other solvent - polymer systems which generally lie in the range -0.5 to 1.0. This large discrepancy between the expected and calculated values of χ_{FH} prove that the d-DBP in the film is not at equilibrium with the region above the film. Clearly a large number of assumptions have been made in these calculations, including the assumption that the system is closed and the numerous assumptions made in estimating the vapour pressure of d-DBP at room temperature. However, in an open system the vapour pressure of d-DBP would tend to be lower than in the closed system and hence the equilibrium ϕ_{av} would be even less.

Neutron reflectometry (NR) can provide unique information on the distribution of d-DBP in polystyrene films. This is because the NR sample is kept in ambient conditions of temperature and pressure during measurement, in contrast to other surface analysis techniques SIMS, NRA and XPS where the sample is placed in a vacuum for measurement. Early on in this work it was found that, when examined using SIMS or XPS, the surface of the DBP plus polystyrene film was completely devoid of DBP. The explanation for this is that despite its high boiling point under high vacuum the DBP is sufficiently volatile to boil out of the sample, at least up to the XPS or SIMS probe depth (i.e. ~50Å).

Although the observed surface excess is very small we can be fairly confident of its existence. The surface excess is clearly visible in the VOLFMEM fits to the Z blend, where the fit quality is high and there are no unphysical structures in the bulk of the film. The one layer models under estimate the reflectivity of the samples at higher Q, whilst the two layer models fit the data rather better with a thin layer rich in d-DBP at the air-polymer interface.

If either the surface excess or the difference (ϕ_1 - ϕ_2), where ϕ_1 and ϕ_2 are the volume fractions of DBP in the first and second layers of the two layer models, are plotted versus ϕ_{av} (see Figure 8.13) then the data can be fitted with a straight line passing through the origin, which is what would be expected for surface enrichment behaviour. The gradients of these straight lines are 36(6) and 0.9(1) for the surface excess and the difference (ϕ_1 - ϕ_2) respectively. There is rather a large scatter in the values of (ϕ_1 - ϕ_2) and the surface excess for the lower values of ϕ_{av}. Such results are not unprecedented, similar work on a tackifier in polyisoprene[12] which also shows an excess at the air polymer interface.

There are two reasons for expecting the excess of d-DBP at the air-polymer interface - firstly DBP has a lower surface energy than polystyrene the values are 33.1 mJ m^{-2} and 40.7 mJ m^{-2} respectively[13]. Secondly the DBP, a small molecule, loses less entropy on being confined to the air-polymer interface then the polystyrene. Self consistent field theory models, using a value of $\Delta\gamma$ calculated from the literature values of the surface energy and values of N = 100 for the non-absorbing polymer (≡ PS) and N = 3 for the absorbing species (≡ DBP) and values of χ of 0 and 0.2, do show an excess of DBP at the air-polymer interface, see Figure 8.14. These models show that the predicted surface excess is qualitatively similar to that observed in the experimental system, although the layer thickness is somewhat thinner. Discrepancies between these models and the experimental data are not unsurprising since the programs used in calculating the theoretical profiles were not written with such a situation in mind.

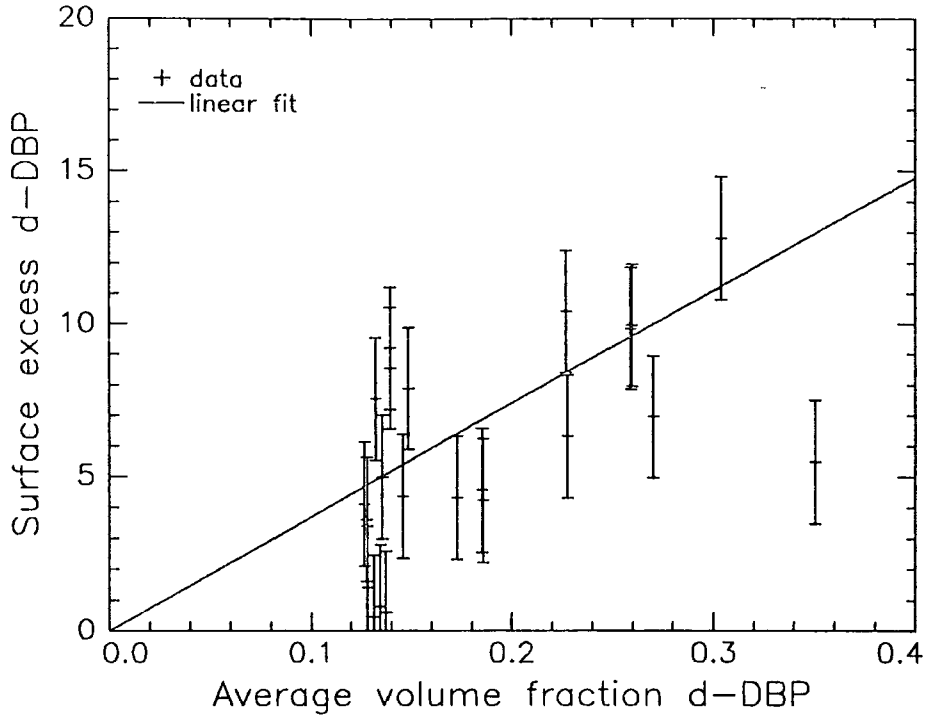

Figure 8.13a: Surface excess vs ϕ_{av} calculated from the two layer model fits to the reflectivity data. Line is a straight line fit with the intercept fixed at zero.

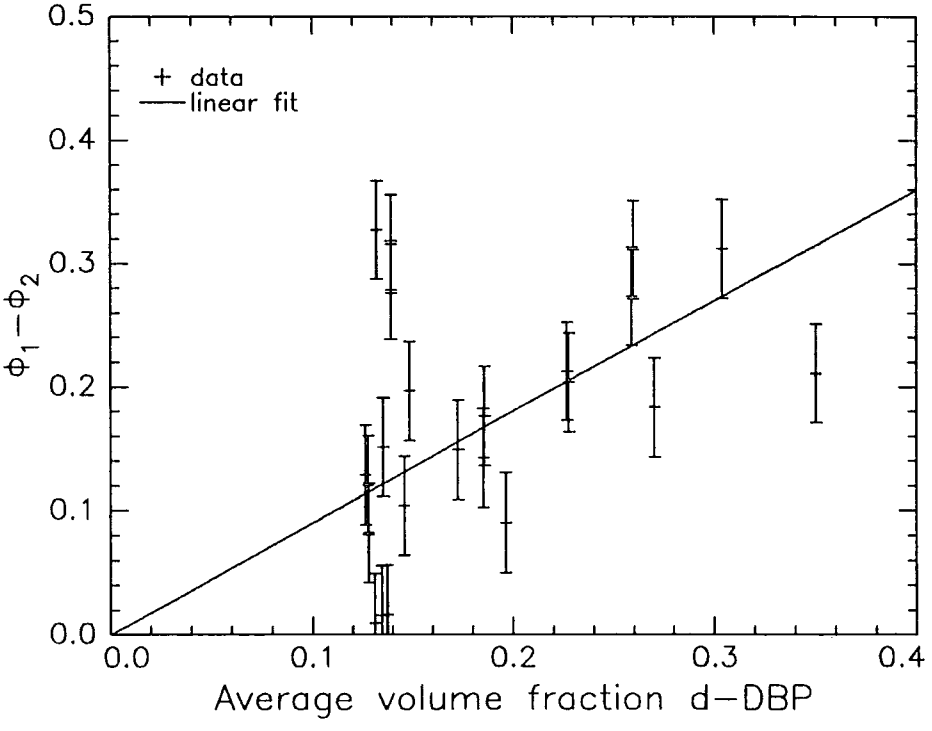

Figure 8.13b: (ϕ_1 - ϕ_2) vs ϕ_{av} calculated from the two layer model fits to the reflectivity data. Line is a straight line fit with the intercept fixed at zero.

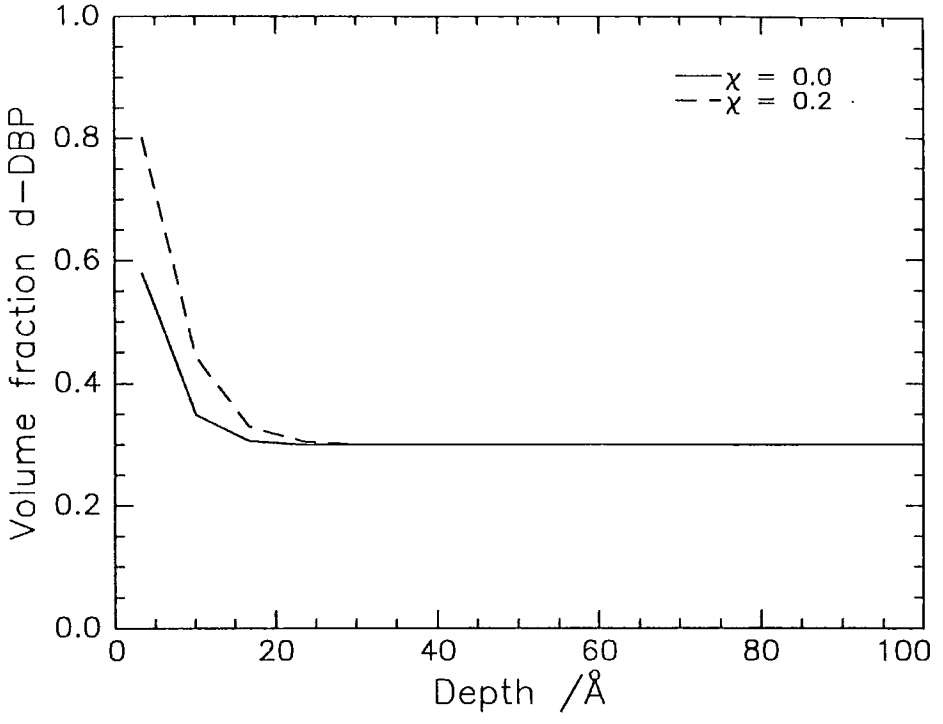

Figure 8.14: Self Consistent field models of the surface excess of d-DBP in polystyrene, with $\Delta\gamma$ = 7.6 mJ m^{-2} and N = 100 for the polymer and 3 for the d-DBP.

8.4 Conclusions

Neutron reflectometry and attenuated total reflection infra red spectrometry both indicate that the average volume fraction of d-DBP in a ~800Å polystyrene film decreases as a function of time after the film is spun cast. The characteristic time of this decrease is around 24 hours and the decrease appears to stop when the average volume fraction of d-DBP reaches ~0.12. It was found that for films with an initial volume fraction of 0.10 d-DBP lost no d-DBP over a period of 17 days, within the experimental error. Calculations show that this level of d-DBP is far higher than would be expected at thermodynamic equilibrium. The lack of a depletion zone near the surface of the film implies that the decrease in ϕ_{av} was determined by the rate of evaporation α, a value of $\alpha = 1.0\times10^{-10}$ cm^3 s^{-1} was calculated.

Neutron reflectometry results showed that there was a small excess of d-DBP at the air-polymer interface, this excess was confined to a layer ~30Å thick. This excess can be modelled broadly using the self consistent field theory of Shull with values of the surface energy difference between dibutyl phthalate and polystyrene found in the literature.

8.5 References for Section 8.

1 . R.W. Richards, unpublished results.

2 . J.K. Sears, N.W. Touchette in 'Encyclopedia of Polymer Science and Engineering Supplement Volume', J. Wiley & Sons, 1989.

3 . J. Crank, 'The Mathematics of Diffusion 2nd ed.', Oxford Science Publications, 1975.

4 . E. Southern, A.G. Thomas, *Transactions of the Faraday Society*, 63, 1967, 1913.

5 . J.S. Vrentas, J.L. Duda in 'Encyclopedia of Polymer Science and Engineering Vol. 5 2nd ed.', J. Wiley & Sons, 1986.

6 . G.T. Fieldson, T.A. Barbari, *Polymer*, 34(6), 1993, 1146.

7 . D.W. Van Krevelen, 'Properties of Polymers 3rd ed.', Elsevier, 1990.

8 . J. Zhang, C.H. Wang, *Macromolecules*, 21, 1988, 1811.

9 . J.L. Xia, C.H. Wang, B.Y. Li, *Macromolecules*, 21, 1990, 2739.

10 . S.L. Vrentas, J.L. Duda, *Journal of Polymer Science, Polymer Physics Edition*, 15, 1977, 403.

11 . R.C. Weast, 'CRC Handbook of Chemistry and Physics 68th ed.', CRC Press, 1988.

12 . X. Li, M.D. Foster, Poster at 'MacroAkron `94' (35th IUPAC Symposium on Macromolecules, Akron, Ohio, 1994).

13 . J. Brandrup, E.H. Immergut, 'Polymer Handbook 3rd ed.', J. Wiley & Sons, 1989.

9. Conclusions and Further Work

Results from each of the systems studied have been summarised at the end of each section, so the intention now is to draw some general conclusions and make suggestions for further work.

The χ data for the syndiotactic d-PMMA/h-PMMA blends exhibited the composition variation predicted for 'repulsive' blends. Further experiments in this area would include a more in depth study of the variation of χ with chain length disparity, an ideal experiment would be to use a fixed temperature ~440K and volume fraction d-PMMA ~0.5 and vary the ratio N_D:N_H from 1:100 to 1:1 keeping the h-PMMA molecular weight fixed at ~1,000,000. The motivation for this work would be to provide a further test for new theories of polymer - polymer thermodynamics. The 'surface enrichment' study of h-PMMA/d-PMMA shows the importance of knowing the thermodynamics of a blend and screening samples using other techniques before embarking on a detailed study using NR. Depending on the results of further SANS work on d-PMMA/h-PMMA it way be worth seeking surface enrichment in symmetric ($N_H = N_D$) high molecular weight blends of d-PMMA/h-PMMA.

The χ data for the PEO/PMMA blends exhibited composition dependence that would be expected for an 'attractive' blend. It would be useful to examine the PEO/PMMA system over a wider range of compositions, but a more important question would be to find the temperature dependence of χ at single composition ($\phi_{d\text{-}PEO} = 0.25$) since there is a discrepancy in this between this work and the work of Russell. As a precautionary note, the exclusion of air bubbles from the SANS samples is critical, this may be done successfully by holding the samples under vacuum during all of the pressing procedure and perhaps keeping samples in a dry atmosphere after fabrication. Note that air bubbles were not apparent in the 'as prepared' samples.

The study of the surface enrichment behaviour of PEO/PMMA can best be described as an 'interesting start', it would appear that the behaviour observed is not described by current theory. This system is worthy of further study because both components can be prepared with good control of molecular weight and narrow molecular weight distributions in both hydrogenous and deuterated form, clearly the hope would be to drive further theoretical developments using results from this blend.

However the extreme roughness of the samples makes the analysis of the NR data difficult. It would be useful to re-examine the d-PEO/h-PMMA blend using NR in the melt state where the air - polymer interface should be rather smoother and with NRA optimised to the polymer - substrate interface.

Clearly d-PS(F), d-PS(F2) / h-PS systems have produced the most complete results - this is in large part due to the substantial amount of information on the surface enrichment and thermodynamics of the d-PS/h-PS blends that is in the literature. It was gratifying to find that the SCF theory was able to describe the brush forming behaviour of these blends, using data in the literature on surface energy and solubility parameters. However it should be noted that the effect of the perfluorohexane end group is relatively small when compared to the size of the effect driven by surface energy differences in heteropolymer blends. Work is already in progress to study the effect of the molecular architecture of the d-PS(F), i.e the location of the fluorinated group(s), on surface segregation behaviour of systems of this sort.

In the d-DBP/PS system an attempt was made to apply some of the methods and ideas from the other systems to an industrially more relevant situation, the use of d-DBP was imposed due to considerations of ease (and cost) of synthesis. The results show some promise for future work on this system, one possibility now that the feasibility of these experiments has been shown would be to try to synthesise a higher molecular weight perdeuterated phthalate, this would reduce problems of evaporation loss and possibly allow the use of high vacuum techniques (such as XPS or SIMS), if the sample were sufficiently cooled.

10. Appendices

10.1 Glossary of Symbols

Roman alphabet

a	statistical segment length
a_T	parameter in the WLF equation
A	parameters of fits to χ of the form $\chi = A+B/T$
A	unit area (Section 8.3 only)
A_{atr}	infra red absorption in ATR mode
A_A	normalisation constant for ϕ_A in SCF theory
A_B	normalisation constant for ϕ_B in SCF theory
$A_{C\text{-}D}$	integration of C-D stretch peak IR absorption band
$A_{C\text{-}H}$	integration of C-H stretch peak IR absorption band
$A_{C\text{-}X}$	either $A_{C\text{-}D}$ or $A_{C=O}$
$A_{C=O}$	integration of C=O stretch peak IR absorption band
b	cube root of the segmental volume, V_m
b	single atom nuclear scattering length (Section 3.1.1 only)
b_i	nuclear scattering length of component i, (including i = H, D, A, B)
B	parameters of fits to χ of the form $\chi = A+B/T$
c	parameter arising from the Clausius - Clapyeron equation
C^0_1	parameter in the WLF equation
C^0_2	parameter in the WLF equation
C_t	concentration at time, t.
C_∞	concentration at $t = \infty$
d	spacing for Bragg peak
d_P	penetration depth for ATR spectroscopy
d_e	effective sample thickness for ATR
d_s	sample detector distance in neutron reflectometry
$\frac{d\sigma}{d\Omega}$	number of neutrons scattered per unit time into solid angle $d\Omega$
D^o	parameter used for describing D_s as a function of M_w and T

D_G	average distance between graft points
D_M	mutual diffusion coefficient
D_S	self diffusion coefficient
E_{atr}	electric field amplitude in ATR crystal
E_D	activation energy for diffusion
E_{max}	most probable energy in Maxwell - Boltzmann distribution
E_{sam}	electric field amplitude in sample
E_o	electric field amplitude at ATR crystal / sample interface
$f_s(\phi_{air})$	surface free energy contribution
g	coefficient in Taylor series expansion for $f_s(\phi_{air})$
$g_D(R_g, Q)$	Debye function for polymer with radius of gyration R_g
$g'_D(R_g, Q)$	modified Debye function for polydisperse blend
G	crystalline growth rate
h	Planck's constant
h	parameter in Schultz - Zimm distribution (section 2.1 only)
I(Q)	coherent elastic neutron scattering
I	segmental ionisation potential
I_o	incident neutron intensity
I_r	reflected neutron intensity
I_{tot}	total neutron scattering intensity
k_B	Boltzmann constant
k	parameter used for describing D_s as a function of M_w and T
k_0, k_1	neutron wavevector perpendicular to surface in mediums 0 and 1
$\mathbf{k}$	incident wavevector (section 3.1 only)
k′	parameter used for describing D_s as a function of M_w and T
$\mathbf{k}'$	scattered wavevector (section 3.1 only)
K	coefficient in expression $z^*_{eq} = K\phi_B$
k_N	calibration constant for LOQ data
l	total film thickness
L	coefficient in expression $z^*_{eq} = K\phi_B + L\phi_B^2$
L	brush height (section 2.3.2 only)
m	segment molar mass
m_j	rest mass of j (=α, D, p, 3He) (section 3.2 only)

m_n	rest mass of neutron
M	mass loss in evaporation / diffusion type experiment
M_x	mass variable in Schultz - Zimm distribution
M_w	weight average molecular weight
M_n	number average molecular weight
M_j	layer matrix for j^{th} layer in neutron reflectivity optical matrix
M_R	product of layer matrices in neutron reflectivity optical matrix calculations
M_{12}	element of M_R
M_{11}	element of M_R
n	neutron refractive index
n_j	neutron refractive index in layer j (where j = 0, 1, j)
n_{atr}	optical refractive index of ATR crystal (section 3.3 only)
n_L	area of one face of a lattice cell in a self consistent field theory
n_{PS}	optical refractive index for polystyrene
n_{sam}	optical refractive index of a sample (section 3.3 only)
n_{Si}	optical refractive index for silicon
N_A	Avogadro's constant, or degree of polymerisation of component A
N_B	degree of polymerisation of component B
N	weight average degree of polymerisation of the specified component
N	number of nuclei in ensemble (section 3.1.1 only)
N_D	weight average degree of polymerisation of the deuterated component
N_H	weight average degree of polymerisation of the hydrogenous component
N_P	number of data points in a neutron reflectivity dataset
N_S	effective degree of polymerisation for d-DBP
p_o	reference pressure
p_j	parameter of j^{th} layer of neutron reflectivity optical matrix
p_v	vapour pressure of DBP
P	parameter for Schultz - Zimm distribution
P^*	vapour pressure of DBP at known temperature T^*
$q_i(x,j)$	distribution functions in self consistent field theory, (i = A, B1, B2 or i)
$\mathbf{Q}$	true scattering vector (section 3.1 only)
Q	commonly named 'scattering vector' (= $\lvert\mathbf{Q}\rvert$)
r	ratio N/N_s (section 8 only)

$\mathbf{r}$	general position vector
r_{01}	Fresnel reflectivity coefficient between layers 0 and 1.
r_j	modified Fresnel reflectivity coefficient for j^{th} layer of neutron reflectivity optical matrix
$\mathbb{R}$	atom position vector (section 3.1.1 only)
$\mathbb{R}_i$	atom position vector of i^{th} atom in ensemble (section 3.1.1 only)
R	neutron reflectivity or universal gas constant
R_{gD}	radius of gyration of the deuterated component
R_{gH}	radius of gyration of the hydrogenous component
R_g	radius of gyration of a specified component
R_o	equilibrium length used in ΔG_{el} calculation (section 2.3.2 only)
R_m	model reflectivity (section 3.1.2 only)
R_D	measured reflectivity (section 3.1.2 only)
s1	height of slit 1 in neutron reflectometer
s2	height of slit 1 in neutron reflectometer
S(Q)	scattering structure factor
S_o	unperturbed mean squared end to end distance
t	reduced parameter used in surface enrichment theory (section 2.2)
t	annealing time or time after spin casting
t_{actual}	actual annealing time
t_c	characteristic time for formation of surface excess
t_{ref}	annealing time at a reference temperature
T	absolute temperature (in K)
T^*	temperature at which DBP as vapour pressure P^*
T_c	crystallisation temperature
T_g	glass transition temperature
T_m	melting temperature
T_s	spinodal temperature
u	the product R_gQ
v	velocity
V	segmental volume for a specified component
v_A, v_B	segmental volumes of components A and B
v_o	reference volume
V(r)	Fermi pseudo potential

V_D, V_H	segmental volume for deuterated and hydrogenous components
V_L	volume of lattice cell in self consistent field theory
v_{max}	most probable velocity of neutron in Maxwell - Boltzmann distribution
V^i_j	velocities of particles j (= α, D, p, 3He) in i (= cm or lab) frame of reference where (section 3.2 only)
w	parameter in Tanh profile fit
w´	component of mean field
$w_i(x)$	mean fields in self consistent field theory (i = A, B, ext, i, Ik, k)
$w_i^o(x)$	component of mean field (i = A, B)
x	lattice layer number in self consistent field theory
x_n	number of lattice layers in SCF model
z	distance from air-polymer interface
z_c	lattice coordination number
z_n	thickness of the n^{th} layer of a multilayer model
z_{off}	parameter in Tanh profile fit
z^*	surface excess
z^*_{air}	surface excess at polymer - air interface
z^*_{dep}	'size' of the depletion zone
z^*_{eq}	equilibrium surface excess
z^*_o	surface excess at t = 0.
z^*_{si}	surface excess at polymer - substrate interface

Greek Symbols

α	evaporation rate (Section 8 only)
α	parameter used for describing D_s as a function of M_w and T
α_D	polarisability of a deuterated segment
α_H	polarisability of a hydrogenous segment
α_{nra}	sample / beam angle in NRA experiment
α_λ	infra red absorption coefficient at wavelength, λ.
β	free energy of end attachment

β_j	neutron optical path length in j^{th} layer of neutron reflectivity optical matrix
λ	parameter for Schultz - Zimm distribution (Section 5.1.3 only)
λ	wavelength of a neutron or infrared radiation
$\delta(x)$	Dirac delta function
δ_{PS}	solubility parameter for polystyrene
δ_{PTFE}	solubility parameter for poly (tetrafluoroethylene)
δ_s	thickness of end confinement region in self consistent field theory
ΔG	Gibbs free energy of a blend, including surface contributions
ΔG_{el}	elastic contribution to the Gibbs free energy of a brush
ΔG_m	Gibbs free energy of mixing for a binary polymer blend
ΔH_{vap}	Enthalpy of vaporisation
ΔR_D	uncertainty in measured reflectivity (section 3.1.2 only)
ΔQ	resolution measured Q (section 3.1.2 only)
$\Delta\gamma$	surface energy difference
$\Delta\mu$	chemical exchange potential
ε	Freed and Bawendi effective interaction energy
ε_{ij}	nearest neighbour pair potentials where i = A, B, j = A, B.
ζ	parameter in self consistent field theory - inversely proportional to compressibility
θ	angle of reflection in neutron reflectometry
θ_j	angle of neutron beam relative to surface in j^{th} layer for neutron reflectivity optical matrix calculation (where j = 0, 1, j)
θ_{atr}	incident angle for ATR
θ_c	critical angle (neutrons or electromagnetic radiation)
θ_{nra}	beam / detector angle in NRA experiment
2θ	scattering angle for neutron techniques
κ	compressibility
$\bar{\mu}_b$	modified chemical potential (section 2.3.1 only)
μ_f	chemical potential of DBP in film
μ^o_f	reference chemical potential for DBP in film
μ_v	chemical potential of DBP vapour

μ^{o}_{v}	reference chemical potential for DBP vapour
ξ	concentration fluctuation correlation length
ξ	concentration fluctuation correlation length at coexistence curve
ξ	decay length for exponential function in PHOENIX (section 4.3.3) only
ρ	mass density
ρ_N	nuclear scattering length density
ρ'_N	Fourier transform of nuclear scattering length density (as a function of depth)
σ	dimensionless grafting density
σ_a	nuclear absorption cross section
σ_i	nuclear incoherent cross section
σ_n	roughness of n^{th} interface of a multilayer model
τ	parameter for Schultz - Zimm distribution (Section 5.1.3 only)
ϕ	volume fraction of the deuterated component or specified component
ϕ	azimuthal angle in SANS (section 4.2 only)
ϕ', ϕ''	composition of coexisting components in a binary blend
ϕ_0	average volume fraction at t = 0
ϕ_1	parameter in Tanh profile fit
ϕ_∞	average volume fraction at t = ∞
ϕ_{air}	maximum volume fraction of deuterated component near the air - polymer interface
ϕ_{av}	integrated average volume fraction
ϕ_d	volume fraction of deuterated component in the bottom of the depletion layer
ϕ_n	volume fraction of deuterated component in the n^{th} layer of a multilayer model
ϕ_t	average volume fraction at time, t.
ϕ_{Si}	maximum volume fraction of deuterated component near the polymer - substrate interface
$\phi_i(x)$	volume fractions of component i in lattice layer x (where i = A, B) (section 2.3.1 only)
ϕ_A^{bulk}, ϕ_B^{bulk}	bulk volume fractions of components A and B (section 2.3.1)

ϕ_B	bulk volume fraction
ϕ_{Si}	maximum volume fraction of deuterated component near the polymer - substrate interface
χ	effective Flory - Huggins interaction parameter
χ^2	the normalised χ^2 fit parameter
χ_b	value of χ at the coexistence curve
χ_d	contribution to χ arising from mixing at constant volume
χ_{de}	enthalpic contribution to χ_d
χ_{ds}	entropic contribution to χ_d
χ^b_e	bulk interaction contribution to attachment energy
χ^s_e	surface interaction contribution to attachment energy
χ_{FH}	the Flory - Huggins interaction parameter
χ_S	the calculated value of χ_{FH} at the spinodal temperature
χ_v	contribution to χ arising from volume change

10.2 Additional Data

χ data for h-PMMA/d-PMMA (section 5.1)

	$\phi_{d\text{-PMMA}}$			
T/K	0.09	0.29	0.49	0.70
408	1.52E-02	4.74E-03	1.26E-03	1.69E-04
435	2.28E-03	-1.02E-03	-1.19E-03	-1.29E-03
453	-2.28E-03	-3.80E-03	-4.07E-03	-6.47E-04
473	-6.84E-03	-1.18E-02	-1.10E-02	-3.96E-03

Table 10.1: χ values obtained from Ornstein - Zernike plots for syndiotactic d-PMMA / h-PMMA blend B.

	$\phi_{d\text{-PMMA}}$		
T/K	0.09	0.29	0.49
298	1.02E-03	1.55E-04	2.43E-04
408	9.10E-04	9.00E-05	2.70E-04
435	1.08E-03	2.10E-04	3.08E-04
453	9.10E-04	1.20E-04	1.40E-04

Table 10.2: χ values obtained using PULLET1 for syndiotactic d-PMMA / h-PMMA blend D.

	$\phi_{d\text{-PMMA}}$		
T/K	0.25	0.50	0.75
408	-1.13E-02	-7.14E-03	-4.72E-03
435	-1.18E-02	-5.68E-03	-4.52E-03
453	-1.17E-02	-5.54E-03	-4.04E-03
473	-1.98E-02	-8.57E-03	-5.71E-03

Table 10.3: χ values obtained using PULLET3 for isotactic d-PMMA / h-PMMA blend I.

χ data for PEO/PMMA (section 6.1)

	$\phi_{d\text{-}PEO}$			
T/K	0.101	0.151	0.199	0.247
423	-1.69E-02	-1.81E-02	-1.81E-02	-1.88E-02
438	-1.79E-02	-1.82E-02	-1.75E-02	-1.78E-02
458	-1.98E-02	-1.88E-02	-1.83E-02	-1.84E-02
473	-2.91E-02	-1.99E-02	-2.12E-02	-2.01E-02

Table 10.4: χ values for d-PEO/h-PMMA blends obtained using PULLET4, fixed radii of gyration, fitted χ, residual background and normalisation constant.

	$\phi_{h\text{-}PEO}$			
T/K	0.126	0.186	0.239	0.272
423	-6.97E-03	-9.63E-03	-9.28E-03	-9.69E-03
438	-8.52E-03	-1.05E-02	-9.94E-03	-1.08E-02
458	-1.37E-02	-1.42E-02	-1.14E-02	-1.18E-02
473	-1.87E-02	-1.53E-02	-1.26E-02	-1.31E-02

Table 10.5: χ values for h-PEO/d-PMMA blends obtained using PULLET4, fixed radii of gyration, fitted χ, residual background and normalisation constant.

10.3 Publications, Lectures and Conferences Attended.

Publications

I. Hopkinson, F,T. Kiff, R.W. Richards, S.M. King, H. Munro, *Polymer*, 35(8), 1994, 1722.

I. Hopkinson, F,T. Kiff, R.W. Richards, S. Affrossman, M. Hartshorne, R.A. Pethrick, H. Munro, J.R.P. Webster, *Macromolecules*, in press.

Lectures

UNIVERSITY OF DURHAM
Board of Studies in Chemistry

1991

October 17	Dr. J.A.Salthouse, (University of Manchester). Son et Lumiere-A Demonstration Lecture.
October 31	Dr. R.Keeley, (Metropolitan Police Forensic Science). Modern Forensic Science.
November 6	Prof. B.F.G.Johnson, (Edinburgh University). Cluster-surface Analogies.
November 7	Dr. A.R.Butler, (St.Andrews University). Traditional Chinese Herbal Drugs: A Different Way of Treating Disease.
November 13	Prof. D.Gani, (St.Andrews University). The Chemistry of PLP Dependent Enzymes.
November 20	Dr. R.More O'Ferrall, (University College, Dublin). Some Acid-Catalysed Rearrangements in Organic Chemistry.
November 28 SCI Lecture	Prof. I.M.Ward, (IRC in Polymer Science, Leeds University). The Science and Technology of Orientated Polymers.
December 4	Prof. R.Grigg, (Leeds University). Palladium-Catalysed Cyclisation and Ion-Capture Processes.
December 5	Prof. A.L.Smith, (Ex. Unilever). Soap, Detergents and Black Puddings.
December 11	Dr. W.D.Cooper, (Shell Research). Colloid Science: Theory and Practice.

1992

January 22	Dr. K.D.M.Harris, (St.Andrews University). Understanding the Properties of Solid Inclusion Compounds.
January 29	Dr. A.Holmes, (Cambridge University). Cycloaddition Reactions in the Service of the Synthesis of Piperidine and Indolizidine Natural Products.
January 30	Dr. M.Anderson, (Sittingbourne, Shell Research). Recent Advances in the Safe and Selective Chemical Control of Insect Pests.
February 12	Prof. D.E.Fenton, (Sheffield University). Polynuclear Complexes of Molecular Clefts as Models for Copper Biosites.
February 13	Dr. J.Saunders, (Glaxo Group Research Limited). Molecular Modelling in Drug Discovery.
February 19	Prof. E.J.Thomas, (University of Manchester). Applications of Organostannanes to Organic Synthesis.
February 20 Musgrave Lecture	Prof. E.Vogel, (University of Cologne). Porphyrins: Molecules of Interdisciplinary Interest.
February 25 Tilden Lecture:	Prof. J.F.Nixon, (University of Sussex). Phosphaalkynes: New Building Blocks in Inorganic and Organometallic Chemistry.
February 26	Prof. M.L.Hitchman, (Strathclyde University). Chemical Vapour Deposition.
March 5	Dr. N.C.Billingham, (University of Sussex). Degradable Plastics-Myth or Magic?.
March 11	Dr. S.E.Thomas, (Imperial College). Recent Advances in Organoiron Chemistry.
March 12	Dr. R.A.Hann, (ICI Imagedata). Electronic Photography-An Image of the Future.
March 18	Dr. H.Maskill, (Newcastle University). Concerted or Stepwise Fragmentation in a Deamination-type Reaction.
April 7	Prof. D.M.Knight, (University of Durham). Interpreting Experiments: The Beginning of Electrochemistry.
May 13	Dr. J-C.Gehret, (Ciba Geigy, Basel). Some Aspects of Industrial Agrochemical Research.
October 15	Dr. M.Glazer and Dr.S.Tarling, (Oxford University and Birbeck College). It Pays to be British!- The Chemist's Role as an Expert Witness in Patent Litigation.
October 20	Dr. H.E.Bryndza, (Du Pont Central Research). Synthesis, Reactions and Thermochemistry of Metal(alkyl)cyanide Complexes and Their Impact on Olefin Hydrocyanation Catalysis.

October 22 **Ingold-Albert Lecture**	Prof. A.G.Davies, (University College, London). The Behaviour of Hydrogen as a Pseudometal.
October 28	Dr. J.K.Cockroft, (Durham University). Recent Developments in Powder Diffraction.
October 29	Dr. J.Emsley, (Imperial College, London). The Shocking History of Phosphorus.
November 4	Dr. T.Kee, (University of Leeds). Synthesis and Coordination Chemistry of Silylated Phosphites.
November 5	Dr. C.J.Ludman, (University of Durham). Explosions, A Demonstration Lecture.
November 11	Prof. D.Robins, (Glasgow University). Pyrrolizidine Alkaloids: Biological Activity, Biosynthesis and Benefits.
November 12	Prof. M.R.Truter, (University College, London). Luck and Logic in Host-Guest Chemistry.
November 18	Dr. R.Nix, (Queen Mary College, London). Characterisation of Heterogeneous Catalysts.
November 25	Prof. Y.Vallee, (University of Caen). Reactive Thiocarbonyl Compounds.
November 25	Prof. L.D.Quin, (University of Massachusetts, Amherst) Fragmentation of Phosphorus Heterocycles as a Route to Phosphoryl Species with Uncommon Bonding.
November 26	Dr. D.Humber, (Glaxo, Greenford). AIDS - The Development of a Novel Series of Inhibitors of HIV.
December 2	Prof. A.F.Hegarty, (University College, Dublin). Highly Reactive Enols Stabilised by Steric Protection.
December 2	Dr. R.A.Aitkin, (University of St.Andrews). The Versatile Cycloaddition Chemistry of $Bu_3P.CS_2$.
December 3 **SCI Lecture**	Prof. P.Edwards, (Birmingham University). What is a Metal?
December 9	Dr. A.N.Burgess, (ICI Runcorn). The Structure of Perfluorinated Ionomer Membranes.

1993

January 20	Dr. D.C.Clary, (University of Cambridge). Energy Flow in Chemical Reactions
January 21	Prof. L.Hall, (University of Cambridge). NMR - A Window to the Human Body.

January 27	Dr. W.Kerr, (University of Strathclyde). Development of the Pauson-Khand Annulation Reaction : Organocobalt Mediated Synthesis of Natural and Unnatural Products.
February 3	Prof. S.M.Roberts, (University of Exeter). Enzymes in Organic Synthesis.
February 10	Dr. D.Gillies, (University of Surrey). NMR and Molecular Motion in Solution.
February 11 **Tilden Lecture**	Prof. S.Knox, (Bristol University). Organic Chemistry at Polynuclear Metal Centres.
February 17	Dr. R.W.Kemmitt, (University of Leicester). Oxatrimethylenemethane Metal Complexes.
February 18	Dr. I.Fraser, (ICI, Wilton). Reactive Processing of Composite Materials.
February 22	Prof. D.M.Grant, (University of Utah). Single Crystals, Molecular Structure and Chemical-Shift Anisotropy
February 24	Prof. C.J.M.Stirling, (University of Sheffield). Chemistry on the Flat-Reactivity of Ordered Systems.
March 3	Dr. K.J.P.Williams, (BP). Raman Spectroscopy for Industrial Analysis.
March 10	Dr. P.K.Baker, (University College of North Wales, Bangor). An Investigation of the Chemistry of the Highly Versatile 7-Coordinate Complexes $[MI_2(CO)_3(NCMe)_2]$ (M=Mo,W).
March 11	Dr. R.A.Jones, (University of East Anglia). The Chemistry of Wine Making
March 17	Dr. R.J.K.Taylor, (University of East Anglia).] Adventures in Natural Product Synthesis.
March 24	Prof. I.O.Sutherland, (University of Liverpool). Chromogenic Reagents for Chiral Amine Sensors.
May 13 **Boys-Rahman Lecture**	Prof. J.A.Pople, (Carnegie-Mellon University Pittsburgh). Applications of Molecular Orbital Theory.
May 21	Prof. L.Weber, (University of Bielefeld). Metallo-phospha Alkenes as Synthons in Organometallic Chemistry
June 1	Prof. J.P.Konopelski, (University of California, Santa Cruz). Synthetic Adventures with Enantiomerically Pure Acetals.
June 7	Prof. R.S.Stein, (University of Massachusetts). Scattering Studies of Crystalline and Liquid Crystalline Polymers.
June 16	Prof. A.K.Covington, (University of Newcastle). Use of Ion Selective Electrodes as Detectors in Ion Chromatography.
June 17	Prof. O.F.Nielsen, (H.C.Ørsted Institute, University of Copenhagen). Low-Frequency IR - and Raman Studies of Hydrogen Bonded Liquids.
October 4	Prof. F.J.Fehler, (University of California at Irvine).

	Bridging the Gap Between Surfaces and Solution with Sessilquioxanes.
October 20	Dr. P.Quayle, (University of Manchester). Aspects of aqueous ROMP Chemistry.
October 23	Prof. R.Adams, (University of S.Carolina) The Chemistry of Metal Carbonyl Cluster Complexes Containing Platinum and Iron, Ruthenium or Osmium and the Development of a Cluster Based Alkyne Hydrogenation Catalyst
October 27	Dr. R.A.L.Jones, (Cavendish Laboratory) Perambulating Polymers
November 10	Prof. M.N.R.Ashfold, (University of Bristol) High Resolution Photofragment Translational Spectroscopy: A New way to Watch Photodissociation
November 17	Dr. A.Parker, (Laser Support Facility) Applications of Time Resolved Resonance Raman Spectroscopy to Chemical and Biochemical Problems
November 24	Dr. P.G.Bruce, (University of St. Andrews) Synthesis and Applications of Inorganic Materials
December 1	Prof. M.A.McKervy, (Queens University, Belfast) Functionalised Calixerenes
January 19	Prof. O.Meth-Cohen, (Sunderland University) Friedel's Folly Revisited
January 26	Prof. J.Evans, (University of Southampton) Shining Light on Catalysts
February 2	Dr. A.Masters, (University of Manchester) Modelling Water without Using Pair Potentials
February 9	Prof. D.Young, (University of Sussex) Chemical and Biological Studies on the Coenzyme Tetrahydrofolic Acid
February 16	Dr. R.E.Mulvey, (University of Strathclyde) Structural Patterns in Alkali Metal Chemistry
February 23	Prof. P.M.Maitlis FRS, (University of Sheffield) Why Rhodium in Homogeneous Catalysis?
March 2	Dr. C.Hunter, (University of Sheffield) Non Covalent Interactions between Aromatic Molecules
April 20	Prof. P.Parsons, (University of Reading) New Methods and Strategies in Natural Product Synthesis

IRC in Polymer Science and Technology International Seminar Series.

1992

March 17	Prof. Sir S.Edwards, (Cavendish Laboratory, University of Cambridge), at Leeds University. Phase Dynamics and Phase Changes in Polymer Liquid Crystals
March 25	Prof. H.Chedron, (Hoechst AG, Frankfurt am Main), at Durham University. Structural Concepts and Synthetic Methods in Industrial Polymer Science.
May 11	Prof. W.Burchard, (University of Freiburg), at Durham University. Recent Developments in the Understanding of Reversible and Irreversible Network Formation.
September 21	Prof. E.L.Thomas, (MIT, Cambridge, Massachusetts), at Leeds University. Interface Structures in Copolymer-Homopolymer Blends.

1993

March 16	Prof. J.M.G.Cowie, (Heriot-Watt University) at Bradford University High Technology in Chains : The Role of Polymers in Electronic Applications and Data Processing
April 1	Prof. H.W.Speiss, (Max-Planck Institut for Polymerforschung, Mainz), at Durham University. Multidimensional NMR Studies of Structure and Dynamics of Polymers.
June 2	Prof. F.Ciardelli, (University of Pisa), at Durham University. Chiral Discrimination in the Stereospecific Polymerisation of α-olefins.
June 8	Prof. B.E.Eichinger, (BIOSYM Technologies Inc. San Diego), at Leeds University. Recent Polymer Modeling Results and a Look into the Future.
July 6	Prof. C.W.Macosko, (University of Minnesota, Minneapolis), at Bradford University. Morphology Development in Immiscible Polymer-Polymer Blending.

Conferences

July 1991
Polymer Surfaces and Interfaces II, Durham University.

December 1991
Polymer Blends and Mixtures, SCI, London.

April 1992
UK Neutron Beam and Muon Beam Users' Meeting

April 1992
Macro Group (UK) Family Meeting, Durham University.

April 1992
High Polymer Research Group ,Mortenhampstead

September 1992
IRC Club Meeting, Leeds University.

April 1993
Macro Group (UK) Family Meeting, Lancaster University.

July 1993
The Polymer Conference, Cambridge University.

September 1993
Neutron Scattering 1993, Sheffield University.

September 1993
Polymers at Interfaces, Bristol University

September 1993
IRC Club Meeting, Durham University.

April 1994
Macro Group (UK) Family Meeting, Birmingham University.

July 1994
MacroAkron '94 IUPAC Meeting, University of Akron, Ohio, USA.

September 1994
Faraday Discussion - Polymers at Surfaces and Interfaces, Bristol University

September 1994
IRC Club Meeting, Leeds University.

10.4 Computer Programs

The computer programs on the following pages are written in VAX FORTRAN.

PHOENIX

```
C
C  PHOENIX , this program replaces Narcissus, Kraftwerk and Puddles.
C  It utilises the Abeles method for calculating neutron reflectivity
C  profiles.  Functions available include modeling, fitting of data,
C  and generation of contour plot and 1-D scan data.
C  Fitting is via the FITFUN utility.
C
C  WARNING: NAMES, TEXT etc. are NOT character variables, they are
C  INTEGERS!!
C
C  Ian Hopkinson 6th July 1992
C
C  Version as of 6th September 1992 uses error weighted fit, and the Beaglehole
C  and Law routine does not yet work.  There are cop outs in the Abeles
C  routine for when temp1=temp2=0 and when pl1=pm=0 (when calculating rm)
C
C  7/9/92 added weighting by fractional error.
C  8/9/92 modified exponential profile to include BETA power, corrected
C       mistake in MODL that had the functional forms mixed up!
C  9/9/92 Added thingy to show work was in progress during 2d calculations
C  27/11/92 Added fiddle to Model that sets yruse(i) to 1.0 so that F(i)
C        can be calculated.
C  15/1/93  Added silicon roughness to the functional form models.
C        Changed READIN so that it treats histogram data formats properly
C        this shouldn't make much difference as long the interval between
C        data points is small.
C  16/3/93 Put in a profile flipper so that functional form profiles can be
C       at the air or silicon surfaces
C  17/11/93 Changed readin routine slightly so that negetive reflectivities
C        don't bugger things up (negetive reflectivities occasionally occur
C        at high Q after background subtraction)
C  9/4/94   Re-wrote the functional form profile part, expunged the Beaglehole
C              and Law 'linear gradient' routine which never seemed to work anyway.
C              And added a READIN routine for VOLFMEM format data files, as long
C              as have the .DEV extension.
C  3/3/94   Added a bit to the model reflectivity so that you can generate
C              R Vs Q profiles from *.map files generated by VOLFMEM
C  26/7/94  Changed multilayer model section such that all layers are indep
C        rather than fixing the total thickness
C  29/7/94  Inserted an addition to functional form models to put SiO2 layer
C        15A nsld=3.676e-6.
C
C
            PROGRAM PHOENIX
C
C  Set up, mainly for FITFUN routine.
C
            EXTERNAL READIN,REFL
            REAL*4 PARM(20),VERP,QMIN,QMAX,RESULT(3,260)
            REAL*4 XUSE(300),YUSE(300),YRUSE(300),F(300),YCALC(300),CHI2
            REAL*4 P1LOWER,P2LOWER,P1UPPER,P2UPPER,TEMP,P1STEPSIZE,P2STEPSIZE
            INTEGER INTTY,IOUTTY,NPARAS,TYPE,NUMBER,OPER,QNUM,I,LOOP1,LOOP2
            INTEGER LOOP3,P1SCAN,P2SCAN,P1STEP,P2STEP,COUNT,INP,AIR
            CHARACTER ANS*1,FILNAM*30,DFILE*34,LFILE*34
            COMMON/TITLES/NAMES(20),TX(5),TY(5),NPARAS
            COMMON/WORK/W(3066)
            COMMON/VERSION/VERP
            COMMON/IO/INTTY,IOUTTY
            COMMON/MODEL/TYPE,NUMBER,AIR
            DOUBLE PRECISION NAMES,THICK(4),VOLFR(4),INTFC(4)
            DATA NAMES/'rho air ','rho sub ','rho h   ','rho d   ','resol   '
     &  ,15*'      '/
            DATA PNAM/'BIRD'/
            DATA TX/'Q /A','^-1 ',3*'   '/
            DATA TY/'LOG1','0 (R','efle','ctiv','ity)'/
            DATA THICK/'Thick 1 ','Thick 2 ','Thick 3 ','Thick 4 '/
            DATA VOLFR/'Vol fra1','Vol fra2','Vol fra3','Vol fra4'/
            DATA INTFC/'Interfc1','Interfc2','Interfc3','Interfc4'/
            VERP=1.0
            INTTY=5
            IOUTTY=6
C
C  PARM(1) is the nsld of air
C  PARM(2) is the nsld of the substrate (silicon))
C  PARM(3) is the nsld of the H-polymer        )--> See ref(1)
C  PARM(4) is the nsld of the D-polymer        )
C  PARM(5) is the instrument resolution
C  All the other parameters are dependent on the model used
C
            PARM(1)=0.0
            PARM(2)=2.095E-6
            PARM(3)=1.034E-6
            PARM(4)=6.792E-6
            PARM(5)=7.0
C
C  Start up screen, title etc
C
            WRITE(6,100)VERP
            WRITE(6,110)
            WRITE(6,120)
```

```
      WRITE(6,130)
      WRITE(6,140)
      WRITE(6,160)
      WRITE(6,170)
      WRITE(6,150)
10    READ(5,*)TYPE,NUMBER
      IF ((TYPE.LT.1).OR.(TYPE.GT.3).OR.(NUMBER.LT.1)) THEN
       WRITE(6,190)
       GOTO 10
      ELSEIF ((TYPE.EQ.1).AND.(NUMBER.GT.2)) THEN
       WRITE(6,190)
       GOTO 10
      ELSEIF ((TYPE.EQ.2).AND.(NUMBER.GT.4)) THEN
       WRITE(6,190)
       GOTO 10
      ENDIF
C
C Ask where which interface this functional form is at
C
       IF (TYPE.EQ.1) THEN
       NPARAS=16
       DO 22 I=11,16
        NAMES(I)='Null   '
22    CONTINUE
21    WRITE(6,370)
      WRITE(6,375)
      READ(5,*)INP
      IF (INP.EQ.0) THEN
       AIR=0
       NAMES(11)='Phi/air'
      ELSEIF (INP.EQ.1) THEN
       AIR=1
       NAMES(14)='Phi/Si'
      ELSEIF (INP.EQ.2) THEN
       AIR=2
       NAMES(11)='Phi/air'
       NAMES(14)='Phi/Si'
      ELSE
       WRITE(6,380)
       GOTO 21
      ENDIF
C
C See which model has been picked and adjust NPARAS and NAMES
C
      NAMES(6)='Bloc siz'
      NAMES(7)='Bulk Fra'
      NAMES(8)='Air ruff'
      NAMES(9)='Si  ruff'
      NAMES(10)='Thicknss'
      IF ((AIR.EQ.0).OR.(AIR.EQ.2)) THEN
       IF (NUMBER.EQ.1) THEN
        NAMES(12)='Beta   '
        NAMES(13)='Char.len'
       ELSE
        NAMES(12)='Xoff   '
        NAMES(13)='Width  '
       ENDIF
      ENDIF
      IF ((AIR.EQ.1).OR.(AIR.EQ.2)) THEN
       IF (NUMBER.EQ.1) THEN
        NAMES(15)='Beta   '
        NAMES(16)='Char.len'
       ELSE
        NAMES(15)='Xoff   '
        NAMES(16)='Width  '
       ENDIF
      ENDIF
C
      ELSEIF (TYPE.EQ.2) THEN
       NAMES(6)='Interfc0'
       DO 20 I=1,NUMBER
        NAMES(4+I*3)=VOLFR(I)
        NAMES(5+I*3)=THICK(I)
        NAMES(6+I*3)=INTFC(I)
20    CONTINUE
C
C      NAMES(5+NUMBER*3)='Tot.thic'
C
       NPARAS=6+3*NUMBER
      ENDIF
C
C Choose function required: (Fit, model, scan (1 or 2-D)
C
      WRITE(6,200)
      WRITE(6,210)
40    READ(5,*)OPER
      IF ((OPER.GT.4).OR.(OPER.LT.1)) THEN
       WRITE(6,190)
       GOTO 40
      ENDIF
C
C If fitting call straight to FITFUN. When using EMU-TEK alterations in set
```

```
C up need to be made, on entry: [alt-s] CODE TEK[enter],DAENABLE NO[enter]
C [alt-s]. On leaving the program [alt-s] CODE ANSI[enter], DAENABLE YES[enter]
C [alt-s]. [alt-e] B clears both the grpahics and text screens.
C
          IF (OPER.EQ.1) THEN
           CALL FITFUN(PNAM,READIN,REFL)
           WRITE(6,220)
           CALL FINITT(0,750)
           GOTO 90
          ENDIF
C
C All other functions need PARM's to be entered, using sub. ALTER
C
          CALL ALTER(NPARAS,NAMES,PARM)
C
C The modelling option, first get the range over which to calculate the model
C actually first you're asked if you'd like to load a *.map file from volfmem
C
          IF (OPER.EQ.2) THEN
           WRITE(6,390)
           READ(5,400)ANS
           IF ((ANS.EQ.'Y').OR.(ANS.EQ.'y')) THEN
            TYPE=3
     ENDIF
          WRITE(6,230)
 50   READ(5,*)QMIN,QMAX
          IF ((QMIN.LT.0.0).OR.(QMIN.GT.QMAX)) THEN
           WRITE(6,210)
           GOTO 50
          ENDIF
          WRITE(6,240)
 60   READ(5,*)QNUM
          IF ((QNUM.LT.2).OR.(QNUM.GT.300)) THEN
           WRITE(6,210)
           GOTO 60
          ENDIF
C
C Calculate the appropriate XUSE values
C
          DO 70 I=1,QNUM
           XUSE(I)=QMIN+(I-1)*(QMAX-QMIN)/(QNUM-1)
           YRUSE(I)=1.
 70   CONTINUE
C
C Call REFL and then save the data
C
          CALL REFL(NPARAS,PARM,QNUM,XUSE,YUSE,YRUSE,YCALC,F)
          WRITE(6,250)
          READ(5,310)FILNAM
          OPEN (UNIT=10,FILE=FILNAM,STATUS='NEW')
          WRITE(10,*)QNUM
          DO 80 I=1,QNUM
           YCALC(I)=10**YCALC(I)
           WRITE(10,*)XUSE(I),YCALC(I)
 80   CONTINUE
          CLOSE(10)
          GOTO 90
         ENDIF
C
C Scan functions require data to be loaded.
C
          CALL READIN(NFIT,XUSE,YUSE,YRUSE,TEXT)
C
C SCANS - first collect one set of parameters
C
 11   WRITE(6,260)NPARAS
          READ(5,*)P1SCAN
          IF ((P1SCAN.LT.5).OR.(P1SCAN.GT.NPARAS)) THEN
           WRITE(6,270)
           GOTO 11
          ENDIF
          WRITE(6,280)
          READ(5,*)P1LOWER,P1UPPER
          IF (P1LOWER.GT.P1UPPER) THEN
           P1LOWER=TEMP
           P1LOWER=P1UPPER
           P1UPPER=TEMP
          ENDIF
          WRITE(6,290)
          READ(5,*)P1STEP
          P1STEPSIZE=(P1UPPER-P1LOWER)/P1STEP
C
C Now get a second set of parameters if 2D scan or generate dummy parameters
C for 1D scan.
C
          IF (OPER.EQ.4) THEN
 12   WRITE(6,260)NPARAS
          READ(5,*)P2SCAN
          IF ((P2SCAN.LT.5).OR.(P2SCAN.GT.NPARAS)) THEN
           WRITE(6,270)
           GOTO 12
          ENDIF
```

```
          WRITE(6,280)
          READ(5,*)P2LOWER,P2UPPER
          IF (P2LOWER.GT.P2UPPER) THEN
           P2LOWER=TEMP
           P2LOWER=P2UPPER
           P2UPPER=TEMP
          ENDIF
          WRITE(6,290)
          READ(5,*)P2STEP
          P2STEPSIZE=(P2UPPER-P2LOWER)/P2STEP
C
C Dummy parameters for the 1d scan option
C
         ELSEIF (OPER.EQ.3) THEN
          P2UPPER=PARM(1)
          P2LOWER=PARM(1)
          P2STEP=0
          P2STEPSIZE=0
         ENDIF
C
C Now step through selected parameters, and calculate chi*chi for each model
C
         COUNT=0
         WRITE(6,350)
         DO 13 LOOP1=0,P1STEP
          PARM(P1SCAN)=P1LOWER+P1STEPSIZE*LOOP1
          DO 14 LOOP2=0,P2STEP
           PARM(P2SCAN)=P2LOWER+P2STEPSIZE*LOOP2
C
          CALL REFL(NPARAS,PARM,NFIT,XUSE,YUSE,YRUSE,YCALC,F)
C
C Now calculate chi*chi for this model, weighted by the exp. error.
C This chi2 is not the kosher chi2 what is in the books
C
          CHI2=0.0
          DO 15 LOOP3=1,NFIT
           CHI2=CHI2+F(LOOP3)*F(LOOP3)
 15     CONTINUE
C
          CHI2=CHI2/NFIT
C
C Store the results in the RESULT array
C
          COUNT=COUNT+1
          WRITE(6,360)COUNT
          IF (OPER.EQ.3) THEN
           RESULT(1,COUNT)=PARM(P1SCAN)
           RESULT(3,COUNT)=CHI2
          ELSEIF (OPER.EQ.4) THEN
           RESULT(1,COUNT)=PARM(P1SCAN)
           RESULT(2,COUNT)=PARM(P2SCAN)
           RESULT(3,COUNT)=CHI2
          ENDIF
 14    CONTINUE
 13   CONTINUE
C
C Write data out to a file (*.1D or *.2D with a *.log file giving model
C details)
C
 16   WRITE(6,300)
          READ(5,310)FILNAM
          IF (INDEX(FILNAM,'.').GT.0) THEN
           GOTO 16
          ENDIF
C
C Generate names for files from root provided by user
C
          LFILE=FILNAM//'.LOG'
          IF (OPER.EQ.3)THEN
           DFILE=FILNAM//'.1D'
          ELSEIF (OPER.EQ.4) THEN
           DFILE=FILNAM//'.2D'
          ENDIF
C
C Write out data
C
          OPEN (UNIT=10,FILE=DFILE,STATUS='NEW')
          DO 17 I=1,COUNT
           IF (OPER.EQ.3) THEN
            WRITE(10,*)RESULT(1,I),RESULT(3,I)
           ELSEIF (OPER.EQ.4) THEN
            WRITE(10,*)RESULT(1,I),RESULT(2,I),RESULT(3,I)
           ENDIF
 17   CONTINUE
          WRITE(10,*)
          CLOSE(10)
C
C Generate .LOG file
C
          OPEN(UNIT=10,FILE=LFILE,STATUS='NEW')
          WRITE(10,320)TYPE,NUMBER
          DO 18 I=1,NPARAS
```

```
          IF ((I.NE.P1SCAN).AND.(I.NE.P2SCAN)) THEN
           WRITE(10,330)NAMES(I),PARM(I)
          ELSEIF ((I.EQ.P2SCAN).AND.(OPER.EQ.4)) THEN
           WRITE(10,340)NAMES(I),P2LOWER,P2UPPER
          ELSEIF (I.EQ.P1SCAN) THEN
           WRITE(10,340)NAMES(I),P1LOWER,P1UPPER
          ELSEIF ((I.EQ.P2SCAN).AND.(OPER.EQ.3)) THEN
           WRITE(10,330)NAMES(I),PARM(I)
          ENDIF
 18   CONTINUE
          CLOSE(10)
C
C  Thats all folks!
C
 100  FORMAT(1X,/,/,34X,'PHOENIX V',F3.1,/,/)
 110  FORMAT(25X,'A program that performs various')
 120  FORMAT(20X,'Neutron reflectivity analysis functions')
 130  FORMAT(/,/,29X,'Written by I. Hopkinson')
 140  FORMAT(/,35X,'July 1992')
 150  FORMAT(/,1X,'What sort of model would you like [number,
     &number]?')
 160  FORMAT(/,1X,'1.  Functional',/,6X,'1. Exponential plus',/,6X,
     & '2. TANH')
 170  FORMAT(/,1X,'2.  Multilayer',/,6X,'n layers (n<4)')
 190  FORMAT(1X,'Invalid input, try again')
 200  FORMAT(/,/,1X,'1. Fit reflectivity data',/,1X,'2. Model reflec
     &tivity data',/,1X,'3. 1-D scan',/,1X,'4. 2-D scan (contour plot)')
 210  FORMAT(1X,'Which function do you require [1-4]?')
 220  FORMAT(1X,'Execution completed')
 230  FORMAT(/,/,1X,'What Q range would you like to model over [number
     &,number]?')
 240  FORMAT(1X,'How many values to be calculated [2-300]?')
 250  FORMAT(1X,'Filename for model data (with extension):'$)
 260  FORMAT(1X,'Which parameter would you like to scan [5-',I2,']?')
 270  FORMAT(1X,'Invalid parameter number')
 280  FORMAT(1X,'Input scan limits [lower,upper]')
 290  FORMAT(1X,'Number of steps')
 300  FORMAT(1X,'File name for output data (no extension):'$)
 310  FORMAT(A)
 320  FORMAT(1X,'Model number ',I1,1X,I1)
 330  FORMAT(1X,A8,3X,G10.4)
 340  FORMAT(1X,A8,3X,G10.4,' to ',G10.4)
 350  FORMAT(1X,'Working')
 360  FORMAT(I4,' '$)
 370  FORMAT(1X,'Structure at :(0) air',/,15X,'(1) silicon interface')
 375  FORMAT(15X,'(2) Both interfaces')
 380  FORMAT(1X,'Invalid entry, see if you can manage it properly this
     & time')
 390      FORMAT(1X,'Would you like to get a profile from a volfmem *.map
     & file? (Y/N)')
 400      FORMAT(A)
 90   END
C
C  Subroutine to alter model parmeters, for all except fitting routine.
C
          SUBROUTINE ALTER(NPARAS,NAMES,PARM)
          INTEGER*4 NPARAS,IPARM
          REAL*8 NAMES(20)
          REAL*4 PARM(20),VALUE
C
C  Print out present values
C
 20   DO 10 I=1,NPARAS
          WRITE(6,100)I,NAMES(I),PARM(I)
 10   CONTINUE
C
C  Interrogate user, for values for end.
C
 30   WRITE(6,110)
          READ(5,*)IPARM,VALUE
          IF (IPARM.GT.NPARAS) THEN
           GOTO 30
          ENDIF
C
C  Exit condition
C
          IF (IPARM.LT.0) THEN
           RETURN
          ELSE
C
C  Alter parameter
C
           PARM(IPARM)=VALUE
           GOTO 20
          ENDIF
          RETURN
C
 100  FORMAT(I3,5X,A8,5X,G10.4)
 110  FORMAT(1X,'Which parameter would you like to alter?',
     * '[Number,Value] or [-1,-1] to end')
          END
C
```

```
C
C  Subroutine to READIN data
C
          SUBROUTINE READIN(NFIT,XUSE,YUSE,YRUSE,TEXT)
          REAL XUSE(300),YUSE(300),YRUSE(300),DUM
          INTEGER NFIT,IN
          LOGICAL EXISTS
          CHARACTER FILNAM*30,TRIPE*3,DUM1*12,DUM2*80
C
C  Get filename and identify extension
C
 10   WRITE(6,100)
          READ(5,110)FILNAM
          INQUIRE(FILE=FILNAM,EXIST=EXISTS)
          IF (.NOT.EXISTS) THEN
           WRITE(6,120)
           GOTO 10
          ENDIF
          IN=INDEX(FILNAM,' ')
          TRIPE=FILNAM((IN-3):(IN-1))
C
C  Read .DRY format (number of points, followed by x y pairs, followed by
C  title).  Fractional error is calculated and placed in YRUSE
C
          IF ((TRIPE.EQ.'DRY').OR.(TRIPE.EQ.'dry')) THEN
           OPEN(UNIT=10,FILE=FILNAM,STATUS='OLD')
           READ(10,*)NFIT
           NFIT=NFIT-4
           DO 20 I=1,NFIT
            READ(10,*)XUSE(I),YUSE(I),YRUSE(I)
C
            IF (YUSE(I).LE.0.0) THEN
             YUSE(I)=10**YUSE(I-1)
             YRUSE(I)=YUSE(I-1)*YRUSE(I-1)
            ENDIF
C
            TEMP=YRUSE(I)/YUSE(I)
            YRUSE(I)=TEMP
            YUSE(I)=LOG10(YUSE(I))
 20   CONTINUE
          READ(10,130)TEXT
          CLOSE(10)
C
C  Read .DEV format (the VOLFMEM format)
C
          ELSEIF ((TRIPE.EQ.'DEV').OR.(TRIPE.EQ.'dev')) THEN
          OPEN(UNIT=10,FILE=FILNAM,STATUS='OLD')
          READ(10,130)TEXT
          READ(10,130)DUM2
          READ(10,*,END=50)(XUSE(I),YUSE(I),YRUSE(I),DUM,I=1,1000)
 50   NFIT=I-1
C
          DO 60 I=1,NFIT
           IF (YUSE(I).LE.0.0) THEN
            YUSE(I)=10**YUSE(I-1)
            YRUSE(I)=YUSE(I-1)*YRUSE(I-1)
           ENDIF
           TEMP=YRUSE(I)/YUSE(I)
           YRUSE(I)=TEMP
           YUSE(I)=LOG10(YUSE(I))
 60   CONTINUE
          CLOSE(10)
C
C  Read .DAT format (the CRISP ASCII format)
C  Fractional error is calculated and placed in YRUSE
C
          ELSEIF ((TRIPE.EQ.'DAT').OR.(TRIPE.EQ.'dat')) THEN
          OPEN(UNIT=10,FILE=FILNAM,STATUS='OLD')
          READ(10,150)DUM1,NFIT
          READ(10,110)DUM2
          READ(10,110)DUM2
          READ(10,110)DUM2
          NFIT=NFIT-1
          DO 30 I=1,NFIT
           READ(10,*)XUSE(I),YUSE(I),YRUSE(I)
           TEMP=YRUSE(I)/YUSE(I)
           YRUSE(I)=TEMP
           YUSE(I)=LOG10(YUSE(I))
 30   CONTINUE
          READ(10,*)XUSE(NFIT+1),YUSE(NFIT+1),YRUSE(NFIT+1)
          READ(10,110)TEXT
          CLOSE(10)
          ELSE
           WRITE(6,140)
           GOTO 10
          ENDIF
C
C  Histogram format conversion
C
          NFIT=NFIT-1
          DO 40 I=1,NFIT
           XUSE(I)=(XUSE(I)+XUSE(I+1))/2
```

```
 40   CONTINUE
C
          RETURN
C
C
 100  FORMAT(1X,'Enter data filename:'$)
 110  FORMAT(A)
 120  FORMAT(1X,'No such file')
 130  FORMAT(A40)
 140  FORMAT(1X,'File extension not recognised')
 150  FORMAT(A12,I4)
 160  FORMAT(I3)
          END
C
C
C The reflectivity calculating subroutine
C
          SUBROUTINE REFL(NPARAS,PARM,NFIT,XUSE,YUSE,YRUSE,YCALC,F)
          REAL PARM(NPARAS),XUSE(NFIT),YUSE(NFIT),YRUSE(NFIT)
          REAL YCALC(NFIT),F(NFIT),SINTH(300)
          REAL TBLOCK(300),ROUGH(300)
          COMPLEX RBLOCK(300),CI,MM(2,2),BIGM(2,2),DUM(2,2),NM,NS,NJ,NJ1
          COMPLEX PM,PS,PA,PL1,BETAL1,BETAM,R1,R2,R3,R4,RM,RS,N0,NL1
          INTEGER NBLOCKS,TYPE,NUMBER,NPARAS
          REAL LAM,PI,CONST1,CONST2,TEMP1,TEMP2,TEMP3
          LOGICAL AIR
          COMMON/MODEL/TYPE,NUMBER,AIR
C
C Some useful constants
C
          PI=3.14159265
          CI=CMPLX(0.0,1.0)
          LAM=12.0
          CONST1=(2*PI)/LAM
          CONST2=LAM*LAM/(2*PI)
C
C Calculate sin theta from XUSE, which are values of Q
C
          DO 10 I=1,NFIT
           SINTH(I)=XUSE(I)/(2*CONST1)
 10   CONTINUE
C
C Get the Model
C
          CALL MODL(PARM,NPARAS,RBLOCK,TBLOCK,ROUGH,NBLOCKS)
C
C The big IF Abeles method for types 1 and 2, Beaglehole and Law for
C type 3 model
C
          IF ((TYPE.EQ.1).OR.(TYPE.EQ.2).OR.(TYPE.EQ.3)) THEN
C
C Abeles, loop through each value of incident Q.
C
          DO 20 I=1,NFIT
C
C Entry conditions (mainly m-1=0)
C
          BIGM(1,1)=1.0
          BIGM(2,2)=1.0
          BIGM(2,1)=0.0
          BIGM(1,2)=0.0
          NL1=1.0-CONST2*PARM(1)
          N0=NL1
          PL1=N0*SINTH(I)
          BETAL1=CONST1*0*PL1
          QL1=XUSE(I)
          CONST3=N0*N0*(1-SINTH(I)*SINTH(I))
C
C Loop through the block model.
C
          DO 30 M=1,NBLOCKS
           NM=1-CONST2*RBLOCK(M)
           PM=SQRT(NM*NM-CONST3)
           QM=(2*CONST1*PM)/NM
           BETAM=CONST1*PM*TBLOCK(M)
C
C Another cop-out to avoid division by zero errors
C
           IF ((PL1.EQ.0.0).AND.(PM.EQ.0.0)) THEN
            RM=EXP(-0.5*QM*QL1*ROUGH(M)*ROUGH(M))
           ELSE
            RM=((PL1-PM)/(PL1+PM))*EXP(-0.5*QM*QL1*ROUGH(M)*ROUGH(M))
           ENDIF
C
           MM(1,1)=EXP(CI*BETAL1)
           MM(2,2)=EXP(-CI*BETAL1)
           MM(1,2)=RM*MM(1,1)
           MM(2,1)=RM*MM(2,2)
           CALL MATRIX(BIGM,MM,DUM)
           BIGM(1,1)=DUM(1,1)
           BIGM(2,2)=DUM(2,2)
           BIGM(1,2)=DUM(1,2)
```

```
            BIGM(2,1)=DUM(2,1)
            BETAL1=BETAM
            QL1=QM
            PL1=PM
 30     CONTINUE
C
C Exit calculations including calculating R for 1 value of Q
C
            NS=1-CONST2*PARM(2)
            PS=SQRT(NS*NS-CONST3)
            QS=2*CONST1*PS/NS
            RS=((PL1-PS)/(PL1+PS))*EXP(-0.5*QL1*QS*(ROUGH(NBLOCKS+1)**2))
            MM(1,1)=EXP(CI*BETAL1)
            MM(2,2)=EXP(-CI*BETAL1)
            MM(1,2)=RS*MM(1,1)
            MM(2,1)=RS*MM(2,2)
            CALL MATRIX(BIGM,MM,DUM)
            BIGM(1,1)=DUM(1,1)
            BIGM(2,1)=DUM(2,1)
            BIGM(2,2)=DUM(2,2)
            BIGM(1,2)=DUM(1,2)
            TEMP1=BIGM(2,1)*CONJG(BIGM(2,1))
            TEMP2=BIGM(1,1)*CONJG(BIGM(1,1))
C
C This bit is a fiddle, because for some reason with functional form models
C temp1=temp2=0. This fiddle allows the program to run and doesn't seem
C to grossly effect the profiles generated.
C
            IF ((TEMP2.EQ.0.0).AND.(TEMP1.EQ.0.0)) THEN
             TEMP1=1
             TEMP2=1
            ENDIF
C
            YCALC(I)=LOG10(TEMP1/TEMP2)
 20     CONTINUE
          ENDIF
C
C Call the resolution routine
C
          CALL RESL(XUSE,YCALC,PARM,NPARAS,NFIT)
C
C Calculate the residual F, this is where error weighting code should
C be inserted. Done - note READIN has also been altered to make YRUSE(i)
C the fractional error in Y.
C
          DO 60 I=1,NFIT
            F(I)=(YUSE(I)-YCALC(I))/YRUSE(I)
 60     CONTINUE
C
C The End
C
          RETURN
          END
C
C Matrix multiplication routine
C
          SUBROUTINE MATRIX(A,B,C)
          COMPLEX A(2,2),B(2,2),C(2,2)
          C(1,1)=A(1,1)*B(1,1)+A(1,2)*B(2,1)
          C(1,2)=A(1,1)*B(1,2)+A(1,2)*B(2,2)
          C(2,1)=A(2,1)*B(1,1)+A(2,2)*B(2,1)
          C(2,2)=A(2,1)*B(1,2)+A(2,2)*B(2,2)
          RETURN
          END
C
C
C The resolution effect routine, this is a modification of the routine
C used previously.
C
          SUBROUTINE RESL(XUSE,YCALC,PARM,NPARAS,NFIT)
          REAL XMIN,XMAX,YCALC(NFIT),XUSE(NFIT),PARM(NPARAS)
          REAL RESULT,YTEMP(300),TEMP,YMIN,YMAX
          INTEGER START,END
C
C Return without doing anything if resolution=0% - otherwise
C you get a division by zero error
C
          IF (PARM(5).EQ.0.0) THEN
           RETURN
          ENDIF
C
C Main loop through all the points
C
          DO 10 I=1,NFIT
           XMIN=XUSE(I)-(PARM(5)/100.0)*XUSE(I)
           XMAX=XUSE(I)+(PARM(5)/100.0)*XUSE(I)
C
C Test for beginning or end of 'point' integral lying outside dataset
C then do loop to identify range of integral
C
           IF (XMAX.GT.XUSE(NFIT)) THEN
            END=NFIT+1
```

```
          ENDIF
          IF (XMIN.LT.XUSE(1)) THEN
           START=0
          ENDIF
          DO 20 J=1,NFIT-1
           IF ((XUSE(J).LE.XMIN).AND.(XUSE(J+1).GT.XMIN)) THEN
            START=J
           ENDIF
           IF ((XUSE(J).GT.XMAX).AND.(XUSE(J-1).LE.XMAX)) THEN
            END=J-1
           ENDIF
 20    CONTINUE
C
C  Bit to work out first part of integral
C
          RESULT=0.0
          IF (XMIN.GT.XUSE(1)) THEN
           TEMP=(XMIN-XUSE(START))/(XUSE(START+1)-XUSE(START))
           YMIN=YCALC(START)+(YCALC(START+1)-YCALC(START))*TEMP
           RESULT=RESULT+0.5*(YMIN+YCALC(START+1))*(XUSE(START+1)-XMIN)
          ENDIF
C
C  Main part of integral
C
          DO 30 J=START+1,END-2
           RESULT=RESULT+0.5*(YCALC(J)+YCALC(J+1))*(XUSE(J+1)-XUSE(J))
 30    CONTINUE
C
C  End part of integral
C
          IF (END.EQ.(NFIT+1)) THEN
           RESULT=RESULT+(YCALC(NFIT))*(XMAX-XUSE(NFIT))
          ELSE
           TEMP=(XMAX-XUSE(END-1))/(XUSE(END)-XUSE(END-1))
           YMAX=YCALC(END-1)-(YCALC(END-1)-YCALC(END))*TEMP
           RESULT=RESULT+0.5*(YMAX+YCALC(END-1))*(XMAX-XUSE(END-1))
          ENDIF
          RESULT=RESULT/(XMAX-XMIN)
          YTEMP(I)=RESULT
 10    CONTINUE
C
C  Transfer integral back to YCALC
C
          DO 40 I=1,NFIT
           YCALC(I)=YTEMP(I)
           YTEMP(I)=0.0
 40    CONTINUE
          RETURN
          END
C
C
C  MODL routine to set up model for REFL.
C
          SUBROUTINE MODL(PARM,NPARAS,RBLOCK,TBLOCK,ROUGH,NBLOCKS)
          INTEGER TYPE,NUMBER,NBLOCKS,AIR,N
          COMMON/MODEL/TYPE,NUMBER,AIR
          COMPLEX RBLOCK(300)
          REAL PARM(NPARAS),TBLOCK(300),ROUGH(300)
          REAL BSIZE,Z,TEMP,TEMP2,TEMP3,TEMP4,TEMP5,TOL,UPPER1,UPPER2
          LOGICAL EXISTS
          CHARACTER*30 MAPFILE
C
C  This is the New Model functional form profile routine.  It takes the
C  block size as a user input, there is no safety check to make sure the
C  program can handle the required number of blocks - so ensure that
C  thick/bsize<300 for safety.  Profiles can be fitted at the air either/and
C  the silicon interface.  Exponential plus or TANH profiles are supported
C
          IF (TYPE.EQ.1) THEN
           BSIZE=PARM(6)
           ROUGH(1)=PARM(8)
           TOL=0.01
           UPPER1=0
           UPPER2=0
           TEMP3=PARM(11)-PARM(7)
     TEMP4=PARM(14)-PARM(7)

C
C  This part works out the upper bounds for the profiles
C  its quite important because on the basis of these results various things
C  are or are not calculated
C
           IF (NUMBER.EQ.1) THEN
            IF ((AIR.EQ.0).OR.(AIR.EQ.2).AND.(TOL.LT.TEMP3)) THEN
             UPPER1=PARM(13)*(LOG(TEMP3/TOL)**(1/PARM(12)))
            ENDIF
            IF ((AIR.EQ.1).OR.(AIR.EQ.2).AND.(TOL.LT.TEMP4)) THEN
             UPPER2=PARM(16)*(LOG(TEMP4/TOL)**(1/PARM(15)))
            ENDIF
           ELSEIF (NUMBER.EQ.2) THEN
            IF ((AIR.EQ.0).OR.(AIR.EQ.2).AND.(TOL.LT.TEMP3)) THEN
             UPPER1=PARM(12)-PARM(13)*(1.34*(-1+2*TOL/TEMP3))/2
```

```
            ENDIF
            IF ((AIR.EQ.1).OR.(AIR.EQ.2).AND.(TOL.LT.TEMP4)) THEN
             UPPER2=PARM(15)-PARM(16)*(1.34*(-1+2*TOL/TEMP4))/2
            ENDIF
           ENDIF
C
           UPPER1=INT(UPPER1/BSIZE)*BSIZE
           UPPER2=INT(UPPER2/BSIZE)*BSIZE
C
C  This next bit actually calculates the profile - the bulk block
C  the two interfaces as necessary - if upper1+upper2> thickness
C  then there is no need to calculate the bulk block
C
           IF ((UPPER1+UPPER2).LT.PARM(6)) THEN
           NBLOCKS=(UPPER1/BSIZE)+(UPPER2/BSIZE)+1
C
C  Calculating the bulk block
C
            IF (UPPER1.EQ.0) THEN
             N=1
            ELSE
             N=(UPPER1/BSIZE)+1
            ENDIF
            TEMP2=PARM(4)*PARM(7)+PARM(3)*(1-PARM(7))
            TBLOCK(N)=PARM(10)-UPPER1-UPPER2
            RBLOCK(N)=CMPLX(TEMP2,0.0)
C
C  This bit calculates the Air interface profile
C
            IF (UPPER1.GT.0) THEN
             DO 10 I=1,(UPPER1/BSIZE)
              TBLOCK(I)=BSIZE
              Z=(I-1)*BSIZE+BSIZE/2
              IF (NUMBER.EQ.1) THEN
               TEMP2=TEMP3*EXP(-(Z/PARM(13))**PARM(12))
              ELSE
               TEMP2=TEMP3*(1+TANH(2*(PARM(12)-Z)/PARM(13)))/2
              ENDIF
              TEMP2=(PARM(7)+TEMP2)*PARM(4)+(PARM(7)+TEMP2-1)*PARM(3)
              RBLOCK(I)=CMPLX(TEMP2,0.0)
 10     CONTINUE
            ENDIF
C
C  This is the silicon interface part
C
            IF (UPPER2.GT.0) THEN
             DO 20 I=1,(UPPER2/BSIZE)
              TBLOCK(N+I)=BSIZE
              Z=UPPER1+(PARM(10)-UPPER2)+(I-1)*BSIZE+BSIZE/2
              IF (NUMBER.EQ.1) THEN
               TEMP2=TEMP4*EXP(-((PARM(10)-Z)/PARM(16))**PARM(15))
              ELSE
               TEMP2=TEMP4*(1-TANH(2*((PARM(10)-PARM(15))-Z)/PARM(16)))/2
              ENDIF
              TEMP2=(PARM(7)+TEMP2)*PARM(4)+(PARM(7)+TEMP2-1)*PARM(3)
              RBLOCK(I)=CMPLX(TEMP2,0.0)
 20     CONTINUE
            ENDIF
C
C  This is what to do if there is no block in the middle
C
           ELSE
       NBLOCKS=INT(PARM(10)/BSIZE)
            DO 30 I=1,INT(PARM(10)/BSIZE)
             TBLOCK(I)=BSIZE
             Z=(I-1)*BSIZE+BSIZE/2
             IF (NUMBER.EQ.1) THEN
              TEMP2=TEMP3*EXP(-(Z/PARM(13))**PARM(12))
              TEMP=TEMP4*EXP(-((PARM(10)-Z)/PARM(16))**PARM(15))
             ELSE
              TEMP2=TEMP3*(1+TANH(2*(PARM(12)-Z)/PARM(13)))/2
              TEMP=TEMP4*(1-TANH(2*((PARM(10)-PARM(15))-Z)/PARM(16)))/2
             ENDIF
             TEMP5=PARM(7)+TEMP2+TEMP
             TEMP5=TEMP5*PARM(4)+(1-TEMP5)*PARM(3)
             RBLOCK(I)=CMPLX(TEMP5,0.0)
 30     CONTINUE
            ENDIF
C  This sticks an SiO2 layer in
C
           NBLOCKS=NBLOCKS+1
       TBLOCK(NBLOCKS)=15.0
       RBLOCK(NBLOCKS)=CMPLX(3.676E-6,0.0)
       ROUGH(NBLOCKS)=PARM(9)
           ROUGH(NBLOCKS+1)=5.0
c
           RETURN
          ENDIF
C
C  Block model
C
           IF (TYPE.EQ.2) THEN
```

```
          NBLOCKS=NUMBER
          ROUGH(1)=PARM(6)
          TEMP3=PARM(5+NUMBER*3)
          DO 40 I=1,NUMBER
           TBLOCK(I)=PARM(5+I*3)
           ROUGH(I+1)=PARM(6+I*3)
           TEMP=PARM(4+I*3)*PARM(4)+(1-PARM(4+I*3))*PARM(3)
           RBLOCK(I)=CMPLX(TEMP,0.0)
           TEMP3=TEMP3-PARM(5+I*3)
 40    CONTINUE
          TEMP3=TEMP3+PARM(5+NUMBER*3)
C  Modification to vary blocks independantly, temp3 is ignored
C         TBLOCK(NUMBER)=TEMP3
          RETURN
         ENDIF
C
C  Read in a *.map file from volfmem, this should only occur for the
C  'Model reflectivity' option.
C
         IF (TYPE.EQ.3) THEN
 50       WRITE(6,100)
          READ(5,110)MAPFILE
          INQUIRE(FILE=MAPFILE,EXIST=EXISTS)
          IF (.NOT.EXISTS) THEN
           WRITE(6,120)
           GOTO 50
          ENDIF
          OPEN(UNIT=10,FILE=MAPFILE,STATUS='OLD')
          DO 60 I=1,300
           READ(10,*,END=70)TBLOCK(I),TEMP,TEMP2
           RBLOCK(I)=CMPLX(TEMP*PARM(4)+(1-TEMP)*PARM(3),0.0)
 60       CONTINUE
 70       NBLOCKS=I-1
          DO 80 I=1,NBLOCKS-1
           TBLOCK(I)=TBLOCK(I+1)-TBLOCK(I)
 80       CONTINUE
          TBLOCK(NBLOCKS)=TBLOCK(NBLOCKS-1)
          RETURN
         ENDIF
 100     FORMAT(1X,'Enter volfmem output filename:'$)
 110     FORMAT(A)
 120     FORMAT(1X,'No file by that name, have another go.')
         END
```

WELDER

```
C
C  WELDER is a program that combines CRISP datasets, the datasets must be
C  rebinned to the same spacing and normalisation factors should have been
C  applied.  Negative values for the reflectivity are replaced by the
C  error in the reflectivity and the number of such replacements is recorded
C  I.H. 11/1/93
C
         PROGRAM WELDER
         CHARACTER DUM1*26,DUM2(8)*80,FILENAM*20
         INTEGER NFIT,I,ERR
         REAL X1(300),Y1(300),YE1(300),X2(300),Y2(300),YE2(300)
         REAL X(300),Y(300),YE(300)
         LOGICAL FLAG1,FLAG2,EXISTS
C
C  Load in datasets to be combined - at present it is assumed that they are
C  called temp1.dat and temp2.dat
C
         OPEN (UNIT=10,FILE='TEMP1.DAT',STATUS='OLD')
C
C  Header 1
C
         DO 10 I=1,6
          READ (10,100)DUM2(I)
 10      CONTINUE
         READ(10,110)DUM1,NFIT
         READ(10,100)DUM2(7)
         READ(10,100)DUM2(8)
C
C  Data 1
C
         DO 20 I=1,NFIT
          READ(10,*)X1(I),Y1(I),YE1(I)
 20      CONTINUE
         CLOSE(10)
C
C  Second dataset
C
         OPEN (UNIT=10,FILE='TEMP2.DAT',STATUS='OLD')
C
C  Header 2
C
         DO 30 I=1,6
          READ (10,100)DUM2(I)
 30      CONTINUE
```

```
      READ(10,110)DUM1,NFIT
      READ(10,100)DUM2(7)
      READ(10,100)DUM2(8)
C
C Data 2
C
      DO 40 I=1,NFIT
       READ(10,*)X2(I),Y2(I),YE2(I)
40    CONTINUE
      CLOSE(10)
C
C Set up combine loop
C
      FLAG1=.TRUE.
      FLAG2=.FALSE.
C
C Start loop
C
      DO 50 I=1,NFIT
       IF ((Y1(I).EQ.0.0).AND.(YE1(I).EQ.0.0)) THEN
        FLAG1=.FALSE.
       ENDIF
       IF (FLAG1.AND.FLAG2) THEN
        X(I)=X1(I)
        Y(I)=(Y1(I)+Y2(I))/2
        YE(I)=(YE1(I)+YE2(I))/2
       ENDIF
       IF (FLAG1.AND.(.NOT.FLAG2)) THEN
        X(I)=X1(I)
        Y(I)=Y1(I)
        YE(I)=YE1(I)
       ENDIF
       IF ((.NOT.FLAG1).AND.FLAG2) THEN
        X(I)=X2(I)
        Y(I)=Y2(I)
        YE(I)=YE2(I)
       ENDIF
       IF ((Y2(I).NE.0.0).AND.(YE2(I).NE.0.0)) THEN
        FLAG2=.TRUE.
       ENDIF
50    CONTINUE
C
C Data is now written out in the *.dry format
C
      WRITE(6,120)
      READ(5,100)FILENAM
      OPEN (UNIT=10,FILE=FILENAM,STATUS='NEW')
      WRITE(10,*)NFIT
      ERR=0
      DO 60 I=1,NFIT
C
C This IF statement traps any negative values for the reflectivity
C
       IF (Y(I).LT.0.0) THEN
        WRITE(10,*)X(I),YE(I),YE(I)
        ERR=ERR+1
       ELSE
        WRITE(10,*)X(I),Y(I),YE(I)
       ENDIF
C
60    CONTINUE
      WRITE(10,130)DUM2(1)
      CLOSE(10)
      WRITE(6,140)ERR

100   FORMAT(A)
110   FORMAT(A26,I4)
120   FORMAT(1X,'Enter name for combined file:'$)
130   FORMAT(A40)
140   FORMAT(1X,I4,'  negative reflectivity values replaced')
      END
```

BANTAM (data fitted as I(Q) vs Q)

```
C
C BANTAM is a program that calculates chi from SANS data
C as well as radii of gyration. (via the Kuhn length, a)
C Written to process d-PS/h-PS standard data, NH=ND and RGH=RGD
C are forced because d-PS and h-PS had identical molecular weights
C See de Gennes p261,p109 and refs 76,84.
C I. Hopkinson 1/10/92
C
      PROGRAM CHICKEN
      EXTERNAL READIN,SCATTER
      COMMON/TITLES/NAMES(20),TX(5),TY(5),NPARAS
      COMMON/WORK/W(3066)
      COMMON/IO/INTTY,IOUTTY
      DOUBLE PRECISION NAMES
      DATA NAMES/'Chi    ','phi(d) ','Rg(h)/A ','Rg(d)/A ','N(d)   ',
     & 'N(h)   ','V      ','b(h)   ','b(d)   ','Instrum ',
```

```
     &      10*'     '/
            DATA TX/'Q/A^',-1  ',3*'   '/
            DATA TY/'I(Q)','/CM^',-1  ',2*'   '/
            DATA PNAM/'SHED'/
            VERP=1.0
            INTTY=5
            IOUTTY=6
            NPARAS=10
            WRITE(6,100)
            WRITE(6,110)
            WRITE(6,120)
            CALL FITFUN(PNAM,READIN,SCATTER)
            CALL FINITT(0,750)
  100       FORMAT(1X,/,/,/,36X,'CHICKEN',/,/,/)
  110       FORMAT(1X,25X,'A program to fit SANS data',/,/,/)
  120       FORMAT(1X,25X,'By Ian Hopkinson (1/10/92)',/,/,/)
            END
C
C READIN data from LOQ
C
            SUBROUTINE READIN(NFIT,XUSE,YUSE,YRUSE,TEXT)
            REAL*4 XUSE(300),YUSE(300),YRUSE(300)
            INTEGER NFIT,I,J
            LOGICAL EXISTS
            CHARACTER FILNAM*60,DUMMY*80
  10        WRITE(6,100)
            READ(5,110)FILNAM
            INQUIRE(FILE=FILNAM,EXIST=EXISTS)
            IF (.NOT.EXISTS) THEN
             WRITE(6,120)
             GOTO 10
            ENDIF
            OPEN (UNIT=10,FILE=FILNAM,STATUS='OLD')
            DO 20 J=1,5
             READ(10,130)DUMMY
  20        CONTINUE
            DO 30 I=1,300
             READ(10,*,END=40)XUSE(I),YUSE(I),YRUSE(I)
             YRUSE(I)=YRUSE(I)/YUSE(I)
  30        CONTINUE
  40        NFIT=I-1
            CLOSE(10)
            RETURN
  100       FORMAT(1X,'Enter filename:'$)
  110       FORMAT(A)
  120       FORMAT(1X,'File does not exist')
  130       FORMAT(A)
            END
C
C Calculation routine
C
            SUBROUTINE SCATTER(NPARAS,PARM,NFIT,XUSE,YUSE,YRUSE,YCALC,F)
            REAL*4 PARM(NPARAS),YCALC(NFIT),YRUSE(NFIT),YUSE(NFIT)
            REAL*4 XUSE(NFIT),S(300),F(NFIT)
            REAL*4 PREFACTOR,RGH,RGD,PHI,CHI,ND,NH,GDH,GDD
            DO 10 I=1,NFIT
             PREFACTOR=(PARM(8)-PARM(9))*(PARM(8)-PARM(9))/PARM(7)
             ND=PARM(5)
             NH=ND
             RGD=PARM(4)
             RGH=RGD
             PARM(3)=RGH
             PHI=PARM(2)
             CHI=PARM(1)
             GDH=GD(RGD,XUSE(I))
             GDD=GD(RGH,XUSE(I))
             TEMP1=1.0/(ND*PHI*GDH)
             TEMP2=1.0/(NH*(1-PHI)*GDD)
             YCALC(I)=PARM(10)*PREFACTOR/(TEMP1+TEMP2-2*CHI)
             F(I)=(YCALC(I)-YUSE(I))/YRUSE(I)
  10        CONTINUE
            RETURN
            END
C
C Debye Function, gd.
C
            REAL FUNCTION GD(RG,Q)
            REAL RG,Q,TEMP
            TEMP=RG*RG*Q*Q
            GD=2*(TEMP+EXP(-TEMP)-1)/(TEMP*TEMP)
            END
```

PULLET3

```
C
C PULLET is a program that calculates chi and radii of gyration
C from SANS data.  Unlike CHICKEN displays fits and data in the Kratky
C format.
C See de Gennes p261,p109 and refs 76,84.
C I. Hopkinson 1/10/92
```

```
C Modified 16/2/93 - seemed to have GDD, GDH mixed up -panic over
C TEMP1 and TEMP2 were mixed up, reversing the effect of GDD and GDH being
C mixed.
C 23/8/93 - Modified to look at 'asymmetric' blends such as PEO/PMMA
C           see ref 113
C 12/10/93 - Modified to look at polydisperse blends such as isotactic PMMA
C           see ref 113
C
      PROGRAM PULLET
      EXTERNAL READIN,SCATTER
      COMMON/TITLES/NAMES(20),TX(5),TY(5),NPARAS
      COMMON/WORK/W(3066)
      COMMON/IO/INTTY,IOUTTY
      DOUBLE PRECISION NAMES
      DATA NAMES/'Chi    ','phi(d) ','Rg(h)/A ','Rg(d)/A ',
     &     'N(d)   ','N(h)   ','DP(d)  ','DP(h)  ',
     &     'Vh     ','Vd     ','b(h)   ',
     &     'b(d)   ','Instrum ',
     &     7*'      '/
      DATA TX/'Q/A^',-1 ',3*'   '/
      DATA TY/'I(Q)','/CM^',-1 ',2*'   '/
      DATA PNAM/'SHED'/
      VERP=1.0
      INTTY=5
      IOUTTY=6
      NPARAS=13
      WRITE(6,100)
      WRITE(6,110)
      WRITE(6,120)
      CALL FITFUN(PNAM,READIN,SCATTER)
      CALL FINITT(0,750)
100   FORMAT(1X,/,/,/,21X,'PULLET 3 - Asymmetry, Polydispersity',/,/,/)
110   FORMAT(1X,25X,'A program to fit SANS data',/,/,/)
120   FORMAT(1X,25X,'By Ian Hopkinson (1/10/92)',/,/,/)
      END
C
C READIN data from LOQ
C
      SUBROUTINE READIN(NFIT,XUSE,YUSE,YRUSE,TEXT)
      REAL*4 XUSE(300),YUSE(300),YRUSE(300)
      INTEGER NFIT,I,J
      LOGICAL EXISTS
      CHARACTER FILNAM*60,DUMMY*80
10    WRITE(6,100)
      READ(5,110)FILNAM
      INQUIRE(FILE=FILNAM,EXIST=EXISTS)
      IF (.NOT.EXISTS) THEN
       WRITE(6,120)
       GOTO 10
      ENDIF
      OPEN (UNIT=10,FILE=FILNAM,STATUS='OLD')
      DO 20 J=1,5
       READ(10,130)DUMMY
20    CONTINUE
      DO 30 I=1,300
       READ(10,*,END=40)XUSE(I),YUSE(I),YRUSE(I)
       YRUSE(I)=YRUSE(I)/YUSE(I)
       YUSE(I)=YUSE(I)*XUSE(I)*XUSE(I)
30    CONTINUE
40    NFIT=I-1
      CLOSE(10)
      RETURN
100   FORMAT(1X,'Enter filename:'$)
110   FORMAT(A)
120   FORMAT(1X,'File does not exist')
130   FORMAT(A)
      END
C
C Calculation routine
C
      SUBROUTINE SCATTER(NPARAS,PARM,NFIT,XUSE,YUSE,YRUSE,YCALC,F)
      REAL*4 PARM(NPARAS),YCALC(NFIT),YRUSE(NFIT),YUSE(NFIT)
      REAL*4 XUSE(NFIT),S(300),F(NFIT)
      REAL*4 PREFACTOR,RGH,RGD,PHI,CHI,ND,NH,GDH,GDD
      REAL*4 DPD,DPH
      REAL*4 VH,VD,V0,NA
      NA=6.022E23
      DO 10 I=1,NFIT
       ND=PARM(5)
       NH=PARM(6)
       DPD=PARM(7)
       DPH=PARM(8)
       VH=PARM(9)
       VD=PARM(10)
       RGD=PARM(4)
       RGH=PARM(3)
       PHI=PARM(2)
       CHI=PARM(1)
       V0=1/((PHI/VD)+(1-PHI)/VH)
       PREFACTOR=V0*((PARM(11)/VH-PARM(12)/VD)**2)
C
C APPEARED TO HAVE THESE TWO MIXED UP PREVIOUSLY
```

```
C THIS IS WHERE POLYDISPERSITY CORECTION GOES IN
C
          GDH=GD(RGH,DPH,XUSE(I))
          GDD=GD(RGD,DPD,XUSE(I))
C
          IF (.NOT.(RGH.EQ.0.OR.RGD.EQ.0)) THEN
      TEMP1=V0/(ND*PHI*GDD*VD)
          TEMP2=V0/(NH*(1-PHI)*GDH*VH)
          ENDIF
          YCALC(I)=PARM(13)*PREFACTOR/(TEMP1+TEMP2-2*CHI)
          YCALC(I)=YCALC(I)*XUSE(I)*XUSE(I)
          F(I)=(YCALC(I)-YUSE(I))/YRUSE(I)
 10       CONTINUE
          RETURN
          END
C
C  Debye Function, gd.
C  Debye function modified to allow polydispersity (12/10/93)
C
          REAL*4 FUNCTION GD(RG,DP,Q)
          REAL*4 RG,Q,TEMP,DP,HI
          TEMP=RG*RG*Q*Q
          HI=1/(DP-1)
          GD=2*((HI/(HI+TEMP))**HI-1+TEMP)/(TEMP*TEMP)
          END
```

Pullet4 (Pullet and Pullet2 simple cases of Pullet4)

```
C
C  PULLET is a program that calculates chi and radii of gyration
C  from SANS data.  Unlike CHICKEN displays fits and data in the Kratky
C  format.
C  See de Gennes p261,p109 and refs 76,84.
C  I. Hopkinson 1/10/92
C  Modified 16/2/93 - seemed to have GDD, GDH mixed up -panic over
C  TEMP1 and TEMP2 were mixed up, reversing the effect of GDD and GDH being
C  mixed.
C  23/8/93 - Modified to look at 'asymmetric' blends such as PEO/PMMA
C            see ref 113
C  18/5/94 - Modified to fit a flat background
C
          PROGRAM PULLET
          EXTERNAL READIN,SCATTER
          COMMON/TITLES/NAMES(20),TX(5),TY(5),NPARAS
          COMMON/WORK/W(3066)
          COMMON/IO/INTTY,IOUTTY
          DOUBLE PRECISION NAMES
          DATA NAMES/'Chi    ','phi(d)  ','Rg(h)/A ','Rg(d)/A ',
     &    'N(d)   ','N(h)   ','Vh     ','Vd     ','b(h)   ',
     &    'b(d)   ','Instrum ','Backgrd ',
     &    8*'      '/
          DATA TX/'Q/A^',-1 ',3*'   '/
          DATA TY/'I(Q)','/CM^',-1 ',2*'   '/
          DATA PNAM/'SHED'/
          VERP=1.0
          INTTY=5
          IOUTTY=6
          NPARAS=12
          WRITE(6,100)
          WRITE(6,110)
          WRITE(6,120)
          CALL FITFUN(PNAM,READIN,SCATTER)
          CALL FINITT(0,750)
 100      FORMAT(1X,/,/,/,29X,'PULLET 2 - Asymmetry'./,/,/)
 110      FORMAT(1X,25X,'A program to fit SANS data',/,/,/)
 120      FORMAT(1X,25X,'By Ian Hopkinson (1/10/92)',/,/,/)
          END
C
C  READIN data from LOQ
C
          SUBROUTINE READIN(NFIT,XUSE,YUSE,YRUSE,TEXT)
          REAL*4 XUSE(300),YUSE(300),YRUSE(300)
          INTEGER NFIT,I,J
          LOGICAL EXISTS
          CHARACTER FILNAM*60,DUMMY*80
 10       WRITE(6,100)
          READ(5,110)FILNAM
          INQUIRE(FILE=FILNAM,EXIST=EXISTS)
          IF (.NOT.EXISTS) THEN
           WRITE(6,120)
           GOTO 10
          ENDIF
          OPEN (UNIT=10,FILE=FILNAM,STATUS='OLD')
          DO 20 J=1,5
           READ(10,130)DUMMY
 20       CONTINUE
          DO 30 I=1,300
           READ(10,*,END=40)XUSE(I),YUSE(I),YRUSE(I)
           YRUSE(I)=YRUSE(I)/YUSE(I)
           YUSE(I)=YUSE(I)*XUSE(I)*XUSE(I)
```

```
 30      CONTINUE
 40      NFIT=I-1
         CLOSE(10)
         RETURN
100      FORMAT(1X,'Enter filename:'$)
110      FORMAT(A)
120      FORMAT(1X,'File does not exist')
130      FORMAT(A)
         END
C
C  Calculation routine
C
         SUBROUTINE SCATTER(NPARAS,PARM,NFIT,XUSE,YUSE,YRUSE,YCALC,F)
         REAL*4 PARM(NPARAS),YCALC(NFIT),YRUSE(NFIT),YUSE(NFIT)
         REAL*4 XUSE(NFIT),S(300),F(NFIT)
         REAL*4 PREFACTOR,RGH,RGD,PHI,CHI,ND,NH,GDH,GDD
         REAL*4 VH,VD,V0,NA
         NA=6.022E23
         DO 10 I=1,NFIT
          ND=PARM(5)
          NH=PARM(6)
          VH=PARM(7)
          VD=PARM(8)
          RGD=PARM(4)
          RGH=PARM(3)
          PHI=PARM(2)
          CHI=PARM(1)
          V0=1/((PHI/VD)+(1-PHI)/VH)
          PREFACTOR=V0*((PARM(9)/VH-PARM(10)/VD)**2)
C
C APPEARED TO HAVE THESE TWO MIXED UP PREVIOUSLY
C
          GDH=GD(RGH,XUSE(I))
          GDD=GD(RGD,XUSE(I))
C
          IF (.NOT.(RGH.EQ.0.OR.RGD.EQ.0)) THEN
     TEMP1=V0/(ND*PHI*GDD*VD)
          TEMP2=V0/(NH*(1-PHI)*GDH*VH)
          ENDIF
          YCALC(I)=PARM(11)*PREFACTOR/(TEMP1+TEMP2-2*CHI)+parm(12)
          YCALC(I)=YCALC(I)*XUSE(I)*XUSE(I)
          F(I)=(YCALC(I)-YUSE(I))/YRUSE(I)
 10       CONTINUE
          RETURN
          END
C
C  Debye Function, gd.
C
          REAL*4 FUNCTION GD(RG,Q)
          REAL*4 RG,Q,TEMP
          TEMP=RG*RG*Q*Q
          GD=2*(TEMP+EXP(-TEMP)-1)/(TEMP*TEMP)
          END
```